



Investigation to the Ride and Handling of Vehicle with Interconnected Suspensions

by

GUANGZHONG XU

A thesis submitted in fulfillment of the requirements for the degree of

Doctor of Philosophy

Faculty of Engineering and Information Technology
University of Technology, Sydney (UTS)

2016

CERTIFICATE of ORIGINAL AUTHORSHIP

I certify that the work in this thesis has not previously been submitted for a degree nor has it been submitted as part of the requirements for a degree except as fully acknowledged within the text.

I also certify that the thesis has been written by me. Any help that I have received in my research work and the preparation of the thesis has been acknowledged. In addition, I certify that all of the information sources and literature used are indicated in the thesis.

Signed:

Guangzhong Xu

ACKNOWLEDGEMENTS

I would like to take the opportunity to thank a number of people for their assistance, encouragement and support throughout my candidature.

I would like to express my deepest gratitude to my supervisor, Professor Nong Zhang, for his excellent guidance, caring, and patience. I am also grateful for the excellent atmosphere that he provided for the purposes of doing my research. I also sincerely thank my co-supervisor Dr. Holger Roser for his assistance and support on the lab work.

I would like to thank my UTS colleagues: Sangzhi Zhu, Jinglai Wu, Jiageng Ruan, Shuo Wang, Anton Tkachev and many others along the way. Their advice, humour, and knowledge were of great benefit throughout this journey.

I would like to thank my parents for their love and support over the years. My mother, in particular, deserves special thanks for her help taking care of my new-born daughter in the last year of my candidature.

Most importantly, I would like to thank my wife, Qi Wang, who has always been there cheering me up and standing by me through the good times and bad.

Lastly, I would like to dedicate this thesis to my beloved daughter Selena. She is so beautiful and brings me more joy than I could have ever imagined.

TABLE OF CONTENTS

CERTIFICATE of ORIGINAL AUTHORSHIP	i
ACKNOWLEDGEMENTS.....	ii
TABLE OF CONTENTS	iii
LIST OF FIGURES	vii
LIST OF TABLES	x
ABSTRACT	xi
Chapter 1: Introduction	1
1.1 Overview of the research.....	1
1.2 Research objectives	3
1.3 Scope of thesis.....	3
1.3.1 Areas that are addressed	3
1.3.2 Areas that are not addressed	4
1.4 Outline of this thesis.....	4
Chapter 2: Background and Literature Review.....	7
2.1 Introduction and rationale	7
2.2 Vehicle system dynamics	7
2.2.1 Vehicle vertical ride dynamics	8
2.2.2 Vehicle pitch dynamics.....	10
2.2.3 Vehicle lateral dynamics.....	14
2.3 Interconnected suspensions	21
2.3.1 Research and applications of interconnected suspension	22
2.3.2 Hydraulically interconnected suspension	26
2.4 Summary	28
Chapter 3: Vehicle with Hydraulically Interconnected Suspensions.....	30
3.1 Introduction	30
3.2 Vehicle-road vibration model.....	31
3.2.1 Vehicle suspension static model.....	31
3.2.2 Vehicle dynamic model	34
3.3 Roll-resistant hydraulically interconnected suspension	39
3.3.1 Description of the RHIS system	39

3.3.2 Static suspension stiffness properties	40
3.3.3 Dynamic modelling of RHIS	45
3.3.4 Modal Analysis of vehicle with RHIS suspension	49
3.3.5 Frequency analysis of RHIS under warp mode	52
3.4 Pitch-resistant hydraulically interconnected suspension	56
3.4.1 Description of the PHIS system.....	56
3.4.2 Static suspension properties of PHIS.....	58
3.4.3 Dynamic model of PHIS.....	61
3.4.4 Modal analysis of PHIS	63
3.4.5 Ride and pitch dynamics of the PHIS	64
3.5 Summary	67
Chapter 4: Nonlinear 3-Dimensional Full Vehicle Model.....	69
4.1 Vehicle model description.....	69
4.1.1 Model definition and assumptions.....	69
4.1.2 Coordinates and transformation.....	73
4.2 Equations of motion	74
4.2.1 Equations of vehicle translational motion	74
4.2.2 Equations of vehicle rotational motion.....	76
4.2.3 Equations of motion of wheels	78
4.2.4 Suspension strut force formulation.....	78
4.3 Nonlinear tyre model.....	80
4.3.1 Tyre model basics	80
4.3.2 Magic Formula tyre model	82
4.4. Vehicle dynamic response of fishhook steering.....	87
4.4.1 Model validation.....	87
4.4.2 The sensitivity of vehicle speed and suspension roll stiffness	89
4.5 Summary	93
Chapter 5: Roll & Pitch Independently Tuned Interconnected Suspension.....	95
5.1 Introduction	95
5.2 Static property of the RPITIS suspension system	98
5.2.1 Model description	98
5.2.2 Static stiffness property of RPITIS.....	100
5.2.3 Static damping property of RPITIS	104

5.3 Time domain analysis of the vehicle with RPITIS suspension	106
5.3.1 Dynamic model of the RPITIS suspension.....	106
5.3.2 Dynamic analysis compared with conventional suspension.....	110
5.3.3 Simulation result highlights	122
5.4 Summary	123
Chapter 6: Zero-warp Hydro-pneumatic Interconnected Suspension	125
6.1 Introduction	125
6.2 Static property of zero-warp hydro-pneumatic interconnected suspension	126
6.2.1 Model description	126
6.2.2 Static stiffness properties	128
6.2.3 Static damping properties	132
6.3 Dynamic modelling of Zero-warp hydro-pneumatic suspension	134
6.3.1 Vehicle equations.....	134
6.3.2 Fluidic equations.....	136
6.4. Model linearization and frequency analysis	139
6.4.1 Model linearization	139
6.4.2 Modal analysis	140
6.4.3 Frequency response under road warp excitation.....	142
6.5. Vehicle dynamic responses in time domain with system nonlinearity	145
6.5.1 Vehicle response under road bump input	145
6.5.2 Tyre dynamic load at warp mode	148
6.6. Summary	150
Chapter 7: Experimental Validation of RHIS at Warp Mode	151
7.1 Introduction	151
7.2 Test facility description	151
7.2.1 Testing vehicle	151
7.2.2 Four-posts multi-channel test rig	153
7.3 Testing methodology	154
7.3.1 Vehicle configurations	154
7.3.2 Testing procedure	155
7.4 Test results.....	157
7.4.1 Steady state of Axle articulation excitation	157
7.4.2 Transient response of bump articulation.....	164

7.4.3 Stochastic road responses	167
7.4.4 Comparison with theory	169
7.5 Discussion	175
7.5.1 Experimental limitations.....	175
7.5.2 Suggestions	177
7.6 Summary	177
Chapter 8: Conclusions and Recommendations.....	179
8.1 Summary of the thesis	179
8.2 Contributions.....	183
8.3 Suggestions for future work	185
Appendix: Publications.....	188
Reference	190

LIST OF FIGURES

Figure 2. 1: Rigid vehicle model.....	14
Figure 2. 2: Kinetic H2 system.	26
Figure 2. 3: FRIC suspension in racecar application.	28
Figure 3. 1: Static suspension property model.....	32
Figure 3. 2: Seven-DOF vehicle model	35
Figure 3. 3: Schematic diagram of the roll-plane RHIS system	39
Figure 3. 4: Static model of the RHIS system.....	41
Figure 3. 5: Static stiffness properties of RHIS: (a) bounce (b) roll (c) pitch (d) warp	43
Figure 3. 6: Vehicle accelerations under warp excitation: (a) C.G vertical (b) Roll	53
Figure 3. 7: Suspension deflection under warp excitation: (a) front left (b) rear right.....	54
Figure 3. 8: Tyre dynamic forces under warp excitation: (a) front left (b) rear right	54
Figure 3. 9: Schematic diagram of the PHIS system	57
Figure 3. 11: Static stiffness of PHIS (a) bounce (b) roll (c) pitch (d) warp	61
Figure 3. 12: Vehicle responses under step pitch moment: (a) pitch angle (b) pitch acceleration (c) C.G vertical displacement (d) C.G vertical acceleration.....	65
Figure 3. 13: Vehicle responses under step road bump at front axle: (a) pitch angle (b) pitch acceleration (c) C.G vertical displacement (d) C.G vertical acceleration.....	66
Figure 4. 1: 14-DOF full-vehicle model: (a) vertical representation; (b) lateral representation; (c) tyre rotational dynamics.....	71
Figure 4. 2: Suspension strut force characteristics (a) Stiffness; (b) Damping.....	80
Figure 4. 3: Tyre coordinate system.....	81
Figure 4. 4: Tyre longitudinal force at pure longitudinal slip (a) Tyre longitudinal force vs. longitudinal slip (b) Tyre longitudinal force vs. longitudinal slip and road friction	84
Figure 4. 5: Tyre lateral force at pure side slip (a) Tyre lateral force vs. side slip angle (b) Tyre lateral force vs. side slip and different road frictions	85
Figure 4. 6: Tyre friction ellipse of the combined slip condition.....	86
Figure 4. 7: Steering wheel input of fishhook maneuver	88
Figure 4. 8: Vehicle responses comparison of 14DOF and CARSIM model: (a) Trajectory (b) Vehicle velocity (c) Yaw rate (d) Roll angle.....	89

Figure 4. 9: Vehicle responses of fishhook maneuver at different vehicle speeds	90
Figure 4. 10: Vehicle responses of fishhook manoeuvre with different roll stiffness	92
Figure 5. 1: Schematic of the roll- and pitch-plane interconnected suspension	99
Figure 5. 2: Static stiffness properties of RPITIS: (a) bounce, (b) roll, (c) pitch, (d) warp	102
Figure 5. 3: Static damping properties of RPITIS: (a) bounce, (b) roll, (c) pitch, (d) warp	106
Figure 5. 4: Damper valve characteristics (a) roll damper; (b) pitch damper	107
Figure 5. 5: Steering input of fishhook maneuver	112
Figure 5. 6: Vehicle response during fishhook manoeuvre. (a) Trajectory (b) Yaw rate (c) Roll angle (d) Dynamics rollover index.....	112
Figure 5. 7: Hard braking inputs	114
Figure 5. 8: Vehicle response at hard braking (a) pitch angle; (b) pitch acceleration; (c) front tyre vertical load; (d) rear tyre vertical load.....	115
Figure 5. 9: RMS of C.G vertical accelerations under different road conditions	116
Figure 5. 10: The speed bump profile in time history.....	117
Figure 5. 11: Vehicle response over one side bump. (a) C.G vertical displacement (b) C.G acceleration (c) pitch angle (d) pitch acceleration (e) roll angle (f) roll acceleration .	118
Figure 5. 12: Tyre dynamic load over one side bump (a) front-left (b) front-right (c) rear left (d) rear right.....	119
Figure 5. 13: The road signals of warp excitation.....	120
Figure 5. 14: Roll response at warp road. (a) roll angle (b) roll acceleration	121
Figure 5. 15: The tyre load at warp road. (a) front left tyre; (b) rear right tyre	121
Figure 6. 1: Schematic diagram of the ZWHPIS suspension.....	127
Figure 6. 2: Static stiffness properties of ZWHPIS: (a) bounce, (b) roll, (c) pitch, (d) warp.....	131
Figure 6. 3: Static damping properties of ZWHPIS: (a) bounce (b) roll (c) pitch (d) warp	134
Figure 6. 4: Frequency response of tyre load at warp modes (a) front left (b) front right (c) rear right (d) rear left	144
Figure 6. 5: Speed bump signals	145
Figure 6. 6: Vehicle response at slow bump (a).....	146
Figure 6. 7: Vehicle response at fast bump.....	148
Figure 6. 8: Tyre load response at 0.2Hz warp road input.....	149

Figure 6. 9: Tyre load response at 1Hz warp road input.....	149
Figure 7. 1: RHIS installation (a) Front installation (b) Rear installation	152
Figure 7. 2: Four poster suspension test rig	152
Figure 7. 3: Suspension deflections (a) front left (b) front right (c) rear left (d) rear right	159
Figure 7. 4: Rotational velocities (a) pitch rate (b) roll rate	159
Figure 7. 5: Tyre dynamic forces (a) front left (b) front right (c) rear left (d) rear right ...	160
Figure 7. 6: Vehicle acceleration at C.G	160
Figure 7. 7: Suspension deflections	162
Figure 7. 8: Rotational velocities	162
Figure 7. 9: Tyre dynamic forces	163
Figure 7. 10: Vehicle accelerations at C.G	163
Figure 7. 11: Suspension deflections	165
Figure 7. 12: Rotational velocities	165
Figure 7. 13: Tyre dynamic forces	166
Figure 7. 14: Vehicle accelerations at C.G	166
Figure 7. 15: Road profile	167
Figure 7. 16: RMS of angular velocity	168
Figure 7. 17: RMS of vehicle C.G acceleration.....	168
Figure 7. 18: Suspension deflections	170
Figure 7. 19: Rotational velocities	170
Figure 7. 20: Tyre dynamic forces	171
Figure 7. 21: Vehicle accelerations at C.G	171
Figure 7. 22: Suspension deflections	173
Figure 7. 23: Angular velocities.....	174
Figure 7. 24: Tyre dynamic forces	174
Figure 7. 25: Vehicle accelerations at C.G	175

LIST OF TABLES

Table 3. 1: Parameters of the 7dof vehicle model.....	36
Table 3. 2: Hydraulic parameters of RHIS	39
Table 3. 3: Modal analysis of a vehicle with SD suspension.....	50
Table 3. 4: Natural frequency comparison of three configurations.	51
Table 3. 5: Hydraulic parameters of PHIS	57
Table 3. 6: Modal analysis of the vehicle with PHIS suspension.	64
 Table 4. 1: Parameters and values of the 14-DOF vehicle dynamic model.....	 72
 Table 5. 1: Parameters of the RPITIS suspension.....	 99
 Table 6. 1: Fluidic parameters of the ZWHPIS	 128
Table 6. 2: Natural frequency comparison of vehicle motion modes	142
 Table 7. 1: Four poster test rig specification.....	 153
Table 7. 2: Specifications of sensors.....	153
Table 7. 3: Summary of lab tests.....	155

ABSTRACT

Conventional passive suspension design often requires a trade-off between ride and handling performance. The unique mode-decoupling property of interconnected suspension presents great potential to improve the compromise between ride and handling. In this thesis, some variants of hydraulically interconnected suspension are presented such as Roll-resistant Hydraulically Interconnected Suspension (RHIS), Pitch-resistant Hydraulically Interconnected Suspension (PHIS), Roll & Pitch Independently Tuned Interconnected Suspension (RPITIS) and Zero Warp Hydro-Pneumatic Interconnected Suspension (ZWHPIS) in order to fully explore the benefits of mode-decoupling and demonstrate the design flexibility of interconnected suspension.

The static property studies of the proposed interconnected suspensions are performed using the fixed vehicle chassis model integrated with the static fluidic model. The characteristics of suspension stiffness and damping are compared with the conventional suspension. Results illustrate that desired mode properties are achieved with the proposed interconnected suspensions. The roll stiffness and damping are favourably increased by the RHIS while the bounce, pitch and warp mode performance are almost unaffected. The pitch stiffness and damping are improved by the PHIS while the influences on the other suspension modes are neutral. The roll and pitch stiffness and damping can be independently tuned by the proposed RPITIS suspension to improve vehicle handling performance while the ride and road holding performance can be further improved with reduced suspension spring stiffness. The off-road vehicle requires suspension warp that is as soft as possible so as to improve the road holding performance. The static property of the ZWHPIS system shows zero warp stiffness is achieved without reducing the ride and anti-roll performance.

Investigations of the ride and handling dynamic performance of the vehicle with various proposed interconnected suspensions are undertaken with a multi-degree rigid body vehicle model coupled with the fluidic model both in the frequency domain and time domain. The linearized models are used in the frequency domain analysis assuming small vibration around the equilibrium position. Modal analyses of the proposed suspension systems are conducted and the results are compared with the conventional suspension. It proves that the decoupled suspension modal properties can be realized favorably through the selected interconnected suspensions. The trends of the ride and handling performances of the vehicle equipped with the proposed suspensions are examined by the frequency response analysis under road inputs or force moments induced by vehicle accelerations. The time domain studies are also performed using the 14 degree-of-freedom nonlinear vehicle model coupled with the nonlinear fluidic model so that more accurate vehicle response can be predicted under complex road conditions and extreme driver maneuvers. The dynamic vehicle responses are compared with a reference vehicle equipped with conventional suspension. The promising improvements both for ride comfort and handling/stability are demonstrated in the simulation results.

The experimental verification of the theoretical modelling of a vehicle with RHIS is performed by bench testing in our suspension lab. Generally, the testing results agree well with the simulation results, especially the tyre dynamic loads under warp mode excitation. The un-modelled effects are discussed and further works are suggested.

Chapter 1: Introduction

1.1 Overview of the research

Vehicle system dynamics including vertical, longitudinal and lateral dynamics is the study of vehicle behavior under various maneuvers and road conditions. The maneuvers includes acceleration, braking, steering and cruising; the roads could be a paved motorway or unpaved rough terrain. The dynamic analysis provides valuable insights into vehicle system design and plays a key role in enhancement of vehicle performance.

Vehicle suspension is the system connecting the vehicle body and its wheels and consists of resilient and damping elements. It is considered the critical system in vehicle dynamics and directly contributes to the ride, handling and safety of the road vehicle. Many types of suspension have been invented, such as solid axle suspension, and independent suspension. The resilient elements take many forms including leaf spring, torsional bar, coil spring, hydro-pneumatic spring and air springs. Hydraulic shock absorber is the most commonly used damping media to provide energy dissipation.

Good handling performance and superior ride comfort are mandatory in the highly competitive automobile market. However a well-known compromise between ride comfort and handling stability exists in the conventional suspension design. Active or semi-active suspensions have been extensively researched and developed in the last three decades and these display a promising performance in terms of breaking the ride-handling compromise. However, broad adoption of controlled suspension has not occurred because of its high overall cost and energy consumption.

Passive interconnected suspension has attracted considerable research attention owing to its unique property of mode decoupling. The interconnections of the individual wheel stations can easily decouple suspension modes and afford the designer great freedom to optimise the mode-based vehicle performance with a greatly reduced compromise between ride comfort and handling.

However, there are gaps between theoretical knowledge and practice application. A few interconnected suspensions have been invented and successfully commercialised in the industry. Some basic types of hydraulic interconnection have been theoretically analysed in the literature applying a simplified linear model [1, 2]. However, due to the flexibility of fluidic connection arrangements, there are many forms of interconnection which have not been explored. Moreover, a complex nonlinear vehicle and fluidic model and a comprehensive dynamic analysis of the interconnected suspension are required to accurately assess performance. The vehicle vibration modes include bounce, roll, pitch, and warp [2]. The dynamics of bounce, roll and pitch are extensively studied, but the dynamics of vehicle warp mode have received little attention. Further, just how the vehicle dynamic behaviour is affected by the warp mode properties remains unclear [3].

This thesis will comprehensively study the ride and handling of vehicles equipped with various interconnected suspensions through the means of the linear vehicle vibration model in the frequency domain and the complex nonlinear full vehicle model in the time domain. The mode decoupling property of hydraulically interconnected suspension will be demonstrated, and two novel variants of interconnected suspensions will be presented and theoretically analysed in terms of ride and handling improvements.

1.2 Research objectives

This thesis is focused on an investigation into the ride and handling of vehicles with various mode-decoupled interconnected suspensions. The main objectives of this research are:

1. Theoretical analysis of interconnected suspension with a focus on the mode decoupling property and warp mode performance.
2. To develop a generalised full vehicle model with multiple nonlinearities and investigate vehicle responses under different maneuvers and road conditions for accurate assessment of vehicle system dynamics.
3. To investigate the ride and handling of vehicles with roll and pitch independently tuned interconnected suspension and demonstrate the capability of mode-based suspension tuning that greatly improves the compromise between ride and handling.
4. To present a novel suspension system with zero-warp suspension stiffness and investigate the off-road performance of vehicles with zero-warp hydro-pneumatic interconnected suspension.
5. Experimental verification of the system model of hydraulically interconnected suspension with a focus on the warp model stiffness and tyre dynamic load response.

1.3 Scope of thesis

1.3.1 Areas that are addressed

The following areas are within the scope of this thesis:

- Linear lumped mass vertical dynamics vehicle modelling.

- Nonlinear 3 dimensional full vehicle modelling with nonlinear tyres.
- Modelling of different interconnected suspension configurations and comparison with conventional suspension.
- Modal analysis and frequency response analysis to evaluate vehicle dynamic performances.
- Numerical simulation in time domain to analyse and compare the performance of different suspension system configurations.
- Experimental validation with direct tyre force measurement.

1.3.2 Areas that are not addressed

The following areas are beyond the scope of this thesis:

- Derivation of suspension model of multi-axle vehicle or rail vehicle on track.
- Dynamics and control of the semi-active or active suspension system.
- Automotive aerodynamic drag and lift.
- Suspension geometry, kinematics and compliance.
- The high order hydraulic model considering fluid compressibility and hose flexibility.
- Individual fluid component experimental or detailed modelling
- High frequency fluid-structure interaction

1.4 Outline of this thesis

This thesis consists of eight chapters, organised as follows:

Chapter 2: this chapter provides some essential background information on the vehicle system dynamics and state-of-the-art development of advanced suspensions. The vehicle system dynamics are reviewed focusing on 4 aspects: the ride comfort, pitch-

plane longitudinal dynamics, roll-plane lateral dynamics and vehicle handling stability. The literature of interconnected suspensions is also extensively reviewed. The gaps in the current knowledge are identified and a synopsis of possible solutions is presented.

Chapter 3: the vehicle vibration model with two different configurations of hydraulically interconnected suspension is developed and the suspension properties and the performance of ride quality and directional stability are studied with a focus on the frequency domain. The results illustrate the mode-decoupling property of the hydraulically interconnected suspension.

Chapter 4: A generalised three dimensional nonlinear full vehicle model is established in this chapter for accurate assessment of vehicle system dynamics. The equations of motion are developed with consideration of the suspension element nonlinearity and tyre nonlinearity. The vehicle dynamic responses under extreme maneuvers are presented and the results are discussed.

Chapter 5: the roll and pitch independently tuned interconnected suspension is proposed and the vehicle system equations are derived in the frequency domain and time domain, respectively. The ride and handling performance of the vehicle with the proposed suspension are comprehensively evaluated both in the frequency domain and time domain.

Chapter 6: based on the model decoupling properties of interconnected suspension, a new hydro-pneumatic interconnected suspension is proposed to realise the zero warp suspension stiffness. The vehicle with the proposed suspension system is modelled and the ride and handling are evaluated in this chapter.

Chapter 7: experimental verification of the mathematic model of the roll-resistant hydraulically interconnected suspension is presented in this chapter. The previously established 4-poster test rig is modified to enable direct measurement of vehicle tyre loads. The experimental results are compared with the numerical results and these are shown to be in good agreement.

Chapter 8: in this chapter, the conclusions are drawn, the contributions of this thesis are summarised and suggestions are given for future work.

Chapter 2: Background and Literature Review

2.1 Introduction and rationale

Vehicle dynamic analysis is essential to evaluate the performance of the vehicle. Vehicle suspension system directly contributes to the ride comfort, handling and safety, and becomes more and more important when the vehicle speed increases. Suspension design has been extensively explored during the past few decades and this has considerably contributed to the improvement of ride, handling and safety for road vehicles.

This chapter presents the state-of-the-art survey of the available literature on road vehicle system dynamics and control focusing on the motion modes specific dynamics. The developments of advanced suspensions including interconnected suspension are reviewed. The gaps in the current knowledge are identified and possible solutions are summarised. Lastly, the methodology employed later in this thesis is outlined.

2.2 Vehicle system dynamics

Along with the rapid development of the automotive industry, the demands on ride comfort, handling, and safety of the vehicle have grown exponentially. The vehicle system dynamics plays a key role in the process of vehicle system development. Generally, a vehicle's dynamical properties are related to three essential motions: longitudinal motion (driving and braking), lateral motion (guidance and steering), and vertical motion (riding and shock absorption). The vehicle system dynamics are

reviewed in relation to three aspects: the ride comfort in the vertical dynamics, longitudinal stability during accelerating and braking, and lateral stability under steering.

2.2.1 Vehicle vertical ride dynamics

The important factor in suspension design is the ride performance of the road vehicle. Vehicle vibration excited by road roughness can lead to fatigue or injury of the driver and passengers. Vibration can also lead to damage of the vehicle and the payload. A few surveys of publications on vehicle dynamics and suspension design are made in [3-10]. Heavy truck ride is reviewed in [4, 7]. The fundamental issues in suspension design for heavy truck vehicles are discussed by Cole in [10]. Crolla [9] reviews the contributions of vehicle dynamics theory to practical vehicle design with a focus on the actively controlled components. Cao, et al [3] provides a comprehensive review of road vehicle suspension design, dynamics and control from an editor's perspective. These articles provide a thorough review of road vehicle dynamics and the issues associated with practical implementation.

Despite extensive use over many years, the two-mass quarter-car model continues to be a useful tool for understanding the bounce mode vibration behaviour of vehicle suspension. The linear quarter-vehicle model is used by many investigators to compare the performance of passive and controlled systems [11-13]. The bounce mode natural frequency is critical to ride comfort and well-being. Rowell [14] suggests that the suspension bounce frequency should be between 1.5 to 2.3Hz based on inquiries and experiments. Nowadays, the suspension of the average family sedan will have a natural frequency of about 1-1.5 Hz while a high performance sports car will have a stiffer suspension with a natural frequency of about 2-2.5 Hz. Although the ride comfort is subjectively assessed, the ISO standard [15] and other equivalent standards provide a

guideline for objective evaluation of human exposure to whole-body vibration. Paddan and Griffin [16] evaluated more than 100 vehicles experimentally and concluded that severity of whole-body vibration can be lessened by improvements in suspension and seat dynamics.

Unsprung weight includes the mass of the tyres, brakes, suspension linkages and other components that move with the wheels. The rest of the mass is on the vehicle side and comprises the vehicle sprung mass. The ratio between the sprung mass and unsprung mass is one of the most important factors of vehicle ride and handling characteristics. The unsprung weight represents a significant portion of the total weight of the vehicle. It reacts directly to roadway irregularities at highway speeds and can generate significant vertical acceleration forces. These forces degrade the ride and also have a detrimental effect on vehicle handling. Gillespie [17] points out that weight reduction of unsprung mass is important. It particularly improves the acceleration level in the 4-8Hz frequency range which is more sensitive to the human head and neck. Light weight unsprung mass not only improves the ride but also benefits the tyre-road contact.

Before modern optimisation methods were introduced, design engineers used to follow the iterative process to find the 'best' parameters of suspension. This was expensive and time-consuming. With the development of computational technology and optimisation theory, multi-objective optimization techniques have been employed in the literature to attain the best compromise between ride quality and road holding [18-23]. RMS of weighted acceleration, wheel dynamics load and suspension dynamic deflections are normally used as evaluation indices to assess the ride comfort performance of the vehicle subject to random excitation from road roughness. The optimisations of the kinetics of suspension linkages are also investigated in [21, 24], and the results show

that compared with suspension stiffness and damping coefficients or inertial property parameters, the geometric parameters also have a significant effect on the ride quality.

Controlled suspension based on the quarter-car model has attracted extensive attention from researchers and industry [9, 11, 25-31]. Semi-active suspension is able to change the suspension damping properties through adjustable dampers. Magneto-rheological damper [28], electro-rheological damper [29] and the control characteristics in the vehicle suspension application are investigated. The ride performance potential of active suspension systems are discussed in [9, 11]. The optimal control strategies are broadly researched in [12, 13, 31-33] such as LQR/LQG, H₂, and H infinity based on the linear model and fuzzy control, and sliding mode control with system nonlinearity. The preview controls are also studied in [20, 31, 34] to improve the ride and reduce the power requirements by utilising previewed road information.

The controlled suspension shows great potential for improved ride and handling performance. However, most modern road vehicles are still equipped with the passive suspension system. The drawbacks of the active suspension are obvious: significantly increased cost, unreliability, high power consumption and inherent complexity.

2.2.2 Vehicle pitch dynamics

As the quarter car model can only predict the vertical bounce dynamic response, a half car pitch plane model is necessary for investigating detailed ride characteristics when pitch mode dynamic analysis is included. From the ride comfort perspective, pitching motion is considered objectionable and annoying [17, 35]. The driver's perception of the path preview is significantly compromised in the presence of excessive pitch motions. Pitch motion can be induced by acceleration and braking, so the pitch mode

should be moderate stiff to minimise the pitching response of the vehicle body to excitations arising from urgent maneuvers.

Pitch and bounce motions are greatly coupled under road excitation. A vehicle's rear wheels are assumed to follow the same road profiles as the front wheels. Since 1930, Maurice Olley, the founder of modern vehicle dynamics and one of the world's foremost experts in ride and handling, has provided many guidelines for ride and handling which are still useful for today's vehicle. Based on the experimental observations, he suggests a softer front axle suspension than the rear suspension in order to obtain a 'flat ride' [35]. This effect is examined more theoretically in papers [36, 37]. The frequency responses of the bounce and pitch motions of the car body on sinusoidal terrain are used to show that the Olley's tuning, involves interference between the responses to the front and rear axle inputs. At higher vehicle speeds, Olley-tuning brings advantages in pitch suppression with very few disadvantages in terms of body acceleration. However at lower speeds, pitch tuning increases vertical acceleration and the suspension stiffness is undesirable for attitude control. The results are useful to guide new suspension designs, especially for rear-engine rear drive vehicles. Cao, et al [38] also attempts to correlate wheel-base filtering and characterisation of random road profiles and concludes that wheelbase filtering has a positive effect on the vehicle vertical ride with a negligible compromise in terms of suspension travel and dynamic tire deflection. The simulation results show that a quarter-car model will overestimate the vertical acceleration responses of the car body when compared with the pitch-plane model.

The suspension design for pitch suppression involves complex challenges. The front-rear suspension tuning with soft suspension may help on the road induced pitch motion but not with the squat and dive during rapid acceleration and braking. The suspension

geometry also plays an important role in the pitch plane dynamics. The influence of anti-dive and anti-squat geometry in combined vehicle bounce and pitch dynamics is investigated by Sharp [39]. It suggests that anti-pitch suspension geometry can effectively reduce the pitch rotating arm of moment which is of benefit for pitch attitude control but it also tends to adversely affect the vehicle handling. The tuning of a pitch-plane model of a passenger car with a 'coupled' suspension system is investigated by Odhams and Cebon [40] and compared to that of a conventional suspension system. Optimum tuning of the coupled system is found to be at lower pitch stiffness, but there is greater pitch damping than that of a popular saloon car. The Olley suspension tuning criterion is found to represent an optimal conventional suspension stiffness tuning for dynamic tyre force minimisation, but not for driver chest acceleration minimisation. It claims that pitch attitude caused by acceleration or braking can be reduced by a stiffer suspension spring.

The conflicting requirements on the high frequency pitch ride and low frequency vehicle body attitude control can be partially alleviated using passive nonlinear springs such as the pneumatic spring or hydro-pneumatic struts which yield lower/higher stiffness at lower/higher amplitude, respectively. Twin-gas chamber strut suspension design is proposed by Cao, et al [41] and the claim is made that it can realise a desirable nonlinear pitch-mode stiffness property in a passive manner. A recent study [42] has explored the pitch dynamics and front-rear suspension tuning of two-axle heavy vehicles. Based on a generalised pitch-plane model of a two-axle heavy vehicle integrating either unconnected or coupled suspension, three dimensionless measures of suspension properties are defined and analysed. These are the pitch margin, pitch stiffness ratio, and the coupled pitch stiffness ratio for different unconnected suspension tunings and load conditions. Fundamental relationships between the vehicle responses

and the proposed suspension measures are established and based on these some basic suspension tuning rules for heavy vehicles with unconnected suspensions are also proposed.

A few recent studies [43, 44] have explored the potential benefits of pitch interconnected suspension systems with higher pitch stiffness. The performance benefits of the pitch-connected hydro-pneumatic suspensions are shown to enhance the pitch attitude control, suspension travel, straight-line braking performance, and vertical ride in [43]. In [44], the hydraulically interconnected suspension system is proposed for the implementation of a resistance control for the pitch and bounce modes of tri-axle heavy trucks. The transfer matrix method is used to evaluate the impedance matrix of the hydraulic subsystem consisting of models of fluid pipes, damper valves, accumulators, and three-way junctions. The modal analysis method is employed to perform the vibration analysis between the trucks with the conventional suspension and the proposed interconnected system. The obtained results show the effectiveness of the proposed system in terms of reducing the pitch motion of sprung mass and simultaneously maintaining the ride comfort. The pitch stiffness is increased while the bounce stiffness is slightly softened. The peak values of sprung mass and wheel hop motions are greatly reduced, and the vibration decay rate of sprung mass is also significantly increased.

The advantage of controlled suspension also has the potential in improving vehicle dynamics in the pitch plane. An active control structure is presented in [45] to allow the road and load transmission paths to be optimised independently. The results demonstrate good anti-dive and anti-squat behaviour together with a soft ride in response to road disturbances. Attitude and vibration control by semi-active suspension is discussed in [27]. The paper introduces a newly developed semi-active anti-roll/pitch

system. The attitude control using semi-actively generated compensation forces prevents the car from rolling in curves and pitching during braking or accelerating. The strength of the system is the small energy consumption. The author claims that the performance of the combination of both attitude and vibration control can compete with a fully active suspension system.

2.2.3 Vehicle lateral dynamics

Rollover accidents are the most dangerous events among all possible accidents. According to the National Highway Traffic Safety Administration of USA [46], although only 8% of light vehicles in crashes rollover, 21% of seriously injured occupants and 31% of occupant fatalities are involved in rollovers. Rollover is defined as any maneuvers that may roll the vehicle more than 90 degrees along the longitudinal axis and make the vehicle body contact the ground. Rollover accidents may be caused by multiple factors, and can be divided into off-road and on-road rollover. On-road rollover can be further divided into tripped and untripped rollover. Rollover crash data show that approximately two-thirds of on-road rollovers are untripped [47].

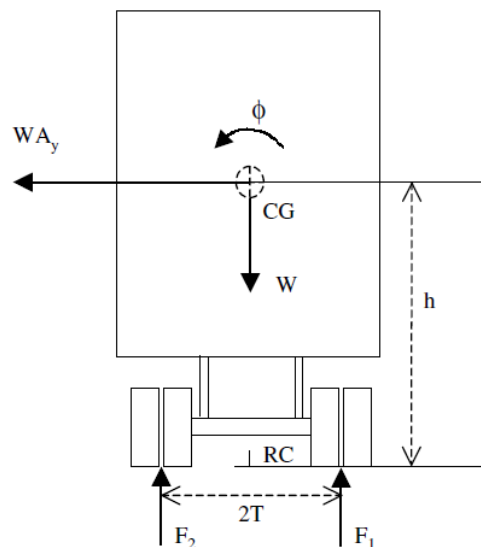


Figure 2. 1: Rigid vehicle model

Roll plane vehicle model and dynamic analysis have been used for investigating the coupled ride and roll-stability characteristics of road vehicles and suspension tuning. Ervin [48] examines the static roll performance of the completely rigid vehicle shown in Figure 2.1.

As the vehicle negotiates a turn, a lateral force WA_y is developed and applied to the center of gravity (C.G.) of the vehicle. The equation of motion can be written as:

$$WA_y h = (F_2 - F_1)T - Wh\phi \quad (2.1)$$

The three terms in the equation are referred to as: the primary overturning moment, the restoring moment and the lateral displacement moment. The rollover will occur when the left side of equation (2.1) is greater than right side. If the $F_1=0$, $F_2=W$, $\phi=0$, it yields the static roll threshold of a rigid vehicle: $A_y=T/h$ which is also called static stability factor (SSF). It provides a useful starting point for the more complex roll models. When the suspension compliance (non-zero roll angle) is considered, the lateral displacement moment reduces the roll threshold as: $A_y = T/h - \phi_T$, where ϕ_T is the maximum angle, the vehicle may roll through until one side of the vehicle lifts off the ground. The SSF of a fully loaded heavy vehicle usually lies below 0.5g, which indicates that a heavy vehicle can rollover before reaching the tyre-road friction limit on dry roads. Ervin[48] has investigated the influence of size and weight variations on the roll stability of heavy vehicles. Roll stability can be improved by increasing the width allowance of vehicles or reducing C.G height. An approximate 3% increase in the roll stability limit can be achieved with only 1% increase in both track width and transverse spring spacing. An increase in the payload CG height yields considerable reduction in the roll stability limit. For such vehicles, even a small improvement in the rollover threshold can significantly improve the vehicle roll stability and reduce the likelihood of

rollover accidents. The weight and dimensions of commercial vehicles, however, are commonly governed by the road regulations.

A more detailed steady-state roll model considering the effects of suspension and tyre is studied by Hac [49]. The model includes the effects of vehicle C.G lateral movement, effects of tyre lateral compliance, effects of suspension jacking forces, effects of changes in track width due to suspension kinematics, gyroscopic forces and effects of dynamic overshoot in the roll angle. Design guidelines for suspension parameters to improve rollover resistance are discussed. Increasing suspension roll stiffness and damping can improve the roll stability of vehicles. The results of analysis and simulations indicate that suspension tuning can change the character of vehicle response from unstable to stable in extreme dynamic rollover tests without changing the SSF.

Many dynamic rollover indexes are proposed by researchers [50-52]. The rollover critical factor (RCF) is presented in [50] to investigate the untripped rollover of light vehicles in the modified fishhook and the sine maneuvers. A 9 degree-of-freedom (DOF) vehicle model is developed to include the roll, yaw, pitch, and bounce modes and passive independent suspensions. RCF is constructed based on the static stability factor (SSF) and taking into account the influence of other key dynamic factors. In general, the larger the RCF, the more kinetically stable is the vehicle. A vehicle becomes unstable when its RCF is less than zero. Simulation results show that a vehicle with certain parameters will rollover during the fishhook maneuver because of roll instability; however, the vehicle with increased suspension stiffness, which does not rollover during the fishhook maneuver, may exceed its rollover threshold because of yaw instability during the sine maneuver. It has been found that the proposed RCF well quantifies the rollover resistance capability of a vehicle for the two specified

manoeuvres. The nominalized RCF is used in [51] to study the effect of vertical and lateral coupling between the tyre and road on vehicle rollover. The RCF is compared with other rollover dynamic indexes such as the lateral tyre load transfer rate and the comparison results show RCF is superior in the rollover analysis because it is more sensitive to the rollover and has a higher safety threshold. In addition, it can express more effects on different factors, such as the oscillation of roll acceleration, and the movement of both roll inertia and vehicle mass. The coupling interactions between vehicle anti-rollover and lateral stability, as well as the effect of road excitation, are taken into account on the vehicle rollover analysis. Tyres with high adhesion capacity imply that the vehicle possesses a high performance ability to keep driving direction, whereas the rollover risk of such a vehicle increases due to the greater lateral force that the tyres can provide. Furthermore, the excitation from road roughness not only diminishes the adhesive condition of the tyres, but also lessens the rollover stability in some extreme cases.

The flexible nature of the tractor frame tends to isolate the driver from the roll motions of the trailer. The compliance of a vehicle's structural frame, suspension, and tyres can also contribute to the rollover process. The effect of structural or articulation compliance may be small, but the combined effect of all compliance on the vehicle dynamics roll stability can be significant. A heavily loaded long vehicle or tractor-trailer truck can exhibit a roll-mode natural frequency as low as 0.5Hz, which is in the range of excitation frequencies rising from emergency type steering manoeuvres. The roll damping becomes important for controlling the roll resonant responses during such emergency manoeuvres. Rearward amplification is a measure of the severity of the rearmost trailer's 'reaction' to inputs from the tractor [53]. It is a frequency dependent measure and is defined as the ratio of the peak lateral acceleration (positive or negative)

of the CG of the rearmost trailer to the amplitude of the tractor's response at a controlled lateral acceleration of 0.15 g measured at the centre of the front axle. The rearward amplification measure may be applied to single or multiple trailer configurations, and it is recommended that it does not exceed 2.2 degree/g.

Conventional passive vehicle suspension system design has to make a compromise between ride comfort and roll stability. The anti-roll bar (ARB) (or sway bar) with softer coil spring suspension to help reduce the body roll of a vehicle during fast cornering has been widely employed from the 1950s. The passive mechanical interconnections (e.g. anti-roll bars) have some inherent limitations in terms of achieving a good compromise. The use of ARB tends to add mass and potentially degrade vehicle ride quality [54]. Further, the use of very stiff anti-roll bars which make the static roll threshold closer to SSF, may be impractical due to the reduced roll mode damping and the resulting increase in the dynamic roll responses under large amplitude and high frequency excitations [55]. Anti-roll bars also tend to reduce the suspension flexibility and increased tyre load transfer on uneven surfaces. The experiment in [56] compares the anti-roll bars with hydraulically interconnected suspension during warp excitation, and shows that anti-roll bar increases the tyre dynamic vertical load 50% more than that of the non-ARB vehicle. Off-road vehicles are subject to large input road motion and appreciable lateral forces, making anti-roll bars undesirable.

Unlike mechanical anti-roll bars that are heavy and do not offer additional roll damping, roll-resistant fluidic interconnected suspension can improve anti-roll properties while maintaining good ride. The hydro-pneumatic suspension systems have been employed in heavy military vehicles for nearly half a century and hold the most significant potential for commercial vehicles. A concept in interconnected pneumatic suspension was described by Lovins and Cramer [57]. The proposed suspension system consists of

four pneumatic and electromagnetic actuators that are interconnected in the roll plane to provide improved roll stiffness. Concepts in roll-interconnected hydro-pneumatic suspensions with hydraulic and pneumatic couplings are developed and analysed for enhancement of anti-roll properties of heavy vehicles in [55]. The roll properties of fluidically connected suspensions are compared with those of unconnected suspensions with and without anti-roll bar, and dynamic responses of a heavy vehicle with different suspensions are investigated under excitations arising from road roughness and directional maneuvers. The results indicate that both interconnected suspensions can considerably improve roll stiffness without affecting vertical ride, while hydraulic interconnections can further enhance the roll mode damping properties.

Active roll control is known to offer substantial improvements in ride and handling performance over the most sophisticated passive suspension systems. The design, development, commissioning and experimental evaluation of a roll control suspension based on active anti-roll bar actuation is reported in [58]. The prototype vehicle demonstrates excellent steady state and dynamic roll cancellation within the lateral acceleration range of 0.5g. Subjective assessments of the system confirm the benefits of a level ride together with the added benefit accrued from the elimination of roll dynamics. Vehicles with Active anti-roll bars in [59] have been tested both in smooth road and rough road conditions, and it is reported that the off-road vehicle handling performance displays significant improvement without sacrificing ride comfort.

Achievable roll stability of heavy road vehicles has been investigated by Sampson & Cebon [60]. Their research puts forward a general purpose numerical model which is suitable for simulating the roll-yaw behaviour of torsionally flexible heavy goods vehicles with an arbitrary arrangement of vehicle units. A controllability analysis is performed to examine the fundamental limitations in achievable roll stability of heavy

vehicles with active roll control systems. The results show that it is not possible to control simultaneously and independently all axle load transfers and body roll angles. The best achievable control objective for maximizing roll stability is shown to be setting the normalised load transfers at all critical axles to equal, while taking the largest inward suspension roll angle to the maximum allowable angle. The results of a simulation of a tractor-semitrailer vehicle with a full-state feedback active roll control system are presented. These show that the roll stability of the vehicle can be increased by 30% to 40% for steady state and transient manoeuvres and that the handling performance improves significantly.

In order to cope with the complicated operation conditions and to improve vehicle safety and ride comfort, various active control systems (such as ABS, 4WS, ESP and semi-active/active suspensions, etc.) were equipped in vehicles one after another since the late 1970s. Their impacts on vehicle dynamics can be usefully separated into three directions, i.e. lateral, longitudinal and vertical. The biggest challenge is in the whole chassis integration of these sub-systems to avoid their interventions and thus to improve the overall vehicle dynamics performance. The research on integrated vehicle dynamics control has become a focus and attracted much attention. A state-of-the-art survey of integrated vehicle dynamics control is conducted in [61]. The roadmap and methodologies of integrated vehicle dynamics control are reviewed, followed by the control strategies of coordination between subsystems. Global integrated control of vehicle suspension and chassis key subsystems are presented in [62]. The effect of a controllable suspension on lateral performance improvement can be observed clearly. The results prove that the global integrated control can significantly improve ride comfort as well as vehicle stability.

The development of green or low-carbon vehicles and research and development on novel powertrains, often based on electric or hybrid technology, has dominated automotive engineering around the world for the first two decades of the twenty-first century. As new powertrains have started to become commercially available, their effects on vehicle dynamic performance have become increasingly important. A recent paper [63] focuses on the integration of new electrified powertrains with vehicle dynamics and control systems. The integration effects are discussed in terms of three generic aspects of vehicle motions, namely roll-plane, pitch-plane and yaw-plane, which are, however, strongly coupled. The authors indicate that the hybrid and electric vehicle powertrain requirements pose additional challenges for suspension design, besides the suspension package, to maintain currently accepted levels of ride, handling and stability performance.

2.3 Interconnected suspensions

The design of passive vehicle suspension constitutes a compromise, since the body-wheel motion-modes of the two-axle vehicle do not share the same preference with reference to suspension stiffness and damping. Vehicle body-wheel motion-modes refer to the relative motions between the body and wheels, and can be sub-classified into several distinct modes through three characteristic features: frequency; moving phase; and damping ratio. For a two-axle four-wheel vehicle, there are seven body-wheel motion-modes, four of which significantly affect vehicle safety and handling performance, namely bounce, roll, pitch, and warp (or axle articulation). Bounce, roll, and pitch are body-dominated motion-modes, whereas warp represents a wheel-dominated motion-mode. For instance, a soft bounce motion-mode is desirable for ride comfort, whilst stiff roll and pitch motion-modes are beneficial for inhibiting vehicle

attitude during steering, braking, and acceleration. Conversely, the warp motion-mode should be as soft as possible in order to enhance vehicle road-holding performance on rough roads.

An interconnected suspension system is one in which a displacement at one wheel station can produce forces at other wheel stations [2]. The two- or four-wheel interconnection between the spring and/or damper at each wheel station is generally realised through either mechanical or hydraulic means. The most commonly claimed advantage of interconnecting wheels is that the suspension designer is afforded more control over the stiffness and damping of each suspension mode, instead of being entirely reliant upon single-wheel stiffness and damping. Interconnected suspensions in a full car level have the theoretical potential to uncouple suspension modes, and can independently tune the stiffness/damping in each of these modes. A comprehensive survey on recent suspension development is presented with a focus on interconnected suspension [3] and a survey of passive interconnected suspension has been carried out in [64].

2.3.1 Research and applications of interconnected suspension

The anti-roll bar system which connects the left and right wheels presents a good example of a mechanically interconnected suspension system and has been widely adopted as the standard configuration for increasing roll stiffness in road vehicles. The first widespread use of suspension interconnections in the automotive industry were pitch-plane arrangements which were realised mechanically on the Citroën 2CV in 1949. The anti-synchronous interconnections served to improve ride performance by softening the pitch and articulation modes relative to the bounce and roll modes. Mechanically interconnected full car suspensions have been developed and investigated in [65] which

may serve to decouple the different suspension modes in order to provide a more favourable compromise between the ride and handling requirements. However, their designs are complex and the added weights are considerable. Besides, they are difficult to tune to adapt to various road and operating conditions.

The fluidic interconnection can be realised through hydraulic fluids, pneumatic fluids, or a combination of those two. Full-vehicle fluidically interconnected suspension systems have been investigated on the topics of pneumatically interconnected suspension [66-68], hydro-pneumatic suspensions [43, 55, 69-72], and hydraulically interconnected suspension [1, 73, 74]. Various fluidically interconnected suspensions are developed for different applications.

Pneumatically interconnected suspension associated with the air-spring has also received much attention. Air-springs have been used for vehicle suspensions over the last 40 years. They are mostly used as independent suspensions. Bhawe [66] has presented a model of a vehicle where the front and the rear springs are connected by a capillary tube. A two-degrees-of-freedom model having motion in bounce and pitch mode is used with the model of pneumatic connections. Road inputs to the front and rear axles are assumed to be identical except for a phase difference between them. The results show that the vehicle body vibration excited by the road irregularities can be suppressed by the interconnected air-spring suspension. Kat and Schalk [67] present the mathematical modelling of the spring force of three interconnected rolling diaphragm type air springs used on a 40-ton tri-axle semi-trailer. The aim of the air spring model is to obtain a validated mathematical model that can be used in full vehicle multi-body dynamic simulations. The model considers the flow effects in the pipes connecting the three air springs as well as the mass transfer between them. Comparisons with experimental results show that the proposed mathematical model of the

interconnected air springs is indeed able to accurately predict the pressures and forces of the air springs. A research project is described in [68] which examines the use of an adaptive interlinked air suspension system to improve driving comfort. Tests were carried out using a complete rear axle system consisting of two air spring modules and modular pipe system. Both the experimental and simulated results show a significant impact on body roll and vertical seat rail acceleration. Accordingly, the conflict between the ride comfort and driving safety of the passenger car can be mitigated.

The interconnection can also be realised through hydro-pneumatic means. Moulton's Hydrolastic and Hydragas systems have been studied widely in the 1950s, 60s and 70s and equipped in many cars produced by British car maker BMC. These anti-synchronous interconnections are similar to the Citroen 2CV but interlinked by hydraulic pipes instead of mechanical springs. Experimental studies [69] showed that the Hydragas system was generally successful in achieving its objectives, with consistently improved ride performance over 'conventional' suspensions at frequencies less than 15 Hz. The roll control system of the interconnected Hydragas suspension are presented by Rosam and Darling [70]. A sealed low bandwidth active roll control suspension has been proposed based on the existing interconnected Hydragas system. Using computer simulation, the system performance is predicted and compared with experimental measurements. It is shown that roll during maneuver can be reduced or eliminated using a minimum of hydraulic components with only moderate power consumption and cost.

Cao etc. [43, 55, 72, 75] investigated the dynamics of interconnected hydro-pneumatic suspensions at a full car level, particularly for heavy vehicle applications. The fluidic coupling are realised through hydro-pneumatic struts, which have a compact design and are claimed to have a larger effective working area than normal hydraulic cylinders. The

struts provide considerable flexibility for various interconnection configurations among the hydraulic and pneumatic chambers, either hydraulically or pneumatically. The passive X-coupled hydro-pneumatic suspension are proposed in [72]. Layouts of various interconnected suspension configurations are illustrated based on two novel hydro-pneumatic suspension strut designs. A vehicle property index is proposed to permit a preliminary evaluation of different interconnected suspension configurations using qualitative scaling of the bounce-, roll-, pitch- and warp-mode stiffness properties. Analytical formulations for the properties of unconnected and three selected X-coupled suspension configurations are derived, and simulation results are obtained to illustrate their relative stiffness and damping properties in the bounce, roll, pitch and warp modes. The results demonstrate that a full-vehicle interconnected hydro-pneumatic suspension can provide enhanced roll- and pitch-mode stiffness and damping, while retaining the soft bounce- and warp-mode properties. The dynamic responses of a vehicle equipped with different configurations of fluidically coupled hydro-pneumatic suspension systems are investigated in [75]. A generalised 14 degree-of-freedom nonlinear vehicle model is developed and validated to evaluate the vehicle ride and handling dynamic responses and suspension anti-roll and anti-pitch characteristics under various road excitations and steering/braking maneuvers. The dynamic responses of the vehicle model with the coupled suspension are compared with those of the unconnected suspensions to demonstrate the performance potential of the fluidic couplings. The results suggest that the full-vehicle-coupled hydro-pneumatic suspension can offer considerable potential in terms of realising enhanced ride and handling performance, as well as improved anti-roll and anti-pitch properties in a very flexible and energy-saving manner. However, the X-coupled suspension cannot decouple the roll and pitch modes. Due to the long wheelbase compared with track width, the pitch mode may be over

stiffened by the X-coupling. Consequently, the ride may be negatively affected with an increased road bump excited pitch motion.

2.3.2 Hydraulically interconnected suspension

Hydraulically interconnected suspensions (HIS) were initially invented and patented by Heyring in 1996 [76]. They were further developed by Australian company Kinetic Pty Ltd (now acquired by Tenneco). The fluidic communication arrangement not only connects the left and right cylinders but also the front and rear cylinders. This connection enables the suspension mode to be fully decoupled both in terms of suspension stiffness and damping. The anti-roll interconnection arrangement shown in Figure 2.2 obtained commercial success and was named Kinetic H2.

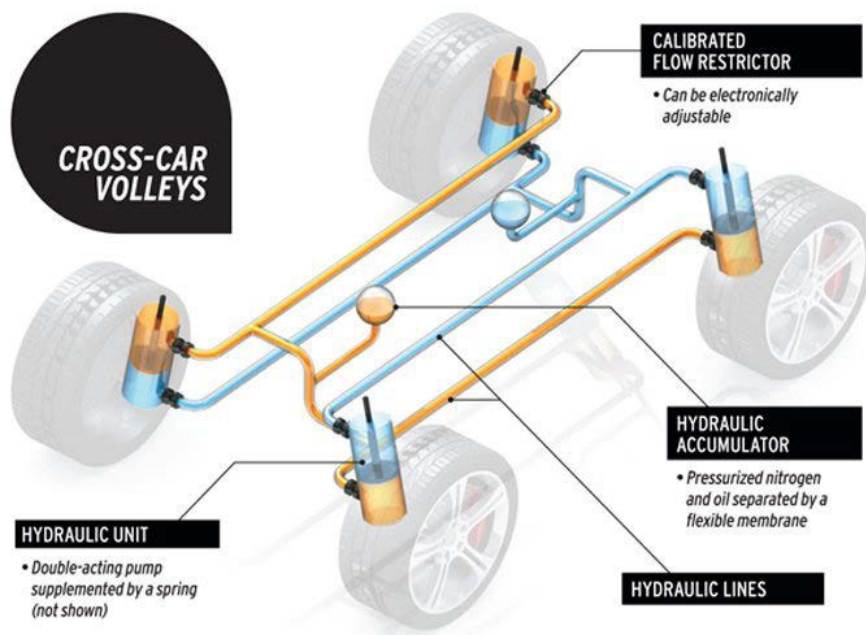


Figure 2. 2: Kinetic H2 system.

The experimental evaluation of the fishhook maneuver performance of a kinetic suspension system is presented in [77]. Improved stability is evaluated by conducting NHTSA's roll rate feedback fishhook tests on a small sport utility vehicle equipped with the Kinetic H2 system. The Kinetic system increased the NHTSA fishhook speed from

43 mph to 60 mph without ever yielding a two wheel-lift condition. The increase in fishhook speed equates to a much safer and more stable vehicle in extreme avoidance maneuvers and decreases the likelihood of an untripped rollover. The body-roll can be greatly reduced while still maintaining a comfortable ride that cannot be matched by conventional dampers and sway bars. The simulation of the ride and handling performance of the Kinetic suspension system has been reported in [78] using commercial simulation software ADAMS. From the simulations, the Kinetic vehicle was shown to offer handling responses that are similar to the standard vehicle. Below the rollover threshold, the Kinetic vehicle responds more quickly to the steering inputs and returns to a neutral position faster than the standard vehicle during the yaw fishhook maneuver. From the ride study, there may be a slight ride penalty for the benefits of increased rollover resistance and handling performance. Most likely, the ride characteristics of the Kinetic vehicle are very similar, if not perceptibly identical, to the standard vehicle.

Zhang & Smith [1, 73, 74] recently studied the dynamics of vehicles fitted with hydraulically interconnected suspension systems with a focus on the multi-body system dynamics and interconnected fluid circuit dynamics. A systematic approach was proposed for studying hydraulically interconnected suspensions in both the time and frequency domains. The finite element modelling of nonlinear hydraulic system is seamlessly connected to a mass-spring vehicle model through hydraulic-mechanical kinetic coupling, and the theoretical analysis is validated by laboratory experiments. The experimental comparison of the anti-roll bar and HIS is presented by Wang, et al. [56] and the results show that the roll resistance and tyre dynamic force of the HIS suspension outperforms the anti-roll bars. It shows that the anti-roll bar stiffens the warp mode which increases warp natural frequency, while with roll-resistant HIS suspension,

the warp natural frequency remains unchanged. The tyre dynamic force at the warp mode also illustrates that tyre load transfer of a vehicle fitted with an anti-roll bar increases 50% more than that of a vehicle fitted with a roll-plane HIS system. Modelling and characteristic analysis of tri-axle trucks with hydraulically interconnected suspensions are presented by Ding, et al. [44]. The obtained results show the effectiveness of the proposed HIS system in reducing the pitch motion of sprung mass and simultaneously maintaining ride comfort.

The FRIC or front and rear inter connected suspension is a system which links the front and rear suspension of the car using hydraulics. The system is first introduced by Mercedes for a Formula 1 race car in 2011, as shown in Figure 2.3. The FRIC reduces the pitch by moving the hydraulic fluid from the front to the rear of the car. So, under braking and cornering, when the nose of the car goes down, the fluid in the rear brings down the back of the car, which in turn brings up the nose and thus maintains a constant ride height.

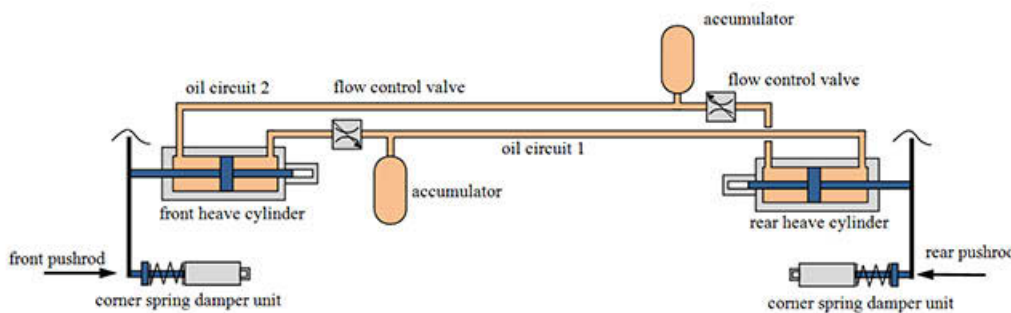


Figure 2. 3: FRIC suspension in racecar application.

2.4 Summary

The literature review in this chapter provides a background on vehicle system dynamics and applications of interconnected suspensions. It shows that there are many conflicting

requirements for suspension tuning in terms of vehicle dynamic performance: the ride comfort vs. tyre grip in the vertical dynamics; the attitude control during manoeuvres vs. pitch ride in the longitudinal dynamics; and the roll stability vs. ride comfort and road holding in the lateral dynamics. The conventional suspension design has evolved to a level that leaves little room for further improvement. The controlled systems have great potential to meet these conflicting requirements; however their high cost and complexity has hindered their large-scale application. From the vehicle motion modes perspective, the interconnected suspensions have the unique property to easily decouple the vehicle motion modes. The above reviewed applications of the interconnected suspension demonstrate some special capabilities to further improve the vehicle dynamics performance in the passive manner and the more advanced interconnections. In addition, the effects of different connection variations to vehicle system dynamics still requires further exploration.

Chapter 3: Vehicle with Hydraulically Interconnected

Suspensions

3.1 Introduction

Smith, et al [1, 73, 74] have published a few papers recently about Hydraulically Interconnected Suspension (HIS). His PhD thesis [79] investigated the dynamics of a vehicle with an HIS system. Previous work focused on detailed fluidic modelling and the transient response. A simple half-car model is used to illustrate the basic principles and to demonstrate the application of the methodology. One of the contributions of Smith's work is the detailed modelling of the fluidic system and its components. The effects of roll-resistant HIS are examined via free vibration analysis and forced vibration analysis.

However, a deeper understanding of the effects of the roll-plane and pitch-plane HIS system to vehicle dynamics still requires more research. The in-plane vehicle model cannot fully demonstrate how the interconnected system influences the vehicle dynamics. For example, one of the merits of HIS is to decouple the vehicle warp mode from other modes, and this mode is a non-planar mode which cannot be predicted by the in-plane vehicle model. The pitch plane HIS is not fully discussed in previous work. The nonlinear properties of the hydraulic system also need to be further discussed in the context of full vehicle dynamics.

The research in this chapter is an extension of Smith's work about hydraulically interconnected suspension. The effects of the passive roll-plane and pitch plane HIS to

vehicle dynamics have been comprehensively studied, respectively, via the full car model in the frequency domain.

3.2 Vehicle-road vibration model

There are basically two methods to study the physic system dynamics: experiment and simulation. The vehicle dynamics can be investigated by conducting experiments under different conditions but the physical experiments can be very expensive and time consuming. In addition, the experiments may not be useful if there is no thorough understanding of how the design change affects vehicle performance. The models of the vehicle and road are important to predict vehicle performance under excitation induced by road roughness.

3.2.1 Vehicle suspension static model

The static property of a vehicle suspension system can be effectively evaluated assuming a fixed vehicle body (or sprung mass) to appropriately reduce the contributions of couplings among various vibration modes of the vehicle body. This can facilitate the characterisation of the stiffness properties of a suspension system in individual modes [80]. This method may be considered to be more suspension oriented and less sensitive to variations in the vehicle inertial parameters. Moreover, this approach is much simpler due to the absence or reduction in coupling between the various vehicle vibration modes. The properties of the interconnected and unconnected configurations can thereby be evaluated using the simplified model of the struts with the fixed sprung mass, as shown in Figure 3.1.

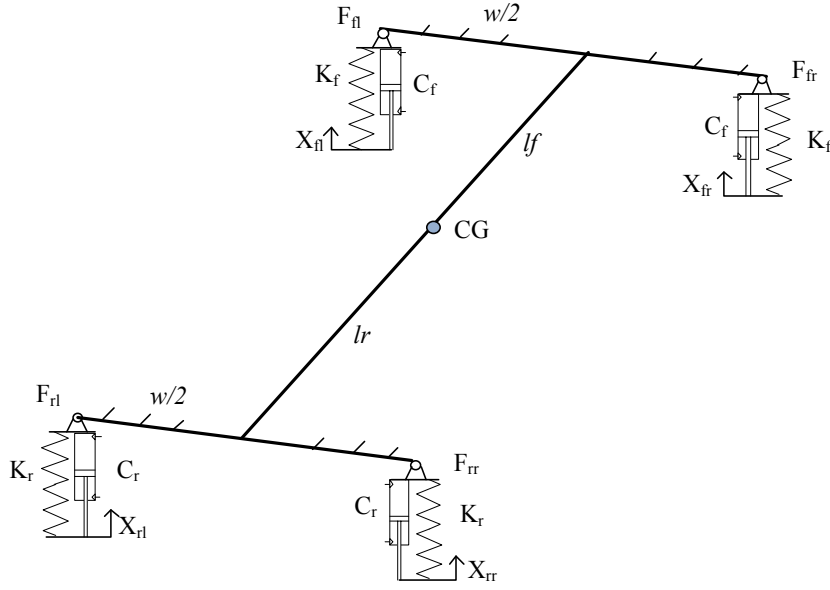


Figure 3. 1: Static suspension property model

In this model, the four struts are subject to four independent excitations (X_{fl} , X_{fr} , X_{rl} , X_{rr}) representing the relative deflection of the struts. The suspension forces (F_{fl} , F_{fr} , F_{rl} , F_{rr}) are the spring forces under struts displacement. The suspension rates K_f and K_r are the linear spring stiffness at the front and rear suspension. The damping rates C_f and C_r are also assumed to be linear for front and rear struts. l_f and l_r are distances from the centre of gravity (C.G) to the front and rear axle, respectively. The vehicle track width w is assumed to be the same for the front and rear axles.

Suspension bounce mode is the vehicle body dominated mode whereby the vehicle body moves vertically related to the ground while the movements of the wheels are negligible. Bounce mode is directly related to the vehicle ride comfort and it is desired to be as soft as possible to isolate the road induced impact. The bounce stiffness properties of the vehicle suspension are evaluated by letting suspension deflections $X_{fl}=X_{fr}=X_{rl}=X_{rr}=x$. The suspension bounce stiffness, K_{Bf} and K_{Br} , of the front and rear suspensions, respectively, are derived from:

$$K_B = K_{Bf} + K_{Br} = \frac{\partial(F_{fl} + F_{fr})}{dx} + \frac{\partial(F_{rl} + F_{rr})}{dx} = 2K_f + 2K_r \quad (3.1)$$

The bounce mode stiffness of the total suspension system is simply the sum of the suspension stiffness of its front and rear suspension.

Suspension roll mode mainly involves the vehicle body roll and lateral movement related to the ground. The vehicle roll mode is critical for lateral stability and is desirable for it to be as stiff as possible. The stiffness property of a full vehicle suspension in the roll mode is evaluated by letting $X_{fl} = X_{rl} = x$ and $X_{fr} = X_{rr} = -x$. The roll-mode stiffness properties, K_{Rf} and K_{Rr} , of the front and rear suspensions, respectively, are evaluated from

$$K_R = K_{Rf} + K_{Rr} = \frac{\partial(F_{fl} - F_{fr})}{dx} \frac{w^2}{4} + \frac{\partial(F_{rl} - F_{rr})}{dx} \frac{w^2}{4} = (K_f + K_r) * \frac{w^2}{2} \quad (3.2)$$

The total roll stiffness of a full vehicle suspension system is the sum of the roll stiffnesses due to the front and rear suspension deflections.

Suspension pitch mode mainly involves the vehicle body pitch and longitudinal movement related to the ground. The pitch mode is related both to the longitudinal stability and ride comfort. Due to the effect of wheelbase filtering, soft pitch stiffness is desired in order to minimise the pitching movement when running over a bump at high frequency. However a stiffer pitch mode is desired at low speed/frequency for attitude control at braking or acceleration. The pitch mode stiffness property of a full vehicle suspension is evaluated by letting $X_{fl} = X_{fr} = x$ and $X_{rl} = X_{rr} = -x$. The pitch stiffness K_p is defined as the pitch moment of the vehicle body vs. the vehicle pitch angle which can be expressed as:

$$K_p = \frac{\partial(F_{fl} + F_{fr})lf - \partial(F_{rl} + F_{rr})lr}{dx} \times \frac{(lf + lr)}{2} = (K_f * lf + K_r * lr) * (lf + lr) \quad (3.3)$$

Suspension warp mode is also known as axle articulation where diagonally-opposed wheels move in phase relative to the vehicle body. Unlike the bounce, pitch and roll modes, the suspension warp mode is wheel dominated and constitutes a non-planar mode, allowing the vehicle to travel on spatial surfaces. The suspension warp stiffness is defined as the torsional moment of the chassis Mt divided by the cross-axle articulation angle θ_w . The warp mode stiffness property of a full vehicle suspension can be assessed by letting $X_{fl}=x$, $X_{fr}=-x$, $X_{rl}=-y$ and $X_{rr}=y$. Assuming zero roll moment, the chassis torsional moment Mt is equal to the front suspension moment Mf and rear suspension moment $-Mr$ such that the rear suspension deflection y is found as $K_f * x / K_r$ where K_f is the front suspension spring rate and K_r is the rear suspension spring rate. The total axle articulation angle θ_w can be found as $2 * x * (ksf + ksr) / (ksr * w)$ and the formulation of the suspension warp stiffness can be obtained as:

$$K_w = \frac{\partial Mt}{\partial \theta_w} = \frac{\partial(F_{fl} - F_{fr})}{\partial \theta_w} \times \frac{w}{2} = \frac{ksf * ksr}{ksf + ksr} \times \frac{w^2}{2} \quad (3.4)$$

The suspension damping coefficients of bounce, roll, pitch and warp modes can also be easily derived by defining the suspension motion with relative speeds of suspension struts $(\dot{X}_{fl}, \dot{X}_{fr}, \dot{X}_{rl}, \dot{X}_{rr})$ which is similar to the mode stiffness formulation.

3.2.2 Vehicle dynamic model

When considering the coupling of sprung mass and unsprung mass, the vehicle dynamic model is needed to predict the vehicle response [81]. The vehicle can be modelled as a

lumped mass system with seven degrees of freedom (DOF) as shown in Figure 3.2. It consists of a rigid sprung mass supported by four independent suspensions, which includes wheel assemblies as four unsprung masses.

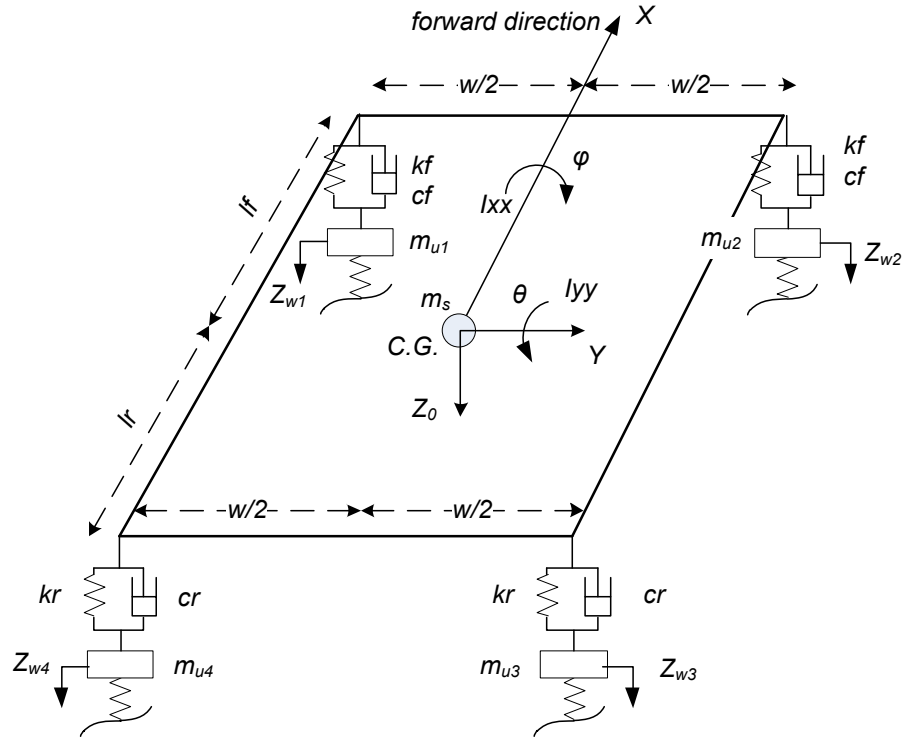


Figure 3. 2: Seven-DOF vehicle model

The sprung mass has inertial properties of mass m_s , roll moment of inertia I_{xx} , and pitch moment of inertia I_{yy} . The roll and pitch rotations are restricted only to the sprung mass. The seven DOF of the vehicle model includes: sprung mass vertical center-of-mass movement Z_0 , roll angle φ , pitch angle θ and four vertical center-of-mass movements of unsprung masses: Z_{w1} , Z_{w2} , Z_{w3} , Z_{w4} . The origin of coordinates is fixed at the center of gravity (CG) of the sprung mass. It is assumed in this section that the suspension springs and shock absorbers have a linear behavior. The parameters of the vehicle model are presented in Table 3.1.

Table 3. 1: Parameters of the 7dof vehicle model

Symbol	Value	Units	Description
m_s	1800	kg	Vehicle sprung mass
I_{yy}	3700	kgm^2	Pitch moment inertia of the sprung mass
I_{xx}	870	kgm^2	Roll moment inertia of the sprung mass
l_f	1.37	m	Distance from the CG to the front axle
l_r	1.48	m	Distance from the CG to the rear axle
w	1.15	m	Width of the vehicle tracks
m_u	42	kg	Unsprung masses of tyre 1, 2, 3, 4
K_f	40	kN/m	Spring rate of front suspension
K_r	44	kN/m	spring rate of rear suspension
C_f, C_r	2500	Ns/m	Damping coefficient at front and rear
K_t	250	kN/m	Vertical stiffness of tyres
k_{af}	32	kNm/rad	Front anti-roll bar stiffness
k_{ar}	8	kNm/rad	Rear anti-roll bar stiffness

By the assumption of small roll and pitch angle, the vertical displacements of sprung mass at each corner assume the relationship as follows:

$$\begin{aligned}
 Z_1 &= Z_0 - \frac{w}{2}\phi - l_f\theta \\
 Z_2 &= Z_0 + \frac{w}{2}\phi - l_f\theta \\
 Z_3 &= Z_0 - \frac{w}{2}\phi + l_r\theta \\
 Z_4 &= Z_0 + \frac{w}{2}\phi + l_r\theta
 \end{aligned} \tag{3.5}$$

Using the free body diagram approach and applying Newton's second law, the equations of the motion of the vehicle body at its C.G are:

$$\begin{aligned}
 m_s \ddot{Z}_s &= C_f(\dot{Z}_{w1} - \dot{Z}_1) + K_f(Z_{w1} - Z_1) + C_f(\dot{Z}_{w2} - \dot{Z}_2) + K_f(Z_{w2} - Z_2) \\
 &\quad + C_r(\dot{Z}_{w3} - \dot{Z}_3) + K_r(Z_{w3} - Z_3) + C_r(\dot{Z}_{w4} - \dot{Z}_4) + K_r(Z_{w4} - Z_4)
 \end{aligned} \tag{3.6}$$

$$I_{xx}\ddot{\theta} = \frac{w}{2}[(C_f(\dot{Z}_{w1} - \dot{Z}_1) + K_f(Z_{w1} - Z_1) - C_f(\dot{Z}_{w2} - \dot{Z}_2) - K_f(Z_{w2} - Z_2))] \\ + \frac{w}{2}[(C_r(\dot{Z}_{w4} - \dot{Z}_4) + K_r(Z_{w4} - Z_4) - C_r(\dot{Z}_{w3} - \dot{Z}_3) - K_r(Z_{w3} - Z_3))] + Mr \quad (3.7)$$

$$I_{yy}\ddot{\psi} = l_f[(C_f(\dot{Z}_{w1} - \dot{Z}_1) + K_f(Z_{w1} - Z_1) + C_f(\dot{Z}_{w2} - \dot{Z}_2) + K_f(Z_{w2} - Z_2))] \\ - l_r[(C_r(\dot{Z}_{w3} - \dot{Z}_3) + K_r(Z_{w3} - Z_3) + C_r(\dot{Z}_{w4} - \dot{Z}_4) + K_r(Z_{w4} - Z_4))] + Mp \quad (3.8)$$

The equations of motion of unsprung masses in the vertical direction are:

$$m_{u1}\ddot{Z}_{w1} = K_T(Z_{g1} - Z_{w1}) + K_f(Z_1 - Z_{w1}) + C_f(\dot{Z}_1 - \dot{Z}_{w1}) \\ m_{u2}\ddot{Z}_{w2} = K_T(Z_{g2} - Z_{w2}) + K_f(Z_2 - Z_{w2}) + C_f(\dot{Z}_2 - \dot{Z}_{w2}) \\ m_{u3}\ddot{Z}_{w3} = K_T(Z_{g3} - Z_{w3}) + K_r(Z_3 - Z_{w3}) + C_r(\dot{Z}_3 - \dot{Z}_{w3}) \\ m_{u4}\ddot{Z}_{w4} = K_T(Z_{g4} - Z_{w4}) + K_r(Z_4 - Z_{w4}) + C_r(\dot{Z}_4 - \dot{Z}_{w4}) \quad (3.9)$$

It can be re-written in the matrix form:

$$M\ddot{Z} + C\dot{Z} + KZ = F \quad (3.10)$$

where $M, C, K \in R^{7 \times 7}$ are the mass, damping and stiffness matrices; Z is the displacement vector at continuous time t ; F is the road excitation force input matrix.

Equation (3.10) can be converted to a continuous-time state space model as:

$$T\dot{X} = SX + F_{ex}, \quad \text{or}$$

$$\begin{bmatrix} I_7 & 0 \\ 0 & M \end{bmatrix} \begin{bmatrix} \dot{Z} \\ \ddot{Z} \end{bmatrix} = \begin{bmatrix} 0 & I_7 \\ -K & -C \end{bmatrix} \begin{bmatrix} Z \\ \dot{Z} \end{bmatrix} + \begin{bmatrix} 0 \\ F_{ex} \end{bmatrix} \quad (3.11)$$

The state vector describing the motion of the sprung and unsprung lumped suspension system is defined as:

$$X_M = [Z \quad \dot{Z}]^T \quad (3.12)$$

where displacement vector is $Z = [Z_{w1} \ Z_{w2} \ Z_{w3} \ Z_{w4} \ Z_0 \ \phi \ \theta]$ and velocity vector is $\dot{Z} = [\dot{Z}_{w1} \ \dot{Z}_{w2} \ \dot{Z}_{w3} \ \dot{Z}_{w4} \ \dot{Z}_0 \ \dot{\phi} \ \dot{\theta}]$.

Anti-roll bar (ARB) connecting the left and right wheels is a commonly used component in suspension to increase the vehicle's roll stiffness for improving the lateral stability. ARB may have simple or complicated irregular shapes for convenient packaging on the vehicle chassis. The ARB modelling is derived by treating it massless torsional spring and integrated into the 7-DOF vehicle model. The torsional stiffness of the front and rear anti-roll bar is assumed to be k_{af} & k_{ar} , and the length of the front and rear anti-roll bar is b_f & b_r respectively. Due to the fact that the anti-roll bar only works when the suspension deflection between the left and right is different, so the additional stiffness K_A caused by anti-roll bars is computed in the matrix form as:

$$K_A = \begin{bmatrix} \frac{k_{af}}{b_f^2} & -\frac{k_{af}}{b_f^2} & 0 & 0 & 0 & 0 & -\frac{k_{af}}{b_f} \\ -\frac{k_{af}}{b_f^2} & \frac{k_{af}}{b_f^2} & 0 & 0 & 0 & 0 & \frac{k_{af}}{b_f} \\ 0 & 0 & \frac{k_{ar}}{b_r^2} & -\frac{k_{ar}}{b_r^2} & 0 & 0 & \frac{k_{ar}}{b_r} \\ 0 & 0 & -\frac{k_{ar}}{b_r^2} & \frac{k_{ar}}{b_r^2} & 0 & 0 & -\frac{k_{ar}}{b_r} \\ 0 & 0 & 0 & 0 & 0 & 0 & 0 \\ 0 & 0 & 0 & 0 & 0 & 0 & 0 \\ -\frac{k_{af}}{b_f} & \frac{k_{af}}{b_f} & \frac{k_{ar}}{b_r} & -\frac{k_{ar}}{b_r} & 0 & 0 & k_{af} + k_{ar} \end{bmatrix} \quad (3.13)$$

If the stiffness coefficient matrix of the original springs is denoted as K_S , then in equation (3.10) the stiffness coefficient matrix K is replaced as:

$$K = K_S + K_A \quad (3.14)$$

3.3 Roll-resistant hydraulically interconnected suspension

3.3.1 Description of the RHIS system

The model of a vehicle fitted with roll-resistant hydraulically interconnected suspension RHIS system contains two subsystems: one mechanical and one hydraulic. The hydraulic layout features right-left symmetry and two identical fluid circuits, as shown in Figure 3.3, and some fluidic parameters are listed in Table 3.2.

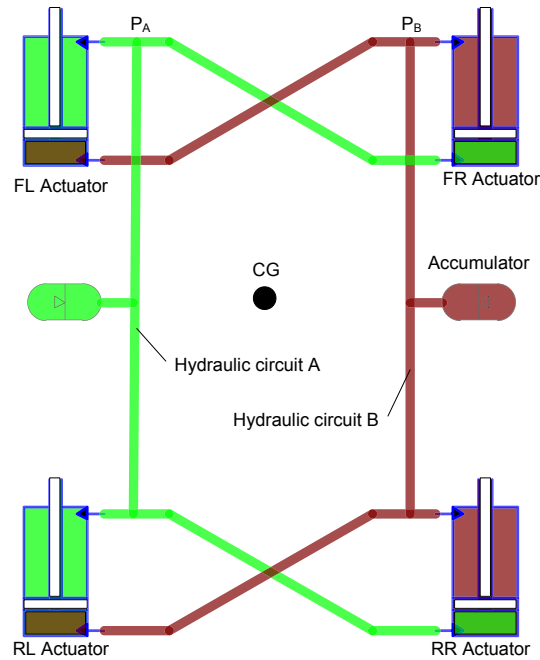


Figure 3. 3: Schematic diagram of the roll-plane RHIS system

Table 3. 2: Hydraulic parameters of RHIS

Symbol	Value	Units	Description
γ	1.4	/	Gas heat factor
D_{r_piston}	0.032	m	Cylinder piston diameter
D_{r_rod}	0.014	m	Cylinder piston rod diameter
V_r	3.2×10^{-4}	m^3	Accumulator volume
P_r	1	Mpa	Accumulator pre-charged gas pressure
\bar{P}_r	2	Mpa	Fluidic system mean working pressure

In the fluid system, it includes two nitrogen-filled diaphragm-type accumulators; interconnecting pipelines; and four double-acting hydraulic cylinders added to the original suspension. The cylinder bodies are mounted to the car chassis, with the piston rods being fixed to the wheel assemblies. Assuming the vehicle is rolling from left to right, the left suspension extend while the right suspension compress. The cylinder chambers linked to circuit A will squeeze the hydraulic fluid out and force it to flow into accumulator A, while cylinder chambers linked to circuit B increases the volume that fluid flows out from accumulator B. Thus the pressure at circuit B decreases while the pressure at the circuit A increases. The generated hydraulic forces act against the vehicle body roll motion. In other modes, there is a small amount or even no fluid flow into or out of the accumulators. Accordingly, the effects on those modes by RHIS are negligible. The interconnection arrangement enables the vehicle roll mode to be decoupled from bounce mode and warp mode.

3.3.2 Static suspension stiffness properties

The strut forces of the roll-plane RHIS consist of spring force and hydraulic force. The strut deflections are X_{fl} , X_{fr} , X_{rl} , X_{rr} at front left, front right, rear left and rear right, respectively. A^T , A^B denotes the effective cylinder chamber area at the top and bottom.

The gas volume change in the accumulators A and B can be found as:

$$\begin{aligned}\Delta V_A &= A^T (X_{fl} + X_{rl}) - A^B (X_{fr} + X_{rr}) \\ \Delta V_B &= A^T (X_{fr} + X_{rr}) - A^B (X_{fl} + X_{rl})\end{aligned}\tag{3.15}$$

Assuming no pressure loss along the pipeline, the pressures of cylinder chambers are equal to the connected accumulator pressures P_A or P_B which can be expressed as:

$$P_A = \frac{P_0 * V_0^\lambda}{(V_0 - \Delta V_A)^\lambda}, \quad P_B = \frac{P_0 * V_0^\lambda}{(V_0 - \Delta V_B)^\lambda} \quad (3.16)$$

where γ is the gas heat factor, P_0 and V_0 are the initial accumulator pressure and volume.

The strut forces are formulated according to the fluid connection, as shown in Figure 3.4:

$$\begin{aligned} F_{fl} &= K_f X_{fl} + P_A A^T - P_B A^B - P_0 (A^T - A^B) \\ F_{fr} &= K_f X_{fr} + P_B A^T - P_A A^B - P_0 (A^T - A^B) \\ F_{rl} &= K_r X_{rl} + P_B A^T - P_A A^B - P_0 (A^T - A^B) \\ F_{rr} &= K_r X_{rr} + P_A A^T - P_B A^B - P_0 (A^T - A^B) \end{aligned} \quad (3.17)$$

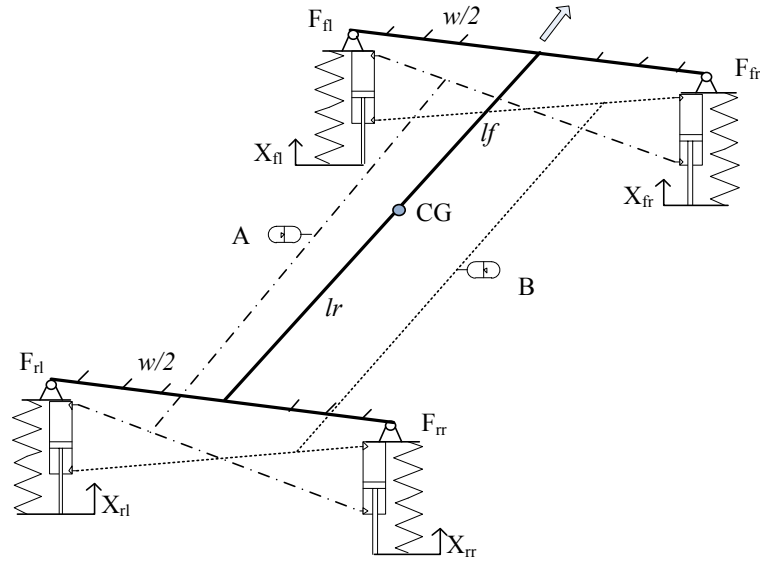


Figure 3. 4: Static model of the RHIS system

By defining the strut deflections of each mode, the static stiffness property of the roll-plane RHIS can be formulated as follows:

The bounce-mode stiffness properties of the roll-plane RHIS suspension are derived using Equations (3.1) and (3.15-3.17), such that

$$K_B = 2(K_f + K_r) + \frac{4(A^T - A^B)P_0 V_0^\lambda}{(V_0 - 2x(A^T - A^B))^\lambda} \quad (3.18)$$

The roll mode stiffness properties of the RHIS are derived from Equations (3.2) and (3.15-3.17), such that

$$K_R = (K_f + K_r) * \frac{w^2}{2} + w(A^T + A^B) \left(\frac{P_0 V_0^\lambda}{(V_0 - 2x(A^T + A^B))^\lambda} - \frac{P_0 V_0^\lambda}{(V_0 + 2x(A^T + A^B))^\lambda} \right) \quad (3.19)$$

Under pitch motion (assuming $l_f=l_r$; $X_{fl}=X_{fr}=x$ and $X_{rl}=X_{rr}=-x$), the volumes of the accumulator are the same, thus the cylinder pressures at the two fluid circuits are the same. It means the hydraulic system doesn't provide additional pitch suspension stiffness. The pitch mode stiffness properties of the RHIS are thereby the same as the unconnected spring-damper suspension, as expressed in Equations (3.3). Similarly, under warp mode motion, ($X_{fl}=x$, $X_{fr}=-x$, $X_{rr}=y$, $X_{rl}=-y$), the fluid flows from one chamber to the other chamber. The gas volume of the accumulators has no change, which means no additional warp stiffness is introduced by the HIS system. The warp mode stiffness of the RHIS system is the same as the unconnected conventional suspension, as expressed in equation (3.4).

The damping valves of the RHIS system can be tuned to have the equivalent damping property as the conventional spring-damper suspension in bounce, pitch and warp modes. Moreover, additional roll dampers can be added and placed in front of the accumulators to increase the overall roll damping which is not possible for the mechanical anti-roll bars system. The enhanced roll-mode damping properties of the RHIS configuration would be beneficial for controlling the transient roll motions and roll stability limits during steering maneuvers [82].

The static stiffness property of each mode are studied and compared with three suspension configurations. These are the roll resistant hydraulic interconnected suspension (RHIS), the conventional unconnected spring-damper suspension (SD) and the conventional spring-damper suspension with anti-roll bars (ARB).

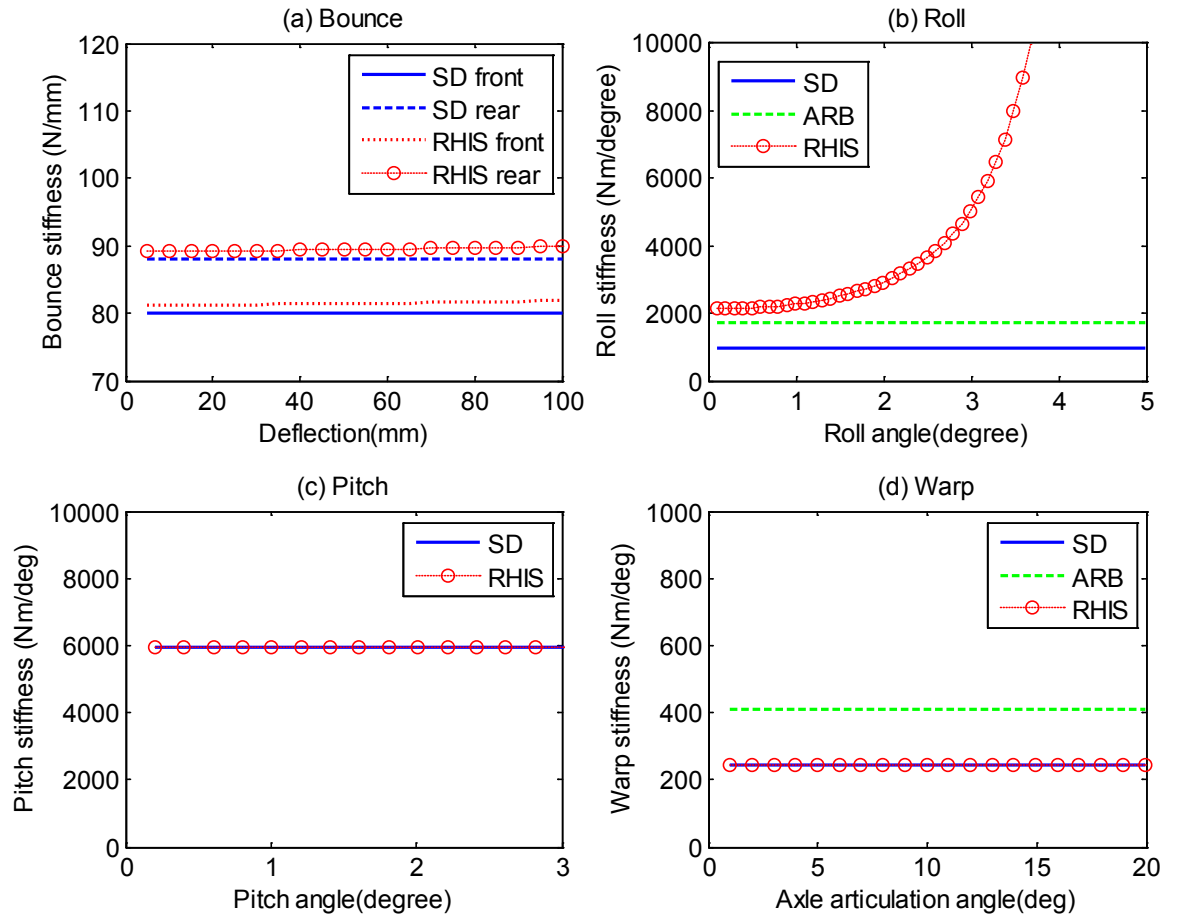


Figure 3. 5: Static stiffness properties of RHIS: (a) bounce (b) roll (c) pitch (d) warp

Figure 3.5 (a) - (d) presents the comparison results of the static modes stiffness property of all the selected suspension configurations (SD, ARB and RHIS). Under the in-phase bounce mode excitations, the ARB suspension yields identical front and rear suspension rates as the SD suspension throughout the deflection range considered. The RHIS suspension has a slightly larger bounce static stiffness than the unconnected SD suspension and exhibits a weekly progressively hardening effect in compression both at

the front and rear axle. The result suggests that the RHIS system introduces a small amount of bounce stiffness and will slightly reduce the ride comfort level compared with the SD suspension. This can be compensated by using slightly reduced unconnected spring stiffness in the RHIS system to obtain the same total bounce stiffness and the equivalent ride comfort.

The differences in the roll stiffness property of the selected configurations are presented in Figure 3.5 (b). The RHIS system exhibits a significantly higher roll mode property when compared with the SD suspension. The additions of passive front and rear anti-roll bars can also yield an upward parallel shift of the effective roll stiffness of the unconnected suspension (SD). Although the anti-roll bar yields static roll stiffness like those of the hydraulically interconnected suspension in the small roll angle range, the RHIS suspensions provide progressively increased roll stiffness corresponding to higher deflections. The nonlinear characteristic of the RHIS in the roll stiffness is desirable to manage the ride comfort in a lateral direction under high speed stochastic road excitation and the roll motion control during fast cornering. Furthermore, the use of very strong anti-roll bars are usually devoid of damping while roll damping can be tuned independent of bounce damping by the RHIS system.

The pitch property of the RHIS system is identical with that of the SD and ARB configurations, as shown in Figure 3.5 (c). The road holding and braking/traction performances of a vehicle are greatly influenced by the warp stiffness of the suspension. Figure 3.5 (d) illustrates a comparison of the warp stiffness properties of the three suspension configurations. Interconnected suspension configurations RHIS yield warp stiffness identical to that of the unconnected spring-damper suspension (SD) over the entire range of the axle articulation angle considered, as in the case of pitch-mode

stiffness. The use of anti-roll bars, however, tends to increase the effective suspension warp stiffness, due to the greater coupling in the roll and warp modes. This suggests that the hydraulic interconnection does not alter the warp property of the suspension, while they yield significant gains in the roll mode properties.

3.3.3 Dynamic modelling of RHIS

The modelling and dynamics of vehicles fitted with the hydraulically interconnected suspension system are investigated by Zhang and Smith [1] with a focus on the roll stability and fluid circuit dynamics. The ride comfort of a vehicle with an RHIS system is analysed in [73]. Experimental studies also confirm the anti-roll performance of the RHIS systems in [83]. However, the road holding performance of the RHIS system as a major advantage has not been thoroughly investigated, particularly at warp mode. In theory, the RHIS system is able to decouple the roll mode from all other modes and enhance vehicle roll stability without compromising on road holding ability. In this section, a quantitative analysis of the warp mode is carried out as well as a tyre-ground force study of the RHIS system via mathematical modelling and simulation.

The equation of motion for the vehicle possessing an integrated mechanical-hydraulic system can be written in a similar form to the vehicle with an unconnected SD suspension:

$$M \ddot{Z} + C \dot{Z} + KZ + D_{r1} \cdot A \cdot P(t) = F_{ext}(t) \quad (3.20)$$

where the displacement vector Z , mass matrix M , damping matrix C , stiffness matrix K and excitation forces F are as defined in the previous section 3.2.2; $D_{r1} \cdot A \cdot P$ describes the forces of the cylinders due to the change of hydraulic pressures; D_1 is the linear transformation matrices. The area matrix A and pressure vector P , related to the

corresponding cylinder chambers (T-top; B- bottom), are defined as:

$$P = \begin{bmatrix} P_T^1 & P_B^1 & P_T^2 & P_B^2 & P_T^3 & P_B^3 & P_T^4 & P_B^4 \end{bmatrix}^T,$$

$$A = \text{diag} \begin{bmatrix} A_T^1 & A_B^1 & A_T^2 & A_B^2 & A_T^3 & A_B^3 & A_T^4 & A_B^4 \end{bmatrix}.$$

In order to reduce the complexity of the fluid circuit system, the following assumptions are made: (a) piston friction is not considered. (b) the fluid is incompressible compared with nitrogen gas in the accumulator. (c) the oil density is constant. (d) pipeline is simplified with no viscous resistance, namely the pressure and flow rate inside the pipelines are equal throughout. The more complicated model taking into account pipeline flexibility and fluid viscous resistance has been developed in reference to studying the transient nature of the fluid system.

The cylinder chambers form the boundary between the mechanical and hydraulic subsystems. The compressibility of the hydraulic fluid in each of the cylinder chambers is shown as:

$$Q_{comp} = \frac{V}{\beta} \frac{dP}{dt} \quad (3.21)$$

where V and β are the volume and effective bulk modulus of the cylinder chamber.

Thus the fluid compressibility in the cylinder chamber is given by

$$Q_{comp} = \dot{Z}_{s-u}(t)A - Q(t) = \frac{V_0 - Z_{s-u}(t)A}{\beta} \dot{P}(t) \quad (3.22)$$

where $Q(t)$ denotes the volume flow rate where the pipeline meets the cylinder chamber; \dot{P} represents the rates of change of the in-chamber pressure; V_0 constitutes the initial volume of the cylinder chambers; and Z_{s-u} is the relative displacement between the unsprung mass and the point of strut contact at the corner of the sprung mass.

When applied to all eight chambers in the fluid system, as shown in Figure 3.2, Equation (3.22) can be re-written as:

$$\dot{Q}(t) = A \cdot D_{r1}^T \cdot \dot{Z}(t) + V(t) \cdot \dot{P}(t) \quad (3.23)$$

in which \dot{Q} is the flow vector defined as $\dot{Q} = [\dot{Q}_T^1 \quad \dot{Q}_B^1 \quad \dot{Q}_T^2 \quad \dot{Q}_B^2 \quad \dot{Q}_T^3 \quad \dot{Q}_B^3 \quad \dot{Q}_T^4 \quad \dot{Q}_B^4]^T$, $V(t)$ is a time-variant matrix of cylinder volume and bulk modulus terms, and D_1^T is a constant linear transformation matrix.

The accumulators are modelled by assuming an adiabatic process. The pressure and volume at any time in the accumulator P_a and V_a are related to the pre-charged values, P_p and V_p , as follows:

$$P_a V_a^\gamma = P_p V_p^\gamma = \text{constant}, \quad (3.24)$$

where γ is the ratio of specific heat for the gas. The adiabatic gas law is used to model the accumulator pressure as a function of gas volume at the pre-charged pressure. Taking the partial time derivative of Equation (10), and noting that the flow into the accumulator is given by $\dot{Q}_a = -\partial V_a / \partial t$, the pressure gradient of the accumulator is written as a nonlinear function of the pressure, i.e.

$$\dot{P}_a = \frac{\gamma \dot{Q}_a P_a}{V_p} \left(\frac{P_a}{P_p} \right)^{1/\gamma} \quad (3.25)$$

This equation shows the gas-spring nonlinearity as the rate of pressure change at any time not only depends on the flow rate but also on the pressure (state dependent). Linearisation can be made by substituting P_a with mean working pressure \bar{P} and gas

heating factor γ is equal to 1. It is valid when the vehicle system vibrates at small amplitude.

Then Equation (3.25) can be rewritten as:

$$\dot{P}_a = \frac{\gamma Q_a \bar{P}^2}{V_p P_p} \quad (3.26)$$

Assuming no fluid resistance in the pipelines, by the arrangement of the interconnection, we have:

$$\begin{aligned} P_1^T &= R_r Q_A + P_A ; & P_1^B &= R_r Q_B + P_B ; \\ P_2^T &= R_r Q_B + P_B ; & P_2^B &= R_r Q_A + P_A ; \\ P_3^T &= R_r Q_B + P_B ; & P_3^B &= R_r Q_A + P_A ; \\ P_4^T &= R_r Q_A + P_A ; & P_4^B &= R_r Q_B + P_B ; \end{aligned} \quad (3.27)$$

$$Q_A = Q_1^T + Q_2^T + Q_3^T + Q_4^T, \quad Q_B = Q_1^B + Q_2^B + Q_3^B + Q_4^B \quad (3.28)$$

where P_A , Q_A are the pressure and flow rate of the accumulator in hydraulic circuit A; P_B , Q_B are the pressure and flow rate of the accumulator in hydraulic circuit B. R_r is the roll damping coefficient.

The state vector describing the dynamic states of the hydraulic subsystem is defined as:

$$X_H = [P_A \quad P_B]^T \quad (3.29)$$

Through integrating the Equation (3.12) and (3.29), the state vector of the full vehicle fitted with a roll-plane RHIS is obtained:

$$X = [X_M^T \quad X_H^T]^T \quad (14+2=16 \text{ elements}) \quad (3.30)$$

By combining Equation (3.20) and Equation (21) – (28), the equations of a full vehicle system in state space form is derived as:

$$T\dot{X} = SX + F, \text{ or}$$

$$\begin{bmatrix} I_7 & 0 & 0 \\ 0 & M_7 & 0 \\ 0 & 0 & (T_H)_2 \end{bmatrix} \begin{bmatrix} \dot{Z} \\ \ddot{Z} \\ \dot{X}_H \end{bmatrix} = \begin{bmatrix} 0 & I_7 & 0 \\ -K & -C - C_H & -D_{r1} \cdot A \cdot D_{r2} \\ K_H & D_{r2}^T \cdot A \cdot D_{r1}^T & S_H \end{bmatrix}_{16 \times 16} \begin{bmatrix} Z \\ \dot{Z} \\ X_H \end{bmatrix}_{16} + \begin{bmatrix} 0 \\ F_M \\ 0 \end{bmatrix}_{16} \quad (3.31)$$

3.3.4 Modal Analysis of vehicle with RHIS suspension

Modal analysis is the study of the dynamic properties of structures under vibrational excitation. The goal of modal analysis in structural mechanics is to determine the natural mode shapes and frequencies of an object or structure during free vibration. In order to perform the modal analysis using the vehicle model derived before, equation (3.31) needs to be alternatively written as the following standard state space equation:

$$\dot{X} = AX + BF \quad (3.32)$$

A represents the system matrix and X is the state variable vector. The eigenvalues and eigenvectors representing the vibration characteristics of the vehicle system can be found by solving the eigen problem of the system matrix A. One eigen pair represents one vibration mode. For the i th eigenvalue and the corresponding eigenvector, λ_i and u_i satisfy

$$Au_i = \lambda_i u_i \text{ and } \lambda_i = s_L \text{ for } \det(A(sL) - sLI) \equiv 0. \quad (3.33)$$

For each complex eigenvalue $\lambda_i = \sigma + j\omega$, the natural frequency ω_{ni} and the damping ratio ζ_i of the vibration mode are given by

$$\omega_{ni} = |\lambda_i| = \sqrt{\sigma^2 + \omega^2} \quad \text{and} \quad \xi_i = \frac{\text{abs}(\sigma)}{\omega_{ni}} \quad (3.34)$$

The first seven elements of u_i ($i=1,\dots,7$) represent the displacement components corresponding to the oscillation frequency ω_{ni} and the maximum element in eigenvector u_i indicates the dominant component of the response under the resonance frequency ω_{ni} . The mode shapes are normalised with respect to the largest element, and the eigenvectors are sorted according to natural frequencies from low to high, leading to the modal matrix.

Table 3. 3: Modal analysis of a vehicle with SD suspension.

	1st	2nd	3rd	4th	5th	6th	7th
Modes	Body roll	Body bounce	Body pitch	Wheel pitch	Wheel roll	Wheel bounce	Warp
Natural Freq. (Hz)	1.253	1.38	1.491	13.09	13.15	13.17	13.29
Damping ratio	0.16	0.185	0.18	0.296	0.293	0.295	0.286
Modal shape							
CG displacement	0	1	1	0.062	0	0.061	0
Pitch angle	0	0.648	-0.749	0.041	0	-0.044	0
Roll angle	1	0	0	0	0.106	0	-0.046
Wheel 1 (front left)	-0.092	-0.309	-0.033	1	0.935	-0.042	1
Wheel 2 (front right)	0.092	-0.309	-0.033	1	-0.935	-0.042	-1
Wheel 3 (rear right)	0.081	0.029	-0.297	0.042	-1	1	0.931
Wheel 4 (rear left)	-0.081	0.029	-0.297	0.042	1	1	-0.931

Table 3.3 is the summary of the natural frequency and modal shape of the vehicle with SD suspension. From the modal shape, we can see the first three are body predominant modes: body roll, body bounce and body pitch; the last four are wheel predominant modes: wheel pitch, wheel roll, wheel bounce and warp. Bounce and pitch mode both involve body vertical movement and pitch angular movement

which illustrate the coupling between these two modes. In warp mode, the body motion is very small compared to wheel motion.

As the inertia properties of the vehicle are kept the same, so the natural frequency indicates the overall stiffness of each mode. Increased natural frequency means the increased stiffness of each mode. For bounce and warp, a soft mode is desirable to improve the ride quality and road holding ability, whereas for roll and pitch, a stiff mode is desirable to enhance the stability and handling performance.

Table 3. 4: Natural frequency comparison of three configurations.

Natural Frequency (Hz)	Body roll	Body bounce	Body pitch	Wheel pitch	Wheel roll	Wheel bounce	Warp
SD	1.27	1.38	1.53	13.09	13.16	13.23	13.33
ARB	1.56	1.38	1.53	13.09	13.97	13.23	14.18
RHIS	1.68	1.39	1.53	13.10	14.04	13.24	13.30

Table 3.4 is a summary of the natural frequency of three different vehicle configurations (SD, ARB and RHIS). From the comparison results, we can see vehicle roll mode natural frequency increased from 1.27Hz to 1.56Hz by the anti-roll bar, and it increased to 1.66Hz by the RHIS. The warp mode natural frequency also increased from 13.33Hz to 14.18Hz by the anti-roll bars, but there is almost no change in terms of the RHIS system which agrees with the static characteristic analysis. The results illustrate that anti-roll bars can improve the roll stiffness while bounce mode maintains the same, but the warp mode is negatively affected. The stiffened warp mode implies a decreased road holding ability. The roll-plane HIS can provide an even stiffer roll mode than the anti-roll bars, which agrees well with the testing results in reference [77]. More importantly, both bounce & warp mode are kept at pretty much the same levels. This clearly

demonstrates the advantage of the useful mode decoupling property of the RHIS system over the anti-roll bars.

3.3.5 Frequency analysis of RHIS under warp mode

The roll stability of the RHIS has been theoretically and experimentally investigated in reference [73]. The decoupled warp mode property of the RHIS system is a unique advantage over the conventional mechanically interconnected anti-roll bar system, but the vehicle dynamics of the vehicle with RHIS at warp mode have not been thoroughly investigated to date, especially in the frequency domain.

The vibration evaluation indexes suggested by Cole [84] include the sprung mass acceleration Y_A , the suspension deflection Y_S , and the tyre dynamic force Y_T . The corresponding transfer function matrices from the state vector X for calculating the outputs are defined as follows:

$$Y_A = H_A X = s^2 \begin{bmatrix} 0_{3 \times 4} & I_{3 \times 3} & 0_{3 \times 9} \end{bmatrix} X, \quad (3.35)$$

$$Y_S = H_S X = \begin{bmatrix} -1 & 0 & 0 & 0 & 1 & lf & w/2 \\ 0 & -1 & 0 & 0 & 1 & lf & -w/2 \\ 0 & 0 & -1 & 0 & 1 & -lr & -w/2 \\ 0 & 0 & 0 & -1 & 1 & -lr & w/2 \end{bmatrix} 0_{4 \times 9} X, \quad (3.36)$$

$$Y_T = H_T X + H_U X = \begin{bmatrix} -K_T & & & & & & \\ & -K_T & & & & & \\ & & -K_T & & & & \\ & & & -K_T & & & \\ & & & & -K_T & & \\ & & & & & 0_{4 \times 12} & \end{bmatrix} X + \begin{bmatrix} K_T \\ -K_T \\ K_T \\ -K_T \end{bmatrix} U \quad (3.37)$$

where $H_U = \begin{bmatrix} K_T \\ -K_T \\ K_T \\ -K_T \end{bmatrix}$ represents the road excitation in the warp/axle-articulation mode.

The outputs Y can be obtained from the state vector X and input U , as follows:

$$Y = \begin{bmatrix} H_A \\ H_S \\ H_T \end{bmatrix} X + \begin{bmatrix} 0 \\ 0 \\ H_U \end{bmatrix} U = CX + DU \quad (3.38)$$

Based on equation (3.32) and (3.38), the transfer function from inputs to the evaluation outputs can be developed as:

$$H = C(sI - A)^{-1} B + D \quad (3.39)$$

The bode plot of the frequency response of a vehicle's C.G acceleration, suspension deflections and tyre dynamic forces under warp excitation are shown from Figure 3.6 to Figure 3.8, respectively. The vehicle fitted with RHIS is compared to vehicles fitted with SD and vehicles fitted with ARB suspension.

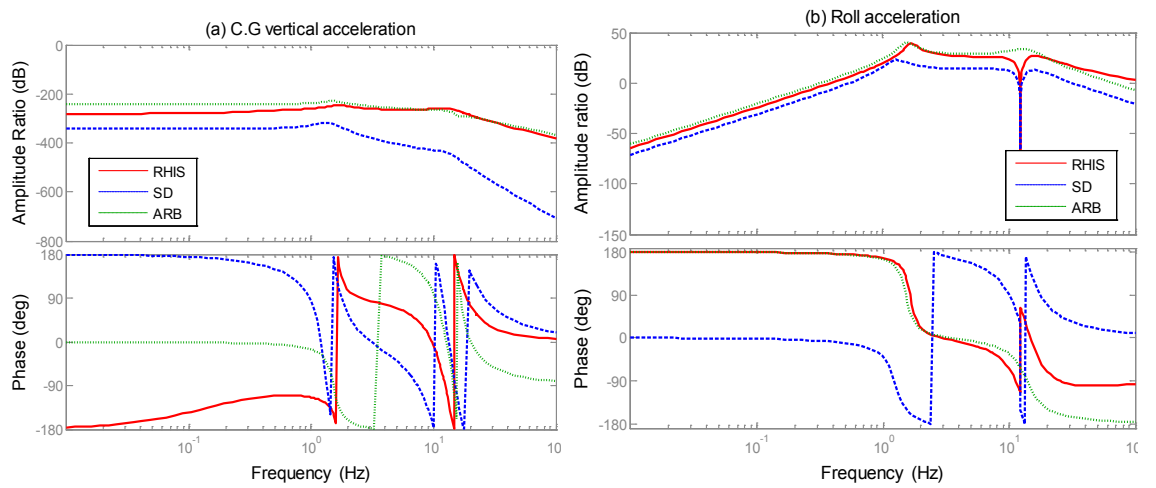


Figure 3. 6: Vehicle accelerations under warp excitation: (a) C.G vertical (b) Roll

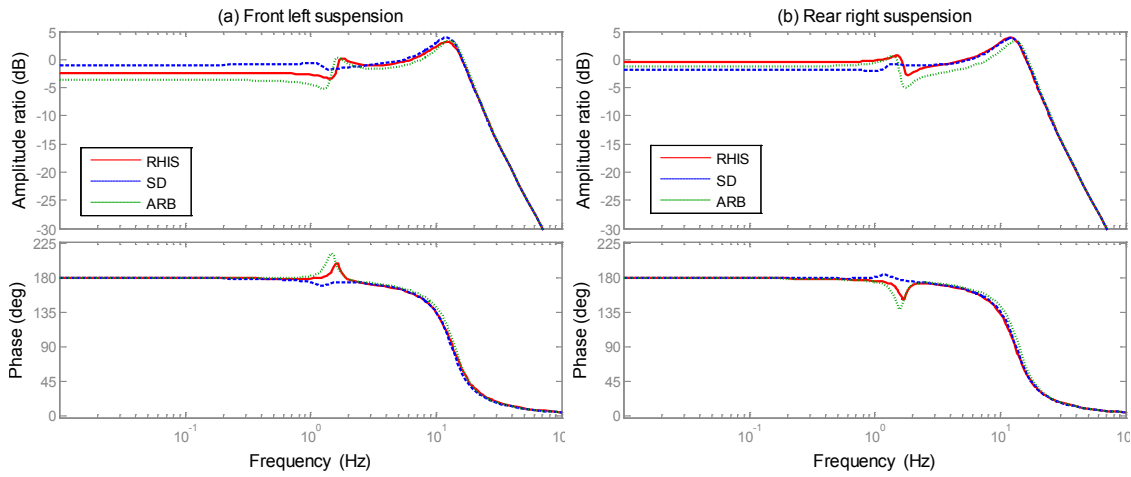


Figure 3. 7: Suspension deflection under warp excitation: (a) front left (b) rear right

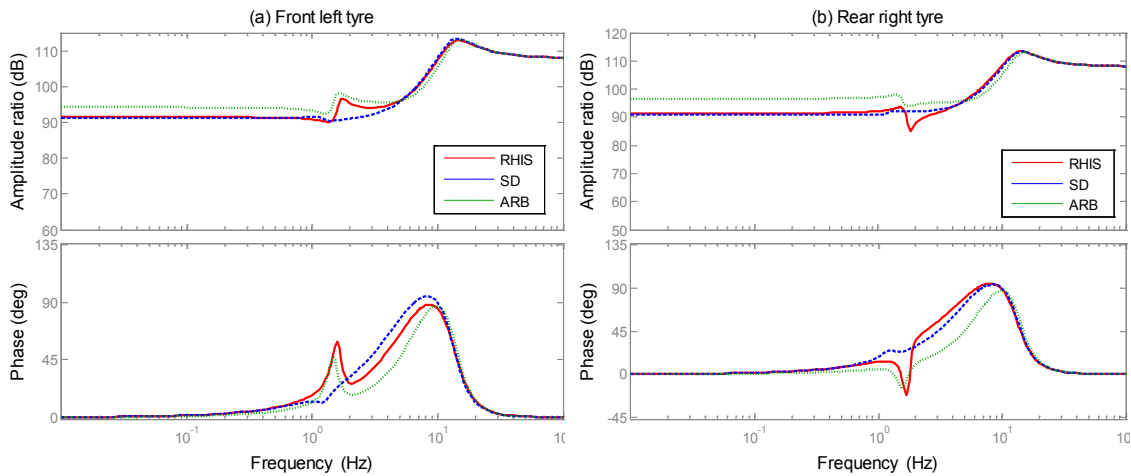


Figure 3. 8: Tyre dynamic forces under warp excitation: (a) front left (b) rear right

It shows that the C.G vertical acceleration of all three vehicles has a very small amplitude ratio compared with body roll motion and tyre motion. RHIS vehicle's vertical acceleration level is larger than the SD vehicle, but lower than the ARB vehicle even though RHIS has the largest total roll stiffness. The roll amplitude ratios of all three vehicle configurations display a similar pattern in general. The RHIS presents the highest body roll natural frequency and SD suspension has the lowest roll natural frequency which agrees well with the modal analysis. There is a deep hole near the second natural frequency for the SD and RHIS vehicles, possibly due to the poor

calculation accuracy of the frequency response. It can be observed that there is a 180 degree phase difference in the roll acceleration between the SD vehicle and the RHIS vehicle/ARB vehicle which is due to the opposite roll stiffness distribution being altered by the anti-roll systems.

The suspension deflection (working space) is important for chassis packaging design. The amplitude ratios of SD suspension deflection of all three vehicles are nearly constant at the low frequency range under the warp excitation and the amplitude ratios become the same in the higher frequency. The suspension deflection is more critical in the low frequency range where the amplitude ratio of SD suspension is observed to be the largest at the front, while it is the smallest at the rear. The RHIS suspension deflection is larger than ARB suspension but lower than the SD suspension at the front and it is the largest at the rear in the low frequency.

The traction and control of the road vehicle is only through the contact patch of the tyres so that the contact between tyre and ground is vital for the vehicle's stability and safety especially under off-road rough terrain conditions. The comparison results of the tyre dynamic force under warp excitation, presented in Figure 3.8, illustrate that the RHIS vehicle has a lower tyre dynamic force similar to the SD vehicle in the whole frequency range, except for some difference presented near the first suspension natural frequency around 1.5Hz owing to the phase changing. By contrast, the ARB vehicle has a higher amplitude ratio of tyre dynamic force in the low frequency range, roughly 3 dB at the front and 5 dB at the rear, respectively. This means that anti-roll bars not only increase the roll stiffness, but also unfavorably increase the warp stiffness. Further, the tyre dynamic force varies to a much larger degree than the vehicle with the SD and RHIS systems. The tyre force amplitude ratio becomes the same for all three suspension configurations in the frequency range that is larger than 10Hz for both the front and rear

tyres. It suggests that the tyre stiffness becomes dominant at high frequency while the suspension warp stiffness has negligible effects on the tyre dynamic force responses.

In a nutshell, the vehicle warp mode is a wheel dominant mode with a small amount of roll motion involved due to the unbalanced roll stiffness distribution. The SD suspension has a roll stiffness distribution biased towards the rear end while the ARB and RHIS suspension have a roll stiffness distribution biased towards the front end to improve the steering. The comparison results of the frequency response analysis show that the RHIS can increase the roll mode stiffness substantially, with minimum influence on the bounce- and warp-mode properties. Such enhanced decoupling of the roll mode from the bounce/warp modes would be beneficial in realising an improved design compromise among various vehicle performance measures under complex driving conditions and road irregularity.

3.4 Pitch-resistant hydraulically interconnected suspension

3.4.1 Description of the PHIS system

The vehicle handling performance can be effectively improved by limiting variations in normal tyre forces, realised by controlling vehicle attitude (roll and pitch motions), and lateral and longitudinal load transfers [42, 43, 85]. Conventional suspensions generally utilise relatively soft stiffness springs in conjunction with anti-roll bars to obtain an improved compromise between roll stability and ride as well as road-friendliness. The use of anti-roll bars can inhibit roll motion and lateral load transfer. However, it has an effect on the longitudinal load transfers and pitch motions. The anti-squat/anti-dive geometry of suspension control arms implemented in the passenger cars can achieve an improved static load distribution on different axles, and they still may induce an unequal

load distribution during braking and acceleration especially when soft springs are applied [86].

Owing to inherent limitations of passive unconnected suspensions in realising complex and contradictory design requirements, active and semi-active controlled suspensions have received extensive attention. The controlled suspensions, however, add considerable costs (hardware as well as power consumption), weight and complexity. Furthermore, a number of studies have raised concerns related to the reliability of fully active suspensions, which amounts to a critical design issue. Alternatively, semi-active suspensions tend to deteriorate the ride vibration performance at higher frequencies, compared to passive unconnected suspensions [43]. Among the various passive suspensions, the interconnected suspensions pneumatically or hydraulically are believed to provide promising alternatives for vehicle suspension applications [3].

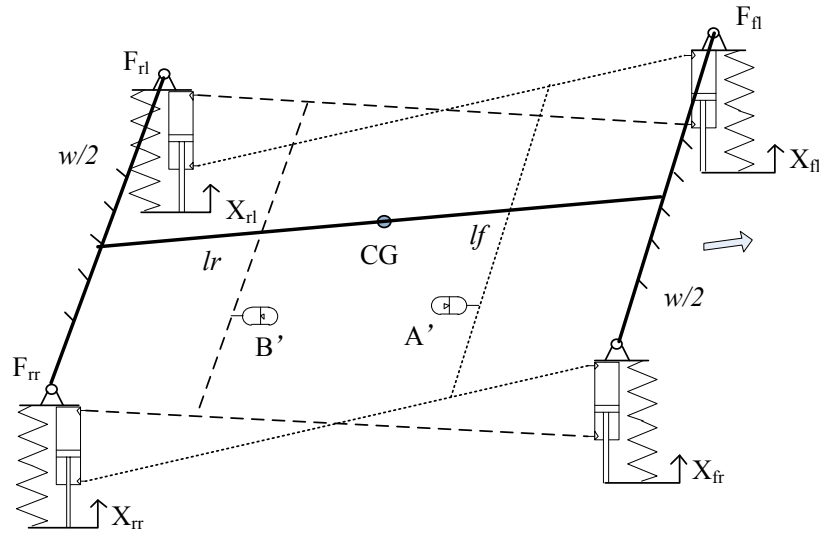


Figure 3. 9: Schematic diagram of the PHIS system

Table 3. 5: Hydraulic parameters of PHIS

Symbol	Value	Units	Description
γ	1.4	/	Gas heat factor
D_{p_piston}	0.025	m	Cylinder piston diameter

D_{p_rod}	0.012	m	Cylinder piston rod diameter
V_p	3.2×10^{-4}	m^3	Accumulator volume
P_p	1	Mpa	Accumulator pre-charged gas pressure
\bar{P}_p	2	Mpa	Fluidic system working pressure

The pitch-resistant hydraulically interconnected suspension (PHIS) system, shown in Figure 3.9, can increase the pitch stiffness nonlinearly while maintaining the soft bounce and warp modes. The PHIS system has 4 double acting cylinders and 2 hydraulic accumulators and communication pipelines which are similar to the RHIS, but the interconnection is arranged in the pitch plane so that the hydraulic system can counteract the car body pitch motion progressively. The parameters of the PHIS system are presented in Table 3.5.

3.4.2 Static suspension properties of PHIS

The static suspension property of the pitch-plane PHIS can be developed in a similar manner to the roll-plane RHIS by defining the strut deflections X_{fl} , X_{fr} , X_{rl} , X_{rr} at the front left, front right, rear left and rear right, respectively. The strut forces consist of mechanical force and hydraulic force developed by the means of the springs and cylinders.

A^T , A^B denotes the effective cylinder piston area at the top and bottom. The gas volume change in the accumulators A' and B' can be found as:

$$\begin{aligned}\Delta V'_A &= A^T (X_{fl} + X_{fr}) - A^B (X_{rl} + X_{rr}) \\ \Delta V'_B &= A^T (X_{fl} + X_{fr}) - A^B (X_{rl} + X_{rr})\end{aligned}\tag{3.40}$$

The pressure of cylinder chambers is equal to the pressure of corresponding accumulator P_A , or P_B , when assuming no pressure loss along the pipeline. Similarly, it can be found by Equation (3.16).

The strut forces are formulated according to the fluid connection as shown in Figure 3.9:

$$\begin{aligned} F_{fl} &= K_f X_{fl} + P_A A^T - P_B A^B - P_0 (A^T - A^B) \\ F_{fr} &= K_f X_{fr} + P_A A^T - P_B A^B - P_0 (A^T - A^B) \\ F_{rl} &= K_r X_{rl} + P_B A^T - P_A A^B - P_0 (A^T - A^B) \\ F_{rr} &= K_r X_{rr} + P_B A^T - P_A A^B - P_0 (A^T - A^B) \end{aligned} \quad (3.41)$$

The bounce-mode ($X_{fl}=X_{fr}=X_{rl}=X_{rr}=x$) stiffness properties of the PHIS suspension are:

$$K_B' = 2(K_f + K_r) + \frac{4(A^T - A^B)P_0 V_0^\lambda}{(V_0 - 2x(A^T - A^B))^\lambda} \quad (3.42)$$

The pitch mode ($X_{fl}=X_{fr}=x$ and $X_{rl}=X_{rr}=-x$) stiffness properties of the PHIS are derived:

$$K_P' = (l_f + l_r) \left[(K_f * l_f + K_r * l_r) + \frac{(A^T + A^B)}{x} \left(\frac{P_0 V_0^\lambda}{(V_0 - 2x(A^T + A^B))^\lambda} - \frac{P_0 V_0^\lambda}{(V_0 + 2x(A^T + A^B))^\lambda} \right) \right] \quad (3.43)$$

Under roll motion ($X_{fl}=x$, $X_{fr}=-x$, $X_{rl}=x$, $X_{rr}=-x$), the fluid in the cylinder chambers exchanges between the left and right through the pipe connection. The gas volumes of the accumulators are kept the same so that there is no change on the cylinder pressures under roll motion. This means the hydraulic system doesn't provide additional roll stiffness. The roll mode stiffness properties of the PHIS are thereby the same as the unconnected spring-damper suspension, as expressed in Equations (3.3). Similarly, under the warp mode motion, ($X_{fl}=x$, $X_{fr}=-x$, $X_{rr}=y$, $X_{rl}=-y$), the fluid exchanges between the left and right chambers. The gas volume of the accumulators does not

change, which means no additional warp stiffness is introduced by the interconnected system. The warp mode stiffness of the PHIS system is the same as the unconnected conventional SD suspension, as expressed in Equation (3.4).

The damping valves of the PHIS system can be tuned to have the equivalent damping property as the spring-damper suspension in bounce, roll and warp modes. Additional pitch dampers can be included and placed in front of the accumulators to tune the overall pitch damping. The enhanced pitch-mode damping properties of the PHIS configuration would be beneficial for controlling the transient pitch motions and longitudinal stability [87].

PHIS's static stiffness properties of all four suspension modes are compared with SD suspension. Figure 3.10 (a) - (d) presents the comparison results of the static modes stiffness property of the PHIS and SD suspension.

Under the in-phase bounce mode excitations, the PHIS suspension has an almost identical bounce static stiffness as the unconnected SD suspension both at the front and rear axle. The roll property of the PHIS system is identical to that of the SD suspension, as shown in Figure 3.10 (b). The differences in the pitch stiffness property between PHIS and SD suspension are presented in Figure 3.10 (c). The PHIS system exhibits a highly nonlinear pitch stiffness compared to the SD suspension. When the pitch angular deflection is small, the PHIS suspensions provide just slightly more pitch stiffness than the SD. The pitch stiffness of the PHIS increases progressively under the large pitch angular deflection (>1 degree). Due to the bounce and pitch coupling in the pitch plane vehicle dynamics, moderate pitch stiffness is required in the small pitch amplitude to control the pitch acceleration level for ride comfort when running over the road bump. However, stiffer pitch stiffness is favourable to inhibit the squat or dive induced by

braking or acceleration. The nonlinear characteristic of the PHIS in the pitch stiffness are highly desirable in order to improve the compromise between ride comfort and vehicle attitude control. Figure 3.10 (d) shows that the warp stiffness properties of the PHIS yields identical warp stiffness as the unconnected spring-damper suspension (SD) over the entire range of the axle articulation angle considered. This suggests that the PHIS system decouples the pitch mode from other modes without affecting the vehicle's warp mode property.

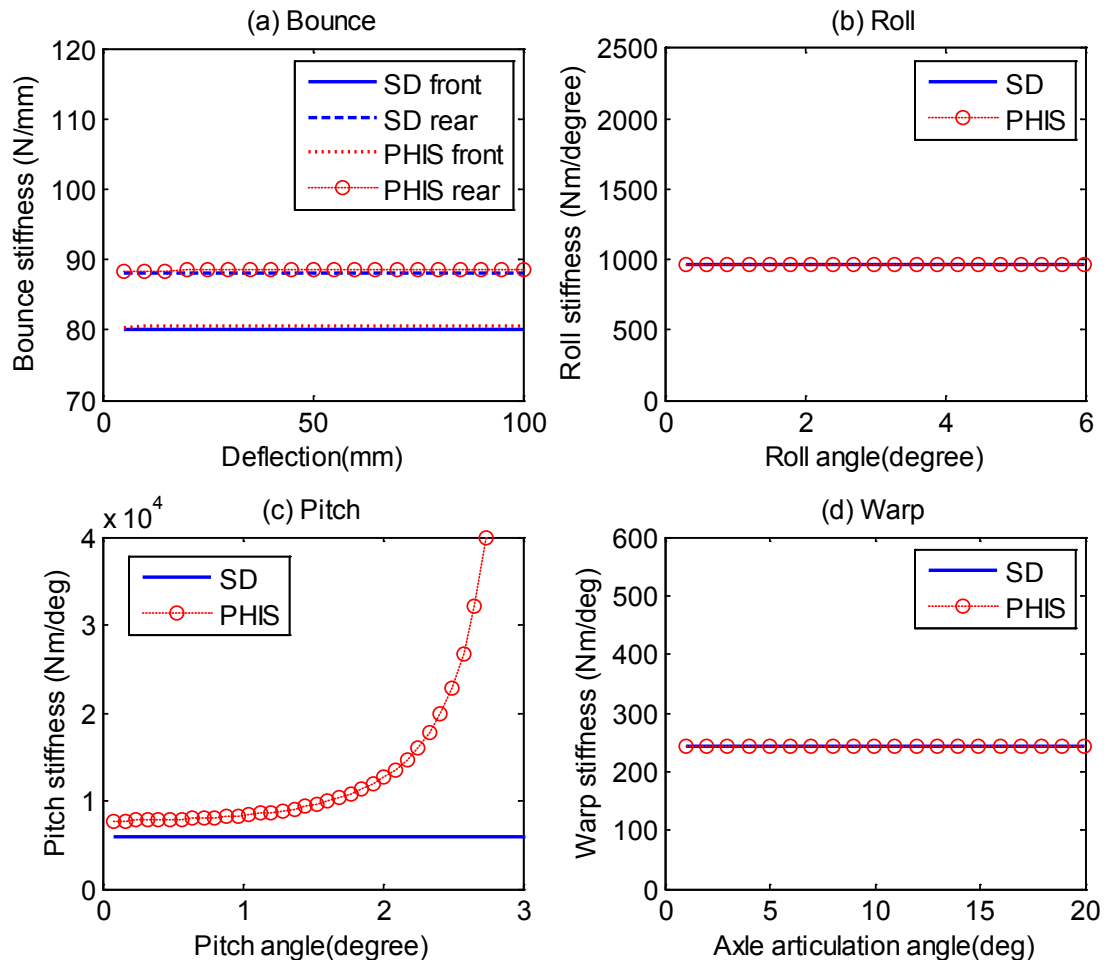


Figure 3. 10: Static stiffness of PHIS (a) bounce (b) roll (c) pitch (d) warp

3.4.3 Dynamic model of PHIS

The dynamic modelling of a vehicle fitted with the PHIS system is very similar to the modelling of the RHIS system. The assumption of the fluidic system in the RHIS is also applied in the PHIS system.

The equations of motion for the vehicle possessing an integrated mechanical-hydraulic system are:

$$M \ddot{Z} + C \dot{Z} + KZ + D_{p1} \cdot A \cdot P(t) = F_{ext}(t) \quad (3.44)$$

where the displacement vector Z , mass matrix M , damping matrix C , stiffness matrix K and excitation forces F are defined as the same; the linear transformation matrices D_{p1} should be modified according to the anti-pitch fluid interconnection.

The pressure and flow equations in the Equation (3.27) should be modified as:

$$\begin{aligned} P_1^T &= R_p Q_{A'} + P_{A'}; & P_1^B &= R_p Q_{B'} + P_{B'}; \\ P_2^T &= R_p Q_{A'} + P_{A'}; & P_2^B &= R_p Q_{B'} + P_{B'}; \\ P_3^T &= R_p Q_{B'} + P_{B'}; & P_3^B &= R_p Q_{A'} + P_{A'}; \\ P_4^T &= R_p Q_{B'} + P_{B'}; & P_4^B &= R_p Q_{A'} + P_{A'}; \end{aligned} \quad (3.45)$$

where R_p denotes the damping coefficient of pitch damper.

The flow equations in the equation (3.28) should be modified as:

$$Q_{A'} = Q_T^1 + Q_T^2 + Q_B^3 + Q_B^4, \quad Q_{B'} = Q_B^1 + Q_B^2 + Q_T^3 + Q_T^4 \quad (3.46)$$

The state vector of the full vehicle fitted with PHIS is the same as:

$$X = \begin{bmatrix} X_M^T & X_H^T \end{bmatrix}^T \quad (14+2=16 \text{ elements}) \quad (3.47)$$

The full vehicle system of PHIS in the state space form is thus modified as

$$T\dot{X} = SX + F, \text{ or}$$

$$\begin{bmatrix} I_7 & 0 & 0 \\ 0 & M_7 & 0 \\ 0 & 0 & (T_H)_2 \end{bmatrix} \begin{bmatrix} \dot{Z} \\ \ddot{Z} \\ \dot{X}_H \end{bmatrix} = \begin{bmatrix} 0 & I_7 & 0 \\ -K & -C - C_H & -D_{p1} \cdot A \cdot D_{p2} \\ K_H & D_{p2}^T \cdot A \cdot D_{p1}^T & S_H \end{bmatrix}_{16 \times 16} \begin{bmatrix} Z \\ \dot{Z} \\ X_H \end{bmatrix}_{16} + \begin{bmatrix} 0 \\ F_M \\ 0 \end{bmatrix}_{16} \quad (3.48)$$

3.4.4 Modal analysis of PHIS

A vehicle's pitch motion is normally coupled with the bounce motion for two-axle vehicles. Olley [35] initially studied the oscillation centres of bounce/pitch coupling. He stated that the displacement amplitude ratio between the vertical bounce and the pitch angle at the CG of sprung mass was the distance from the CG to each of the two oscillation centres. The oscillation centres that fall within and outside the wheelbase are regarded as the pitch and bounce oscillation centres, respectively.

The modal property of the PHIS is analysed using the same method mentioned in section 3.3.4. The natural frequency, damping ratio and modal shape are summarised in Table 3.6. When compared with the modal property of the unconnected SD suspension listed in Table 3.3, the pitch natural frequency is increased from 1.491 Hz to 1.62 Hz and the bounce natural frequency is also slightly increased from 1.38 Hz to 1.43 Hz by the PHIS suspension. The roll and warp modal properties are not affected by the PHIS. By using Olley's method to calculate the position of the oscillation centre, we can see that the pitch oscillation centre of the vehicle with PHIS is shifted towards the C.G while the bounce oscillation centre is shifted away from the C.G. It suggests that the coupling of the pitch and bounce motion in the SD suspension are decoupled to some extent by the PHIS system.

The increased pitch mode stiffness is favourable to control the brake/acceleration induced pitch motion. However, the complete decoupling of pitch mode from bounce mode may not be desirable for the vehicle's ride comfort due to the wheelbase filtering. When the vehicle's front axle runs over a bump, the rear axle will follow the same bump in a time delay depending on the vehicle speed and wheelbase length. It can result in an amplified pitch motion if the wheelbase delay time falls into the pitch resonant frequency. Because of the shifting of the pitching centre towards the CG, the pitch oscillation due to the road bump may become more severe. To minimise the effects of amplified pitch oscillation over bumps, one possible improvement of the pitch-plane PHIS is to control the pitch damping by adding pitch damping valves in front of the accumulators.

Table 3. 6: Modal analysis of the vehicle with PHIS suspension.

Modes	1st	2 nd	3rd	4 th	5th	6th	7th
	Body roll	Body bounce	Body pitch	Wheel bounce	Wheel roll	Warp	wheel pitch
Natural Freq. (Hz)	1.253	1.43	1.62	13.09	13.14	13.284	13.29
Damping ratio	0.17	0.209	0.208	0.337	0.308	0.3	0.41
Modal shape							
Wheel 1 (front left)	-0.092	0.197	0.150	1	-0.939	1	-0.990
Wheel 2 (front right)	0.092	0.197	0.150	1	0.939	-1	-0.990
Wheel 3 (rear right)	0.081	0.082	-0.320	0.84	1	0.991	1
Wheel 4 (rear left)	-0.081	0.082	-0.320	0.84	-1	-0.991	1
CG displacement	0	1	-0.556	-0.031	0	0	-0.002
Pitch angle	0	0.278	1	-0.001	0	0	0.030
Roll angle	1	0	0	0	-0.106	-0.041	0

3.4.5 Ride and pitch dynamics of the PHIS

The vehicle response under a step pitch moment input can be used to simulate the vehicle's behaviour at braking/acceleration. The comparison results of the vehicles' step response under pitch moment input are shown in Figure 3.11. It shows that the pitch angle of the PHIS vehicle is smaller than the SD vehicle. However, owing to the increased pitch natural frequency, the pitch acceleration levels of the two vehicles are comparable. Regarding C.G vertical displacement and acceleration, the PHIS vehicle has smaller amplitude than the SD vehicle; however, as the magnitude of the vertical response is small under pitch moment input, the effects of vertical acceleration are not significant.

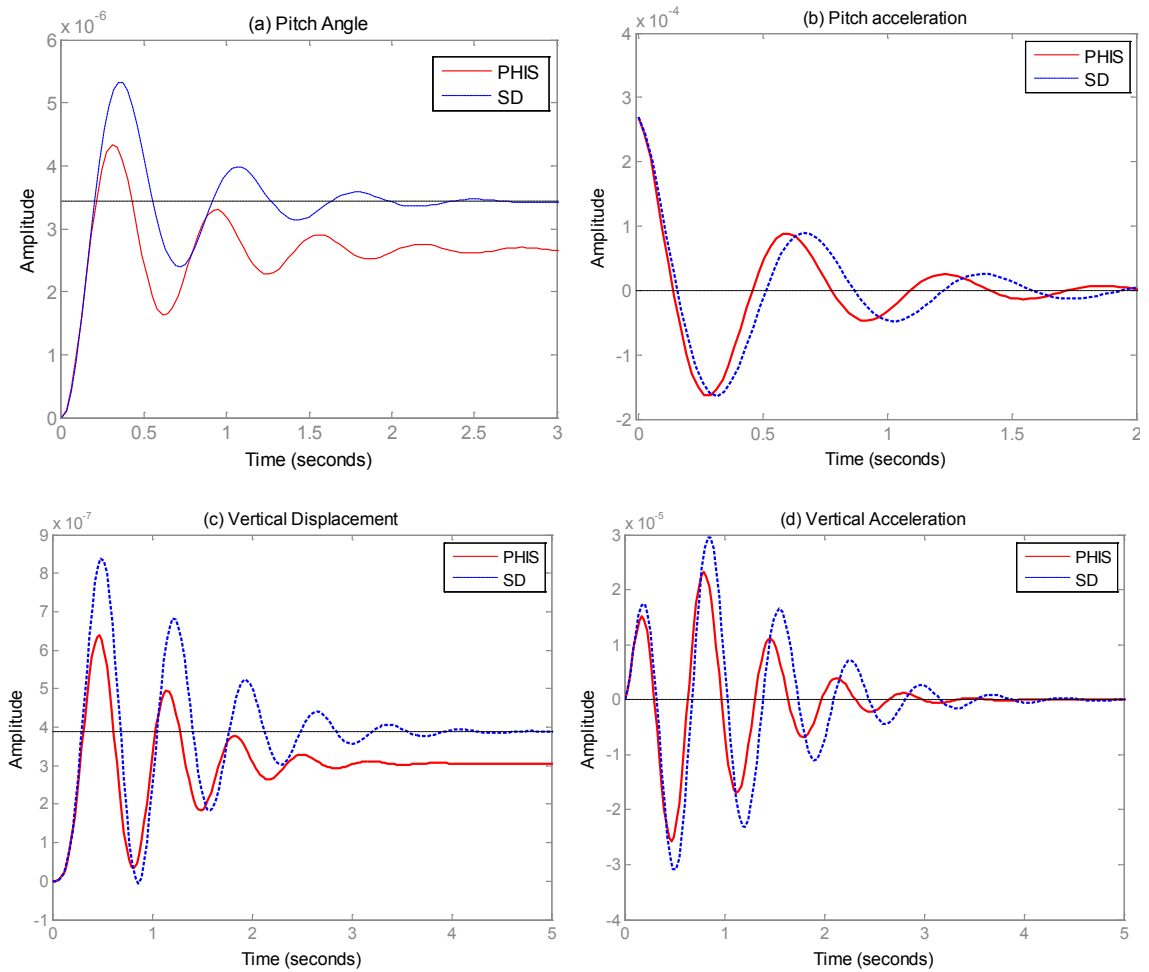


Figure 3. 11: Vehicle responses under step pitch moment: (a) pitch angle (b) pitch acceleration (c) C.G vertical displacement (d) C.G vertical acceleration.

How the vehicle responds under the road axle bump input is directly related to ride comfort. Figure 3.12 show the vehicle's step response results under the front axle bump input. It can be seen that the peak value of the PHIS vehicle's pitch acceleration is slightly higher than that of the SD vehicle due to the increased pitch stiffness.

This suggests that the PHIS suspension system can effectively control the vehicle's longitudinal attitude under braking or acceleration at the cost of a slightly increased pitch angular acceleration level under the axle bump input. The contradictory requirement of the attitude control and ride comfort can be alleviated by the nonlinear pitch stiffness of the PHIS system.

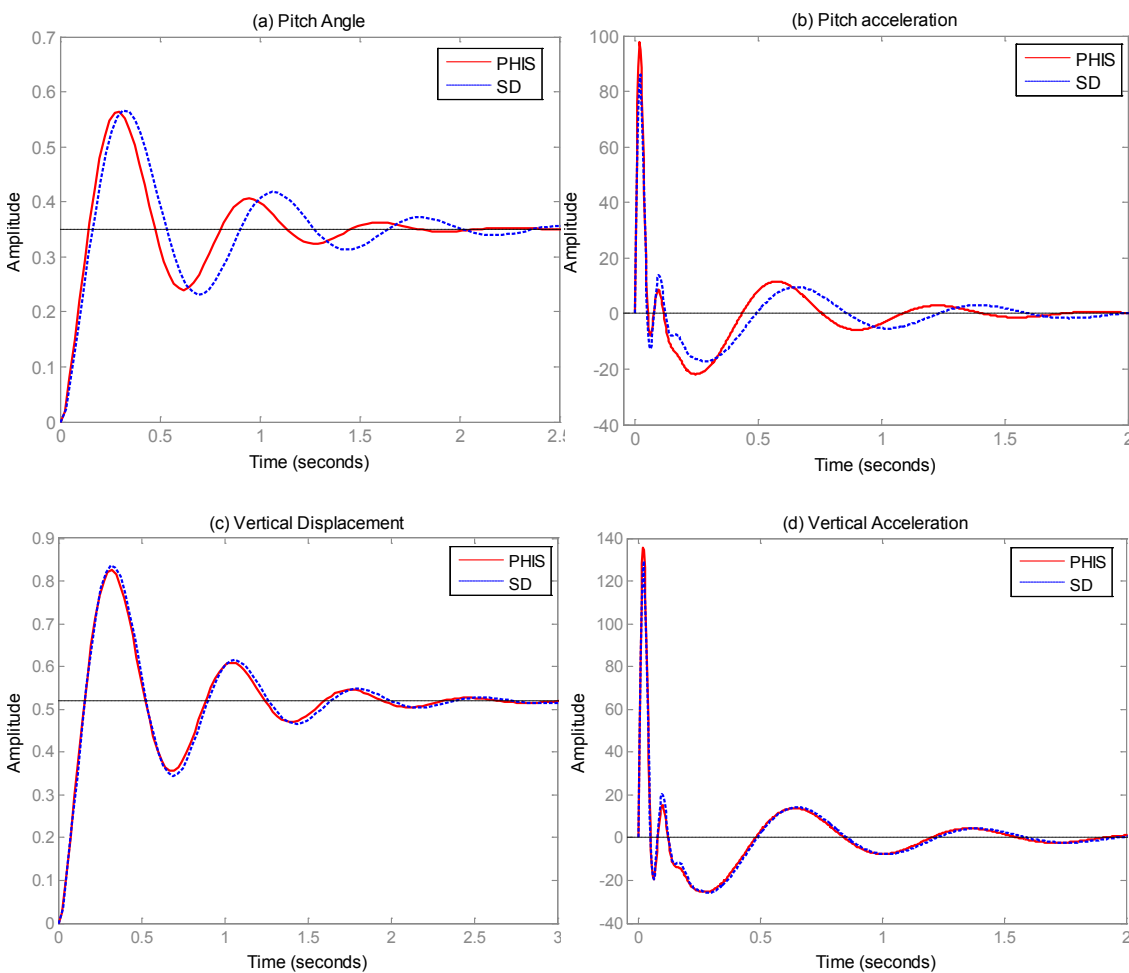


Figure 3. 12: Vehicle responses under step road bump at front axle: (a) pitch angle (b) pitch acceleration (c) C.G vertical displacement (d) C.G vertical acceleration

3.5 Summary

In this chapter, the static and dynamic characteristics of the vehicles with the roll-resistant RHIS system and pitch-resistant PHIS are investigated respectively.

The static suspension characteristics illustrate that the roll stiffness is increased by the RHIS with minimum effects in terms of the other modes; similarly, the pitch stiffness is increased by the PHIS with minimum effects in terms of the other modes. It demonstrates the mode decoupling property of the hydraulically interconnected suspension. The nonlinear roll stiffness of RHIS and the nonlinear pitch stiffness of the PHIS are favourable in order to improve the compromise between ride comfort and directional stability.

The dynamic model of the vehicle with roll plane RHIS or pitch plane PHIS are developed by integrating the full vehicle model and the fluidic model. The gas-spring effects of the accumulators are linearised to facilitate the frequency response analysis of the vehicle system. The models are then used to conduct the modal analysis and frequency response analysis under various road inputs to study the system dynamics.

The modal property of the vehicle with RHIS suspension shows that the roll natural frequency is increased while the bounce, pitch and warp natural frequencies are kept almost the same. In contrast, the anti-roll bars not only increase the roll stiffness, but also stiffen the warp mode which is not desirable for vehicle road holding under rough terrain. The additional roll dampers in the RHIS system provide more parameters for the suspension engineer to fine tune the vehicle's performance under complex driving and road conditions. The vehicle responses under warp road excitation are studied and compared with different suspension configurations to provide a deep understanding of

the vehicle's warp mode characteristics. It shows that roll motion is excited under warp road inputs due to unbalanced roll stiffness distribution while the bounce motion is very small. At the low frequency, the tyre dynamic loads (weight transfer) are directly associated with the suspension warp stiffness. The comparison analysis shows that RHIS has soft suspension warp stiffness while anti-roll bars tend to increase the suspension warp stiffness. Soft suspension warp stiffness is vital for off-road vehicle application because the traction and control are improved and the torsional load/stress on the vehicle body/chassis are reduced with the reduced tyre dynamic loads.

The dynamic characteristics of the pitch controlled PHIS system are also investigated. Modal results show that the pitch natural frequency is increased by the PHIS with minimum effects in terms of the other modes. However, the modal shape of the pitch and bounce mode are affected by the PHIS. By calculating the position of the oscillation center, the pitching center is shifted towards C.G while the bounce center is shifted away from C.G by the PHIS. The step response of the PHIS under vehicle body pitch moment input and front axle road bump input are presented and the results show that the pitch attitude is well controlled during braking or acceleration, but the ride comfort is slightly decreased compared to the SD vehicle.

Chapter 4: Nonlinear 3-Dimensional Full Vehicle Model

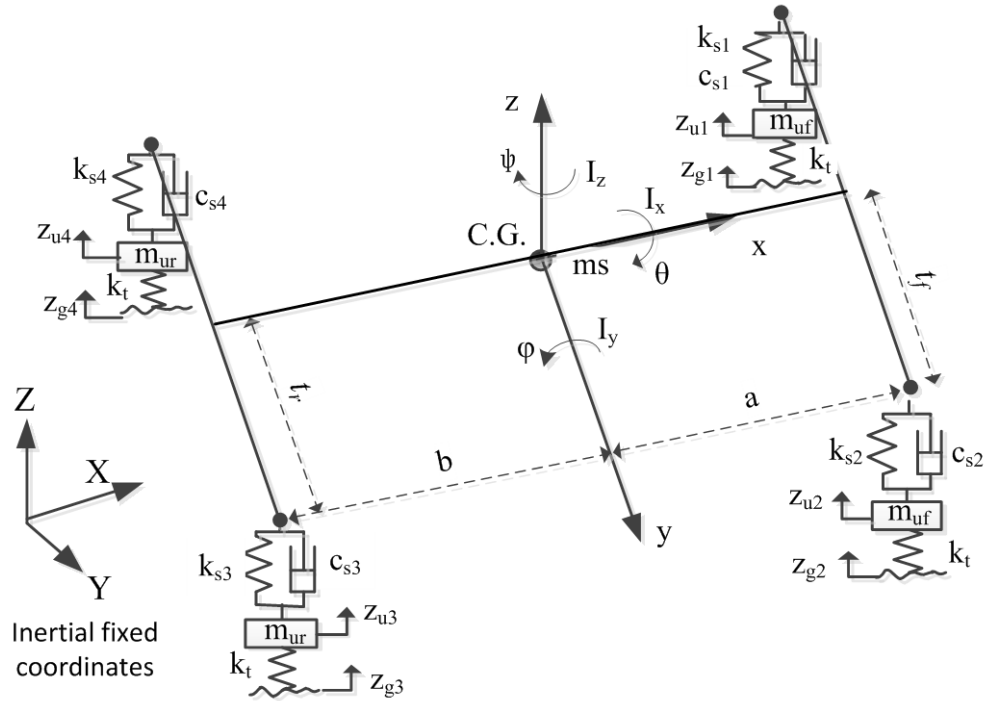
4.1 Vehicle model description

In order to more accurately predict the dynamic response of a practical vehicle, a generalised 14 DOF nonlinear full vehicle model is established. The model incorporates the essential deflection modes of the sprung and unsprung rigid bodies. It also offers the flexibility of modelling nonlinear springs and damping and can simulate the vehicle responses to normal force inputs in case of an active suspension system. It can predict the vehicle behaviour even after wheel lift-off and thus can be used in developing or testing the validity of rollover prediction/prevention strategies. It is considered to be a good compromise between high computational efficiency and accurate predictions of the dynamic response characteristics compared to the complex high order multi-body dynamics model [88, 89].

4.1.1 Model definition and assumptions

Figure 4.1 exhibits the schematic of the two-axle, 14 degree-of-freedom nonlinear vehicle model and the parameter values used for this study are presented in Table 4.1. These parameters are obtained from a Ford SUV. The rigid vehicle body includes six degrees of freedom (DOF) at the vehicle lumped mass centre of gravity which are translational freedoms of motion in the longitudinal, lateral, vertical directions, and rotational freedoms of motion in yaw, roll, and pitch directions. The wheel assemblies are assumed to move together with the vehicle body in the yaw plane. The lateral roll motion of the wheel related to the ground is ignored as it is very small. Thus each

unsprung mass (wheel assemblies) has 2 DOFs which are translational freedom of motion in the vertical direction and rotational freedom of motion in the wheel plane.



(a)

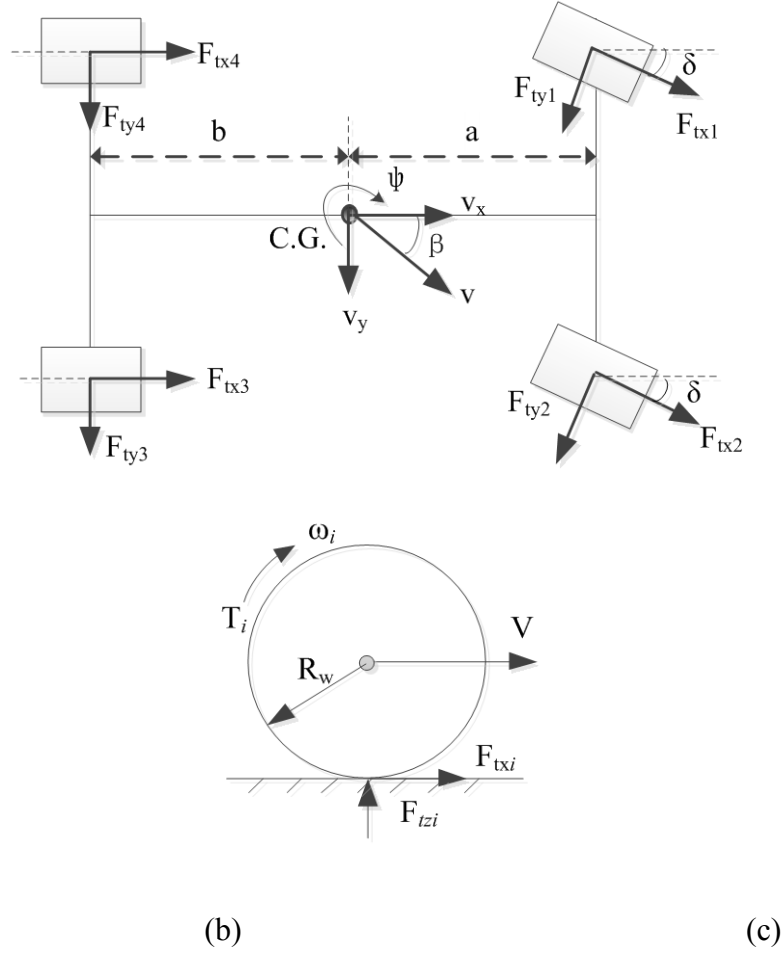


Figure 4. 1: 14-DOF full-vehicle model: (a) vertical representation; (b) lateral representation; (c) tyre rotational dynamics

The position of the vehicle body's center of gravity (C.G) is denoted $O(x,y,z)$ where the roll, pitch and yaw angle are denoted as θ , ϕ , ψ . The vertical displacement of the wheels are denoted Z_{ui} ($i=1,2,3,4$ denotes the front-left, front-right, rear-right, rear-left wheels respectively). m_s , m_{ui} , are the mass of the sprung mass and unsprung mass. The inertial moments of the vehicle body are denoted as I_x , I_y , I_z . The suspension spring stiffness and damping coefficient are denoted as k_{si} , c_{si} , respectively. K_t is the vertical stiffness of the tyres. F_{txi} , F_{tyi} ($i=1,2,3,4$) are the tyre lateral force and longitudinal force of the i th tyre, respectively. Steering angle at front axle is denoted as δ . The distance from C.G to the front axle is a and the distance from C.G to the rear axle is b . The track width of the vehicle at front axle and rear axle are t_f , t_r respectively.

Table 4. 1: Parameters and values of the 14-DOF vehicle dynamic model

Parameters	Symbol	Value
Vehicle sprung mass	m_s	1800 kg
Roll moment inertia of the sprung mass	I_x	870 kgm ²
Pitch moment inertia of the sprung mass	I_y	3700 kgm ²
Yaw moment inertia of the sprung mass	I_z	3800 kgm ²
Roll yaw cross moment inertia	I_{xz}	50 kgm ²
Rolling moment inertia of wheel assemblies	I_w	1 kgm ²
Effective tyre radius	R_w	0.34 m
Distance from the sprung mass CG to the front axle	a	1.37 m
Distance from the sprung mass CG to the rear axle	b	1.48 m
Half width of the front axle	t_f	0.575 m
Half width of the rear axle	t_r	0.575 m
Height from CG to roll axis	h_s	0.4 m
Height from CG to ground	h_g	0.65 m
Front unsprung masses	$m_{u1,2}$	40 kg
Rear unsprung masses	$m_{u3,4}$	42 kg
Spring rate of front suspension	$k_{s1,2}$	42 kN/m
spring rate of rear suspension	$k_{s3,4}$	46 kN/m
Vertical stiffness of tyres	$k_{t1,2,3,4}$	250 kN/m
Front anti-roll bar stiffness	k_{af}	35 kNm/rad
Rear anti-roll bar stiffness	k_{ar}	10 kNm/rad

To simplify the model, a few assumptions are made and some small effects are ignored without affecting the accuracy. They are listed as follows:

- 1) Unless stated, the small angle is assumed in the modelling of the vehicle, such as roll and pitch.
- 2) The changing of the axis position of the roll, pitch and yaw are ignored as it is usually small.

- 3) The mass center of the whole vehicle is the same as the mass center of the sprung mass considering the unsprung mass is small compared to the sprung mass.
- 4) The whole vehicle is in symmetry to the XZ plane so that the inertia product $I_{yz}=I_{yx}=0$. However, I_{xz} is non-zero as the vehicle is normally not symmetrical to the YZ plane.
- 5) The damping characteristic of the tyre is normally small and ignored in the modelling.
- 6) The effects of wheel alignment and camber angle due to the suspension deflection are ignored.
- 7) The suspension geometry and compliance is not considered in this thesis.
- 8) The suspension jack force and roll steering are ignored.

4.1.2 Coordinates and transformation

The vehicle system is a typical multi-body dynamic system. It can be described in the global coordinates (ground-fixed) or the local coordinates (vehicle body- or wheel-fixed coordinates). The body-fixed coordinate frame $oxyz$ is attached to the center-of-gravity (C.G.) of the vehicle body, and aligned along the principle directions of the vehicle. The global coordinate frame $OXYZ$ is fixed on the ground. In the different coordinates, the vehicle has a different inertia tensor and it can be transformed between different coordinates through the Euler angle. The vehicle translational and rotational velocities in the body-fixed coordinates frame $oxyz$ are expressed as:

$$\begin{bmatrix} V_x \\ V_y \\ V_z \end{bmatrix}_b = \begin{bmatrix} u \\ v \\ w \end{bmatrix}; \quad \begin{bmatrix} \omega_x \\ \omega_y \\ \omega_z \end{bmatrix}_b = \begin{bmatrix} \dot{\theta} \\ \dot{\phi} \\ \dot{\psi} \end{bmatrix} \quad (4.1)$$

The translational movement of the vehicle is a related movement with reference to the ground-fixed inertial coordinates. The rotational movement of the vehicle body is related to the body-fixed coordinates. It is simpler to formulate the equations of the motion of the vehicle in the body-fixed coordinates as the inertia tensor remains independent of time in the reference frame. The z axis of the vehicle body-fixed coordinates frame $oxyz$ is parallel to the Z axis of ground-fixed coordinates frame $OXYZ$ and it rotates related to the ground-fixed coordinates frame with a course angle τ which is the sum of the side slip angle β and the yaw angle ψ . The vehicle trajectory with respect to the ground-fixed inertial coordinate frame $oxyz$ can be derived such that:

$$\begin{aligned} X &= \int \dot{X} dt = \int V \cos \tau dt \\ Y &= \int \dot{Y} dt = \int V \sin \tau dt \end{aligned} \quad (4.2)$$

where $V = \sqrt{u^2 + v^2}$, $\tau = \beta + \psi$, $\beta = \text{atan} \frac{v}{u}$.

4.2 Equations of motion

4.2.1 Equations of vehicle translational motion

The vehicle dynamics in the spatial movement of a rigid body includes the translational motions and rotational motions. Translational motions include the forward or backward movement along the x axis, the side slip movement along the y axis and the vertical movement along the z axis. The wheel assemblies (unsprung mass) are assumed to have the same translation motion of the vehicle body in the longitudinal and lateral direction. Rotational motions are only considered for the vehicle body which include the roll movement around the x axis, the pitch movement around the y axis and the yaw movement around the z axis.

The tyre forces are the main external forces of the vehicle system which can be developed from the Magic formula tyre model. The aero resistance and grade resistance can be included as the disturbance forces. Assuming small motion, the equations of motion for the sprung mass are developed by applying Newton's second law.

The longitudinal motion along the x axis is coupled with the pitch and yaw motion, the equation is expressed as:

$$\sum F_X = m_s a_x + \sum_{i=1}^4 m_{ui} a_x \quad (4.3)$$

$$\sum F_X = \sum_{i=1}^4 F_{txi} \cos \delta_i - \sum_{i=1}^4 F_{tyi} \sin \delta_i + w_x$$

$$a_x = \dot{u} - v\dot{\psi} + w\dot{\phi}$$

where a_x is the longitudinal acceleration, w_x is the disturbance forces in the X direction, $\sum F_X$ is the total of the longitudinal forces received by the vehicle. The tyre lateral forces and longitudinal force of the i th tyre are F_{txi} , F_{tyi} ($i=1,2,3,4$) can be obtained from the tyre model. δ_i is the steering angle at the i th wheel. An identical front-wheel steering input δ is assumed for the front wheels and the rear steering wheel is zero for the front steering vehicle.

When the aero and grade resistance is not considered, equation (4.3) is rewritten as:

$$(m_s + 4m_u)(\dot{u} - v\dot{\psi} + w\dot{\phi}) = (F_{tx1} + F_{tx2}) \cos \delta + (F_{ty1} + F_{ty2}) \sin \delta + F_{tx3} + F_{tx4} - m_s g \sin \varphi \quad (4.4)$$

Similarly, the lateral motion along the y axis is coupled with the yaw and roll motion.

The lateral equation is expressed as:

$$\sum F_y = m_s a_y + \sum_{i=1}^4 m_{ui} a_y \quad (4.5)$$

$$\sum F_y = \sum_{i=1}^4 F_{txi} \sin \delta_i + \sum_{i=1}^4 F_{tyi} \cos \delta_i + w_y$$

$$\alpha_y = \dot{v} + u\dot{\psi} - w\dot{\theta}$$

which can be rewritten as:

$$\begin{aligned} (m_s + 4m_u)(\dot{v} + u\dot{\psi} - w\dot{\theta}) &= (F_{tx1} + F_{tx2}) \sin \delta + (F_{ty1} + F_{ty2}) \cos \delta \\ &+ F_{ty3} + F_{ty4} + m_s g \cos \varphi \sin \theta \end{aligned} \quad (4.6)$$

In the vertical direction, the vehicle body (sprung mass) has the loads of suspension strut forces which are transmitted from the tyre vertical dynamic loads. The vertical motion of vehicle body is coupled with the pitch and roll motion. The equation of the motion of the vehicle body along the z axis is expressed as:

$$m_s a_z = \sum F_Z^s = \sum_i F_{si} + w_z \quad (4.7)$$

$$\alpha_z = \dot{w} - u\dot{\varphi} + v\dot{\theta}$$

where $\sum F_Z^s$ is the total vertical forces in the z direction received by the vehicle body, F_{si} is the suspension strut force of the *i*th wheel. The equation can be rewritten as:

$$m_s (\dot{w} - u\dot{\varphi} + v\dot{\theta}) = F_{s1} + F_{s2} + F_{s3} + F_{s4} - m_s g \cos \varphi \cos \theta \quad (4.8)$$

4.2.2 Equations of vehicle rotational motion

In classical mechanics, Euler's rotation equations are a vectorial quasi-linear first-order ordinary differential equation describing the rotation of a rigid body, using a rotating reference frame with its axes fixed to the body and parallel to the body's principal axes of inertia. Their general form is:

$$I \cdot \dot{\omega} + \omega \times (I \cdot \omega) = M \quad (4.9)$$

where M is the applied torques, I is the inertia matrix, and ω is the angular velocity about the principal axes.

In the vehicle body-fixed coordinates, they become:

$$\begin{aligned} I_x \dot{\omega}_x + (I_z - I_y) \omega_y \omega_z - I_{xz} (\omega_x \omega_y + \dot{\omega}_z) &= M_x \\ I_y \dot{\omega}_y + (I_x - I_z) \omega_x \omega_z + I_{xz} (\omega_x^2 - \omega_z^2) &= M_y \\ I_z \dot{\omega}_z + (I_y - I_x) \omega_x \omega_y + I_{xz} (\omega_y \omega_z - \dot{\omega}_x) &= M_z \end{aligned} \quad (4.10)$$

where M_i ($i=x,y,z$) are the components of the applied torques, I_i are the moments of inertia and ω_i are the components of the angular velocity about the axes.

The applied torques on the vehicle body can be expressed as:

$$\begin{aligned} M_x &= t_f (F_{s1} - F_{s2}) + t_r (F_{s4} - F_{s3}) + h_s [(F_{x1} + F_{x2}) \sin \delta + (F_{y1} + F_{y2}) \cos \delta \\ &\quad + F_{y3} + F_{x4} + m_s g \cos \varphi \sin \theta] \\ M_y &= a(F_{s1} + F_{s3}) - b(F_{s2} + F_{s4}) + h_g [(F_{x1} + F_{x2}) \cos \delta + (F_{y1} + F_{y2}) \sin \delta \\ &\quad + F_{x3} + F_{x4} - m_s g \sin \varphi] \\ M_z &= a[(F_{y1} + F_{y2}) \cos \delta - (F_{x1} + F_{x2}) \sin \delta] - b(F_{y3} + F_{y4}) + t_f [(F_{x1} - F_{x2}) \cos \delta \\ &\quad + (F_{y1} - F_{y2}) \sin \delta] + t_r (F_{x4} + F_{x3}) \end{aligned} \quad (4.11)$$

where h_s is the roll center height, h_g is the center of gravity height of vehicle body.

When we substitute the equation (4.1) and (4.11) into equation (4.10), the equations of rotational motion of the vehicle body can be expressed as:

$$I_x \ddot{\theta} = (I_y - I_z) \dot{\phi} \dot{\psi} + I_{xz} (\dot{\theta} \dot{\phi} + \dot{\psi}) + t_f (F_{s1} - F_{s2}) + t_r (F_{s4} - F_{s3}) \\ + h_s [(F_{x1} + F_{x2}) \sin \delta + (F_{y1} + F_{y2}) \cos \delta + F_{y3} + F_{x4} + m_s g \cos \varphi \sin \theta] \quad (4.12)$$

$$I_y \ddot{\phi} = (I_z - I_x) \dot{\theta} \dot{\psi} - I_{xz} (\dot{\theta}^2 - \dot{\psi}^2) + a(F_{s1} + F_{s3}) - b(F_{s2} + F_{s4}) \\ + h_g [(F_{x1} + F_{x2}) \cos \delta + (F_{y1} + F_{y2}) \sin \delta + F_{x3} + F_{x4} - m_s g \sin \varphi] \quad (4.13)$$

$$I_z \ddot{\psi} = (I_x - I_y) \dot{\theta} \dot{\phi} - I_{xz} (\dot{\phi} \dot{\psi} - \ddot{\theta}) + a[-(F_{x1} + F_{x2}) \sin \delta + (F_{y1} + F_{y2}) \cos \delta] \\ - b(F_{y3} + F_{y4}) + t_f [(F_{x1} - F_{x2}) \cos \delta + (F_{y1} - F_{y2}) \sin \delta] + t_r (F_{x4} + F_{x3}) \quad (4.14)$$

4.2.3 Equations of motion of wheels

For unsprung mass (wheels), the equations of motion at vertical direction are expressed as the function of road elevation z_{gi} :

$$m_{ui} \ddot{z}_{ui} = -F_{si} + k_{ti} (z_{gi} - z_{ui}), \quad i = 1, 2, 3, 4 \quad (4.15)$$

The vertical properties of pneumatic tyres are represented by linear stiffness k_t assuming point-contact with the road surface. The tyre damping is normally small and can be ignored.

The rotational dynamics of each wheel assembly is derived from the forces and moments acting on the wheel, as illustrated in Figure 4.1 (c):

$$I_{wi} \dot{\omega}_i = F_{xi} R_{wi} - T_i, \quad i = 1, 2, 3, 4 \quad (4.16)$$

where I_{wi} is the moment of inertia of the wheel, ω_i is the wheel rotating velocity, R_{wi} is the effective radius of the tyre, T_i is the braking or accelerating torque applied on the wheel.

4.2.4 Suspension strut force formulation

In the above equations, the strut forces F_{si} ($i=1, 2, 3, 4$) consist of spring forces, damping forces and forces from anti-roll bars. The equations are shown as:

$$F_{si} = F_{ki}(X_{si}) + F_{ci}(\dot{X}_{si}) + F_{ARBi} \quad (4.17)$$

where spring force F_{ki} is a function of relative displacement X_{si} between the unsprung mass and each corner of the sprung mass, damping force F_{ci} is a function of the relative velocity \dot{X}_{si} .

Suspension stiffness nonlinearity such as bump stop can be conveniently included if needed. The vehicle suspension damping ratio is usually direction and velocity dependant. The damping is small in compression (bump) but large in extension (rebound). The damping rate is relatively high at low speed to control the vehicle attitude; it is relatively low at high speed for improved ride. Figure 4.2 are the typical basic stiffness and damping force characteristics obtained from a median sized sport utility vehicle, with the extension force being positive, and the compression force being negative. Look-up tables can be used to represent the actual characteristics of the stiffness and damping of suspension struts from experimental testing.

According to geometry relationship, X_{si} is expressed as:

$$\begin{aligned} X_{s1} &= z_{u1} - z - t_f \theta - a\varphi; & X_{s2} &= z_{u2} - z + t_f \theta - a\varphi \\ X_{s3} &= z_{u3} - z + t_f \theta + a\varphi; & X_{s4} &= z_{u4} - z - t_f \theta + a\varphi \end{aligned} \quad (4.18)$$

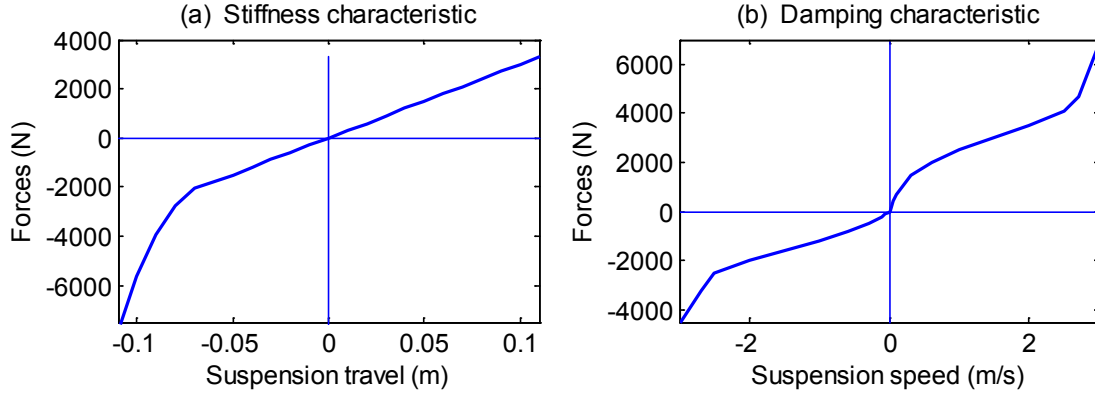


Figure 4. 2: Suspension strut force characteristics (a) Stiffness; (b) Damping

The anti-roll bar model is derived by treating it massless torsional spring. Assuming linear front and rear rotational stiffness of the ARBs as k_{af} and k_{ar} , respectively, the ARB forces $F_{ARBi(i=1,2,3,4)}$ are expressed as:

$$\begin{aligned} F_{ARB1} &= (X_{s1} - X_{s2}) \frac{k_{af}}{4t_f^2}; & F_{ARB2} &= (X_{s2} - X_{s1}) \frac{k_{af}}{4t_f^2} \\ F_{ARB3} &= (X_{s3} - X_{s4}) \frac{k_{ar}}{4t_r^2}; & F_{ARB4} &= (X_{s4} - X_{s3}) \frac{k_{ar}}{4t_r^2} \end{aligned} \quad (4.19)$$

When we substitute equation (4.18) and (4.190) into the equation (4.17), the suspension strut forces can be obtained.

4.3 Nonlinear tyre model

4.3.1 Tyre model basics

Tyres are essential components interacting with the road. The tyre contact patch is the only point of contact of the vehicle with the ground, it must allow for acceleration, cornering and braking whatever the road, driving or weather conditions. At the same time, it gives drivers and their passengers a feeling of comfort.

The force system that a tyre receives from the ground is assumed to be located at the center of the tyre print and can be developed along x , y , z axes. Therefore, the interaction of a tyre with the road generates a 3D force system including three forces and three moments, as shown in Figure 4.3 [90]. It includes longitudinal force F_{tx} , lateral force F_{ty} , normal force F_z , roll moment M_x , pitch moment M_y , and yaw moment M_z . The effects of tyre force moments to the vehicle dynamics are normally small. In the actual application, the tyre is mainly in a combined condition of longitudinal slip, side slip and vertical load. The tyre vertical load can be presented by the tyre vertical stiffness and damping.

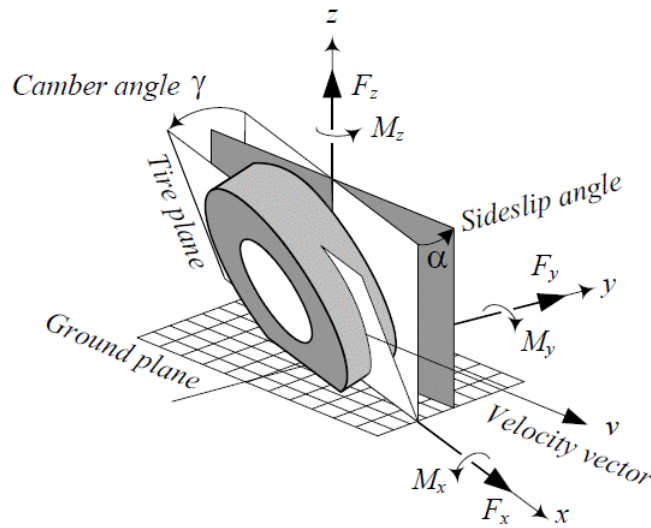


Figure 4. 3: Tyre coordinate system

The inputs of the tyre model include the normal tyre load, the longitudinal slip ratio and the sideslip angle; the outputs include the longitudinal tyre force F_{xi} and lateral tyre force F_{yi} . The aligning torque is ignored here as it is usually very small. By assuming small roll and pitch angles, the longitudinal slip ratio κ_i and side-slip angle α_i used in the tyre model can be expressed in equation (4.20) and (4.21) as:

$$\begin{aligned}
\kappa_1 &= \left(1 - \frac{R_{w1}\omega_1}{(u + t_f\dot{\psi})\cos\delta + (v + a\dot{\psi})\sin\delta}\right) \\
\kappa_2 &= \left(1 - \frac{R_{w2}\omega_2}{(u - t_f\dot{\psi})\cos\delta + (v + a\dot{\psi})\sin\delta}\right) \\
\kappa_3 &= \left(1 - \frac{R_{w3}\omega_3}{u - t_r\dot{\psi}}\right) \\
\kappa_4 &= \left(1 - \frac{R_{w4}\omega_4}{u + t_r\dot{\psi}}\right)
\end{aligned} \tag{4.20}$$

$$\begin{aligned}
\alpha_1 &= \delta - \arctan\left(\frac{v + a\dot{\psi}}{u + t_f\dot{\psi}}\right); \quad \alpha_2 = \delta - \arctan\left(\frac{v + a\dot{\psi}}{u - t_f\dot{\psi}}\right) \\
\alpha_3 &= -\arctan\left(\frac{v - b\dot{\psi}}{u - t_r\dot{\psi}}\right); \quad \alpha_4 = -\arctan\left(\frac{v - b\dot{\psi}}{u + t_r\dot{\psi}}\right)
\end{aligned} \tag{4.21}$$

The tyre normal load includes the static tyre load and dynamic tyre load. The static tyre load is:

$$\begin{aligned}
F_{tz1}^s &= F_{tz2}^s = \frac{b \cdot m_s g}{2(a+b)} + m_{uf} g \\
F_{tz3}^s &= F_{tz4}^s = \frac{a \cdot m_s g}{2(a+b)} + m_{ur} g
\end{aligned} \tag{4.22}$$

The tyre dynamic load is:

$$F_{tzi}^D = k_{ti}(Z_{gi} - Z_{ti}) + c_{ti}(\dot{Z}_{gi} - \dot{Z}_{ti}) \tag{4.23}$$

Then, the total tyre normal load is the sum of static load and dynamic load, which is:

$$F_{tzi} = F_{tzi}^D + F_{tzi}^s \tag{4.24}$$

4.3.2 Magic Formula tyre model

Pacejka [91, 92] has developed a series of tyre design models over the last 20 years.

They were named the 'magic formula' because there is no particular physical basis for

the structure of the equations chosen, but they fit a wide variety of tyre constructions and operating conditions. Each tyre is characterised by a few coefficients for each important force that it can produce at the contact patch, typically lateral and longitudinal force, and self-aligning torque, as a best fit between experimental data and the model. These coefficients are then used to generate equations showing how much force is generated for a given vertical load on the tyre, camber angle and slip angle.

The tyre force is formulated as the trigonometric function of the generalised theoretical slip quantity x (that is: at either lateral slip α or longitudinal slip κ):

$$Y = D \sin \left\{ C \arctan \left[Bx - E(Bx - \arctan(Bx)) \right] \right\} + S_v \quad (4.25)$$

where Y is output variable F_{tx} or F_{ty} ; X is input variable α or κ . And,

B : stiffness factor

C : shape factor

D : peak value

E : curvature factor

S_v : vertical shift

The parameters are further related to the tyre normal load and road friction with a number of coefficients which can be physically tested by the tyre manufacturer. For the longitudinal tyre force in the pure longitudinal slip, they are defined as:

$$\begin{aligned} C_x &= a_0 \\ D_x &= (a_1 F_{tz}^2 + a_2 F_{tz}) \\ BCD_x &= (a_3 F_{tz}^2 + a_4 F_{tz}) e^{-a_5 F_{tz}} \\ B_x &= \frac{BCD_x}{C_x D_x} \\ Ex &= (a_6 F_{tz}^2 + a_7 F_{tz} + a_8) \\ S_{hx} &= a_9 F_{tz} + a_{10} \\ S_{vx} &= 0 \\ x &= \alpha + S_{hx} \end{aligned}$$

where the factors a_0 to a_{10} can be obtained from the empirical data of tyre testing.

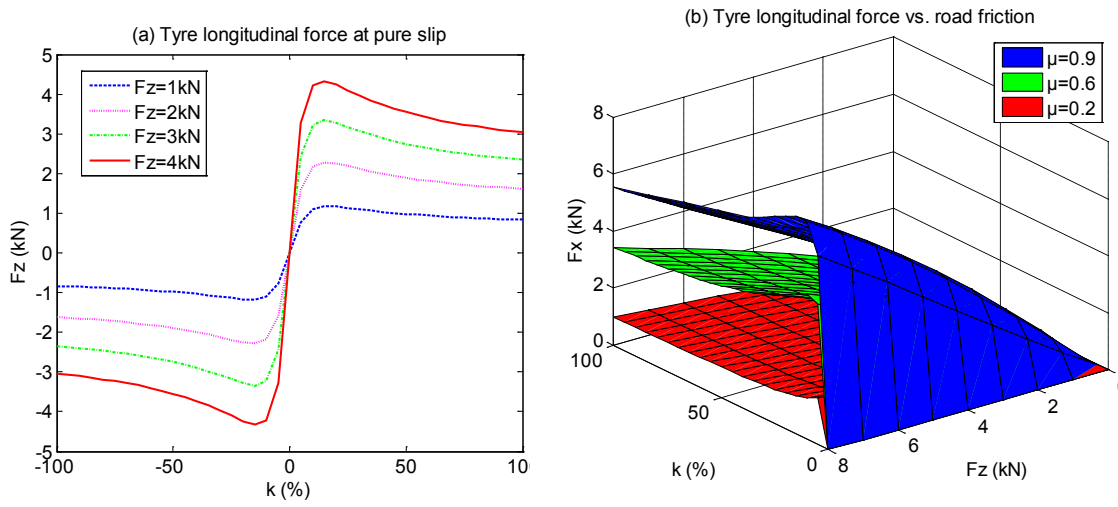


Figure 4. 4: Tyre longitudinal force at pure longitudinal slip (a) Tyre longitudinal force vs. longitudinal slip (b) Tyre longitudinal force vs. longitudinal slip and road friction

The relationship of pure longitudinal slip ratio and the tyre longitudinal force according to the tyre magic formula is presented in Figure 4.4 with tyre data obtained from a typical car tyre 235/60 R16. It can be seen that the tyre longitudinal force is not only related to the longitudinal slip ratio but also related to the tyre normal force and the road friction coefficient. The tyre longitudinal force increases when the slip ratio increases, but it saturates at around slip ratio of 10-20%. The tyre longitudinal force will decrease when the slip ratio further increases after the saturation. Therefore, for the optimal braking performance, the slip ratio needs to be controlled to maintain the point of maximum longitudinal force to achieve the maximum deceleration.

Similarly for the lateral tyre force in the pure side slip, the coefficients are defined as:

$$\begin{aligned}
C_y &= b_o \\
D_y &= (b_1 F_{tz}^2 + b_2 F_{tz}) \\
BCD_y &= b_3 \sin(2 \arctan \frac{F_{tz}}{b_4})(1 - b_5 |\gamma|) \\
B_y &= \frac{BCD_y}{C_y D_y} \\
E_y &= (b_6 F_{tz} + b_7) \\
S_{hy} &= b_8 \gamma + b_9 F_{tz} + b_{10} \\
S_{vy} &= b_{11} F_{tz} \gamma + b_{12} F_{tz} + b_{13} \\
x &= \kappa + S_{hy}
\end{aligned}$$

where b_0 - b_{13} could be obtained from the tyre manufacturer.

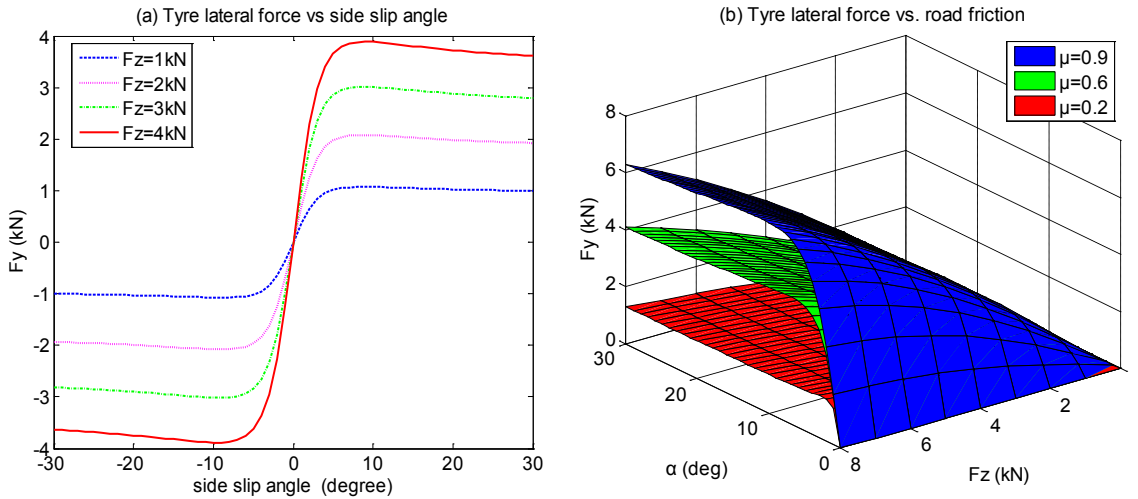


Figure 4. 5: Tyre lateral force at pure side slip (a) Tyre lateral force vs. side slip angle
(b) Tyre lateral force vs. side slip and different road frictions

The relationship of tyre lateral force with the side slip angle, tyre normal force and road friction are presented in Figure 4.5. Similarly, in order to obtain the maximum lateral tyre force, the slip angle needs to be controlled at the optimal range. It also shows that the road friction will greatly affect the lateral tyre force. The vehicle is more likely to spin out on a wet or icy road at cornering due to the low lateral force.

In the real vehicle application, the tyres are normally in a combined slip situation which involves not only side slip but also longitudinal slip. The equivalent theoretical slip quantities can be expressed in a general form as:

$$\begin{aligned}\sigma_x &= \frac{\kappa}{1 + \kappa} \\ \sigma_y &= \frac{\tan \alpha}{1 + \kappa}\end{aligned}\quad (4.26)$$

And,

$$\sigma = \sqrt{\sigma_x^2 + \sigma_y^2} \quad (4.27)$$

In the combined slip model, the longitudinal and lateral tyre force components can be obtained by employing the theoretical slip from the pure slip characteristics as:

$$F_{tx} = \frac{\sigma_x}{\sigma} F_{tx0}(\sigma), \quad F_{ty} = \frac{\sigma_y}{\sigma} F_{ty0}(\sigma) \quad (4.28)$$

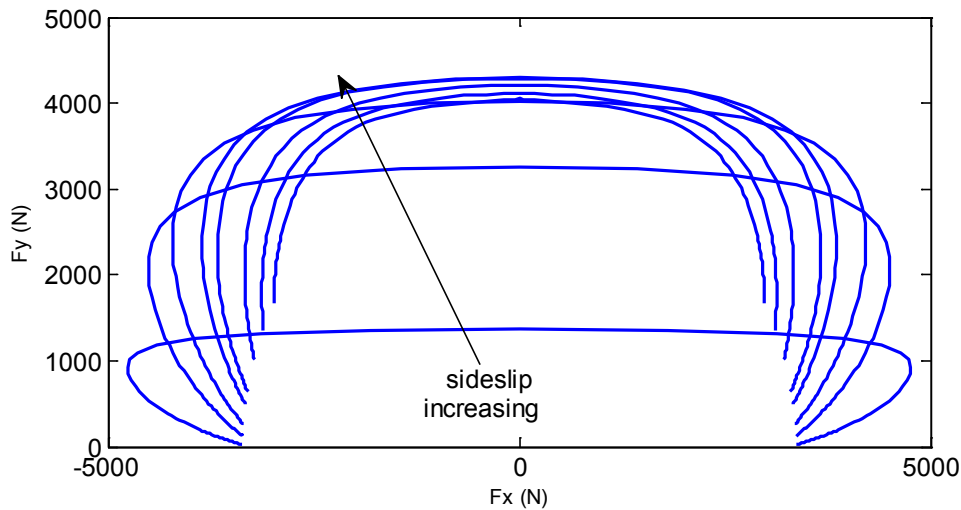


Figure 4. 6: Tyre friction ellipse of the combined slip condition

Figure 4.6 presents the coupling of tyre lateral force and longitudinal force with a constant tyre normal load. From the bottom to the top, the side slip angle of the

envelope curves are 2° , 4° , 6° , 8° , 10° , 15° , 20° , 25° . It shows that the tyre adhesive limit is not a circle but an ellipse. The friction limitation is described by the envelope curve. However, when the slip angle exceeds 8° , the semi-minor axis of the ellipse will decrease with respect to the increase of side slip angle.

4.4. Vehicle dynamic response of fishhook steering

A generalised 14-DOF vehicle model which includes ride model, handling, and a tyre model is developed for the study of vehicle dynamics. This model is highly nonlinear which includes the coupling of rigid body motions, spring and damping nonlinearity and the tyre nonlinearity. In this section, the coupling of vehicle yaw and roll is investigated in the fishhook maneuver with the developed vehicle model.

4.4.1 Model validation

The fishhook maneuver is a dynamic test adopted by the National Highway Traffic Safety Administration (NHTSA) of the United States of America to evaluate the vehicle's rollover resistance instead of the Static Stability Factors (SSF) [93]. The maneuver uses steering inputs that approximate the steering a driver acting in panic might use in an effort to regain lane position after dropping two wheels off the road way onto the shoulder. NHTSA has often described it as a road edge recovery maneuver. There are two types of fishhook maneuver, the fixed time fishhook and the roll rate feedback fishhook. Due to the simplicity of implementation, the fixed time fishhook is chosen to investigate the effect of lateral coupling. The steering wheel signal is shown in Figure 4.7.

14 DOF full vehicle model based on Matlab/Simulink is verified by using CARSIM (commercial vehicle dynamic analysis software). The vehicle initial entrance speed is

set to 60km/h. The vehicle responses of trajectory, longitudinal speed, yaw rate and roll angle are compared in Figure 4.8. From the comparison results, the trend between the 14DOF model and CARSIM simulations was similar with a small difference in the magnitude. The difference arises due to the model simplification such as the tyre chamber and toe changes, suspension kinematics and compliance, as well as roll center changes. The validation result has proven that the 14 DOF vehicle model is accurate enough to be used to represent actual vehicle dynamic behaviour.

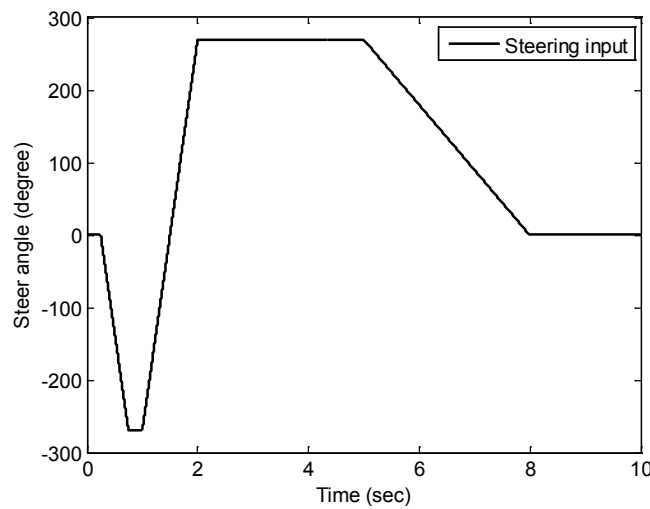
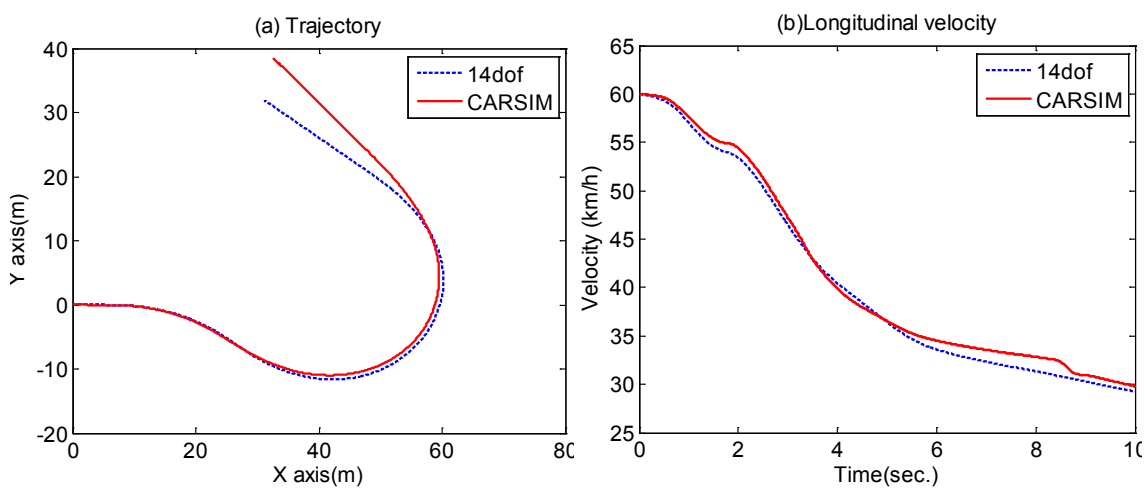


Figure 4. 7: Steering wheel input of fishhook maneuver



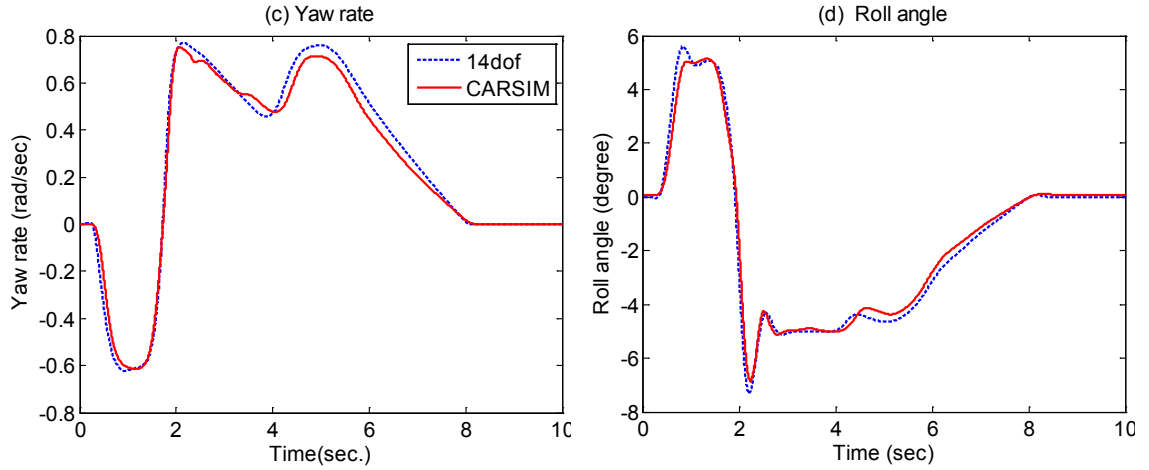


Figure 4. 8: Vehicle responses comparison of 14DOF and CARSIM model: (a) Trajectory (b) Vehicle velocity (c) Yaw rate (d) Roll angle

4.4.2 The sensitivity of vehicle speed and suspension roll stiffness

Rollover accidents are dangerous events. The crash data shows that approximately two-thirds of on-road rollovers are untripped [50]. Rollover incidents involve a variety of factors, while the vehicle speed and suspension roll stiffness are critical to the untripped rollover of light vehicles (passenger car, pick-ups, vans and sport utility vehicles).

The effects of vehicle speed in the fishhook maneuver are evaluated by varying the vehicle speed from 40km/h to 70km/h in the simulation. The vehicle responses are presented in Figure 4.9 with vehicle parameters obtained from a typical Sport Utility Vehicle (SUV).

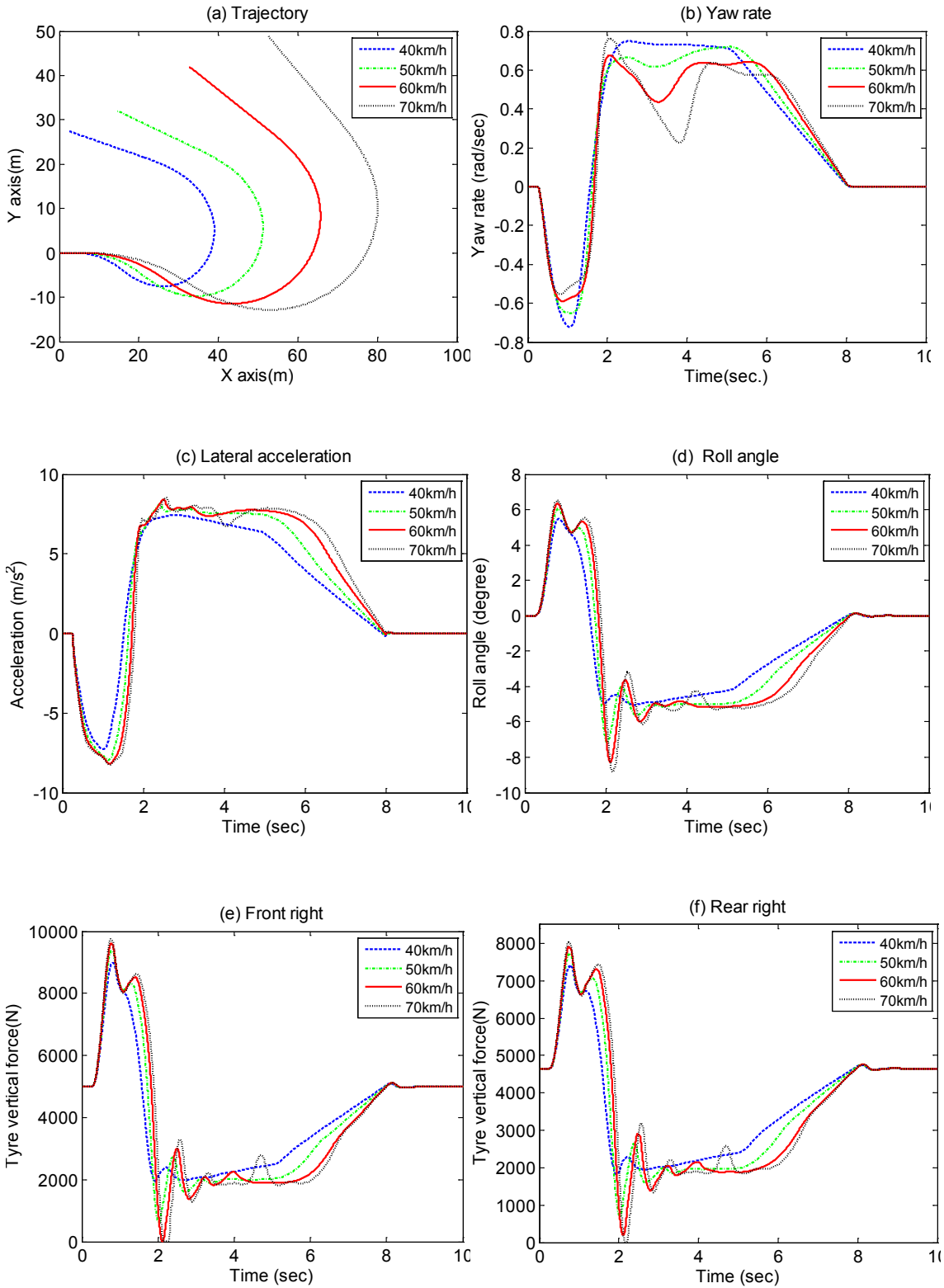
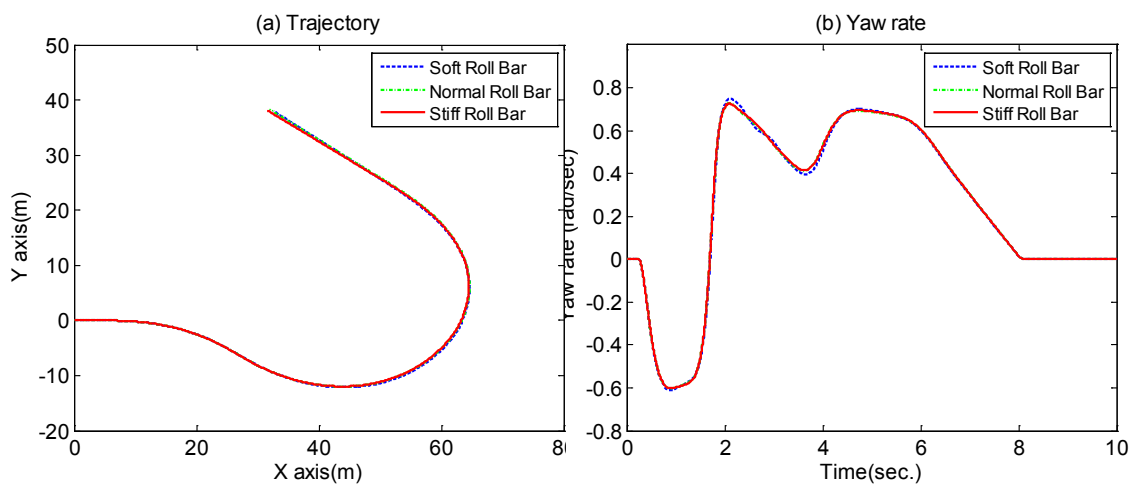


Figure 4. 9: Vehicle responses of fishhook maneuver at different vehicle speeds

The vehicle trajectory and yaw rate responses are shown in Figure 4.9 (a) and (b). It can be seen from the results that the trajectory is longer when the vehicle speed increases.

The amount of yaw rate indicates a vehicle's steering characteristics. If the yaw rate is higher than the desired yaw rate, this means there is an over-steering situation but if the yaw rate is lower than the desired yaw rate, this means that the vehicle is under-steering. The yaw rate responses show that the under-steering tendency becomes more evident with the high vehicle speed, especially at a time range of between 3 seconds and 5 seconds. The vehicle's lateral and roll responses are presented in Figure 4.9 (c) and (d). The developed vehicle lateral acceleration is not proportional to the vehicle speed. The maximum lateral acceleration is determined by the road friction such that it won't continue to increase when the maximum lateral acceleration is reached at about 50km/h on the dry road, and the vehicle starts to slide out when speed goes up further. The magnitude of roll angle is directly related to the roll moment induced by vehicle lateral acceleration. It shows the roll angle gets larger when the vehicle entrance speed is higher. When the lateral acceleration saturates, the increment of vehicle roll angle becomes small. The tyre load transfers are mainly related to the roll angle and lateral acceleration. Figure 4.9 (e) and (f) present the tyre loads at the wheel station of front right and rear right. It can be seen that the front right tyre load approaches zero when the initial vehicle speed is 60km/h. As the vehicle speed increases to 70km/h, both front and rear right side tyres lift off the ground which means a greater risk of rollover.



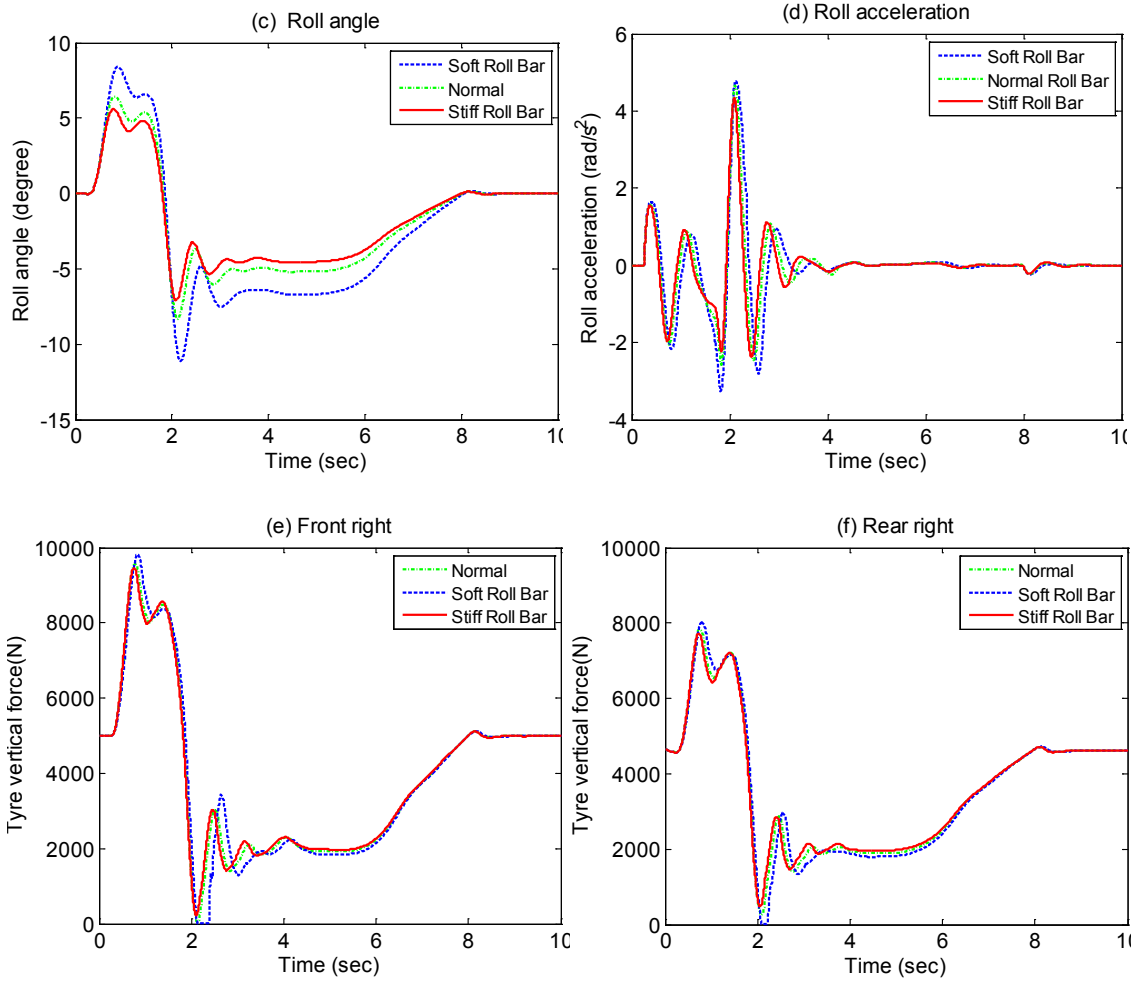


Figure 4. 10: Vehicle responses of fishhook manoeuvre with different roll stiffness

In some cases, vehicle rollovers take place due to roll instability. To evaluate the effects of suspension roll stiffness, three sets of anti-roll bars parameters are used in the simulation. In addition to the normal parameters in Table 4.1, the total anti-roll bar stiffness is reduced to 40% of its original value for the second case and increased to 140% of its original value for the third case. The roll stiffness distribution has a significant influence on the vehicle yaw dynamics. The roll stiffness distribution biased towards the rear axle will result in severe under-steering in extreme steering condition such as the fishhook maneuver. To eliminate the effects of vehicle yaw instability, the roll stiffness distribution is tuned to have the same yaw rate for all three cases.

The responses of three different roll stiffness vehicles are compared in the fishhook tests with 60 km/h initial vehicle velocity. Figure 4.10 (a) and (b) illustrate that all three cases have a similar trajectory and yaw rate response to the same steering inputs. Figure 4.10 (c) and (d) present the comparison of the roll angle and roll acceleration responses of the vehicles. The vehicle with a soft roll bar has the largest magnitude of roll angle and acceleration while the vehicle with a stiff roll bar has the smallest magnitude of roll angle and roll acceleration. The vehicle tyre loads are presented in Figure 4.10 (e) and (f). It shows that the soft roll bar vehicle's tyres have lost contact with the ground while the stiff roll bar vehicle still maintains tyre ground contact. The lost contact between tyre and ground presents a higher rollover risk and the roll instability can be improved by employing the stiff anti-roll bars but at the same time not significantly reducing the ride comfort.

4.5 Summary

A generalised 14 DOF nonlinear vehicle model is developed to predict the coupling of longitudinal, lateral and vertical dynamics of the on-road two-axle vehicle in this chapter. The magic formula tyre model is used to include the nonlinear behaviour of the pneumatic tyre. The proposed model is validated by the commercial software CARSIM and the results illustrate the 14 DOF is accurate enough for a vehicle dynamics study.

The sensitivity of the vehicle speed and roll stiffness are investigated in the fishhook maneuver test. Severe under-steering is presented when the vehicle speed is too high. The lateral tyre force saturates at its maximum value so that the vehicle starts to slide out when the vehicle speed continues to increase, and the vehicle reaches its maximum roll angle and presents a high risk of rollover. The roll stability is critical to vehicle

handling and safety. With the same SSF, the stiff roll mode is desirable to inhibit the roll motion and increase the rollover threshold of the vehicle at cornering.

Chapter 5: Roll & Pitch Independently Tuned

Interconnected Suspension

5.1 Introduction

Vehicle suspension systems which have been extensively studied [3, 5] play a very important role for a ground vehicle's comfortable and safe driving. Conventional vehicle suspension design generally involves a trade-off between handling and ride comfort as the requirements for spring and damper settings are opposite [94].

Assuming rigid vehicle body and unsprung (wheel) elements, there are typically four suspension modes: bounce, pitch, roll and warp [2]. Bounce mode is related to vertical ride quality; warp mode (also called axle articulation) is a non-planar mode which indicates road holding ability on rough terrain; roll and pitch mode are directly related to lateral/longitudinal stability. These modes don't share the same preference with reference to suspension stiffness and damping. For instance, soft bounce/warp modes are desirable for a comfortable ride and an even load distribution of tyres, whilst stiff roll and moderate stiff pitch modes are beneficial for inhibiting vehicle attitude during cornering, braking, and acceleration. The conflicting requirement between ride and handling is the main challenge for conventional suspension design.

Active/semi-active controlled suspensions have received much attention in research and industry because they are able to provide the best ride comfort performance while maintaining good handling stability [95-97]. The main obstacle for commercialisation of such systems is the significant power consumption and associated costs. Passive suspension systems still remain the dominant type in production vehicles mainly due to

their reliability and cost energy effectiveness. Interconnected suspensions, unlike active/semi-active suspensions, can easily decouple different vehicle vibration modes in a passive manner [2]. The interconnections can be realised by various means, such as mechanical, hydraulic and pneumatic. Anti-roll bars (ARB) are one of the typical examples of mechanical interconnection as they decouple the roll mode from bounce and pitch. But the drawback is obvious in that it is unable to decouple the warp mode. Warp stiffness is increased unfavourably which affects the vehicle's road holding performance due to increased variation of the tyre dynamic load on an uneven surface. Anti-roll bars also tend to add more weight, and yield a very lightly damped roll mode that is known to be detrimental to transient roll responses [54].

Roll-resistant interconnected suspension systems have been studied theoretically and experimentally as the unique modes-decoupling property allows the ride quality to be maintained with improved roll stability. Cao et al. [82] investigate the roll-plane interconnection with the proposed twin-gas-chamber hydro-pneumatic suspension strut and compare the roll property of different connection patterns. Zhang & Smith et al. [73, 74] investigate the modelling and dynamics of vehicles fitted with roll resistant hydraulically interconnected suspension system with a focus on the roll stability and fluid circuit dynamics. The ride comfort of the vehicle with roll-plane interconnected suspension is analysed in [73]. Experimental studies also confirm the performance of hydraulically interconnected systems in [56, 83]. The road holding performance of anti-roll hydraulically interconnected suspension particularly at warp mode is investigated and compared with anti-roll bars in [56], it shows that anti-roll bars stiffen the warp mode which increases warp natural frequency, while with roll-resistant interconnected suspension, the warp natural frequency remains unchanged. It also illustrates that the tyre load transfer of a vehicle fitted with an anti-roll bar increases 50% more than that of

a vehicle fitted with a roll-plane interconnected suspension system. Tenneco's Kinetic H2/CES suspension is one of the commercialised hydraulically interconnected suspensions developed to improve the lateral stability and road holding performance [98].

The pitch plane dynamics should be considered during acceleration or braking if the suspension design is biased towards ride comfort, especially for vehicles with a short wheelbase and high centre of gravity. When bounce stiffness is reduced, the ride comfort can become a problem as the pitch natural frequency may drop into an uncomfortable range of less than 1Hz [42]. This rotational movement can induce sickness in passengers. Cao, et al. [43] analyse the dynamic property of the pitch interconnected hydro-pneumatic suspension for two-axle heavy vehicle application. The pitch plane hydraulically interconnected suspension for a tri-axle heavy truck is also analysed in [44]. Roll and pitch coupled hydro-pneumatic suspension systems are proposed in [72, 75], however the stiffness and damping of roll and pitch modes are not able to be tuned independently. Normally the vehicle wheelbase is much longer than the track width. The roll and pitch coupled suspension may cause over-stiffened pitch mode so that the ride comfort may be negatively affected. Roll and pitch controlled interconnected suspension is proposed in paper [99]. The linearized model is used for modal analysis and the results show that the roll and pitch stiffness increase independently, but system nonlinearity is ignored.

In this chapter, a generalised 14 DOF full vehicle model with the roll and pitch independently tuned interconnected suspension (RPITIS) system is established. The vehicle model incorporates the stiffness and damping nonlinearity and tyre nonlinearity is represented by the Magic Formula tyre model. The damping valves and accumulators

are included in the hydraulic model to represent the nonlinear properties of the interconnected system. Comprehensive dynamic analyses, such as the fishhook manoeuvre, hard braking, stochastic ride, speed bump and warp excitation tests, are carried out and the results are compared with conversional suspension configurations.

5.2 Static property of the RPITIS suspension system

5.2.1 Model description

The vehicle fitted with the RPITIS system contains additional strut forces developed from the hydraulic actuators. The hydraulic layout is shown in Figure 5.1 and fluidic parameters are listed in Table 5.1. The inside 4 cylinders and fluid communication circuits A and B form the roll-resistant interconnected sub-system. An additional set of 4 cylinders at the outside and fluid communication circuits C and D form the pitch-resistant interconnected sub-system. It includes four nitrogen filled diaphragm type accumulators; interconnecting pipelines; and eight double-acting hydraulic cylinders in total. Cylinders are designed to make the upper and lower chamber cross-section areas as close as possible. The cylinder bodies are mounted to the car chassis with the piston rods being fixed to the wheel assemblies.

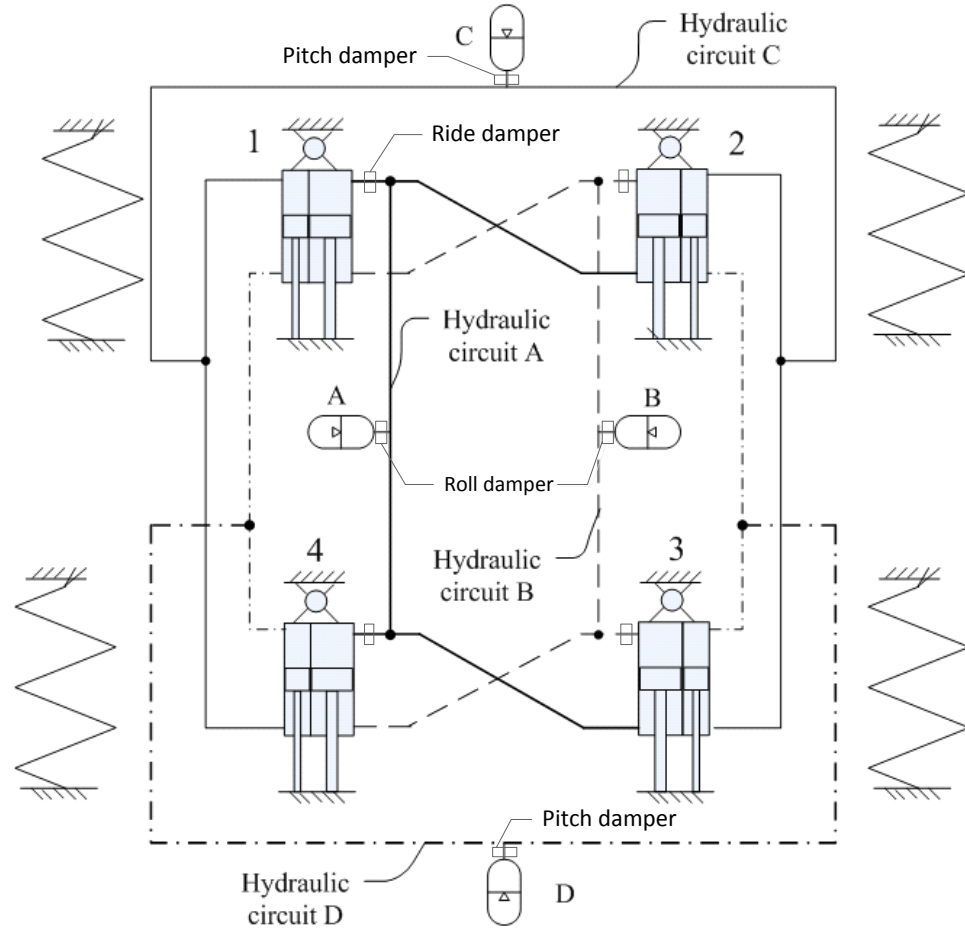


Figure 5. 1: Schematic of the roll- and pitch-plane interconnected suspension

Table 5. 1: Parameters of the RPITIS suspension

Parameters	Symbol	Value
Gas heat factor	γ	1.4
Roll accumulator volume	V_r	$3.2 \times 10^{-4} \text{ m}^3$
Roll accumulator pre-charged gas pressure	P_r	1 Mpa
Roll cylinder piston diameter	D_{r_piston}	0.032 m
Roll cylinder piston rod diameter	D_{r_rod}	0.014 m
Roll sub-system working pressure	\bar{P}_r	2 Mpa
Pitch accumulator volume	V_p	$3.2 \times 10^{-4} \text{ m}^3$
Pitch accumulator pre-charged gas pressure	P_p	1 Mpa
Pitch cylinder piston diameter	D_{p_piston}	0.025 m
Pitch cylinder piston rod diameter	D_{p_rod}	0.012 m
Pitch sub-system working pressure	\bar{P}_p	2 Mpa

The interconnected system can decouple the roll and pitch modes. In the roll motion, pressure in the chambers of roll-plane (inside) cylinders changes due to gas volume change in the accumulators, and the generated cylinder forces are against the roll motion to provide additional roll stiffness. In the meantime, the circuit connection of pitch-plane cylinders makes the fluid flow from one side to the opposite side with minimum pressure changes and a negligible influence on the vehicle suspension during roll motion. Similarly in pitch motion, interconnection of pitch-plane (outside) cylinders provides additional pitch stiffness whilst the roll-plane cylinders have a negligible impact on it. The decoupled roll and pitch modes enable the mode based performance to be independently tuned by the proposed interconnected suspension.

5.2.2 Static stiffness property of RPITIS

The definition of static suspension modes is the same as stated in Chapter 3 by defining the suspension deflection with respect to the fixed vehicle body/chassis. The pressures of the interconnected hydraulic system will change at different suspension modes due to the gas-spring effects of the hydraulic accumulators. Assuming zero flow rate in the connection pipelines between accumulators and the hydraulic cylinders in the mode stiffness calculation, the pressure of cylinder chambers is equal to the pressure of the corresponding accumulators. Following this, the suspension mode stiffness can be found.

The volume changes of accumulators are:

$$\begin{aligned}
 \Delta V_A &= X_1 A_{R1}^T - X_2 A_{R2}^B - X_3 A_{R3}^B + X_4 A_{R4}^T \\
 \Delta V_B &= -X_1 A_{R1}^B + X_2 A_{R2}^T + X_3 A_{R3}^T - X_4 A_{R4}^B \\
 \Delta V_C &= X_1 A_{P1}^T + X_2 A_{P2}^T - X_3 A_{P3}^B - X_4 A_{P4}^B \\
 \Delta V_D &= -X_1 A_{P1}^B - X_2 A_{P2}^B + X_3 A_{P3}^T + X_4 A_{P4}^T
 \end{aligned} \tag{5.1}$$

where ΔV_A , ΔV_B , ΔV_C and ΔV_D are the gas volume changes of accumulator A, B, C and D as shown in the Figure 5.1. X_i ($i=1, 2, 3, 4$) denotes the suspension deflections at front left, front right, rear right and rear left. Subscript Ri , Pi denote the roll, pitch cylinders and the superscript T , B denote the top and bottom chamber, respectively.

The bounce mode stiffness of the RPITIS suspension is formulated as:

$$K_B = 2(K_f + K_r) + \sum_{i=1}^4 \frac{(A_{Ri}^T - A_{Ri}^B)P_{R0}V_{R0}^\lambda}{(V_{R0} - \Delta V_A)^\lambda} + \sum_{i=1}^4 \frac{(A_{Pi}^T - A_{Pi}^B)P_{P0}V_{P0}^\lambda}{(V_{P0} - \Delta V_C)^\lambda} \quad (5.2)$$

where V_{R0} , P_{R0} are the size and pre-charge gas pressure of roll accumulator A and B; V_{P0} , P_{P0} are the size and pre-charge gas pressure of pitch accumulator C and D;

The roll mode of the RPITIS suspension is determined by the suspension springs and the roll-plane hydraulically interconnected sub-system where the pitch sub-system has no effects at roll mode. The roll stiffness is formulated as:

$$K_R = \frac{w^2}{2}(K_f + K_r) + \frac{w^2}{4x} \left(\begin{array}{l} (A_{R1}^T + A_{R2}^B + A_{R3}^B + A_{R4}^T) \frac{P_{R0}V_{R0}^\lambda}{(V_{R0} - \Delta V_A)^\lambda} \\ -(A_{R1}^B + A_{R2}^T + A_{R3}^T + A_{R4}^B) \frac{P_{R0}V_{R0}^\lambda}{(V_{R0} - \Delta V_B)^\lambda} \end{array} \right) \quad (5.3)$$

Similarly, the roll-plane sub-system has no effect at the pitch mode. The pitch mode of the RPITIS suspension is determined by the suspension springs and the pitch-plane hydraulically interconnected sub-system, and the pitch stiffness is formulated as:

$$K_P = (l_f + l_r) \left(K_f * l_f + K_r * l_r \right) + \frac{1}{2x} \left(\begin{array}{c} (A_{p1}^T + A_{p2}^T - A_{p3}^B - A_{p4}^B) \frac{P_{p0} V_{p0}^\lambda}{(V_{p0} - \Delta V_C)^\lambda} \\ -(A_{p1}^T + A_{p2}^T - A_{p3}^B - A_{p4}^B) \frac{P_{p0} V_{p0}^\lambda}{(V_{p0} - \Delta V_D)^\lambda} \end{array} \right) \quad (5.4)$$

The warp mode stiffness of RPITIS is the same as the unconnected suspension owing to the unchanged gas volume of all four accumulators at warp mode.

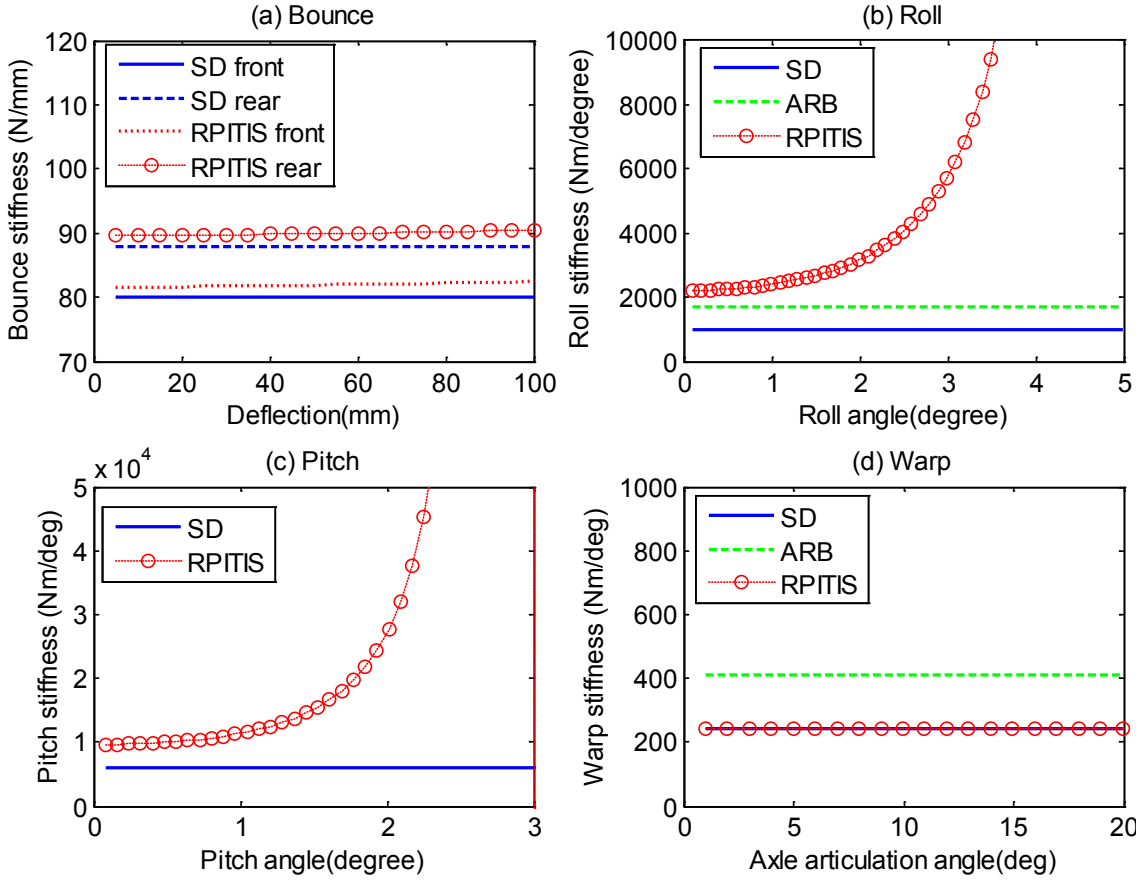


Figure 5. 2: Static stiffness properties of RPITIS: (a) bounce, (b) roll, (c) pitch, (d) warp

Figure 5.2 presents the comparison results of the static modes stiffness property of RPITIS suspension and conventional suspensions. Under the in-phase bounce mode excitations, The RPITIS suspension has a slightly larger bounce static stiffness than the unconnected SD suspension and exhibits a weekly progressively hardening effect in

comparison, both at the front and rear axle. The result suggests that the RPITIS system introduces a small amount of bounce stiffness and will slightly reduce the ride comfort level compared with the SD suspension. This can be compensated by using slightly softer individual springs in the RPITIS system to obtain the same total bounce stiffness in order to achieve the equivalent ride comfort.

The differences in the roll stiffness property of the selected configurations are presented in Figure 5.2 (b). The RPITIS system exhibits a significantly higher roll mode property when compared with the SD suspension. The additions of passive front and rear anti-roll bars can also yield an upward parallel shift of the effective roll stiffness of the unconnected suspension (SD). Although the anti-roll bar can yield static roll stiffness similar to those of the hydraulically interconnected suspension in the small roll angle range, the RPITIS suspensions provide progressively increased roll stiffness corresponding to higher deflections. The nonlinear characteristic of the RPITIS in the roll stiffness are desirable to manage the ride comfort in lateral direction under the high speed stochastic road excitation and the roll motion control during fast cornering. Furthermore, the use of very strong anti-roll bars usually lack damping while roll damping can be tuned independent of bounce damping by the RPITIS system.

Figure 5.2 (c) shows the differences in the pitch stiffness property between RPITIS and SD suspension. The RPITIS system exhibits a highly nonlinear pitch stiffness compared with the SD suspension. When the pitch angular deflection is small, the RPITIS suspensions provide just slightly larger pitch stiffness than the SD. The pitch stiffness of the RPITIS increases progressively under the large pitch angular deflection (>1 degree). Due to the bounce and pitch coupling in the pitch plane vehicle dynamics, moderate pitch stiffness is required in the small pitch amplitude to control the pitch

acceleration level for ride comfort when running over road bumps. However, stiffer pitch stiffness is desirable to inhibit the squat or dive induced by the braking or acceleration. The nonlinear characteristic of the RPITIS in the pitch mode is highly desirable in order to improve the compromise between ride comfort and vehicle longitudinal attitude control.

Figure 5.2 (d) illustrates a comparison of the warp stiffness properties of the selected suspension configurations. Interconnected suspension configurations RPITIS yield warp stiffness identical to that of the unconnected spring-damper suspension (SD) over the entire range of the axle articulation angle considered. The use of anti-roll bars, however, tends to increase the suspension warp stiffness, due to the greater coupling in the roll and warp modes. This suggests that the hydraulic interconnection does not alter the warp property of the suspension, while it yields nonlinear improvement in the roll and pitch mode properties.

5.2.3 Static damping property of RPITIS

The mode damping property of the vehicle system can be defined by the suspension relative velocities at each corner with respect to the fixed vehicle body, namely \dot{X}_i ($i=1,2,3,4$) at front left, front right, rear right, rear left, respectively. The size of the four accumulators in the RPITIS system is assumed to be infinite to ignore the gas-spring effects. The flow rates at each chamber fluid port are defined as the product of suspension velocity \dot{X}_i and the chamber area as:

$$Q_{Ri}^j = \dot{X}_i A_{Ri}^j; \quad Q_{Pi}^j = \dot{X}_i A_{Pi}^j \quad (5.5)$$

where $i=1,2,3,4$; $j=T$ or B (denotes the top or bottom chamber); and R, P represent the roll, pitch sub-system cylinders.

The flow rates of the accumulators are defined according to the interconnection of the fluid circuits as:

$$\begin{aligned}
 Q_a &= Q_{R1}^T - Q_{R2}^B - Q_{R3}^B + Q_{R4}^T, \\
 Q_b &= -Q_{R1}^B + Q_{R2}^T + Q_{R3}^T - Q_{R4}^B, \\
 Q_c &= Q_{P1}^T + Q_{P2}^T - Q_{P3}^B - Q_{P4}^B, \\
 Q_d &= -Q_{P1}^B - Q_{P2}^B + Q_{P3}^T + Q_{P4}^T
 \end{aligned} \tag{5.6}$$

The front left suspension strut damping force as an example is calculated:

$$\begin{aligned}
 F_{D1} = F_{R1} + F_{P1} &= A_{R1}^T \left(P_{R0} + P_{ride} (Q_{R1}^T) + P_{roll} (Q_a) \right) - A_{R1}^B \left(P_{R0} - P_{roll} (Q_b) \right) \\
 &+ A_{P1}^T \left(P_{P0} + P_{pitch} (Q_c) \right) - A_{P1}^B \left(P_{R0} - P_{pitch} (Q_d) \right)
 \end{aligned} \tag{5.7}$$

where the pressure losses of ride damper P_{ride} , roll damper P_{roll} and pitch damper P_{pitch} are a function of the corresponding flow rates which can be tuned by the fixed leaking area, pre-load pressure and valve shim opening stiffness [100].

The other strut forces can be formulated similarly. The bounce mode damping force is the sum of all strut forces; the roll, pitch and warp mode damping torques can be formulated with the struts force and the vehicle geometric dimensions (track width, distances of front / rear axle to the C.G).

The static damping property of RPITIS suspension is compared with the SD suspension in Figure 5.3. The damping valves of the RPITIS vehicle is tuned to have the same level of bounce damping as the SD vehicle as shown in Figure 5.3 (a). Due to the additional roll and pitch dampers included in the RPITIS system, the considerable roll and pitch mode damping gain is yield by the RPITIS system compared with the unconnected SD suspension. The enhanced roll and pitch mode damping properties of the RPITIS suspension would be beneficial for controlling the transient motions and stability during steering, acceleration or braking. RPITIS suspension yields a slightly lower warp

damping compared with the SD vehicle. It is because the warp damping is only determined by the ride dampers in the RPITIS system while the roll and pitch damper has a negligible effect at the warp mode.

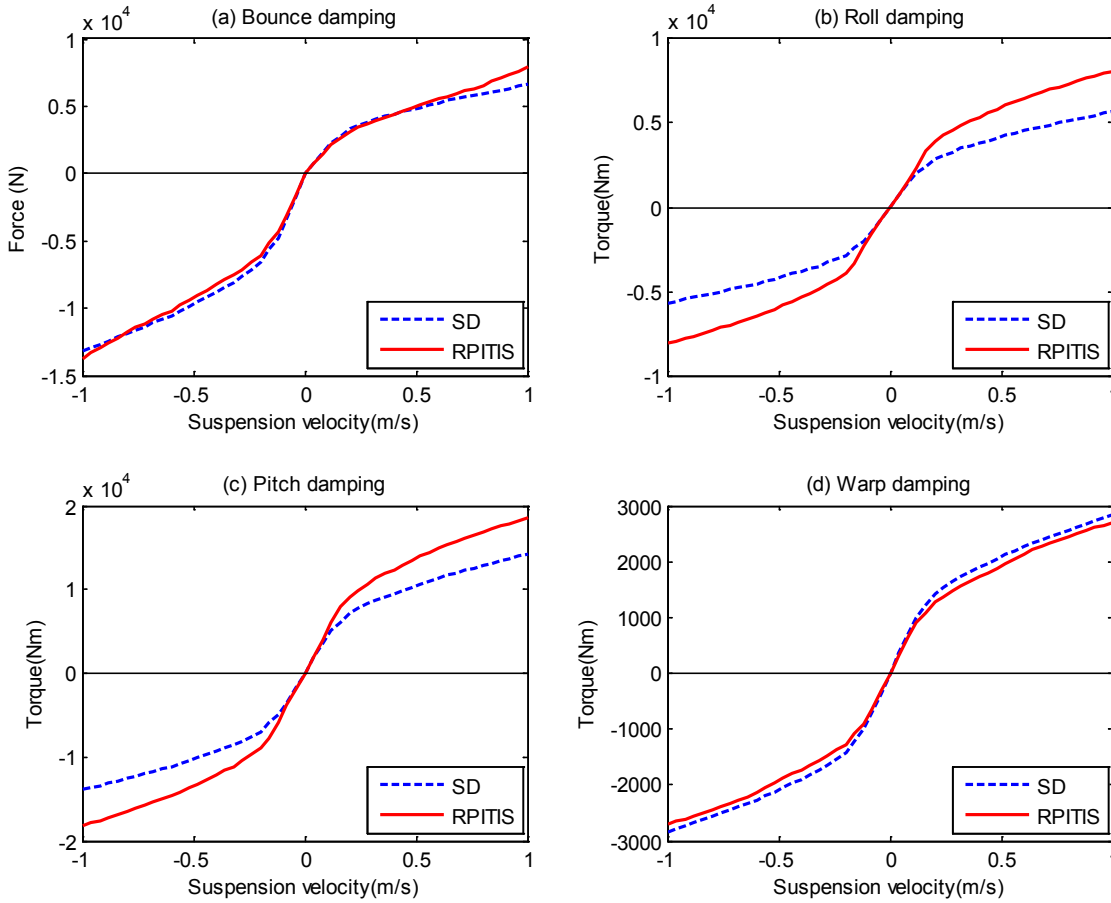


Figure 5.3: Static damping properties of RPITIS: (a) bounce, (b) roll, (c) pitch, (d) warp

5.3 Time domain analysis of the vehicle with RPITIS suspension

5.3.1 Dynamic model of the RPITIS suspension

To simplify the modelling, the following assumptions are made in this paper: (a) piston friction is relatively small and not considered; (b) the hydraulic fluid is not compressible compared with gas; (c) the pipeline is regarded as rigid so that the flow rate inside the pipelines is equal throughout.

A vehicle fitted with RPITIS doesn't require shock absorbers and anti-roll bars. The cylinder hydraulic forces (F_{Hi}) of the RPITIS system include both nonlinear stiffness developed from air-spring effects in the accumulators and the damping effects provided by the hydraulic damping valves integrated in the hydraulic circuits. Ride control damping can be set equivalent to the original shock absorber damping characteristic. The roll and pitch damping characteristic can be tuned to have a high damping rate at low flow rate for attitude control and low damping rate at high flow rate for ride comfort, as shown in Figure 5.4. The pipeline pressure loss is not considered as it is small compared to the pressure loss from damper valves when the pipe size is properly chosen.

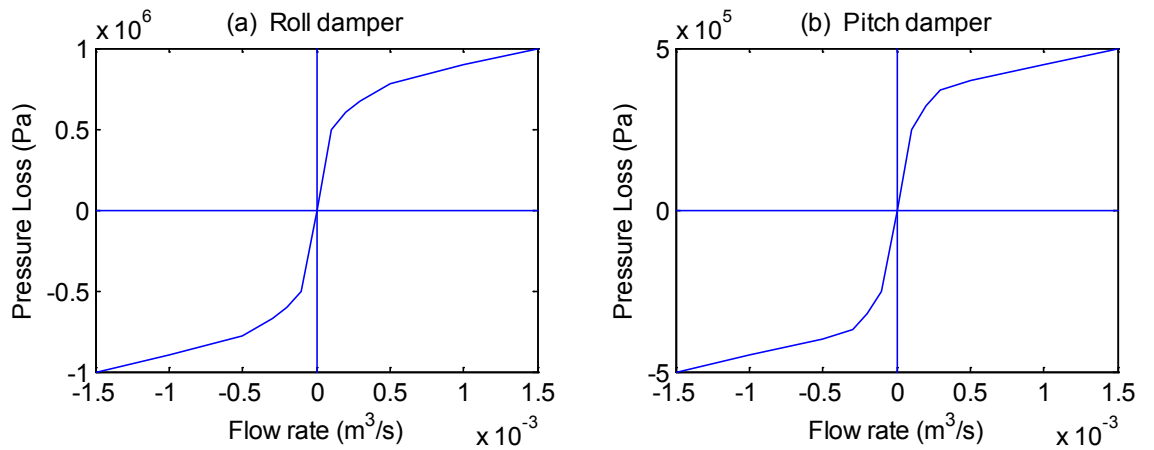


Figure 5. 4: Damper valve characteristics (a) roll damper; (b) pitch damper

The cylinder chambers form the boundary between the vehicle system and hydraulic subsystems. The volume flow rate at the cylinder port is the product of suspension strut speed \dot{X}_s and the effective piston area which is expressed in Equation (5.5). According to the fluid interconnection arrangement, the flow rates of the accumulators A, B, C and D are obtained in Equation (5.6).

For the roll-plane interconnected sub-system, it includes the roll dampers connected with accumulator A and B, and the ride dampers connect with roll cylinder ports. The pressure losses from ride damper P_{di} are related to cylinder flow rate Q_{Ri}^T . The pressure losses from roll damper P_{ra} , P_{rb} are related to accumulator flow rates Q_a , Q_b . The pressure equations of the roll-plane cylinders are:

$$\begin{aligned} P_{R1}^T &= P_{d1}(Q_{r1}^T) + P_{ra}(Q_a) + P_a, & P_{R1}^B &= P_{rb}(Q_b) + P_b, \\ P_{R2}^T &= P_{d2}(Q_{r2}^T) + P_{rb}(Q_b) + P_b, & P_{R2}^B &= P_{ra}(Q_a) + P_a, \\ P_{R3}^T &= P_{d3}(Q_{r3}^T) + P_{rb}(Q_b) + P_b, & P_{R3}^B &= P_{ra}(Q_a) + P_a, \\ P_{R4}^T &= P_{d4}(Q_{r4}^T) + P_{ra}(Q_a) + P_a, & P_{R4}^B &= P_{rb}(Q_b) + P_b. \end{aligned} \quad (5.8)$$

For the pitch-plane interconnected sub-system, only pitch dampers are included which connect with accumulators C and D. As the pitch-plane cylinder size is relatively small, ride control dampers are not required. The pressure losses from pitch damper P_{pc} , P_{pd} are functions of accumulator flow rates Q_c , Q_d . Then the pressure equations of the pitch-plane cylinders can be given as:

$$\begin{aligned} P_{P1}^T &= P_{pc}(Q_c) + P_c, & P_{P1}^B &= P_{pd}(Q_d) + P_d, \\ P_{P2}^T &= P_{pc}(Q_c) + P_c, & P_{P2}^B &= P_{pd}(Q_d) + P_d, \\ P_{P3}^T &= P_{pd}(Q_d) + P_d, & P_{P3}^B &= P_{pc}(Q_c) + P_c, \\ P_{P4}^T &= P_{pd}(Q_d) + P_d, & P_{P4}^B &= P_{pc}(Q_c) + P_c. \end{aligned} \quad (5.9)$$

The accumulators are modelled by assuming an adiabatic process. The pressure P_a and volume V_a at any time in the accumulator A are related to the pre-charged values, P_0 and V_0 , as:

$$P_a V_a^\gamma = P_0 V_0^\gamma = \text{const.} \quad (5.10)$$

The adiabatic gas law is used to model the accumulator pressure as a function of gas volume at the pre-charged pressure, where γ is the specific heat factor for the gas. Taking the partial time derivative of Equation (18), and noting that the flow into the accumulator is given by $Q_a = -\partial V_a / \partial t$, the pressure gradient of the four accumulators can be written as a nonlinear function of the pressure and flow rate, that is,

$$\begin{aligned} \dot{P}_a &= \frac{\gamma Q_a P_a}{V_{r0}} \left(\frac{P_a}{P_{r0}} \right)^{1/\gamma} ; \dot{P}_b = \frac{\gamma Q_b P_b}{V_{r0}} \left(\frac{P_b}{P_{r0}} \right)^{1/\gamma} ; \\ \dot{P}_c &= \frac{\gamma Q_c P_c}{V_{p0}} \left(\frac{P_c}{P_{p0}} \right)^{1/\gamma} ; \dot{P}_d = \frac{\gamma Q_d P_d}{V_{p0}} \left(\frac{P_d}{P_{p0}} \right)^{1/\gamma} . \end{aligned} \quad (5.11)$$

The derived Equations (5.11) are highly nonlinear in nature which represents the air-spring effect of accumulators. The hydraulically interconnected system has low stiffness at small motion, but exhibits fast increased stiffness at large motion which is an advantage over the mechanically interconnected linear system.

The hydraulic forces F_{Hi} of the interconnected system can be obtained as:

$$\begin{aligned} F_{H1} &= (P_{r1}^T A_r^T - P_{r1}^B A_r^B) + (P_{p1}^T A_p^T - P_{p1}^B A_p^B), \\ F_{H2} &= (P_{r2}^T A_r^T - P_{r2}^B A_r^B) + (P_{p2}^T A_p^T - P_{p2}^B A_p^B), \\ F_{H3} &= (P_{r3}^T A_r^T - P_{r3}^B A_r^B) + (P_{p3}^T A_p^T - P_{p3}^B A_p^B), \\ F_{H4} &= (P_{r4}^T A_r^T - P_{r4}^B A_r^B) + (P_{p4}^T A_p^T - P_{p4}^B A_p^B). \end{aligned} \quad (5.12)$$

By combining Equation (5.5) – (5.12), the RPITIS hydraulic forces F_{Hi} are derived.

The strut forces F_{si} in Equation (4.17) are rewritten to contain suspension spring forces F_{ki} and hydraulic forces F_{Hi} as Equation (5.13):

$$F_{si} = F_{ki}(X_{si}) + F_{Hi} \quad (5.13)$$

With the integration of the vehicle model developed in Chapter 4, the whole vehicle model with RPITIS suspension is established. Numerical methods can be applied to solve the equations such as the fourth-order Runge-Kutta algorithm to obtain the whole vehicle responses in the time domain.

5.3.2 Dynamic analysis compared with conventional suspension

Like the improved properties in roll and pitch modes by the RPITIS suspension, the suspension spring stiffness can be reduced to achieve better ride comfort without affecting the roll and pitch stability. In this session, a vehicle fitted with RPITIS and soft suspension springs is compared with conventional suspensions under different maneuvers and road conditions. Roll and pitch dynamics, ride comfort and the tyre dynamic load are investigated according to the simulation results. To demonstrate the advantage of the proposed system, the vehicle suspension configurations for comparison are defined as below:

- 1) SD: conventional spring-damper suspension;
- 2) SD-half: SD with suspension spring stiffness reduced to 50% ;
- 3) ARB: conventional spring-damper suspension integrated with anti-roll bars (SD with anti-roll bars);
- 4) ARB-half: ARB with suspension spring stiffness reduced to 50% (SD-half with anti-roll bars);
- 5) RPITIS: the proposed interconnected system with the suspension spring stiffness set as 50% of SD. (same as SD-half, or ARB-half)

Not all of the configurations are compared at each test. Configuration with anti-roll bars are not compared at the straight line braking and ride quality tests as the anti-roll bar

does not influence the outcomes when vehicle roll is not involved. They are used in the tests where the roll and warp motions are excited. The vehicle parameters are obtained from a typical sport utility vehicle, as listed in Table 4.1.

Emergency steering (fishhook)

Several studies have reported that a significant proportion of the serious heavy-vehicle accidents involve rollover. US accident statistics are surveyed by Winkler et al.[24], and a strongly negative correlation between roll stability and the average likelihood of rollover accidents is reported. It is clear that even a modest increase in roll stability can lead to a significant reduction in the probability of rollover accidents. For vehicles with the same static rollover threshold, a larger roll movement during cornering will decrease the dynamic rollover threshold, which will greatly increase the rollover propensity.

Dynamic stability indexes are used in the literature [50, 51]. The indicators include the effects of the lateral movement of vehicle CG during vehicle body roll motion, suspension jacking forces, the dynamic overshoot in the roll angle or other factors. In this paper, nomalized rollover critical factor (RCF) [51] is compared for different suspension configurations:

$$RCF = 1 - \left[\frac{g}{2}(t_f + t_r) - h_s g |\theta| - |\alpha_y| (h - z_s) - \frac{|\ddot{\theta}| I_x}{m_s} \right] / \left[\frac{g}{2}(t_f + t_r) \right] \quad (5.14)$$

There are two types of the fishhook manoeuvre, the fixed time fishhook (fishhook 1a) and the roll rate feedback fishhook (fishhook 1b). Due to the simplicity of implementation, the fishhook 1a is chosen, as shown in Figure 5.5 with 60km/h initial vehicle speed. The performance of the three configurations, that is ARB, ARB-half and RPITIS, are compared in Figure 5.6.

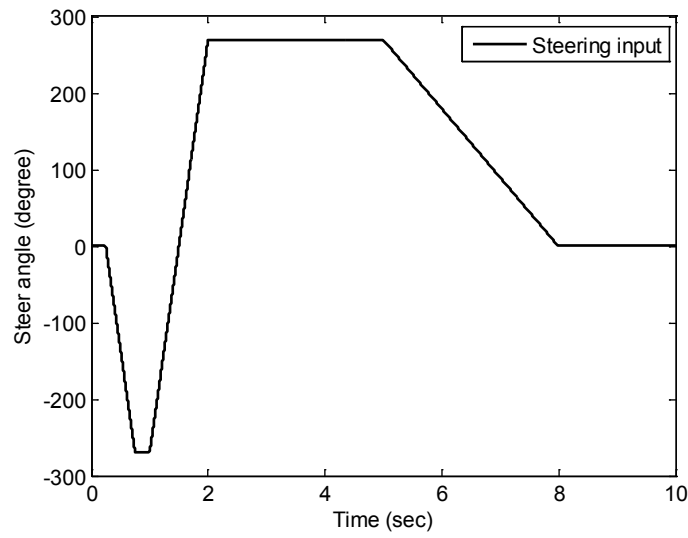


Figure 5. 5: Steering wheel input of fishhook maneuver

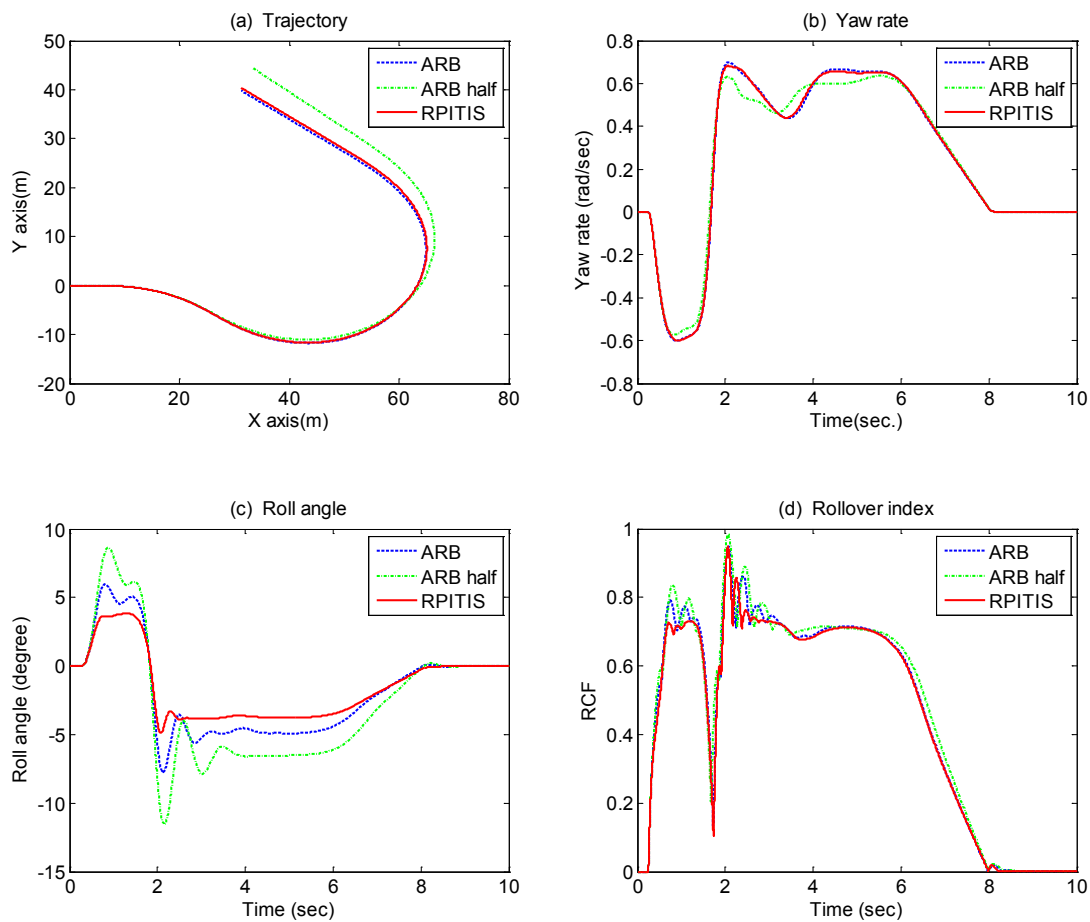


Figure 5. 6: Vehicle response during fishhook manoeuvre. (a) Trajectory (b) Yaw rate

(c) Roll angle (d) Dynamics rollover index

Normally a vehicle with equally distributed roll stiffness at the front and rear will experience an over-steering tendency at extreme conditions such as the fishhook manoeuvre. RPITIS suspension parameters, mainly relating to the cylinder size, can be tuned to have a similar steering performance as the ARB vehicle which is assumed to be optimal at steering. From Figure 5.6(a) and 5.6(b), a slightly understeering tendency is observed for the ARB-half vehicle while RPITIS and ARB vehicles have similar trajectories and yaw rates. Figure 5.6(c) and 5.6(d) show that the RPITIS vehicle has the smallest roll angle and lowest RCF, while the ARB-half vehicle has the largest roll angle and its RCF approaches to 1, which means rollover will very likely occur at that moment.

Emergency braking

The longitudinal stability also becomes important when the vehicle suspension setting is biased towards soft ride. The front diving under braking and the rear squatting under acceleration is normally annoying and the excessive tyre load transfer may also reduce the acceleration/braking performance, especially for the high CG and short wheel-base vehicles [86]. Pitch stiffness is coupled with bounce stiffness for conventional suspension [37, 45]. Soft spring may help on the isolation of vertical vibration, but it can become unfavourable because the motion sickness can be an issue when the pitch rotational frequency is less than 1Hz.

To simulate the emergency braking in a straight lane, the maximum braking torque is chosen by trial and error in order that the wheel lock is not triggered. Figure 5.7 is the ramped step inputs of brake torque applied on front and rear wheels. Configurations with anti-roll bars are not considered here as it has no effect on straight line braking.

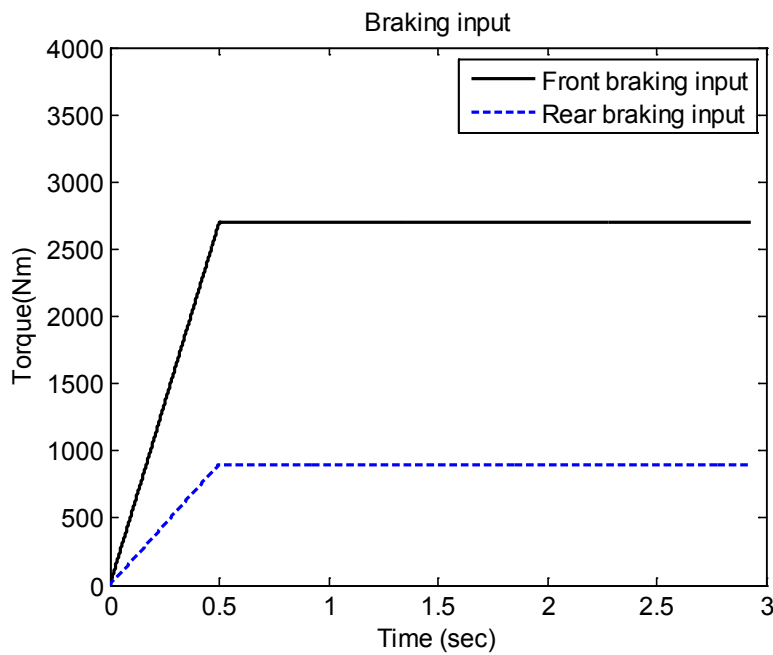


Figure 5. 7: Hard braking inputs

The system responses of a vehicle with SD, SD-half and RPITIS are shown in Figure 5.8. It can be seen that the maximum pitch angle of SD-half in Figure 5.8(a) is twice that of SD because the pitch stiffness is reduced to half when the suspension spring rate is reduced by 50 percent. RPITIS configuration has the smallest pitch angle even if it has the same suspension spring stiffness as the SD-half. The larger dynamic tyre load of the SD-half is observed in Figure 5.8 (c) and (d), while the tyre load of RPITIS is similar to SD suspension. The pitch damping is enabled to be tuned as well as the pitch stiffness in the RPITIS system to control the dynamic overshoot and quickly dampen down the oscillation. The pitch and bounce mode are coupled to some extent in the vertical dynamic, while excessive pitch stiffness and damping is not recommended. The merit of the RPITIS system in the pitch plane is that it provides more freedom in the design and tuning of stiffness and damping which cannot be achieved by conventional suspension or the roll and pitch coupled suspension as proposed in [72].

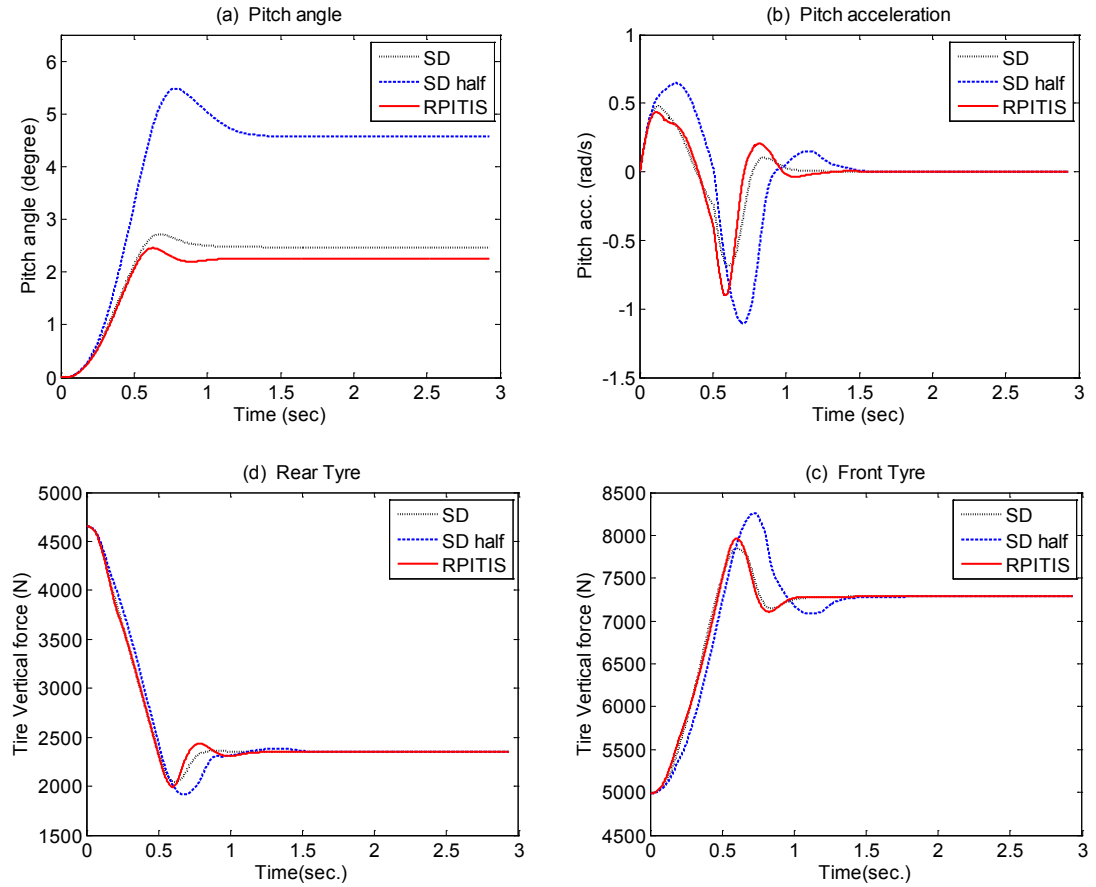


Figure 5. 8: Vehicle response at hard braking (a) pitch angle; (b) pitch acceleration; (c) front tyre vertical load; (d) rear tyre vertical load

Ride quality under road excitation

According to ISO 8608, B, C, D class roads are selected and referred to as ‘smooth’, ‘medium-rough’ and ‘rough’, respectively, to study the ride comfort on a stochastic road [101]. The left and right tracks are assumed to be identical, and the rear wheels follow the front wheels with a time delay. The vertical ride vibration responses of the vehicle model with different suspensions are evaluated under excitations arising from the three random road surfaces and different vehicle speeds (30, 60, 90, 120 and 150 km/h). Human perception of ride comfort related to vertical vibration has been associated with root mean square (RMS) acceleration responses [15, 16].

The RMS vertical acceleration values of the sprung mass of the vehicle model employing three different suspension configurations (SD, SD-half and RPITIS) are compared in Figure 5.9. The results show that the SD-half and RPITIS yield a comparable vertical ride for most of the road conditions and vehicle speeds that are considered while the SD yields higher responses in all conditions. This phenomenon illustrates a well-known property that soft suspension springs bring a favourable ride. It should be noticed the vehicle fitted with RPITIS can improve the ride comfort and does not have a compromised roll and pitch performance, as demonstrated in previous section.

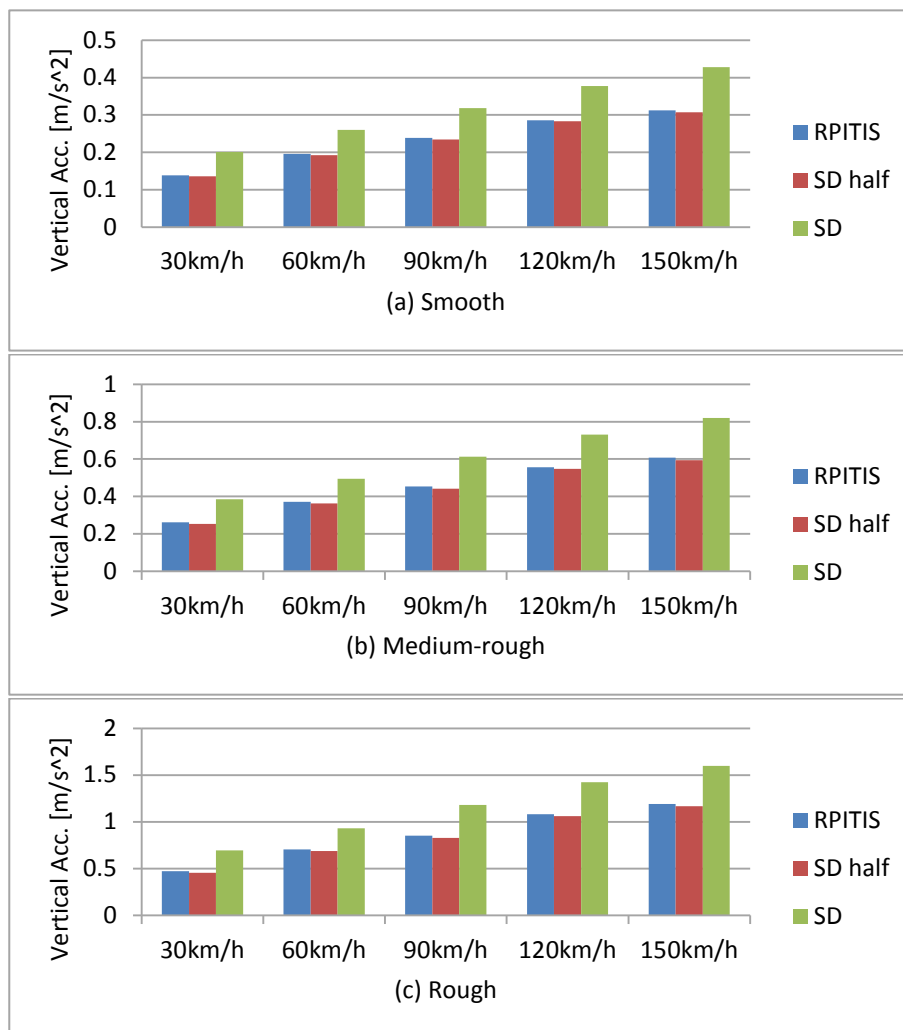


Figure 5. 9: RMS of C.G vertical accelerations under different road conditions

Single wheel bump

A single side speed bump can excite both the roll and pitch motion, and it simulates the situation of only one side of the tyres running over obstacles which is frequently encountered in daily drive scenarios.

A bump signal is given as:

$$d = \begin{cases} \frac{h}{2} (1 - \cos(\frac{2\pi v}{l} t)), & 0 \leq t \leq \frac{l}{v}, \\ 0 & t > \frac{l}{v}. \end{cases} \quad (1)$$

with $h = 0.08$ m, $\ell = 0.5$ m and vehicle speed $v = 5$ m/s, as shown in Figure 5.10.

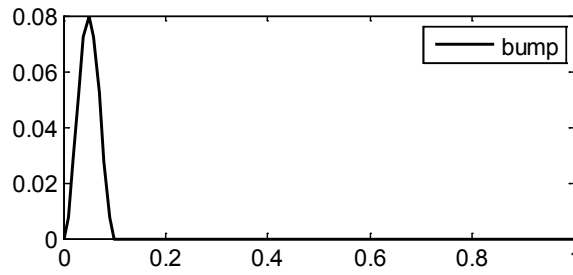


Figure 5. 10: The speed bump profile in time history

Under the left side bump road input, the vehicle body responses and dynamics tyre loads are compared with the four suspension configurations (SD, ARB, ARB-half and RPITIS). From figure 5.11, it can be seen that the vehicle C.G displacement and acceleration for RPITIS has the smallest magnitude compared to others and this indicates the improved ride. The RPITIS vehicle observes the largest pitch angle due to the increased overall pitch stiffness and shifted pitch oscillation centre towards the centre of the vehicle body mass in the pitch plane. However the pitch accelerations of all four configurations are comparable which is more critical to ride comfort.

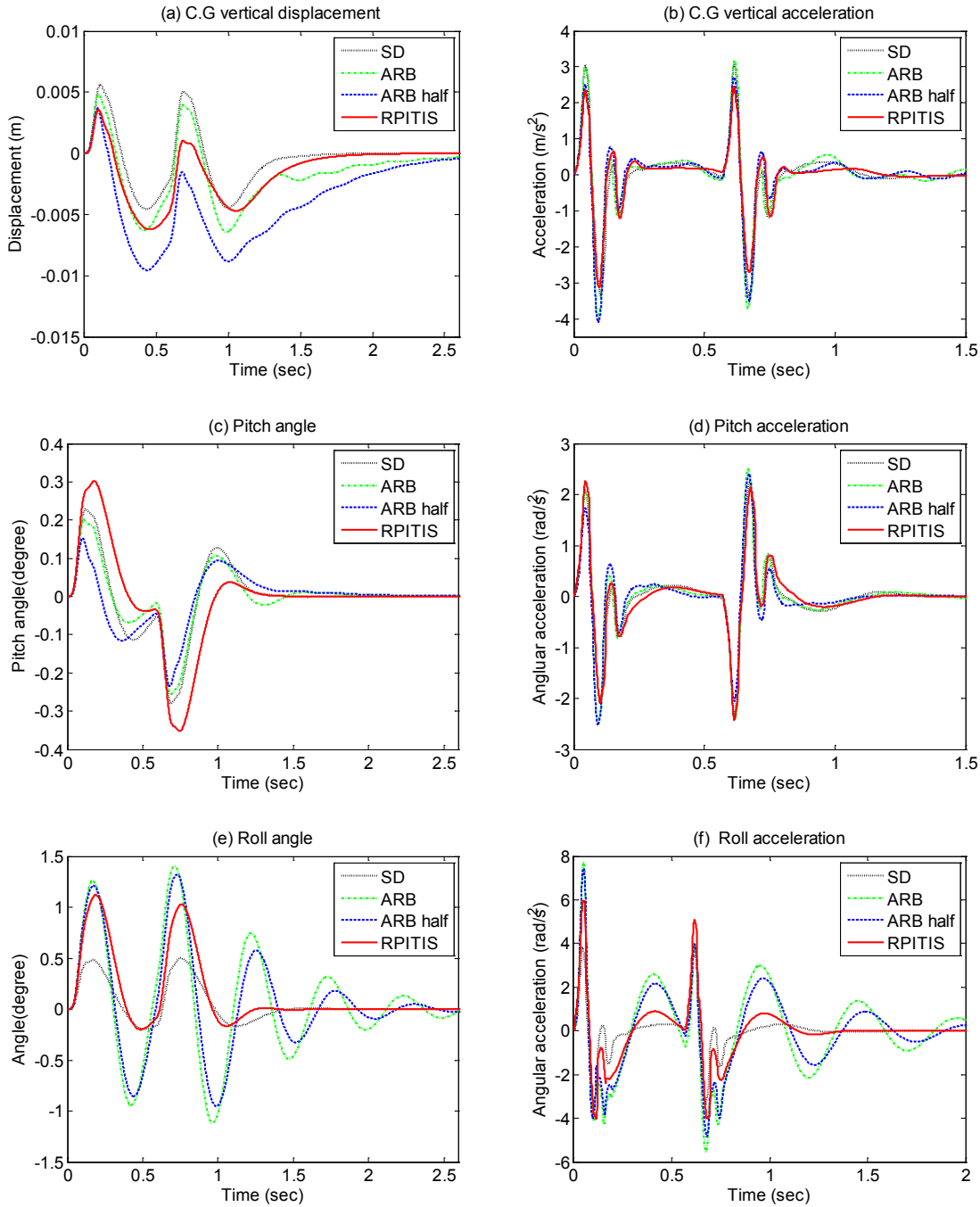


Figure 5.11: Vehicle response over one side bump. (a) C.G vertical displacement (b) C.G acceleration (c) pitch angle (d) pitch acceleration (e) roll angle (f) roll acceleration

The vehicle body roll angle and acceleration are shown in Figure 5.11(e) and 5.11(f), the spring-damper configuration (SD) has the lowest roll response but it is not applicable as there is insufficient roll stiffness. The maximum roll angle of the RPITIS

vehicle is larger than that of the SD vehicle but smaller than those of the vehicles with anti-roll bars. Server roll oscillation can be observed for configurations of ARB and ARB-half, while it is quickly damped for RPITIS. The reason of this is that vehicles fitted with anti-roll bars generally lack damping in the roll motion, while additional roll damping can be provided by the roll dampers in the RPITIS.

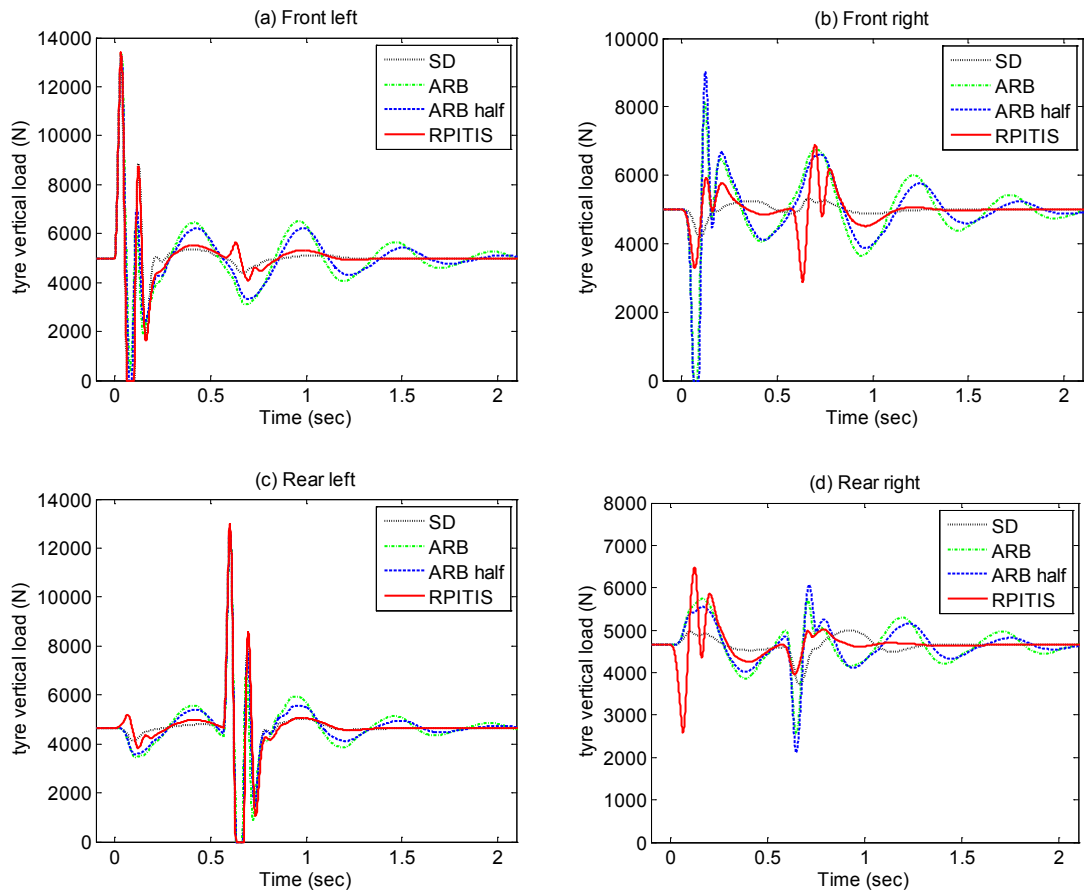


Figure 5.12: Tyre dynamic load over one side bump (a) front-left (b) front-right (c) rear left (d) rear right

Figure 5.12 shows the dynamic tyre load of vehicles fitted with selected suspensions. The left-side tyres present similar tyre load responses for all suspension configurations. For the right-side tyres, the ARB and ARB-half have a larger magnitude than the RPITIS. In particular, the lost contact between the front-right tyre and the ground can be observed for ARB and ARB-half configurations in Figure 5.12 (b) due to the small

suspension travel which is limited by the strong front anti-roll bar. In contrast, the tyre load variation is much smaller for the vehicle with the RPITIS system due to warp mode decoupling. Besides peak forces, the tyre load oscillation of RPITIS flattened out much quicker than the ARB configurations due to the nonlinear damping provided by hydraulic valves.

Tyre dynamic load under warp bumpy road

The front-rear axle articulation is frequently encountered in the off-road environment, and a flexible suspension in the warp mode is critical for tyres to hold the road and provide traction and control. Warp simulation is studied here to understand how the road-holding ability is affected by different suspension configurations.

Figure 5.13 is the road input of warp excitation. The left track and right track of the road profile are out of phase, and the wavelength of the road is intentionally designed so that the front and rear tyres also move in an opposite direction. This is the worst case scenario that tyre load transfer will encounter most on off-road driving.

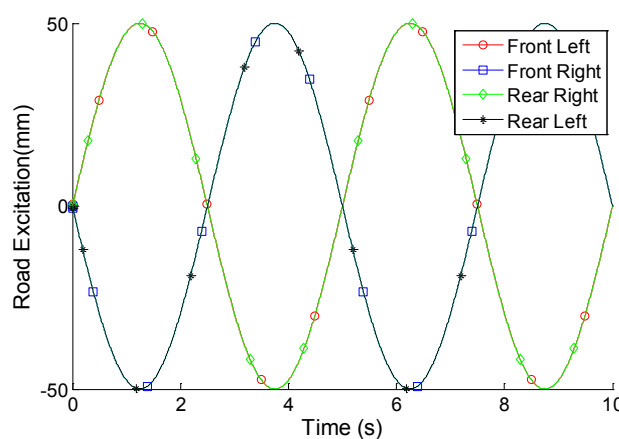


Figure 5. 13: The road signals of warp excitation

Figure 5.14 presents the vehicle roll angle and acceleration response under warp excitation. The roll motion at warp excitation is determined by the roll stiffness

distribution. A 180 degree phase difference between SD and the other three configurations can be observed. It is because the SD suspension has a slightly stiffer rear spring than the front one, which results in the body roll motion being dominated by the rear suspension. In opposition, the RPITIS and Anti-roll bar configurations have more front roll stiffness than the rear one due to the steering/handling requirement. This causes the roll motion of vehicle configurations with the RPITIS and ARBs to follow the front axle. However, even the RPITIS has a similar roll stiffness distribution to the ARB, and the steady state roll angle and transient roll acceleration of RPITIS is much smaller than that of the ARBs due to the warp decoupling by the front-rear interconnection.

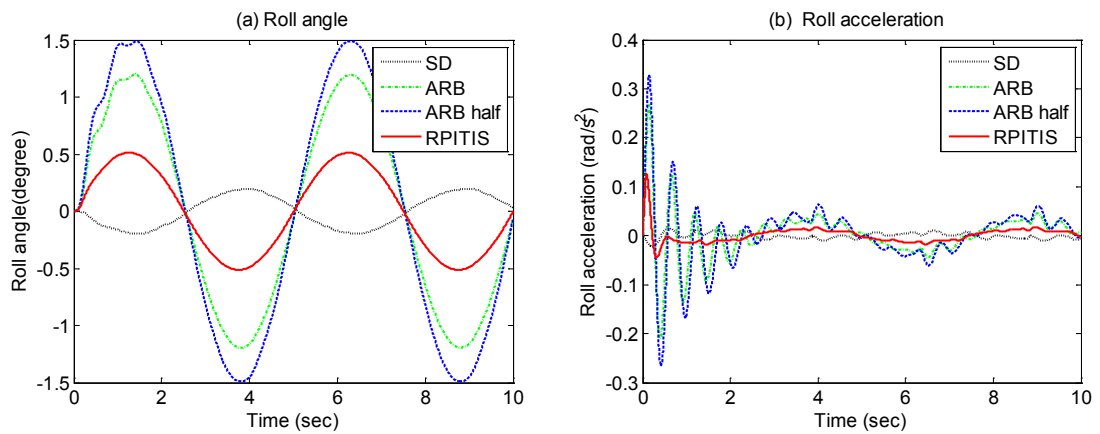


Figure 5.14: Roll response at warp road. (a) roll angle (b) roll acceleration

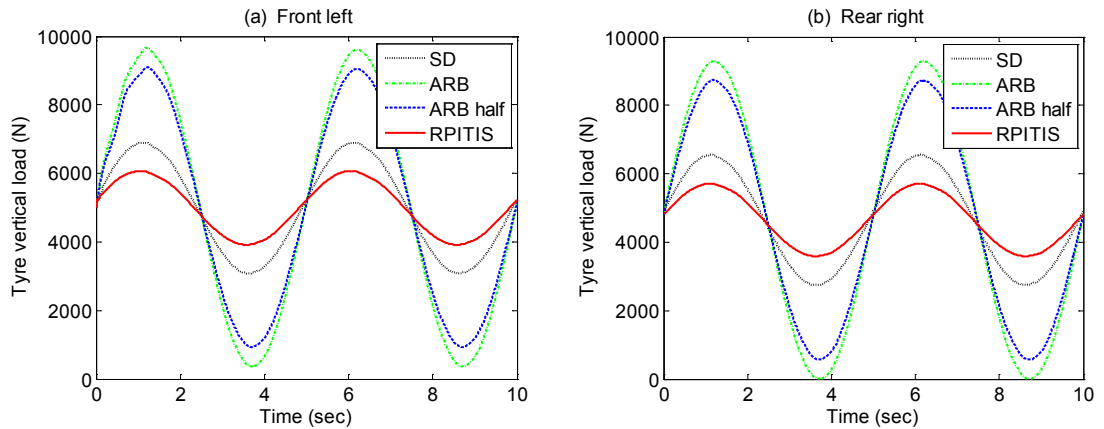


Figure 5.15: The tyre load at warp road. (a) front left tyre; (b) rear right tyre

The variations of the front left and rear right tyre vertical force are shown in Figure 5.15. The smaller the tyre load variation indicates the better tyre grip. From the figure we can see that the tyre load variations of a vehicle with anti-roll bars (ARB, ARB-half) are observed to be significantly larger, and those of the RPITIS vehicle are the smallest. The RPITIS system ensures no additional warp stiffness is introduced to the suspension system by itself, and the vehicle warp stiffness is mainly provided by the individual suspension spring elements. Anti-roll bars not only increase the roll stiffness, but also introduce extra warp stiffness to make the suspension inflexible for axle articulation. That is why anti-roll bars are usually required to be detached when vehicles need to go off- road.

5.3.3 Simulation result highlights

In this section, the dynamic modelling and time domain analysis of a two-axle vehicle with integration of the passive RPITIS system is conducted. Simulation results are presented based on vehicle parameters obtained from a typical sport utility vehicle. Comprehensive analyses including roll and pitch dynamics, ride quality and tyre load transfer are carried out and the performance of RPITIS is compared with conventional suspension configurations.

The vehicle with RPITIS has better roll resistance and an improved dynamic rollover index at the fishhook maneuver and the roll stiffness distribution can be varied to achieve improved steering at extreme conditions. At straight line hard braking, the proposed suspension shows improved pitch resistance and reduced tyre longitudinal load transfer. The ride comfort of the RPITIS vehicle is improved for different road conditions and vehicle speeds by the reduced suspension spring stiffness without jeopardising the lateral and longitudinal stability. The single-side bump and warp tests

illustrate vehicle warp mode is decoupled by the RPITIS. The tyre load transfer is reduced significantly and the roll and pitch damping can be improved by the integrated damper valves. By contrast, the vehicles with anti-roll bars show excessive tyre load variation and severe under-damped oscillation.

The demonstrated results illustrate the decoupled modes by the RPITIS system. The bounce and warp stiffness are provided mainly by the suspension springs at each corner while extra nonlinear roll and pitch stiffness are provided by the interconnected system. The mode based performance can be optimised by tuning mode stiffness and damping independently. The mode decoupling property of the proposed RPITIS system is meaningful for suspension design engineers as the long existing compromise between ride and handling can be greatly improved.

5.4 Summary

The vehicle fitted with the RPITIS suspension system is presented in this chapter. The roll and pitch stiffness and damping can be independently tuned by the proposed system without affecting the vehicle's ride quality in the bounce mode and the tyre dynamic load in the vehicle warp mode. The static and dynamic forces developed by the struts of the RPITIS suspension are analysed to derive suspension stiffness and damping properties in the four fundamental vibration modes, namely bounce, roll, pitch and warp. The results show that the RPITIS system can increase the roll- and pitch-mode stiffness and damping substantially, with minimum influence on the bounce/warp mode properties. Such enhanced decoupling of the roll/pitch from the bounce/warp modes would be beneficial in realising an improved design compromise among various vehicle performance measures under complex driving conditions. The dynamic analysis of the proposed interconnected suspension is performed and compared with conventional

suspensions to investigate the potential benefits on the vehicle ride, handling, roll and pitch dynamics response under various road excitation and braking/steering maneuvers. The simulation results demonstrate that the proposed RPITIS suspension system can yield considerably enhanced anti-roll and anti-pitch properties, and handling performance. The ride quality of the vehicle is also improved by the reduced vehicle bounce stiffness. The systematic analysis of suspension properties, design sensitivity and vehicle dynamic responses clearly demonstrate the considerable potential of the roll and pitch decoupled interconnected suspension. The decoupled modes by the hydraulically interconnected system enable the vehicle design engineer to optimise vehicle performance at each mode independently and this serves to enhance the overall vehicle ride, handling performance and driving stability in an energy-saving manner.

Chapter 6: Zero-warp Hydro-pneumatic Interconnected Suspension

6.1 Introduction

For off-road applications such as military vehicles, in order to further improve the vehicle's mobility performance on rough terrain, it is meaningful to completely decouple the warp mode from other modes to achieve zero warp suspension stiffness.

The anti-roll and anti-pitch hydraulically interconnected suspensions are studied in the previous chapters. These show that roll stability at cornering has been improved with a negligible effect on ride comfort and road holding performance by the roll-resistant interconnected suspension. Pitch-resistant interconnected suspension shows improved pitch stability at acceleration/braking. Roll and pitch coupled hydro-pneumatic suspension are investigated in [102] and roll and pitch independently tuned hydraulically interconnected suspension are also presented in [99]. However, the dynamics of the warp mode have received limited attention by the researcher. In [72], the warp property of the x-coupled hydraulic pneumatic suspension is investigated and low warp stiffness is achieved which parallels the unconnected suspension configuration. In [56], an experimental study is conducted to compare the roll-plane hydraulically interconnected suspension with anti-roll bars, and this proves that the hydraulically interconnected system has relatively low warp stiffness while anti-roll bars tend to increase the warp stiffness and increase the tyre load transfer at warp road inputs.

Tenneco's kinetic suspension H2/CES is the commercialised hydraulically interconnected suspension system with low warp stiffness. But the existence of unconnected steel coil springs as the vehicle weight supporting means at each corner will introduce a certain amount of warp suspension stiffness.

In this chapter, a new Zero-Warp Hydro-Pneumatic Interconnected Suspension (ZWHPIIS) is proposed with zero warp suspension stiffness. The static and dynamic properties of the vehicle equipped with the zero-warp suspension are presented.

6.2 Static property of zero-warp hydro-pneumatic interconnected suspension

6.2.1 Model description

The hydro-pneumatic interconnected suspension with zero warp stiffness is proposed, and the hydraulic layout is shown in Figure 6.1. It includes four nitrogen filled diaphragm type accumulators; interconnecting pipelines; and 8 hydraulic cylinders in total. The cylinder bodies are mounted to the car chassis with the piston rods being fixed to the wheel assemblies.

The four hydro-pneumatic single acting struts (on the outsides) are used as resilient elements instead of steel springs to support the vehicle weight and provide bounce/pitch stiffness. The hydro-pneumatic struts are left-right interconnected (through circuit C at the front and circuit D at the rear) in order to enable the free warp/articulation of the front and rear axle.

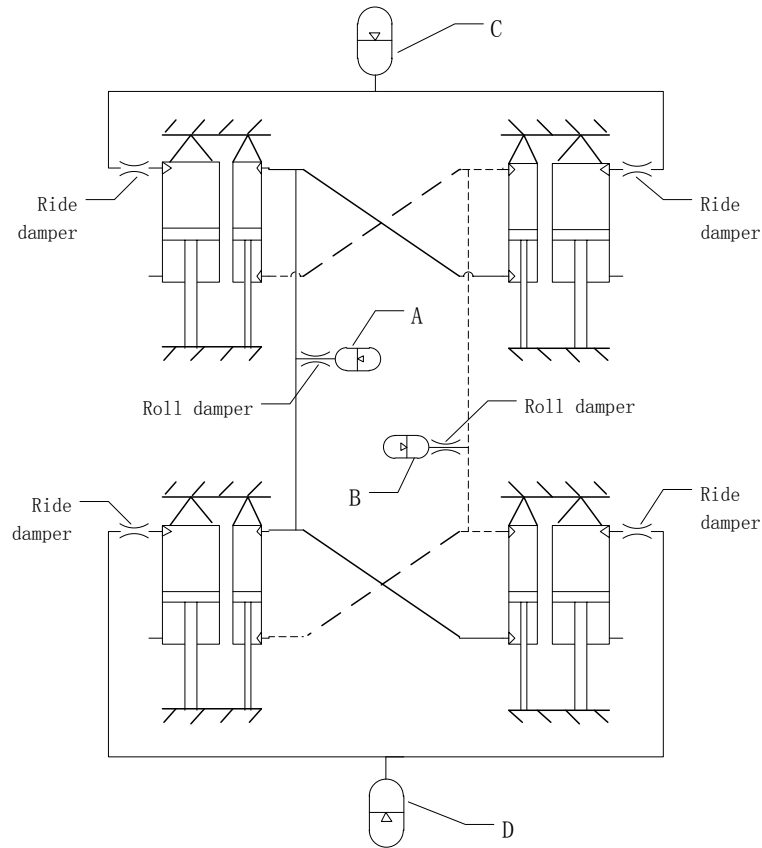


Figure 6. 1: Schematic diagram of the ZWHPIS suspension

The roll-resistant hydraulic subsystem is comprised by the smaller double acting roll cylinders parallel to the struts and the chambers are interconnected through circuit A & B. In the roll motion, pressures in the chamber of roll cylinders change due to the gas volume change in the accumulators A and B, and the generated hydraulic forces are against the roll while the roll stiffness can be independently tuned without affecting ride quality. The roll-resistant hydraulic subsystem, as proved by theory and experiments, provides roll stiffness with no additional warp stiffness. Together with the left-right interconnected hydro-pneumatic struts, zero warp stiffness is achieved. The proposed interconnected suspension enables it to decouple warp modes from all other vehicle modes.

The parameters of the proposed ZWHPIS system are presented in Table 6.1 and the vehicle parameters are the same as those listed in Table 3.1.

Table 6. 1: Fluidic parameters of the ZWHPIS

Symbols	Values	Units	Descriptions
γ	1.3	/	Gas heat factor
ρ	870	kg/m^3	Hydraulic fluid density
β	1400	Mpa	Bulk modulus
V_r	2.4×10^{-4}	m^3	Volume of accumulator A & B
P_r	1	Mpa	Pre-charged pressure of A & B
V_s	1.2×10^{-3}	m^3	Volume of accumulator C & D
P_s	1	Mpa	Pre-charged pressure of C & D
Dr_{piston}	32	mm	Diameter of roll cylinder piston
Dr_{rod}	14	mm	Diameter of roll cylinder rod
Ds_{piston}	50	mm	Diameter of strut cylinder piston
\bar{P}_r	2.0	Mpa	Roll control mean working pressure
C_{ride}	5e8	/	Ride valve damping co-efficient
C_{roll}	3e8	/	Roll valve damping co-efficient

In the proposed system, ride damper valves are included to provide ride damping so that traditional shock absorbers are not required. Additional roll damping can be provided by the roll damper in the circuits A and B which is normally not possible for anti-roll bars. It is worth mentioning that by utilising the hydraulic pump (which can be shared with the braking, power steering system), the proposed system can realise vehicle height/attitude control function in a low cost manner compared with air suspension which usually needs a set of air compressors and a tank. Another advantage of the hydro-pneumatic suspension is that the height adjustment is independent to suspension stiffnesses.

6.2.2 Static stiffness properties

The static suspension stiffness property of the ZWHPIS suspension can be developed in a similar manner to the roll and pitch combined RPITIS suspension derived in Chapter 5 by defining the suspension strut deflections X_1, X_2, X_3, X_4 at the front left, front right, rear left and rear right, respectively. The suspension force consists of hydraulic force developed from hydro-pneumatic struts. Assuming zero flow-rate in the connection pipelines between accumulators and the hydraulic cylinders in the mode stiffness calculation, the fluid pressure of the cylinder chambers is equal to the pressure of the corresponding connected accumulators. A_{wf}, A_{wr} denotes the effective piston areas of the single acting hydro-pneumatic strut at the front and rear. A_{Ri}^T, A_{Ri}^B denotes the effective piston areas of the double acting roll cylinders at the top or bottom. The gas volume change in the accumulators can be found as:

$$\begin{aligned}\Delta V_A &= X_1 A_{R1}^T - X_2 A_{R2}^B - X_3 A_{R3}^B + X_4 A_{R4}^T \\ \Delta V_B &= -X_1 A_{R1}^B + X_2 A_{R2}^T + X_3 A_{R3}^T - X_4 A_{R4}^B \\ \Delta V_C &= A_{wf} (X_1 + X_2) \\ \Delta V_D &= A_{wr} (X_3 + X_4)\end{aligned}\tag{6.1}$$

where $\Delta V_A, \Delta V_B, \Delta V_C$ and ΔV_D are the gas volume changes of accumulator A, B, C and D as shown in the Figure 6.1.

By defining $X_1 = X_2 = X_3 = X_4 = x$, the bounce mode stiffness forces of the ZWHPIS suspension is formulated as:

$$\begin{aligned}F_{Bf} &= 2A_{wf} \cdot \left(\frac{P_{C0} V_{C0}^\lambda}{(V_{C0} - \Delta V_C)^\lambda} - P_{C0} \right) + \sum_{i=1}^2 \frac{(A_{Ri}^T - A_{Ri}^B) P_{R0} V_{R0}^\lambda}{(V_{R0} - \Delta V_A)^\lambda} \\ F_{Br} &= 2A_{wr} \cdot \left(\frac{P_{D0} V_{D0}^\lambda}{(V_{D0} - \Delta V_D)^\lambda} - P_{D0} \right) + \sum_{i=3}^4 \frac{(A_{Ri}^T - A_{Ri}^B) P_{R0} V_{R0}^\lambda}{(V_{R0} - \Delta V_A)^\lambda}\end{aligned}\tag{6.2}$$

where F_{Bf} , F_{Br} are the stiffness forces developed by the hydraulic struts at the front and rear. V_{R0} , P_{R0} are the size and pre-charge gas pressure of roll accumulator A and B; V_{C0} , V_{D0} , P_{C0} , P_{D0} are the size and pre-charge gas pressure of the accumulator C and D.

The bounce stiffness can be obtained by calculating the derivatives of the bounce stiffness forces over the increment of suspension deflection dx .

The roll mode is defined by $X_1 = X_4 = x$, $X_2 = X_3 = -x$ and the anti-roll moment of the ZWHPIS suspension is only provided by the roll-plane sub-system where the left-right interconnected hydro-pneumatic struts have no effects at the roll mode. The roll stiffness is formulated as:

$$K_R = \frac{w^2}{4x} \left(\begin{aligned} &(A_{R1}^T + A_{R2}^B + A_{R3}^B + A_{R4}^T) \frac{P_{R0} V_{R0}^\lambda}{(V_{R0} - \Delta V_A)^\lambda} \\ &-(A_{R1}^B + A_{R2}^T + A_{R3}^T + A_{R4}^B) \frac{P_{R0} V_{R0}^\lambda}{(V_{R0} - \Delta V_B)^\lambda} \end{aligned} \right) \quad (6.3)$$

The pitch mode is defined by $X_1 = X_2 = x$, $X_3 = X_4 = -x$, and the anti-pitch moment is provided by the hydro-pneumatic struts as:

$$K_P = \frac{(l_f + l_r)}{x} \left(A_{wf} l_f \cdot \left(\frac{P_{C0} V_{C0}^\lambda}{(V_{C0} - \Delta V_C)^\lambda} - P_{C0} \right) + A_{wr} l_r \cdot \left(\frac{P_{D0} V_{D0}^\lambda}{(V_{D0} - \Delta V_D)^\lambda} - P_{D0} \right) \right) \quad (6.4)$$

The warp mode is defined as $X_1 = X_3 = x$, $X_2 = X_4 = -x$. Under warp mode, the gas volume of all the accumulators is kept the same as no fluid flows in or out of the accumulators. Thus, the suspension stiffness forces are zero which means zero torsional moment is exerted on the vehicle chassis or body.

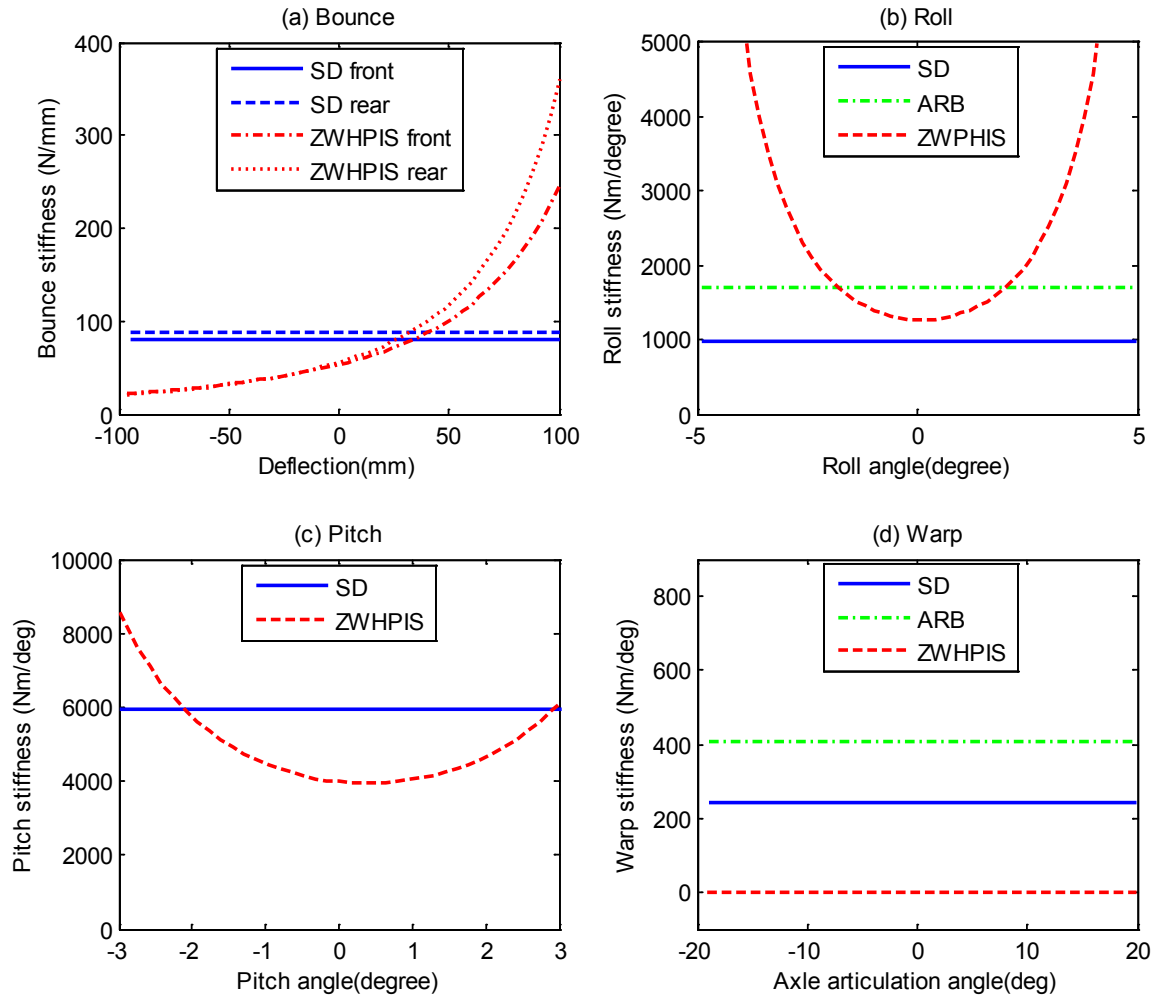


Figure 6. 2: Static stiffness properties of ZWHPIS: (a) bounce, (b) roll, (c) pitch, (d)

warp

Figure 6.2 (a) - (d) presents the static stiffness property of the ZWHPIS suspension at each mode. Generally, the hydro-pneumatic zero warp suspension exhibits a highly nonlinear property compared to the linear SD or ARB suspension. Under the in-phase bounce mode excitations, the bounce stiffness of the ZWHPIS is smaller than that of the linear SD suspension at zero suspension deflection which will help improve the ride comfort at a small amplitude vibration. The bounce stiffness increases progressively in suspension compression. The stiffness hardening effects could greatly reduce the chances of the suspension bottoming out under large impact. Similarly, the roll and pitch stiffness of the ZWHPIS are nonlinear along the roll and pitch angle range. The

rotational stiffness is small when the roll or pitch angle is small and it increases exponentially when the roll or pitch angle becomes larger. The nonlinear behavior of the roll and pitch stiffness is favourable to control vehicle attitude at larger motion and ride comfort at high frequency small motion. Figure 6.2 (d) illustrates a comparison of the warp stiffness properties of the selected suspension configurations. Interconnected ZWHPIS suspension yields zero warp stiffness as the fluid interconnection enables vehicle axles to articulate freely. The use of anti-roll bars, however, tends to increase the suspension warp stiffness, due to the greater coupling in the roll and warp modes.

6.2.3 Static damping properties

As demonstrated in Chapter 5, the mode damping property of the vehicle system can be defined by the suspension relative velocities at each corner with respect to the fixed vehicle body, namely \dot{X}_i ($i=1,2,3,4$) at the front left, front right, rear right, and rear left, respectively. The size of the four accumulators in the ZWHPIS system is assumed to be infinite to ignore the gas-spring effects. The flow rates at each chamber fluid port are defined as the product of suspension velocity \dot{X}_i and the effective chamber area, expressed as:

$$Q_{Wi} = \dot{X}_i A_{Wi}; \quad Q_{Ri}^j = \dot{X}_i A_{Ri}^j \quad (6.5)$$

where $i=1,2,3,4$; $j=T$ or B (denotes the top or bottom chamber); W , R represent the warp struts and roll cylinders, respectively.

The flow rates of the accumulators A and B in the roll-plane subsystem are defined according to the interconnection of the fluid circuits as:

$$\begin{aligned}
Q_A &= Q_{R1}^T - Q_{R2}^B - Q_{R3}^B + Q_{R4}^T, \\
Q_B &= -Q_{R1}^B + Q_{R2}^T + Q_{R3}^T - Q_{R4}^B, \\
Q_C &= Q_{W1} + Q_{W2}, \\
Q_D &= Q_{W1} + Q_{W2}.
\end{aligned} \tag{6.6}$$

The total suspension damping is the sum of damping forces developed from the ride damper and the roll damper as illustrated in Figure 6.1. The suspension strut damping force can be formulated as:

$$\begin{aligned}
F_{D1} &= F_{W1} + F_{R1} = A_{W1} P_{ride}(Q_{W1}) + \left(A_{R1}^T (P_{R0} + P_{roll}(Q_A)) - A_{R1}^B (P_{R0} - P_{roll}(Q_B)) \right), \\
F_{D2} &= F_{W2} + F_{R2} = A_{W2} P_{ride}(Q_{W2}) + \left(A_{R2}^T (P_{R0} + P_{roll}(Q_B)) - A_{R2}^B (P_{R0} - P_{roll}(Q_A)) \right), \\
F_{D3} &= F_{W3} + F_{R3} = A_{W3} P_{ride}(Q_{W3}) + \left(A_{R3}^T (P_{R0} + P_{roll}(Q_B)) - A_{R3}^B (P_{R0} - P_{roll}(Q_A)) \right), \\
F_{D4} &= F_{W4} + F_{R4} = A_{W4} P_{ride}(Q_{W4}) + \left(A_{R4}^T (P_{R0} + P_{roll}(Q_A)) - A_{R4}^B (P_{R0} - P_{roll}(Q_B)) \right).
\end{aligned} \tag{6.7}$$

where the pressure losses of ride damper P_{ride} , roll damper P_{roll} are a function of the corresponding flow rates which can be tuned by the fixed leaking area, pre-load pressure and valve shim opening stiffness [100].

The suspension damping property at each mode can be obtained by formulating the suspension strut damping forces according to the mode definition. The static damping property of ZWHPIS suspension is compared with the SD suspension in Figure 6.3. The ride damping valves of the hydro-pneumatic suspension are tuned to have the same level of bounce damping as the SD vehicle, as shown in Figure 6.3 (a). ZWHPIS suspension yields similar pitch and warp damping compared with the SD vehicle owing to the equivalent ride damper setting. Due to the additional roll dampers included in the proposed fluid system, the considerable roll mode damping gain is yielded by the ZWHPIS system compared to the unconnected SD suspension. The enhanced roll mode

damping properties are beneficial for controlling the transient motions and handling stability during cornering.

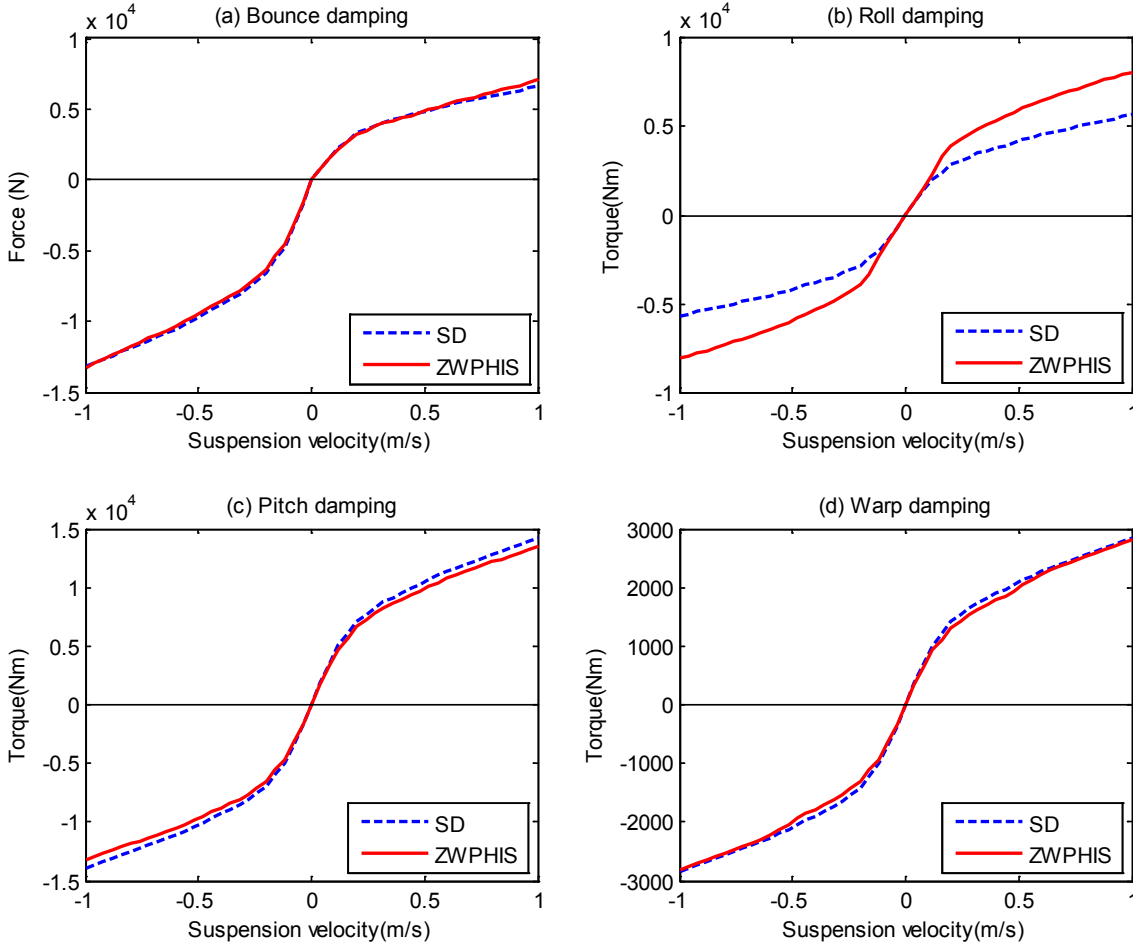


Figure 6. 3: Static damping properties of ZWHPIS: (a) bounce (b) roll (c) pitch (d) warp

6.3 Dynamic modelling of Zero-warp hydro-pneumatic suspension

6.3.1 Vehicle equations

As the warp mode dynamic analysis of the vehicle system usually do not involve the lateral and longitudinal dynamic, a 7-DOF full vehicle vertical model is sufficient for warp mode study.

As shown in Figure 3.2, m_s , m_{u1} , m_{u2} , m_{u3} , m_{u4} represent the sprung mass and unsprung masses, respectively. I_{xx} and I_{yy} is the roll and pitch moment of inertia. Z_0 , Z_{w1} , Z_{w2} , Z_{w3} , Z_{w4} denote the vertical displacement of the sprung mass and unsprung mass. Z_{g1} , Z_{g2} , Z_{g3} , Z_{g4} are the ground excitation inputs. ϕ , θ denote the pitch and roll angles of the sprung mass. The tyres are simplified to linear spring, and the stiffness is represented by k_t . The dynamic equation of vehicle motion can be expressed as:

$$m_{ui}\ddot{Z}_{wi} = -F_{Hi} + F_{ti}, (i = 1, 2, 3, 4.) \quad (6.8)$$

$$m_s\ddot{Z}_0 = F_{H1} + F_{H2} + F_{H3} + F_{H4} \quad (6.9)$$

$$I_{yy}\ddot{\phi} = l_f(F_{H1} + F_{H2}) - l_r(F_{H3} + F_{H4}) \quad (6.10)$$

$$I_{xx}\ddot{\theta} = \frac{t_f}{2}(F_{H1} - F_{H2}) + \frac{t_r}{2}(F_{H4} - F_{H3}) \quad (6.11)$$

where F_{Hi} are the hydraulic strut forces of the interconnected fluidic system. F_{ti} are the tyre forces.

By the assumption of small roll and pitch angle, the vertical displacements of wheels related to sprung mass at each corner have the relationship as:

$$\begin{aligned} Z_{s1} &= Z_0 + l_f\phi + \frac{t_f}{2}\theta - Z_{w1}; Z_{s2} = Z_0 + l_f\phi - \frac{t_f}{2}\theta - Z_{w2} \\ Z_{s3} &= Z_0 - l_r\phi - \frac{t_r}{2}\theta - Z_{w3}; Z_{s4} = Z_0 - l_r\phi + \frac{t_r}{2}\theta - Z_{w4}. \end{aligned} \quad (6.12)$$

The relative velocity of suspension travel is:

$$\begin{aligned} \dot{Z}_{s1} &= \dot{Z}_0 + l_f\dot{\phi} + \frac{t_f}{2}\dot{\theta} - \dot{Z}_{w1}; \dot{Z}_{s2} = \dot{Z}_0 + l_f\dot{\phi} - \frac{t_f}{2}\dot{\theta} - \dot{Z}_{w2} \\ \dot{Z}_{s3} &= \dot{Z}_0 - l_r\dot{\phi} - \frac{t_r}{2}\dot{\theta} - \dot{Z}_{w3}; \dot{Z}_{s4} = \dot{Z}_0 - l_r\dot{\phi} + \frac{t_r}{2}\dot{\theta} - \dot{Z}_{w4}. \end{aligned} \quad (6.13)$$

The hydraulic suspension force is directly related to the relative velocity of suspension travel. The vehicle model and the fluidic system model can be integrated through the suspension travel speed.

6.3.2 Fluidic equations

Assumptions are made the same as mentioned in the previous chapter being: (a) piston friction is not considered. (b) the fluid is incompressible compared with nitrogen gas in the accumulator. (c) the oil density is constant. (d) the pipeline is simplified with no viscous resistance, namely the pressure and flow rate inside the pipelines are equal throughout. A more complicated model with consideration of fluid viscous resistance has been developed to study the damping effects of the pipelines in reference [103].

The hydraulic strut forces (F_{Hi}) of the ZWHPIS system include both nonlinear stiffness developed from the air-spring effects in the accumulators and the damping effects provided by the hydraulic damping valves integrated in the hydraulic circuits. Ride control damping can be set equivalent to the individual shock absorber damping characteristics as shown in Figure 6.1. The roll damping characteristic can be tuned to have a high damping rate at low flow rate for attitude control and a low damping rate at high flow rate for ride comfort. The pipeline pressure loss is not considered as it is small compared with pressure loss from damper valves when the pipe size is properly chosen.

The cylinder chambers form the boundary between the mechanical and hydraulic subsystems. The volume flow rate at the cylinder port is the product of suspension strut velocity \dot{X}_{si} and the effective chamber area which is expressed in Equation (6.5). According to the fluid interconnection arrangement, the flow rates of the accumulators A, B, C and D are obtained in Equation (6.6).

The pressure losses from ride damper P_{ride} are related to strut flow rate Q_{wi} . The pressure losses from roll damper P_{ra}, P_{rb} are related to accumulator flow rates Q_a, Q_b which can be obtained from Equation (6.6). The pressure equations of the ZWHPIS fluid system are:

$$\begin{aligned} P_{R1}^T &= P_{roll}(Q_A) + P_A, & P_{R1}^B &= P_{roll}(Q_B) + P_B, \\ P_{R2}^T &= P_{roll}(Q_B) + P_B, & P_{R2}^B &= P_{roll}(Q_A) + P_A, \\ P_{R3}^T &= P_{roll}(Q_B) + P_B, & P_{R3}^B &= P_{roll}(Q_A) + P_A, \\ P_{R4}^T &= P_{roll}(Q_A) + P_A, & P_{R4}^B &= P_{roll}(Q_B) + P_B. \end{aligned} \quad (6.14)$$

$$\begin{aligned} P_{W1} &= P_{ride}(Q_{W1}) + P_C, & P_{W2} &= P_{ride}(Q_{W2}) + P_C, \\ P_{W3} &= P_{ride}(Q_{W3}) + P_D, & P_{W4} &= P_{ride}(Q_{W4}) + P_D. \end{aligned} \quad (6.15)$$

The accumulators are modelled by assuming an adiabatic process. The pressure and volume at any time in the accumulator P and V are related to the pre-charged values, P_0 and V_0 , as follows:

$$PV^\gamma = P_0V_0^\gamma = \text{Constant} \quad (6.16)$$

where γ is the specific heat factor for the gas. The adiabatic gas law is used to model the accumulator pressure as a function of gas volume at the pre-charged pressure. Taking the partial time derivative of Equation (6.13), and noting that the flow into the accumulator is given by $Q = -\partial V / \partial t$, the pressure gradients for the four accumulators are written as a nonlinear function of the pressure, i.e.

$$\begin{aligned} \dot{P}_A &= \frac{\gamma Q_A P_A}{V_{A0}} \left(\frac{P_A}{P_{A0}} \right)^{1/\gamma}; & \dot{P}_B &= \frac{\gamma Q_B P_B}{V_{B0}} \left(\frac{P_B}{P_{B0}} \right)^{1/\gamma}; \\ \dot{P}_C &= \frac{\gamma Q_C P_C}{V_{C0}} \left(\frac{P_C}{P_{C0}} \right)^{1/\gamma}; & \dot{P}_D &= \frac{\gamma Q_D P_D}{V_{D0}} \left(\frac{P_D}{P_{D0}} \right)^{1/\gamma}. \end{aligned} \quad (6.17)$$

The equations show the gas-spring nonlinearity as the rate of pressure change at any time not only depends on the flow rate but also depends on the pressure at that time (state dependent).

According to the arrangement of the fluid interconnection, for fluid circuit A to D, we have:

$$\begin{aligned} P_A &= P_{R1}^T = P_{R2}^B = P_{R3}^B = P_{R4}^T \\ Q_A &= Q_{R1}^T + Q_{R2}^B + Q_{R3}^B + Q_{R4}^T \end{aligned} \quad (6.18)$$

$$\begin{aligned} P_B &= P_{R1}^B = P_{R2}^T = P_{R3}^T = P_{R4}^B \\ Q_B &= Q_{R1}^B + Q_{R2}^T + Q_{R3}^T + Q_{R4}^B \end{aligned} \quad (6.19)$$

$$P_C = P_{W1} = P_{W2}; \quad Q_C = Q_{W1} + Q_{W2} \quad (6.20)$$

$$P_D = P_{W3} = P_{W4}; \quad Q_D = Q_{W3} + Q_{W4} \quad (6.21)$$

where P_A , Q_A are pressure and flow rate of the accumulator in the hydraulic circuit A; Similarly, P_B , Q_B ; P_C , Q_C ; P_D , Q_D are the pressure and flow rate of the accumulator in the hydraulic circuit B, C and D respectively.

Thus, the hydraulic suspension forces F_{Hi} of the zero warp suspension fluidic system can be obtained as:

$$\begin{aligned} F_{H1} &= (P_{R1}^T A_{R1}^T - P_{R1}^B A_{R1}^B) + P_{W1} A_{W1}, \\ F_{H2} &= (P_{R2}^T A_{R2}^T - P_{R2}^B A_{R2}^B) + P_{W2} A_{W2}, \\ F_{H3} &= (P_{R3}^T A_{R3}^T - P_{R3}^B A_{R3}^B) + P_{W3} A_{W3}, \\ F_{H4} &= (P_{R4}^T A_{R4}^T - P_{R4}^B A_{R4}^B) + P_{W4} A_{W4}. \end{aligned} \quad (6.22)$$

By integrating Equations (6.8) - (6.22), the whole vehicle model with ZWHPIS suspension is established.

6.4. Model linearization and frequency analysis

6.4.1 Model linearization

The equations of motion for the seven-DOF vehicle with integrated mechanical-hydraulic suspension system can be written in the matrix form:

$$M\ddot{Z} + D_{R1} \cdot A_R \cdot P_R + D_{W1} \cdot A_W \cdot P_W = F_{ext}(t) \quad (6.23)$$

where $M, C, K \in R^{7 \times 7}$ are the mass, damping and stiffness matrices; \ddot{Z} is the acceleration vector at continuous time t ; F_{ext} is the road excitation forces input. The term of $D_{R1} \cdot A_R \cdot P_R + D_{W1} \cdot A_W \cdot P_W$ describes the suspension strut forces of the hydraulic struts/cylinders due to the hydraulic pressure change including both gas-spring and damping effects; D_{R1} and D_{W1} are linear transformation matrices. The area matrix A_R , A_W and pressure vector P_R, P_W related to the corresponding cylinder chambers (T-top; B- bottom), are defined as:

$$A_R = \text{diag} \begin{bmatrix} A_{R1}^T & A_{R1}^B & A_{R2}^T & A_{R2}^B & A_{R3}^T & A_{R3}^B & A_{R4}^T & A_{R4}^B \end{bmatrix};$$

$$P_R = \begin{bmatrix} P_{R1}^T & P_{R1}^B & P_{R2}^T & P_{R2}^B & P_{R3}^T & P_{R3}^B & P_{R4}^T & P_{R4}^B \end{bmatrix}^T;$$

$$A_W = \text{diag} \begin{bmatrix} A_{W1} & A_{W2} & A_{W3} & A_{W4} \end{bmatrix};$$

$$P_W = \begin{bmatrix} P_{W1} & P_{W2} & P_{W3} & P_{W4} \end{bmatrix}^T$$

The state vector of the full vehicle fitted with the zero warp hydro-pneumatic interconnected suspension is defined as:

$$X_M = \begin{bmatrix} Z & \dot{Z} & P \end{bmatrix}^T \quad (6.24)$$

where displacement vector is $Z = [Z_{W1} \ Z_{W2} \ Z_{W3} \ Z_{W4} \ Z_{V0} \ \phi_V \ \theta_V]^T$, the velocity vector is $\dot{Z} = [\dot{Z}_{W1} \ \dot{Z}_{W2} \ \dot{Z}_{W3} \ \dot{Z}_{W4} \ \dot{Z}_{V0} \ \dot{\phi}_V \ \dot{\theta}_V]^T$, and pressure vector $P = [P_A \ P_B \ P_C \ P_D]^T$ which describes the dynamic states of the hydraulic subsystem.

Linearisation of the accumulator equations can be made by substituting the pressure variable with mean working pressure \bar{P} and the gas heating factor is equal to 1. It is valid when the system vibrates in small amplitude near the equilibrium position. Then equation (6.17) can be rewritten as:

$$\begin{aligned} \dot{P}_A &= \frac{\gamma Q_A \bar{P}_A^2}{V_{A0} P_{A0}}; \quad \dot{P}_B = \frac{\gamma Q_B \bar{P}_B^2}{V_{B0} P_{B0}}; \\ \dot{P}_C &= \frac{\gamma Q_C \bar{P}_C^2}{V_{C0} P_{C0}}; \quad \dot{P}_D = \frac{\gamma Q_D \bar{P}_D^2}{V_{D0} P_{D0}}. \end{aligned} \quad (6.25)$$

Then the full vehicle system state space equations are derived and written in matrix form as:

$$T\dot{X} = SX + F, \text{ or}$$

$$\begin{bmatrix} I & 0 & 0 \\ 0 & M & 0 \\ 0 & 0 & T_H \end{bmatrix} \begin{bmatrix} \dot{Z} \\ \ddot{Z} \\ \dot{X}_H \end{bmatrix} = \begin{bmatrix} 0 & I_7 & 0 \\ 0 & -D_{R1} \times A_R \times R_R \times A_R \times D_{R1}' - D_{W1} \times A_W \times R_W \times A_W \times D_{W1}' & -D_{R1} \times A_R \times D_{R2} - D_{W1} \times A_W \times D_{W2} \\ K_H & D_{R2}' \times A_R \times D_{R1}' + D_{W2}' \times A_W \times D_{W1}' & S_H \end{bmatrix} \begin{bmatrix} Z \\ \dot{Z} \\ X_H \end{bmatrix} + \begin{bmatrix} 0 \\ F_M \\ 0 \end{bmatrix} \quad (6.26)$$

where, $D_{R1}, D_{R2}, D_{W1}, D_{W2}$ are linear transformation matrices according to the vehicle geometry and fluid connection arrangement.

6.4.2 Modal analysis

Modal analysis is the study of the dynamic properties of structure under vibrational excitation. The goal of modal analysis in structural mechanics is to determine the

natural mode shapes and frequencies of an object or structure during free vibration. In order to perform the modal analysis using the linearised vehicle model derived in the previous section, equation (6.26) is alternatively written as the following standard state space equation:

$$\dot{X} = AX + BF \quad (6.27)$$

A and X represent the system matrix and the state variable vector. With solving the Eigen problem of the system matrix A , seven pairs of conjugate eigenvalues and eigenvectors of the structural system can be obtained.

Three vehicle configurations are selected for comparison of the modal analysis, they are:

- 1) SD: vehicle with conventional spring-damper (SD) suspension as a baseline where the parameters are listed in Table 4.1.
- 2) ARB: vehicle with SD suspension plus anti-roll bars (ARB).
- 3) ZWHPIS: vehicle with the proposed ZWHPIS suspension where the bounce stiffness and damping are set equivalent to SD configuration.

Table 6.2 is a summary of the natural frequency of three different vehicle configurations in which the suspension modes are determined by the modal shapes. As the inertia properties of the vehicle are kept the same, so the natural frequency indicates the overall stiffness of each mode. Increased natural frequency means the increased stiffness of each mode. For bounce and warp, a soft mode is desirable to improve the ride quality and road holding ability, whereas for roll and pitch, a stiff mode is desirable to enhance the handling performance.

Table 6. 2: Natural frequency comparison of vehicle motion modes

Natural Frequency (Hz)	Body roll	Body bounce	Body pitch	Wheel bounce	Wheel roll	Wheel pitch	Warp
SD vehicle	1.26	1.38	1.49	13.09	13.16	13.2	13.31
ARB vehicle	1.62	1.38	1.49	13.1	13.65	13.21	14.01
ZWHPIS vehicle	1.78	1.31	1.38	12.88	14.4	13.21	12.28

From the comparison we can see vehicle roll mode natural frequency is increased by both ARB and ZWHPIS. But for warp mode natural frequency, the difference is obvious that ARB increases the warp stiffness to 14.01 *Hz* but ZWHPIS reduces it to 12.28 *Hz*. When ignoring the suspension effects, for a single degree of freedom spring-mass system with a wheel unsprung mass of 42 KG and a tyre stiffness of 250 KN/M, the natural frequency can be found as:

$$f = \frac{1}{2\pi} \sqrt{\frac{k}{m}} = \frac{1}{2\pi} \sqrt{\frac{250000}{42}} = 12.28 \text{ (Hz)} \quad (6.28)$$

The result shows that the warp natural frequency of the ZWHPIS vehicle is equal to the natural frequency of a single wheel vibration, which means that apart from the tyres, the proposed interconnected suspension have zero warp suspension stiffness.

6.4.3 Frequency response under road warp excitation

From the above mode frequency analysis result, the zero warp suspension stiffness of the ZWHPIS suspension is concluded, but how the zero warp suspension stiffness affects the vehicle's dynamic performance is still not clear. The tyre vertical force variation is also called load transfer, and it is studied under warp excitation (axis articulation) in this section to understand how the road holding ability is affected. Three

cases are compared which are the vehicle with the SD suspension (individual conventional spring and damper suspension), the vehicle with ARB suspension (SD plus anti-roll bars) and the vehicle with ZWPHIS suspension.

Tyre dynamic loads as the output are defined as the product of tyre vertical stiffness K_T and the relative displacements X from the tyres to the ground. It can be rewritten from the state vector X and input U as follows:

$$Y_T = CX + DU = \begin{bmatrix} -K_T & & & \\ & -K_T & & \\ & & -K_T & \\ & & & -K_T \end{bmatrix} X + \begin{bmatrix} K_T \\ -K_T \\ K_T \\ -K_T \end{bmatrix} U \quad (6.29)$$

where $H_U = \begin{bmatrix} K_T \\ -K_T \\ K_T \\ -K_T \end{bmatrix}$ represents the road excitation in the warp/axle-articulation mode.

Warp mode excitation means that one pair of diagonal wheels are forced to move vertically in one direction, while the other pair of diagonal wheels moves opposite at the same time. The tyre load responses are evaluated by the transmissibility based on the amplitude ratios in the frequency domain. Based on Equations (6.27) and (6.29), the transfer function from input to the evaluation output can be developed as:

$$H = C(sI - A)^{-1} B + D \quad (6.30)$$

Figures 6.4 are the magnitude gain of the tyre dynamic load outputs in the frequency range of 0.01Hz to 100Hz under the warp road inputs. The red solid line represents the tyre load of a vehicle fitted with ZWHPIS suspension. The blue dashed line represents the tyre load of a vehicle fitted with conventional SD suspension. The green dotted line represents the tyre load of a vehicle fitted with ARB suspension.

In general, the results show that the tyre dynamic load of a vehicle fitted with ARBs is larger than that of vehicle fitted with SD suspension at the frequency range of less than 4Hz. At the frequency of around 1.5Hz, a slight increase of magnitude gain for tyre 1 & 2 (front tyres) and a decrease of magnitude gain for tyre 3 & 4 (rear tyres) are observed for a vehicle with ARBs, and this may be owing to the phase change of the vehicle body roll. The tyre dynamic loads of a vehicle fitted with ZWHPIS are less than that of vehicle fitted with SD or ARB at a frequency of less than 3Hz, and unlike SD and ARB, the tyre loads decrease significantly when the warp frequency reduces.

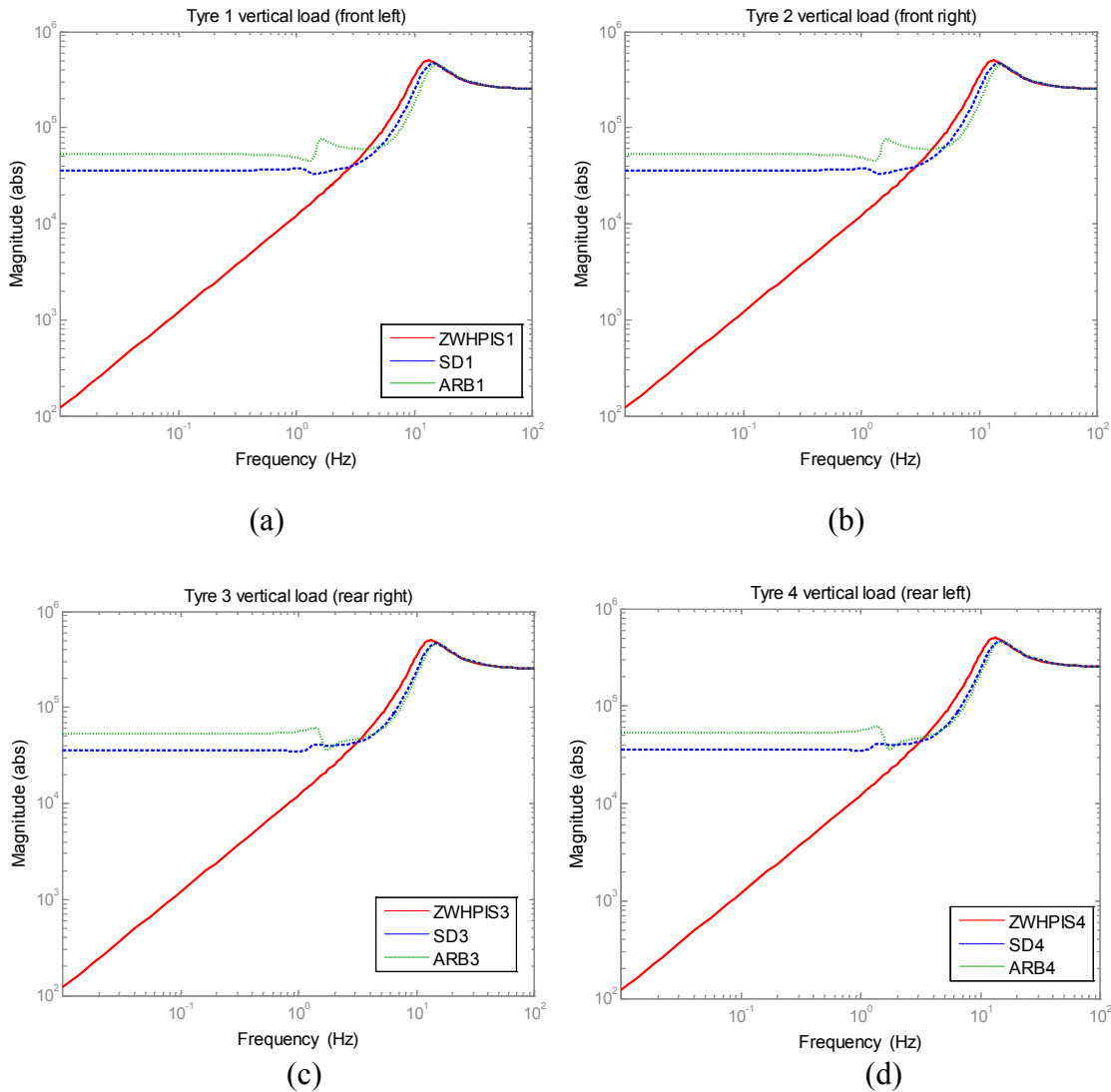


Figure 6. 4: Frequency response of tyre load at warp modes (a) front left (b) front right
(c) rear right (d) rear left

At the high frequency range of greater than 12Hz , the tyre dynamic loads are the same no matter how they are equipped in terms of suspension configurations. This is because at a high frequency, the tyre movements are dominant while the influence of the suspension becomes negligible.

6.5. Vehicle dynamic responses in time domain with system nonlinearity

6.5.1 Vehicle response under road bump input

Speed bump simulation tests are carried out to study how the proposed ZWHPIS system performs when running over a speed bump. One test is performed at low speed where the excitation frequency is close to the vehicle suspension low frequency range (1-2Hz). The other is performed at high speed where the excitation frequency is close to the suspension high frequency range ($>10\text{Hz}$). Figure 6.5 displays the speed bump signals against the time.

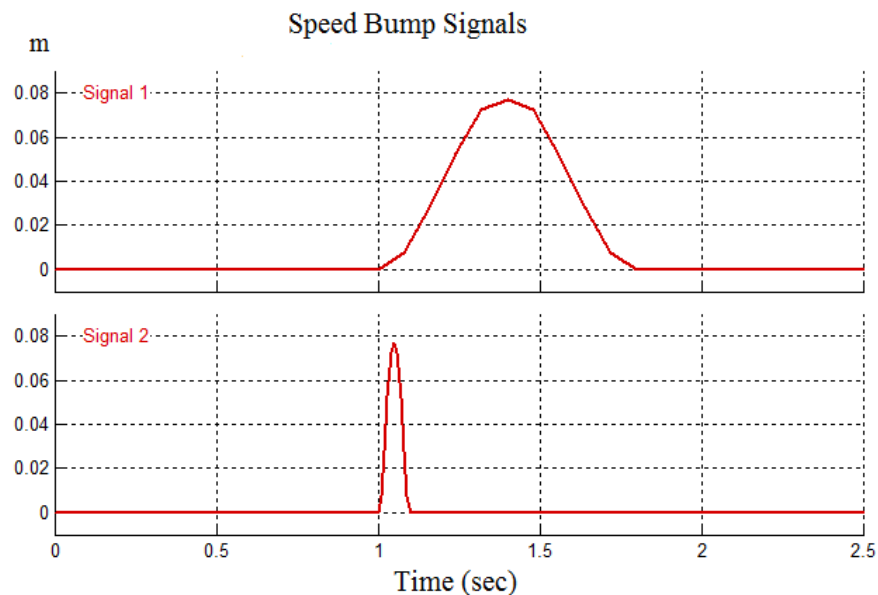


Figure 6. 5: Speed bump signals

The vehicle equipped with ZWHPIS suspension is compared with the reference vehicle with SD suspension under the speed bump tests. The static stiffness and damping properties of the ZWHPIS and SD suspension are presented in section 6.2.

Slow bump:

At the slow bump, the bump width is set to 0.8m and the height is set to 0.08m. The vehicle runs over the speed bump at a speed of 3.6 km/h (=1m/s). So it takes 0.8s for the tyres to run over the speed bump. As the wheelbase effects, the rear tyres will follow the front tyres to run over the speed bump with a time delay $T_d = \text{wheelbase}/\text{vehicle speed} = 2.8$ seconds.

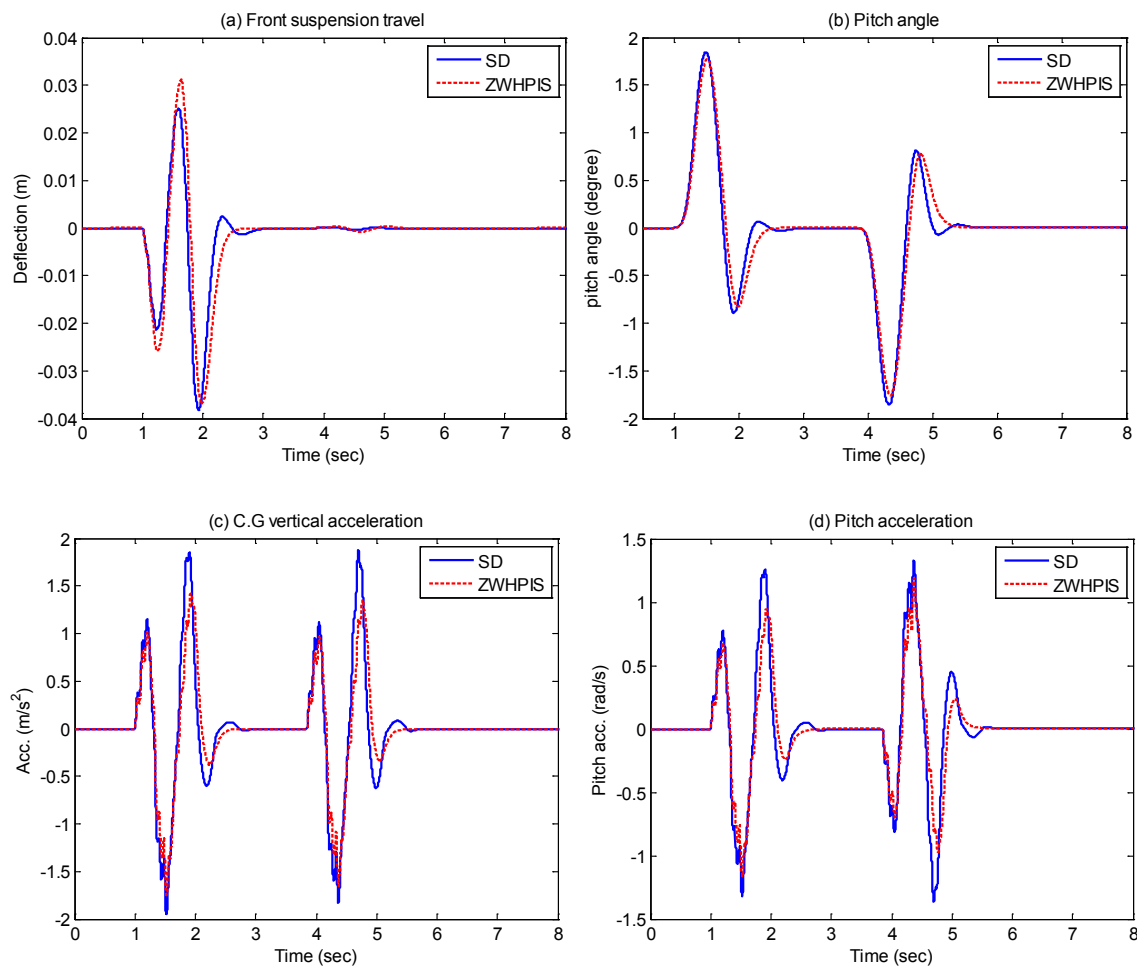


Figure 6. 6: Vehicle response at slow bump (a) front suspension travel (b) pitch angle (c) C.G vertical acceleration (d) pitch acceleration

Figure 6.6 shows the vehicle dynamics response when running over the speed bump at low speed. It includes the suspension travel, pitch angle, vertical acceleration at C.G and the pitch acceleration at C.G. Compared with the conventional SD suspension, the vehicle with the proposed ZWPHIS suspension has similar suspension travel and pitch angle responses. But the ZWPHIS vehicle has a much smaller magnitude of the vertical and pitch accelerations compared to the SD vehicle. The improved ride comfort of ZWPHIS suspension is mainly due to the nonlinear characteristics of the stiffness and damping of the hydro-pneumatic struts.

Fast bump:

At the fast bump test, the bump width is set to 0.4m and the height is the same as 0.08m. The vehicle runs over the speed bump at a speed of 14.4 km/h ($= 4\text{m/s}$) so that it takes 0.1s for the tyres to run over the speed bump. The time delay due to wheelbase is 0.7s.

Figure 6.7 shows the vehicle dynamics response when running over the speed bump at fast speed. Compared with the conventional SD suspension, the vehicle with the proposed ZWPHIS suspension has a smaller peak value of suspension travel and a slightly larger pitch angle response. The ride comfort of ZWPHIS is slightly reduced by the ZWPHIS suspension due to the small amount of increased vertical and pitch accelerations. However, the reduced suspension travel distance is more important at the high speed conditions as it prevents the suspension from bottoming-out which results in passenger discomfort.

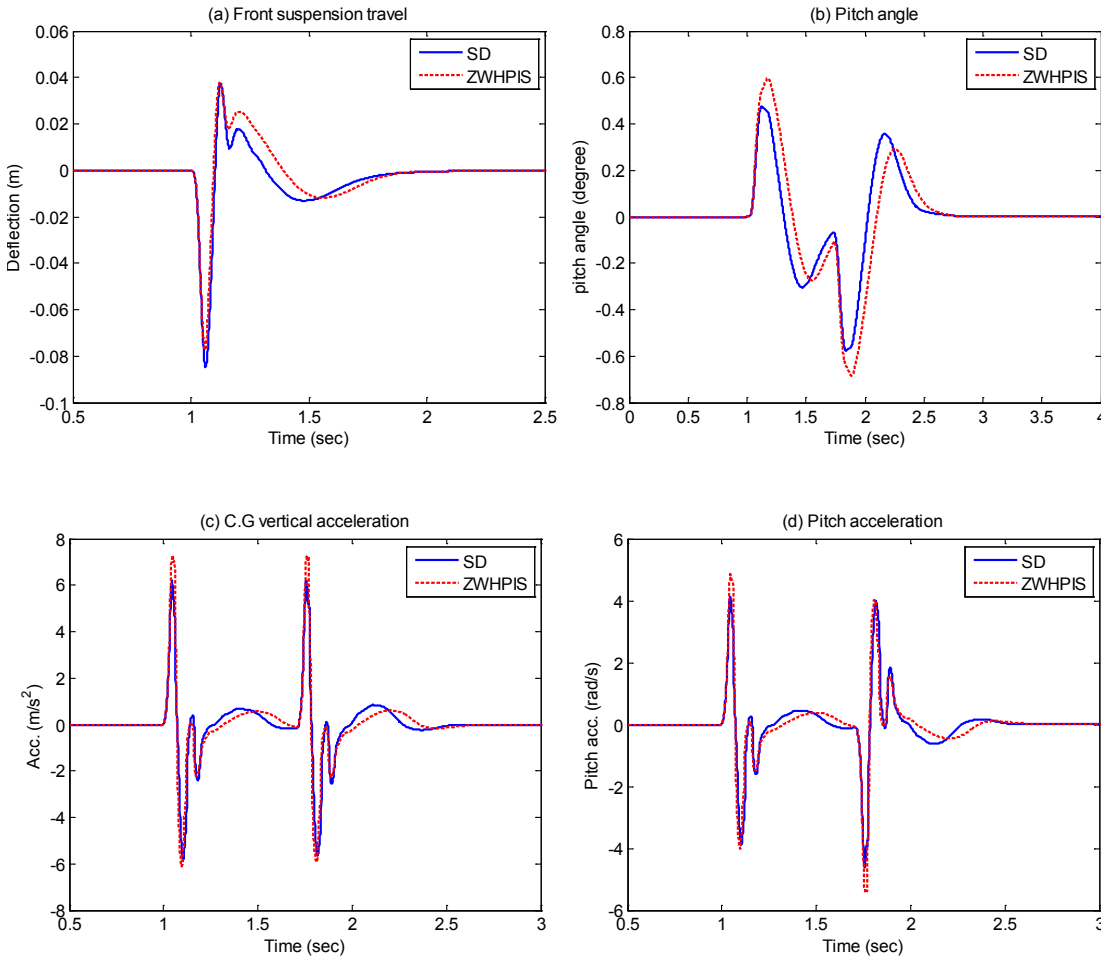


Figure 6. 7: Vehicle response at fast bump (a) front suspension travel (b) pitch angle (c) C.G vertical acceleration (d) pitch acceleration

The speed bump test results show that the nonlinearity of hydro-pneumatic suspension is desirable to improve the ride comfort of the vehicle in a wide speed range. It worth mentioning that the ZWHPIS suspension can conveniently integrate the vehicle height adjustment function into the suspension system so that the off-road performance will be further improved.

6.5.2 Tyre dynamic load at warp mode

Tyre dynamic load is also called weight transfer, and it is studied here to understand how the road-holding ability is affected by different suspension configurations. The less the tyre load varies, the better the tyre grips the road. When the variation of tyre load is

too much, one of the tyres may lose contact with the ground, resulting in a loss of traction and control if the locking differential is not equipped. The tyre warp inputs can be referred to Figure 5.13.

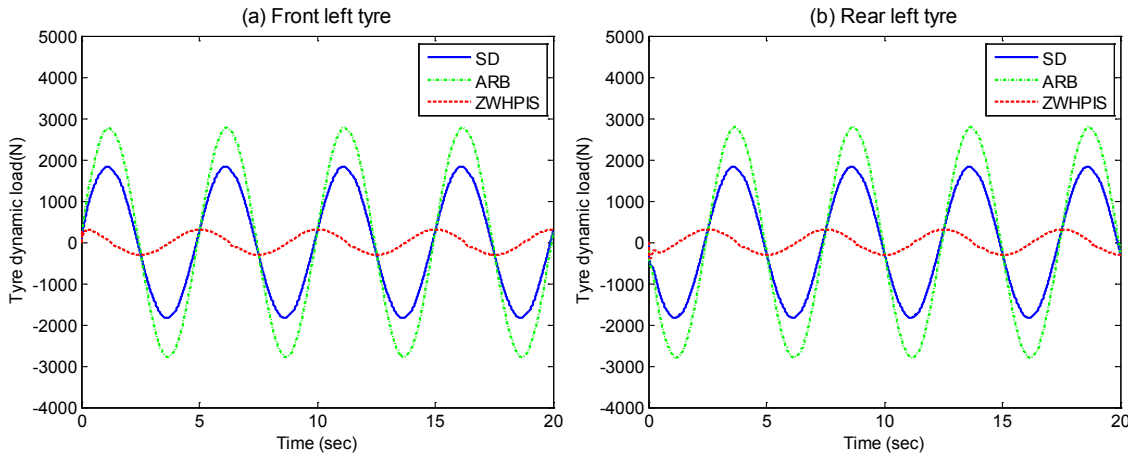


Figure 6. 8: Tyre load response at 0.2Hz warp road input

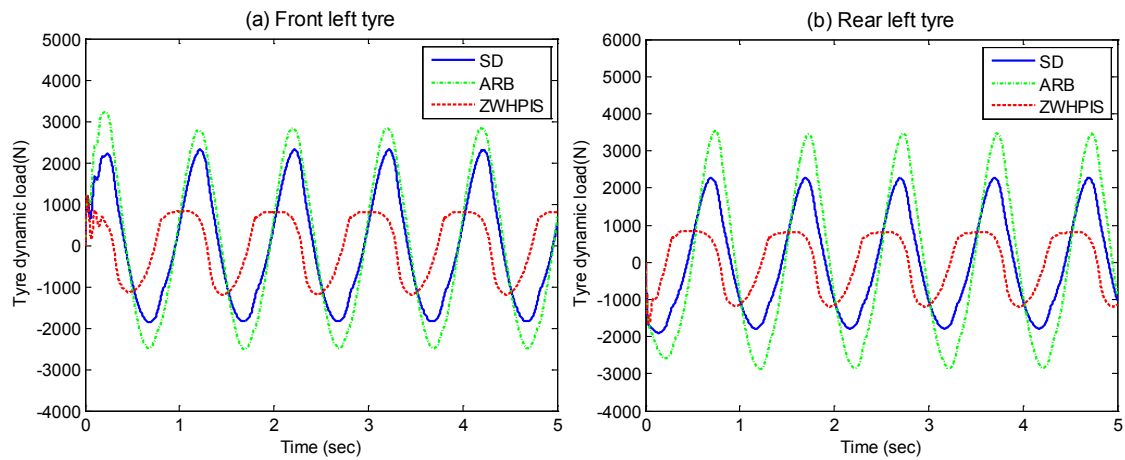


Figure 6. 9: Tyre load response at 1Hz warp road input

Figure 6.8 shows the vehicle tyre vertical load under warp excitation at the low frequency of 0.2Hz. It is shown that tyre load variation of the anti-roll bar vehicle is observed to be the largest, and that of the ZWHPIS vehicle has much smaller tyre forces, approximately one tenth of those of the anti-roll bar vehicle. As the ZWHPIS suspension has zero warp suspension stiffness, the small amount of tyre force variation is due to the damping effects of the interconnected suspension struts.

Figure 6.9 shows the vehicle tyre vertical load under warp excitation at a frequency of 1Hz. The results show that the tyre dynamic load of the ZWPHIS vehicle is still lower than those of the ARB and SD vehicles, but the magnitude of the tyre dynamic load becomes larger compared with the tyre load response at 0.2Hz warp excitation. It agrees well with the frequency response analysis presented in the previous section. When the excitation frequency increases, the tyre deflection and suspension damper start to play more and more of a role in the tyre dynamic load responses. Normally the speed of the off-road vehicle is very small when passing through large road obstacles, so the trait of zero warp suspension stiffness is really useful for off-highway applications.

6.6. Summary

In this paper, the modelling and tyre load analysis of a vehicle with a zero warp interconnected suspension system are presented based on parameters obtained from a typical sport utility vehicle. At the assumption of small oscillation amplitude, the gas spring of the accumulators are linearised in order that modal analysis can be performed to compare the suspension performance of different configurations. The results clearly illustrate that the proposed ZWHPIS suspension can achieve zero warp suspension stiffness, while at the same time maintaining soft bounce and improved roll stability. The results of tyre load analysis in the frequency domain and time domain under warp excitation both show that the vehicle fitted with the ZWHPIS has much less tyre load variation compared with conventional suspensions at low frequencies. The smaller the tyre dynamic load means the better road holding ability and the less vehicle body/frame torsional stress which is meaningful for off-road applications such as those which pertain to military vehicles.

Chapter 7: Experimental Validation of RHIS at Warp Mode

7.1 Introduction

A sport utility vehicle equipped with Roll-resistant Hydraulically Interconnected Suspension has been built in the suspension test lab at the University of Technology Sydney. The experimental validation of the RHIS system has been conducted in the lab. Due to time and resources limits, only the configuration of RHIS has been experimentally verified using the four-poster test rigs. The variations of the Hydraulically Interconnected System (HIS) are all so similar in nature that the verification of the roll-plane interconnection could be confident enough to apply to the other interconnection configurations. The test results are also compared with anti-roll bars to demonstrate the advantages of the fluidic interconnected system over the mechanical left-right interconnected system.

7.2 Test facility description

7.2.1 Testing vehicle

A full size sport utility vehicle (Ford Territory) by Ford Australia is used for testing. Some parameters are provided by the company and those parameters such as sprung mass inertias which need to be estimated are obtained through the parameter estimation process. The detailed method and estimation process can be found in the literature [104].

The testing vehicle has a McPherson independent suspension at the front and a semi-trailing arm suspension at the rear. A stronger anti-roll bar is fitted at the front and a small roll bar is fitted at the rear.

A roll-plane interconnected system has been designed and installed into the testing vehicle for experimental evaluation. The hydraulic piping system is placed underneath the vehicle chassis, interconnecting the hydraulic cylinders into two circuits according to the schematic in Figure 3.3. Flexible hoses are used to connect the ports of the four cylinders to the rigid piping system in order to allow free movement of cylinders. Each circuit employs a hydraulic accumulator to control roll stiffness.



(a) Front installation



(b) Rear installation

Figure 7. 1: RHIS installation (a) Front installation (b) Rear installation

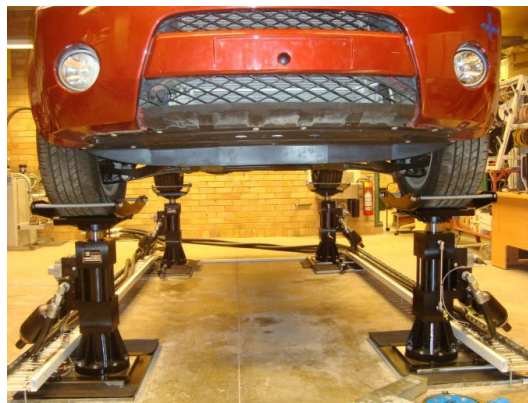


Figure 7. 2: Four poster suspension test rig

The RHIS System implementation required the removal of the anti-roll bar from the testing vehicle. At the front, the cylinder bodies pivot on the vehicle chassis, whilst the cylinder rod ends are attached to the lower control arm of the wishbone suspension, as

shown in Figure 7.1 (a). The overall stroke of the cylinders matches the suspension travel, and the mounting location of the cylinder does not affect wheel turning. At the rear, the cylinders are installed alongside the coil springs, mounted to the vehicle body at the top, and attached to the control arm at the bottom, as shown in Figure 7.1 (b).

7.2.2 Four-poster multi-channel test rig

The suspension test rig as pictured in Figure 7.2 consists of four independently controlled servo actuators, a hydraulic power unit, and a central control system. The actuators are positioned and fixed according to the vehicle's wheel base and track width. Each wheel sits on a suitable wheel pan which is mounted to the actuator's piston rod and features guard rails to laterally restrain the wheels; however, the wheels are not restrained in a vertical direction. The four-post system's operating limitations are listed in Table 7.1:

Table 7. 1: Four poster test rig specification

Amplitude (max.)	± 80 mm
Frequency (max.)	25 Hz
Force (max.)	40 kN
Acceleration (max.)	20 g
Velocity (max.)	0.8 m/s

Table 7. 2: Specifications of sensors

Code	Category	Mounted position	Quantity	Permanently installed
500Kg*4	Load cell	On the wheel plates	4	√
HP_24DCTC	LVDT	Rear wheel stations	2	√
HP_7DCTC	LVDT	Front wheel stations	2	×
AST4000C	Pressure transducer	Inside cylinders	2	√
MMA7361L	Two-axis acceleration sensor	Mass centre	2	×
LPY503AL	Two-axis Gyro meter	Mass centre	2	×

The linear variable displacement transducer (LVDT) is mounted at each corner along the shock absorber. The load cells are mounted under each wheel pan to directly measure the dynamic tyre load. Accelerometer and gyros are mounted at the C.G of vehicle body. We acquired the data from mounted sensors that can cover most aspects of the vehicle dynamics. NI data acquisition system and LABVIEW are used to log the data. The specifications of these sensors are shown in the Table 7.2. The sensor power board is capable of powering up to 20 sensors, and the NI data acquisition board can host 32 analogy input channels.

7.3 Testing methodology

7.3.1 Vehicle configurations

Comparative vehicle tests are carried out under different excitations for three suspension configurations:

- 1) SD: conventional spring-damping suspension without anti-roll bar;
- 2) ARB: conventional spring-damper with anti-roll bars;
- 3) HIS: the roll-resistant Hydraulically Interconnected Suspension (anti-roll bars removed).

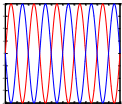
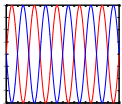
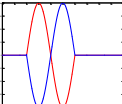
All three configurations have the same suspension springs and shock absorbers which are originally fitted, similar to the production specification. The ARB vehicle is the same as the production version without modification. The SD configuration is the same as the ARB configuration except the anti-roll bars at the front and rear are removed from the vehicle. The RHIS vehicle is modified from the SD vehicle. The hydraulic interconnected system is installed to achieve improved roll stability. The hydraulic

accumulators of the RHIS configuration need to be pre-charged with nitrogen to a specific working pressure; the higher the pre-charged pressure, the greater the roll stiffness the RHIS system holds, and vice versa. For the purpose of this analysis, the pre-charge pressure of 3.0MPa has been chosen.

7.3.2 Testing procedure

The field test of a roll-resistant RHIS vehicle at cornering on smooth road is conducted by Wang [83], and the testing results show agreement with simulation results as the roll stability is greatly improved. The nonlinear roll stiffness of the roll-resistant HIS can greatly reduce the vehicle roll angle at fast cornering. However the property of the decoupled warp mode by the RHIS system still needs to be further verified by experiments. The lab test in this paper is specially designed with a focus on the vehicle performance under the axle articulation (warp mode) induced by the rough road surface.

Table 7. 3: Summary of lab tests

Tess Items	Ground excitation	Amplitude	Frequency
Axle articulation at low frequency		50mm	0.2HZ
Axle articulation at high frequency		3mm	10 HZ
Impule axle articulation		50mm	2.5HZ
Random road	B-class road	N/A	N/A

The steady state responses of a vehicle under axle articulation are investigated at low and high frequencies respectively. Then, the impulse axle articulation test is performed to investigate the vehicle's transient performance. Lastly, the random road test is conducted for ride comfort evaluation. The mathematical expressions of road inputs are listed below and the lab tests are summarised in Table 7.3.

Test 1: Axle articulation at low frequency

The road excitation to the front-left and rear right wheels is expressed as:

$$Zg(t) = 0.05 * \sin(2\pi * 0.2 * t) \quad (7.1)$$

The road excitation to the front-right and rear-left wheels is expressed as

$$Zg(t) = 0.05 * \cos(2\pi * 0.2 * t) \quad (7.2)$$

while the amplitude is $0.05m$, frequency is $0.2Hz$

Test 2: Axle articulation at high frequency

The road excitations are expressed the same as test 1 except the amplitude is $0.003m$, and the frequency is $10Hz$.

Test 3: Axle articulation impulse test

The road excitation to the front-left and rear-right wheels is expressed as

$$Zg(t) = \begin{cases} 0.05 * \sin(2\pi * 2.5 * t), & 0 < t < 0.2s \\ 0, & t \geq 0.2s \end{cases} \quad (7.3)$$

The road excitation to the front-right and rear-left wheels is expressed as

$$Zg(t) = \begin{cases} 0.05 * \cos(2\pi * 2.5 * t), & 0 < t < 0.2s \\ 0, & t \geq 0.2s \end{cases} \quad (7.4)$$

Test 4: Random road roughness test

The road profile of B class road according ISO 8608 is used in this test. The road input is derived from the integration by the road model:

$$\dot{Z}_g = -2\pi f_0 Z_g + 2\pi\omega\sqrt{G_0 V} \quad (7.5)$$

while $f_0=0.01$ is the cut-off frequency, w is the random gauss noise, $G_0=256e-6$ is roughness index which represent the motorway smooth road. Vehicle longitudinal velocity V is 22.2 m/s which is equal to 80km/h.

Vehicle vertical and lateral accelerations are measured by the 3-axis accelerometers mounted at the C.G of vehicle body. Four linear displacement transducers are installed to measure the suspension travel of the four wheels. The vehicle rotational response is measured by the gyro mounted at the same position of accelerometers. Finally, two pressure transducers are fitted at point P_A and P_B (see Figure 7.1) to monitor the hydraulic system response. The tyre load at each corner is directly measured by the load cells installed under the wheel pans. The sensor data are logged by means of a National Instruments acquisition system (USB-6343 X-series) in conjunction with LABVIEW.

7.4 Test results

The vehicle responses with the three suspension configurations are presented and compared in this section.

7.4.1 Steady state of Axle articulation excitation

1). *Warp mode 0.2Hz, 50mm amplitude*

The effects of the warp motion-mode on vehicle handling are more pronounced at lower frequencies, for instance when the vehicle is driving over an uneven surface at relatively low speed. Hence, the wheels of the test vehicle are excited at a frequency of 0.2 Hz and amplitude of 50 mm.

In Figure 7.3, the front suspension deflections of a vehicle fitted with anti-roll bars are smaller than those of vehicles with spring-damper or HIS suspension. On the other hand, the rear suspension deflections of a vehicle fitted with anti-roll bars are smaller than those of vehicles with spring-damper or HIS suspensions. The front anti-roll bar is much stronger so that ARB vehicle's the roll stiffness distribution is towards the front while SD and ARB vehicles have more equally distributed roll stiffness. The front suspension with ARB is less flexible under axle articulation and the vehicle's roll motion is dominated by the front suspension. It can be observed in Figure 7.4 that the roll rate of the ARB vehicle has a 180 phase different to those of the SD and HIS vehicle.

The tyre dynamic loads are measured and compared in Figure 7.5. Larger tyre dynamic forces can be observed at all four wheels for ARB vehicle while the HIS vehicle has a similar tyre dynamic force as the SD vehicle. It shows that HIS does not increase the tyre dynamic forces even with a greater roll resistance at a warp (axle articulation) road situation.

The vehicle vertical and lateral accelerations at vehicle body C.G. are also compared and shown in Figure 7.6. The ARB vehicle has a significantly larger vertical acceleration level compared with the SD and HIS configurations and the high frequency oscillation can be observed. This may be partly due to the warp deflection of the vehicle body and a reaction with the anti-roll bars. It is evident that a vehicle with HIS suspension has a similar acceleration level as a spring-damper only vehicle.

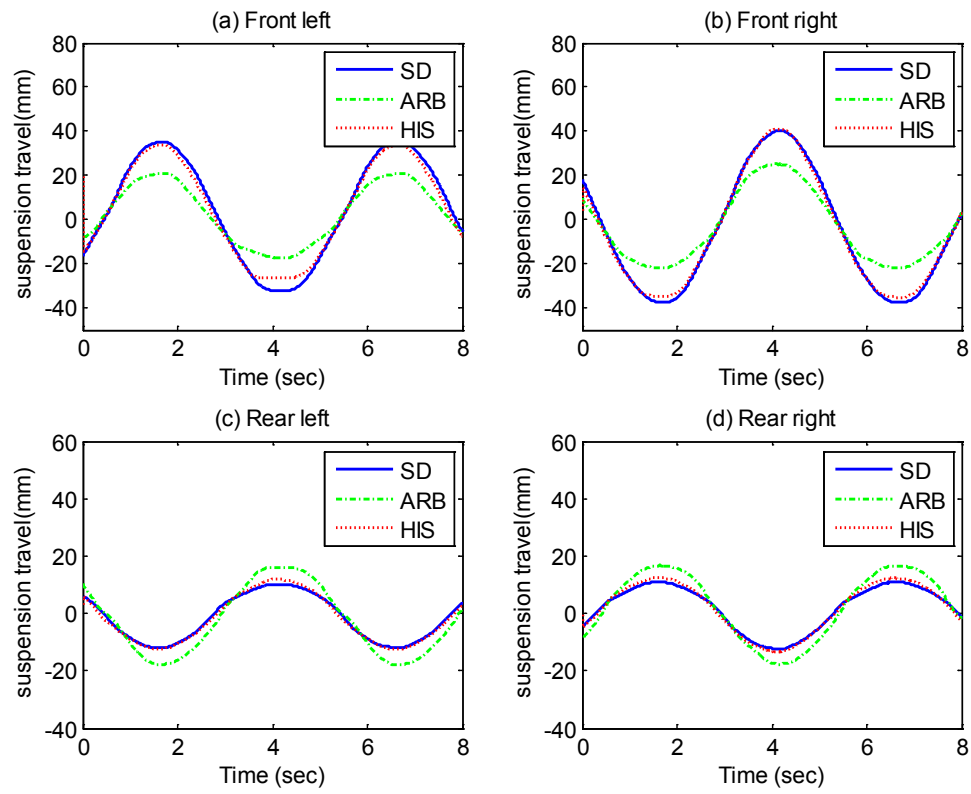


Figure 7. 3: Suspension deflections (a) front left (b) front right (c) rear left (d) rear right

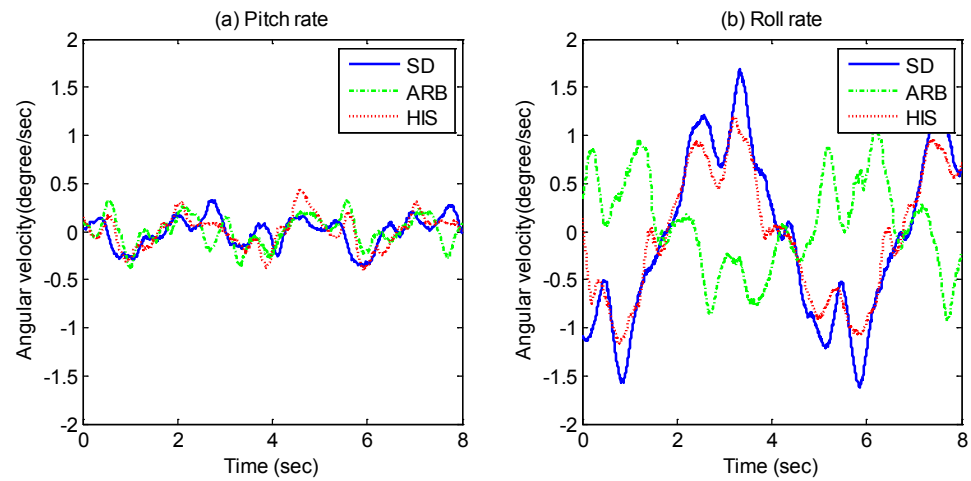


Figure 7. 4: Rotational velocities (a) pitch rate (b) roll rate

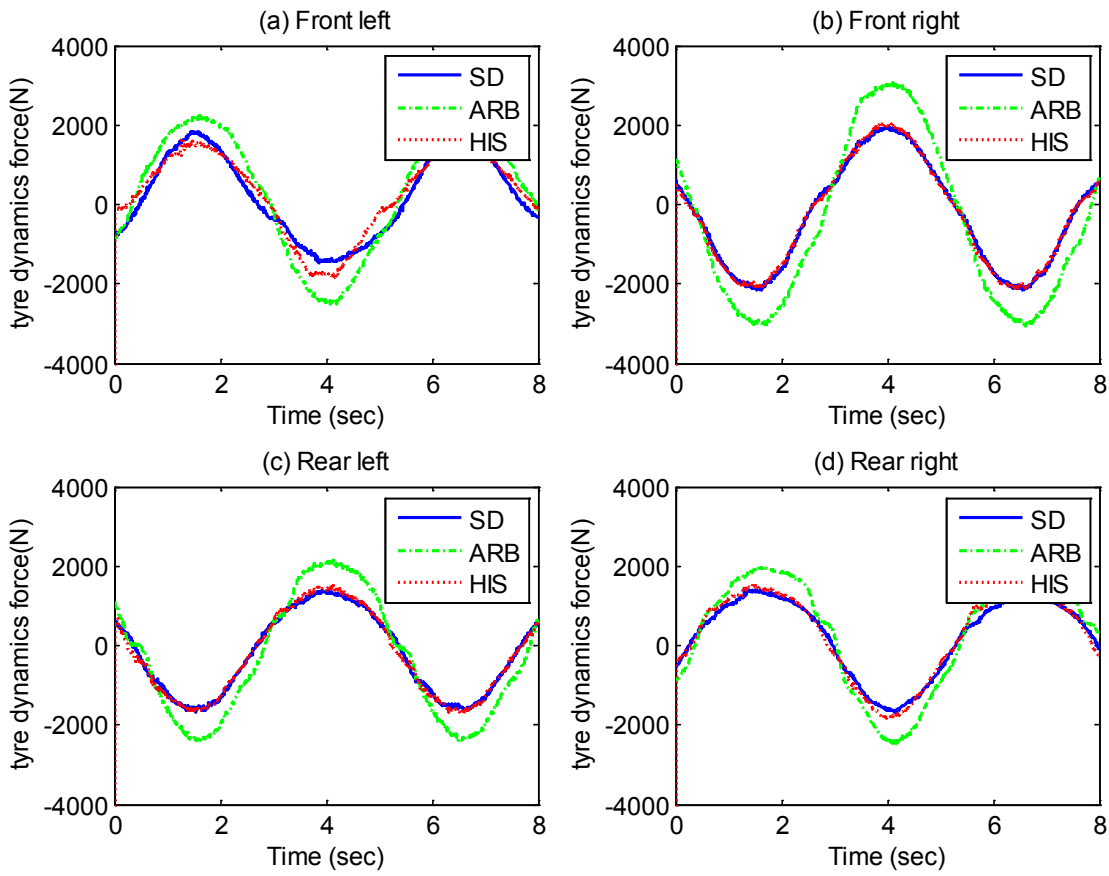


Figure 7. 5: Tyre dynamic forces (a) front left (b) front right (c) rear left (d) rear right

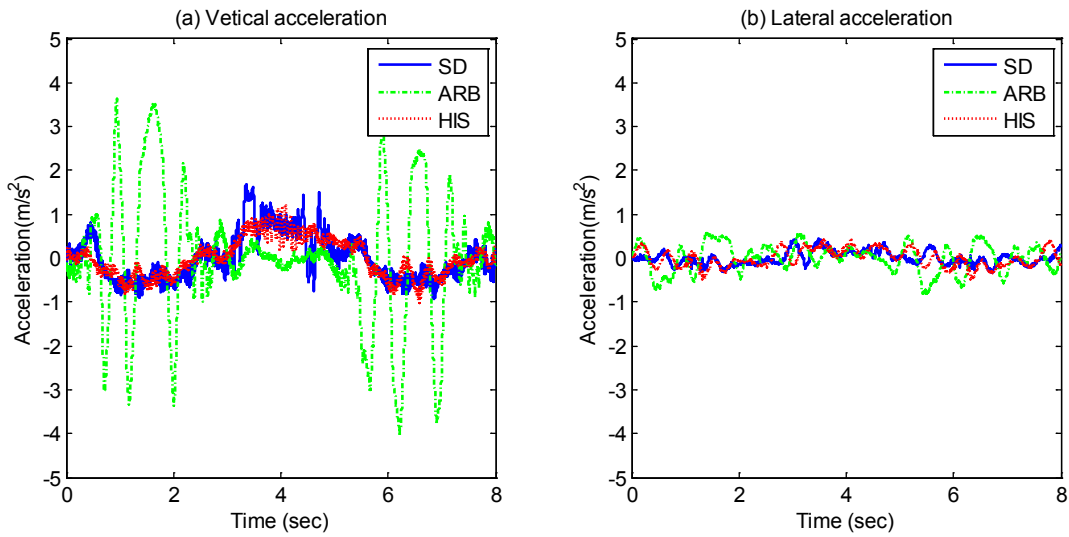


Figure 7. 6: Vehicle acceleration at C.G

2). Warp mode 10Hz, 3mm amplitude

The vehicle performances under high frequency warp excitation are also studied with three different suspension configurations. The excitation frequency is chosen as 10Hz which is close to the vehicle unsprung tyre frequency. The amplitude is 3 mm.

It can be seen in Figure 7.7 and Figure 7.9 that the ARB vehicle presents similar responses of suspension deflection and tyre dynamic loads as the SD vehicle. The suspension deflections are smaller and the tyre dynamic forces are relatively larger for the HIS vehicle, and this is especially more obvious at the front. This indicates that the effects of the anti-roll bars are small at the low amplitude high frequency warp excitations while the hydraulic fluid damping effects of HIS suspension become evident and have some negative effects to the vehicle's road holding ability at the high frequency condition. However, this high frequency road warp excitation is rare in real driving scenarios. In contrast, the low frequency warp is more important for off-road driving.

In Figure 7.8, the magnitudes of roll and pitch rates of all three vehicles are small and comparable. It shows the rotational motions are not evident under small amplitude warp excitation for different suspension configurations. In Figure 7.10, the vertical accelerations of the HIS vehicle and the SD vehicle are comparable while those of the ARB vehicle are relatively higher. It may be due to the additional friction effects introduced by the rubber bushings of anti-roll bars which worsen the vehicle ride comfort.

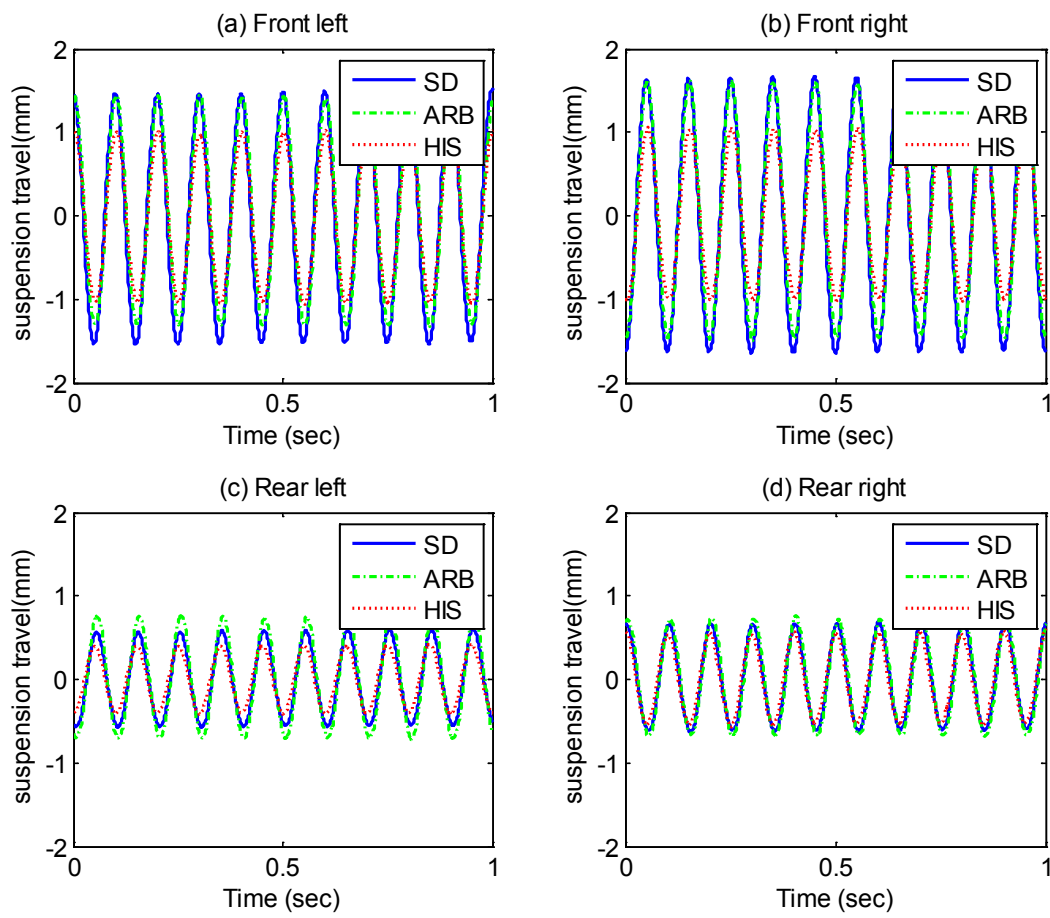


Figure 7. 7: Suspension deflections

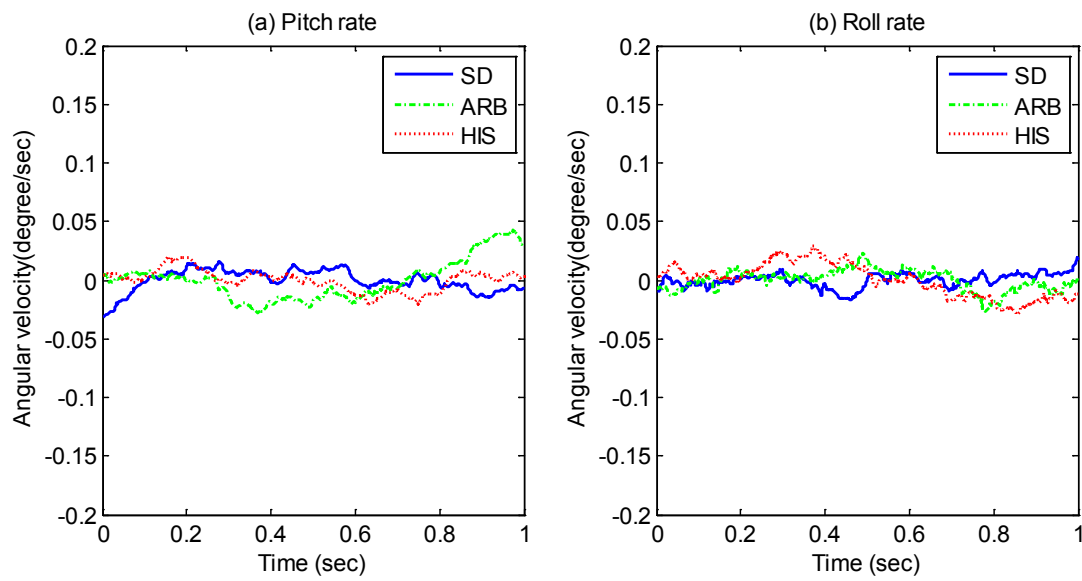


Figure 7. 8: Rotational velocities

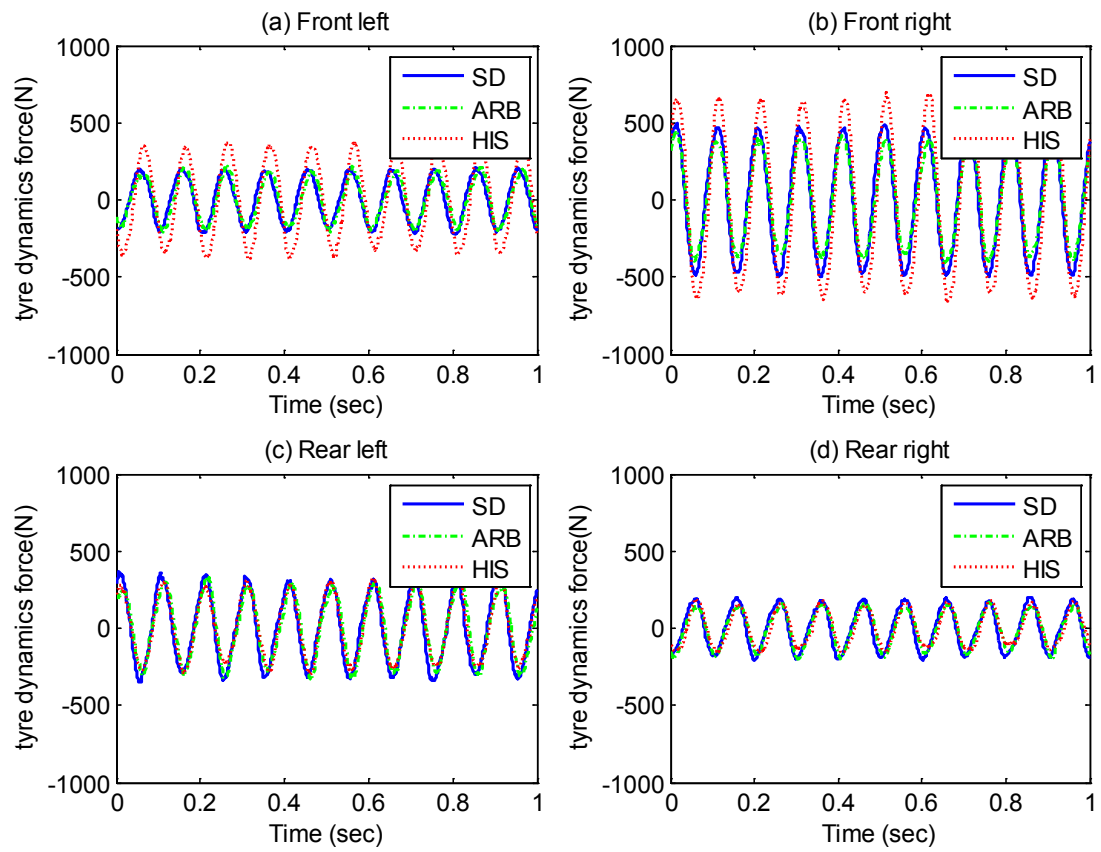


Figure 7. 9: Tyre dynamic forces

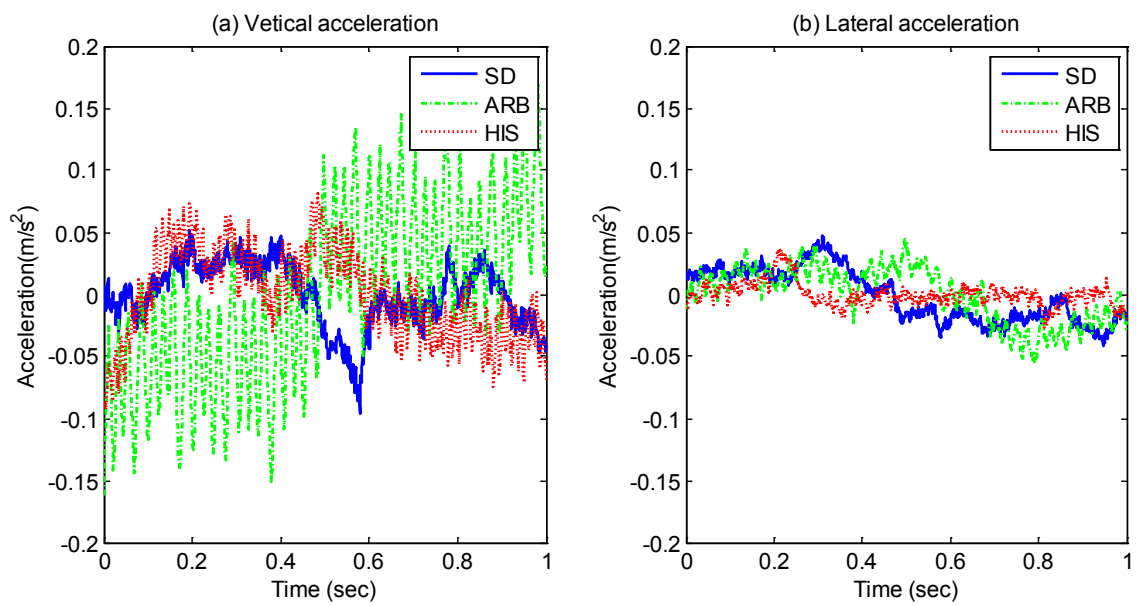


Figure 7. 10: Vehicle accelerations at C.G

7.4.2 Transient response of bump articulation

The vehicle transient responses are investigated under impulse bump articulation which simulates the event when a vehicle's one diagonal wheels run over road bumps while the other diagonal wheels run into road holes simultaneously.

The transient responses of the vehicles are measured and compared from Figure 7.11 to 7.14. These show that the ARB vehicle has the smallest peak value of suspension deflections at the front and the largest peak value of suspension deflection at the rear. The SD vehicle has the largest magnitude of suspension deflection at the front and the smallest peak value at the rear. The response of the HIS vehicle is in between. It can be seen in Figure 7.13 that the ARB vehicle has a greater tyre dynamic load at the front left wheel, but the other three wheels present similar tyre loads. It could be the effects of the vehicle's flexible body frame which absorbs some shock loads. The ARB vehicle body has 180 phase differences for pitch/roll velocities and vertical/lateral accelerations compared to those of the SD vehicle and HIS vehicle. The phase change by the anti-roll bars may be due to the altered roll stiffness distribution.

In Figure 7.14, the magnitudes of the vertical acceleration of vehicles with three suspension configurations are comparable, though the ARB vehicle presents slightly smaller vertical acceleration. For the lateral acceleration, it can be observed that the ARB vehicle has a larger magnitude and presents more serious oscillation. By contrast, the SD vehicle and the HIS vehicle have a smaller lateral acceleration and the oscillation is quickly dampened down. The results indicate that the vehicle with stronger anti-roll bars lacks roll damping while the HIS system not only increases the roll stiffness but also provides addition roll damping without affecting the ride damping performance. The roll mode decoupling properties in terms of both stiffness and

damping are unique and useful for suspension design and mode-based suspension optimisation.

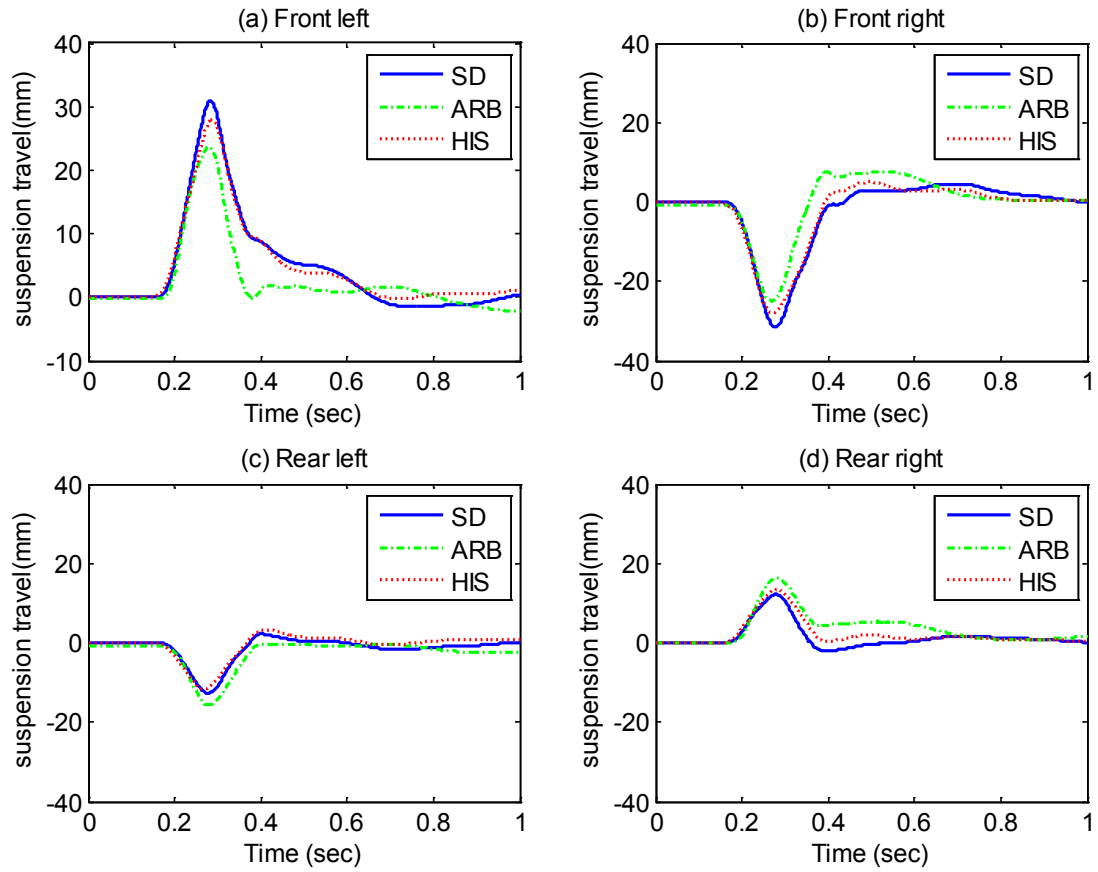


Figure 7.11: Suspension deflections

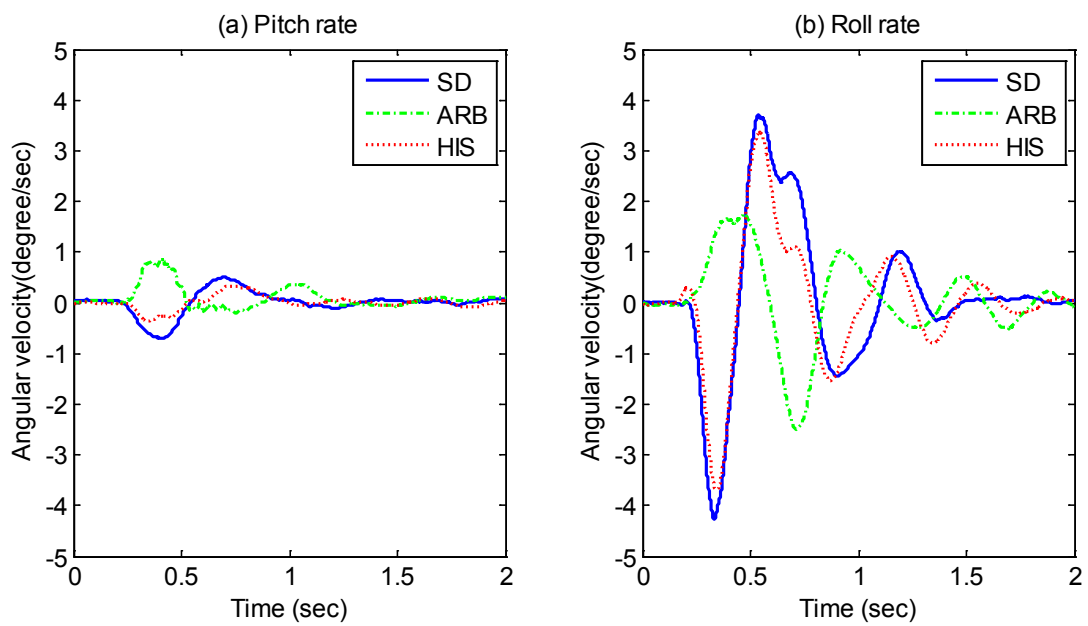


Figure 7.12: Rotational velocities

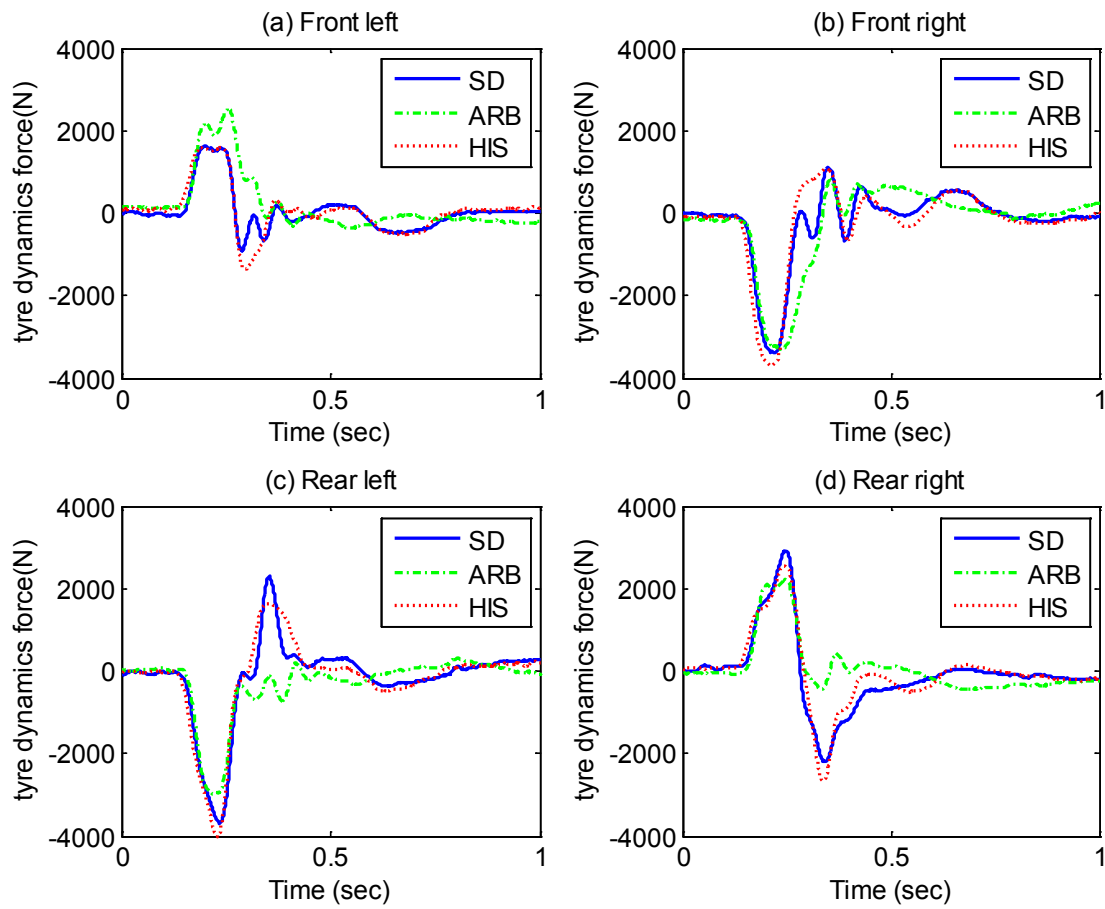


Figure 7.13: Tyre dynamic forces

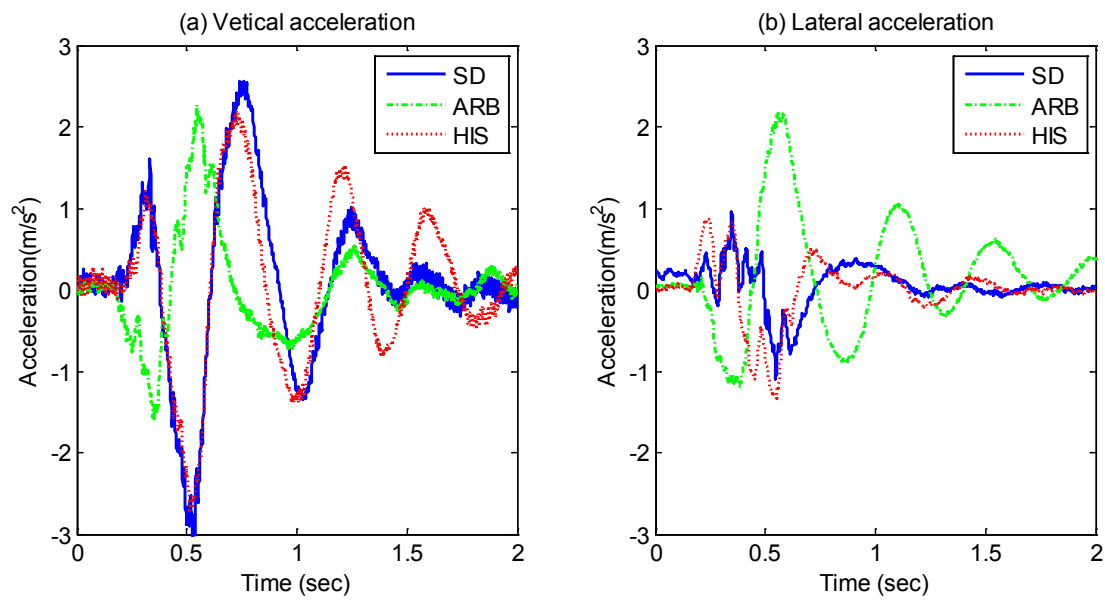


Figure 7.14: Vehicle accelerations at C.G

7.4.3 Stochastic road responses

According to the ISO 8608, the B-class (motorway) stochastic road is used in our lab test to investigate how the vehicle ride is affected by the different suspension configurations. The road profile in time history is shown in Figure 7.15 assuming that the left and right track are identical and the rear-wheels undergo the same profile as the front wheels with a time delays of 0.128 sec. It equals 80km/h of vehicle speed in the straight line.

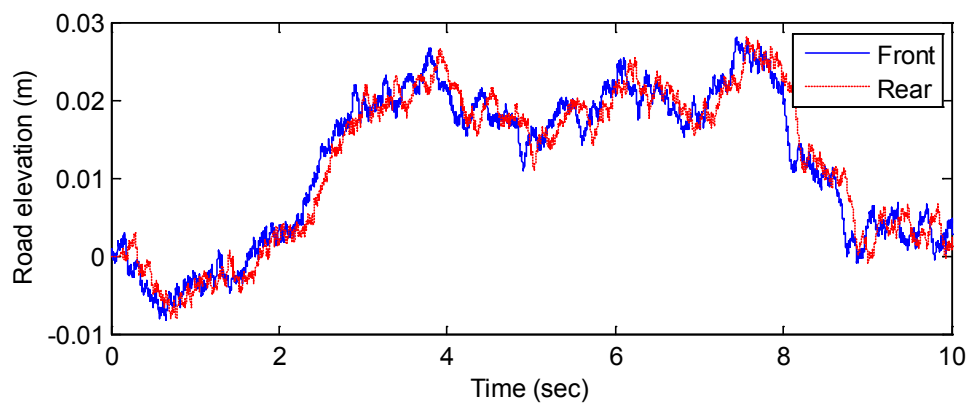


Figure 7. 15: Road profile

Figure 7.16 is the comparison of root mean square (RMS) of the vehicle body's pitch and roll rates with three suspension configurations (SD, ARB and HIS). It shows that HIS suspension slightly increases the pitch rate compared with SD suspension and the pitch rate of the ARB vehicle is smaller than the SD vehicle, although the differences among the three suspension configurations are small. HIS suspension also increases the roll rate slightly compared with SD suspension, but the roll rate of the ARB vehicle is significantly larger than that of the SD vehicle and the HIS vehicle. As the input signals of the left and right track are identical, the roll motion excited during the tests are small but due to the lack of damping by the anti-roll bars, the ARB vehicle experiences a larger roll motion.

Figure 7.17 is a comparison of vehicle body accelerations both at the vertical and lateral level. As mentioned before, the inputs of left and right road roughness are the same, and the lateral motion of the vehicle is minimal compared to the vertical motion. For the C.G vertical acceleration, the RMS values of the SD vehicle and the HIS vehicle are similar while the RMS value of the ARB vehicle is significantly higher being more than 20% (from 0.4 m/s² to 0.5 m/s²). This means that the HIS system doesn't affect the ride comfort while the Anti-roll bars have a negative influence on the vehicle's ride comfort possibly due to the friction introduced by the rubber bushings at the connection between the anti-roll bars and the vehicle body.

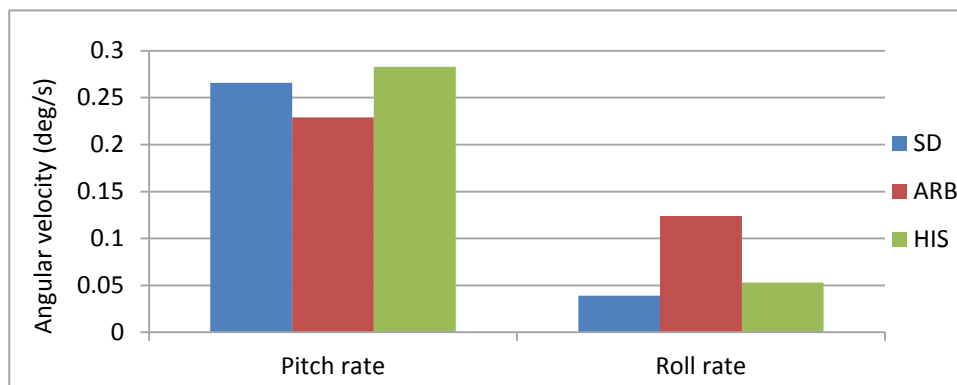


Figure 7. 16: RMS of angular velocity

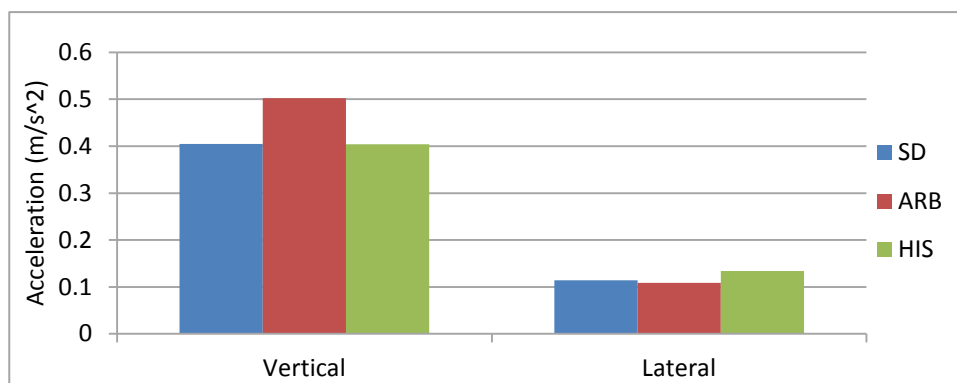


Figure 7. 17: RMS of vehicle C.G acceleration

7.4.4 Comparison with theory

The simulation results are presented in this section and discussed in relation to experimental results. Due to limited space, only the axle articulation at 0.2Hz and the impulse bump articulation are discussed here.

1). Warp mode 0.2Hz, 50mm amplitude

The simulated vehicle responses of suspension deflection, rotational velocity, tyre dynamic load and vehicle body acceleration are presented in Figure 7.18 to 7.21 under the low frequency large amplitude axle articulation road excitation. The ARB vehicle has a smaller suspension deflection at the front and a larger suspension deflection at the rear compared with the SD vehicle or HIS vehicle. For the tyre dynamic load, the ARB vehicle has larger magnitudes both at the front and at the rear. The roll rate and lateral acceleration of the ARB vehicle are considerably larger than those of the SD vehicle or HIS vehicle while the pitch rate and vertical acceleration of all three configurations are similar.

Compared with the vehicle responses of experiments shown in Figure 7.3 to 7.6, it can be seen that simulation results of suspension deflection and tyre dynamic force agree well with the experiments except for small differences in relation to the magnitudes, particularly at the rear suspension. The phase change of roll motion is also predicted by the mathematic models. Both experiment and simulation results show that the ARB vehicle presents less flexible suspension and larger tyre dynamic forces, while the HIS suspension offers the same flexibility as the SD suspension at the warp mode.

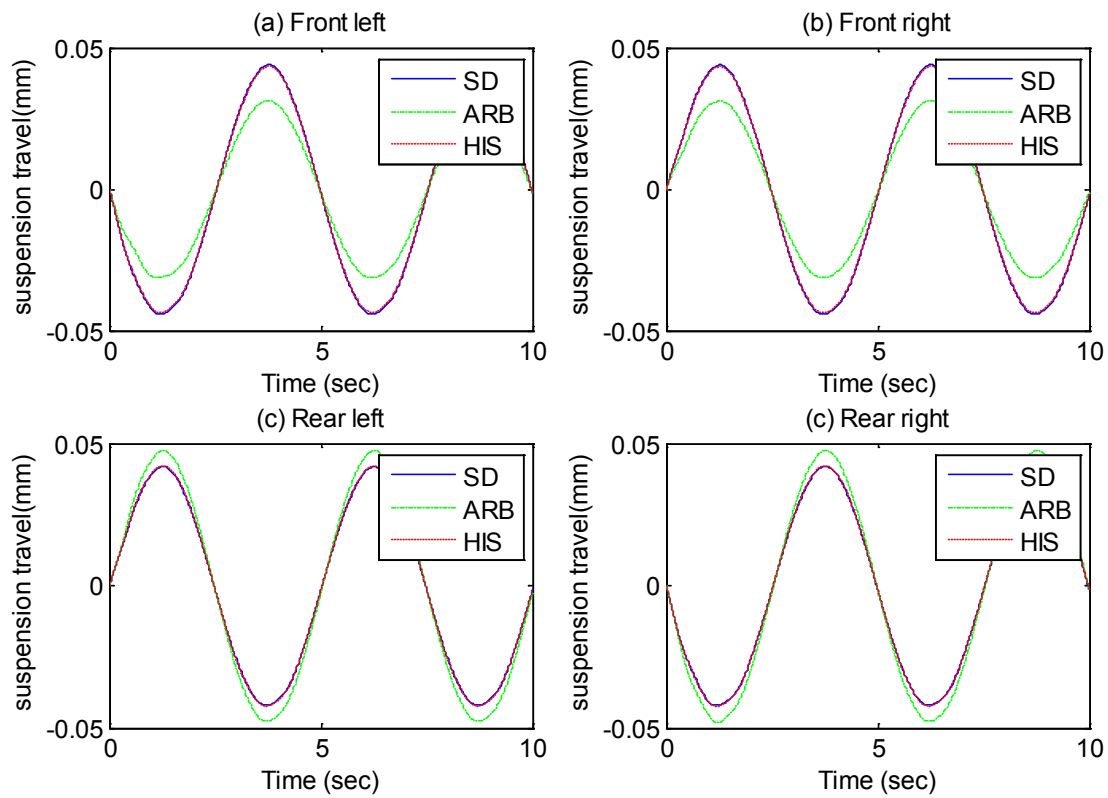


Figure 7.18: Suspension deflections (a) Front left (b) Front right (c) Rear left (d) Rear right

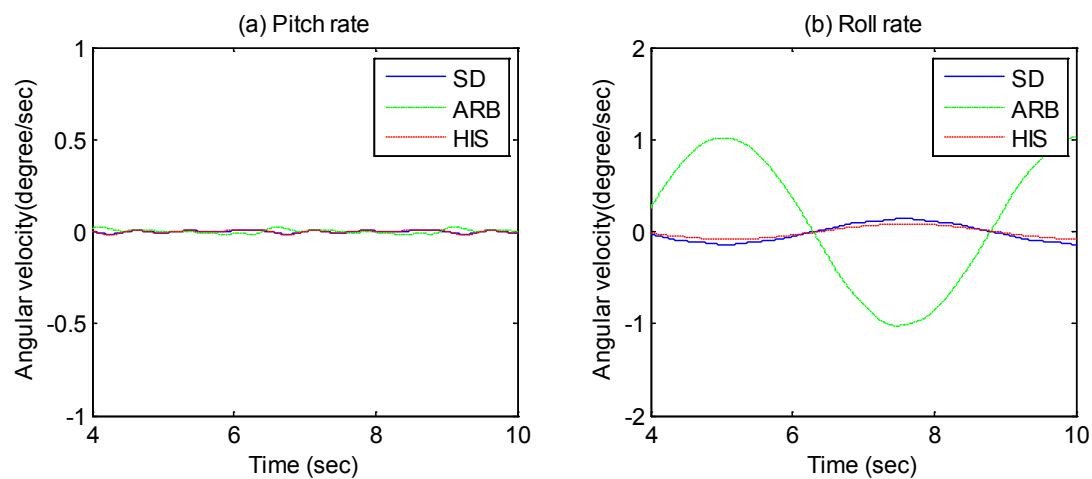


Figure 7.19: Rotational velocities (a) Pitch rate (b) Roll rate

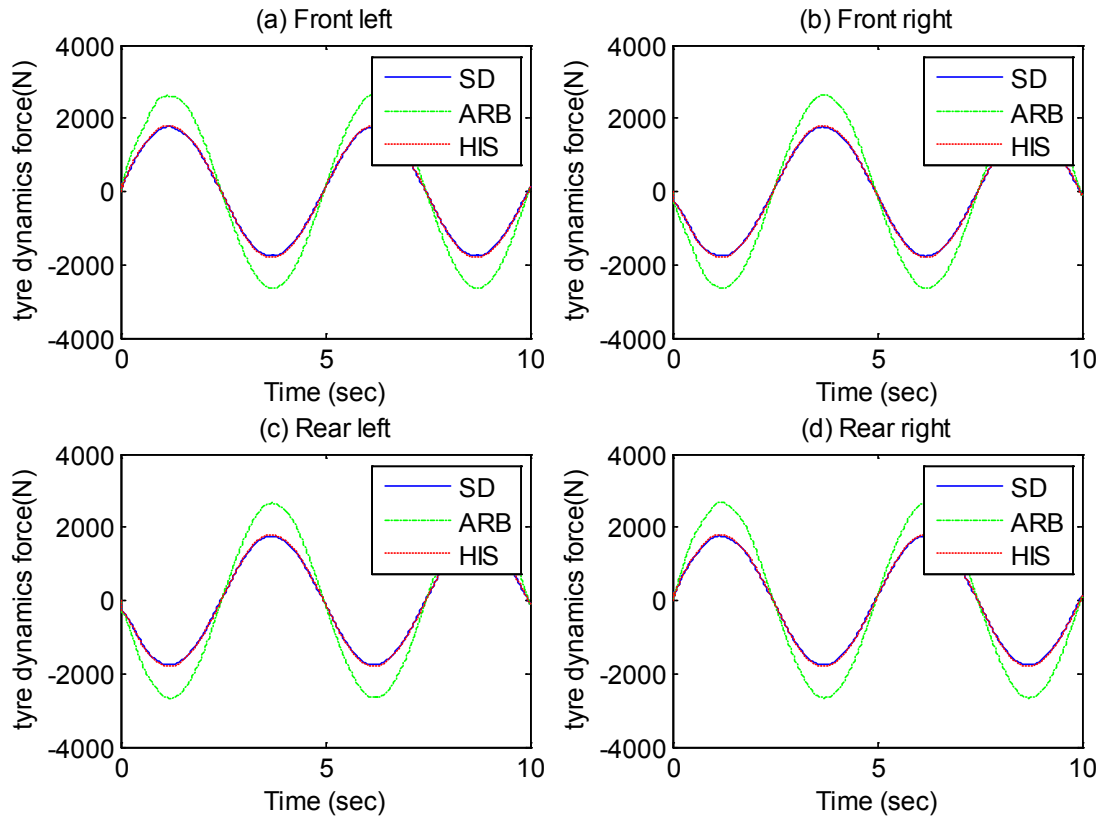


Figure 7. 20: Tyre dynamic forces (a) Front left (b) Front right (c) Rear left (d) Rear right

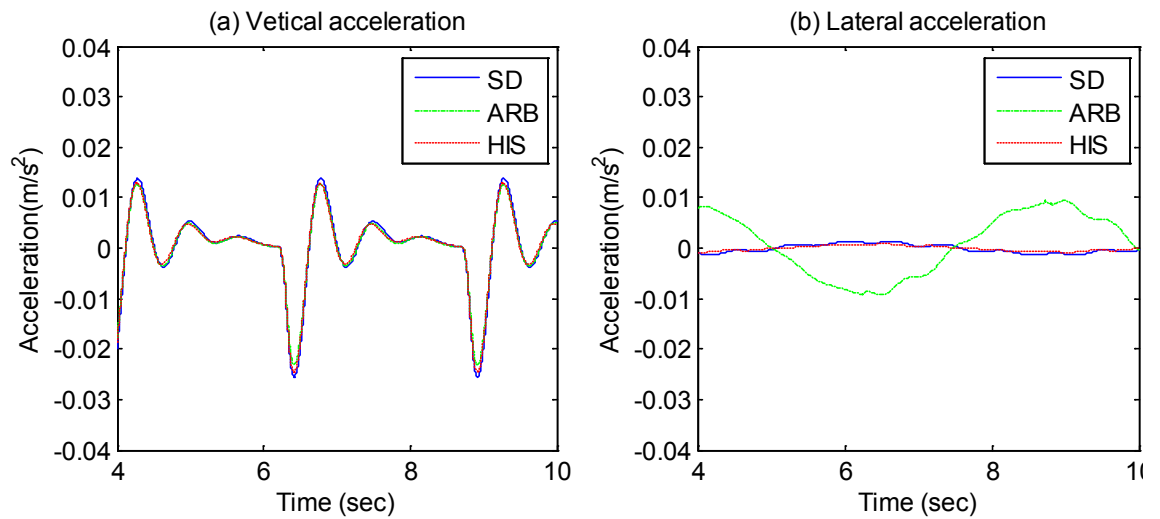


Figure 7. 21: Vehicle accelerations at C.G

However, for the vehicle roll motion, the responses are different between the experiment and simulation. The roll rate of the ARB vehicle in simulation is significantly larger than the SD vehicle and ARB vehicle, while comparable magnitudes are observed in the experiment. For the vehicle body acceleration, the responses are also different between the experiment and simulation. The vertical accelerations of all three vehicle configurations in simulation are small, but the ARB vehicle in the experiment presents a significantly larger acceleration in the vertical direction. The discrepancy is most likely caused by the flexible vehicle body/frame. The assumption of a rigid vehicle body in the mathematical model is not valid in the road warp excitation. The vehicle body/frame's stiffness has a large influence on the vehicle roll response. Another contributor may be the suspension compliance which is not modelled in simulation.

2). Impulse bump articulation

The simulated vehicle responses of suspension deflection, rotational velocity, tyre dynamic load and vehicle body acceleration under impulse bump articulation are shown in Figure 7.22 to 7.25. The ARB vehicle has a smaller suspension deflection at the front compared with the SD vehicle or HIS vehicle. For the tyre dynamic load, the ARB vehicle has larger magnitudes at the front while it displays similar tyre forces to the SD and HIS vehicle at the rear. The roll rate and lateral acceleration of the ARB vehicle are considerably larger than those of the SD vehicle or the HIS vehicle while the pitch rate and vertical acceleration of all three configurations are comparable.

Compared with the vehicle responses of experiments shown in Figure 7.11 to 7.14, it can be seen that the simulation results of suspension deflection and tyre dynamic force agree well with the experiments except for the small difference in the magnitudes, particularly at the rear suspension. The phase change of roll motion is also predicted by

the mathematic models. Both experiment and simulation results shows that the ARB vehicle presents less flexible suspension and larger tyre dynamic forces, while the HIS suspension offers the same flexibility as the SD suspension at warp mode.

The discrepancies between experiment and simulation are mainly found on the magnitudes of roll rate and vehicle body acceleration. The ARB vehicle has the largest roll rate in simulation among all three vehicle configurations but the difference is not significant in the experiment. The vertical acceleration of the ARB and SD vehicle are the same and those of the HIS are slightly larger in simulation, but the experiment shows the vertical acceleration of the SD and HIS vehicle is similar and that of the ARB vehicle is the smallest among all three.

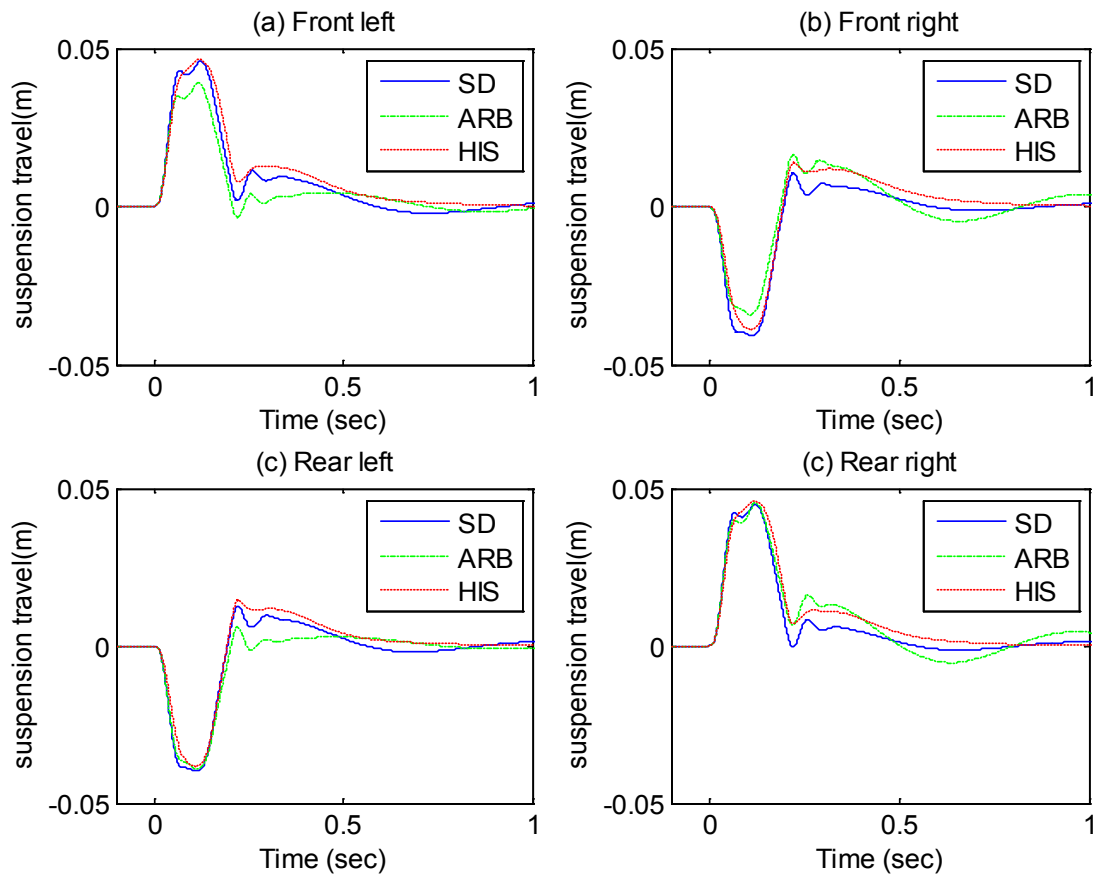


Figure 7. 22: Suspension deflections (a) Front left (b) Front right (c) Rear left (d) Rear right

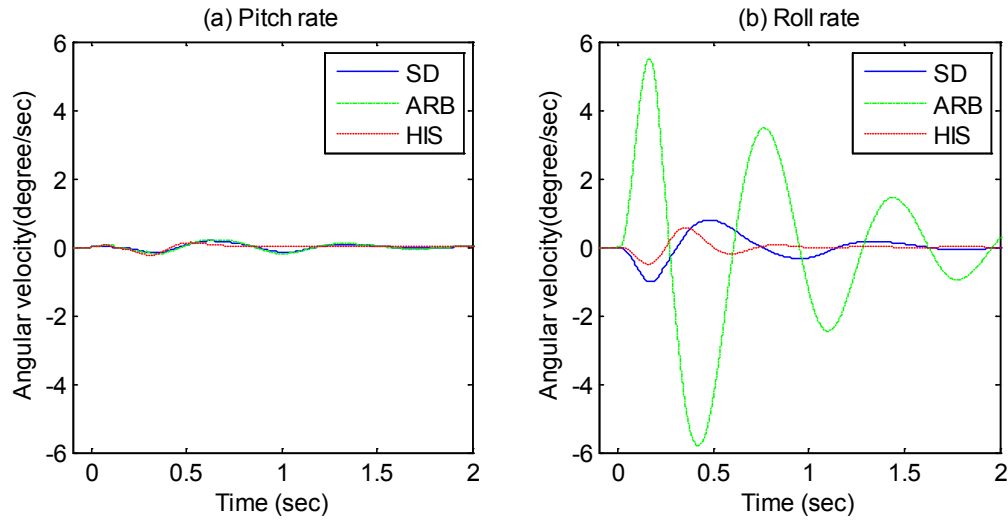


Figure 7.23: Angular velocities

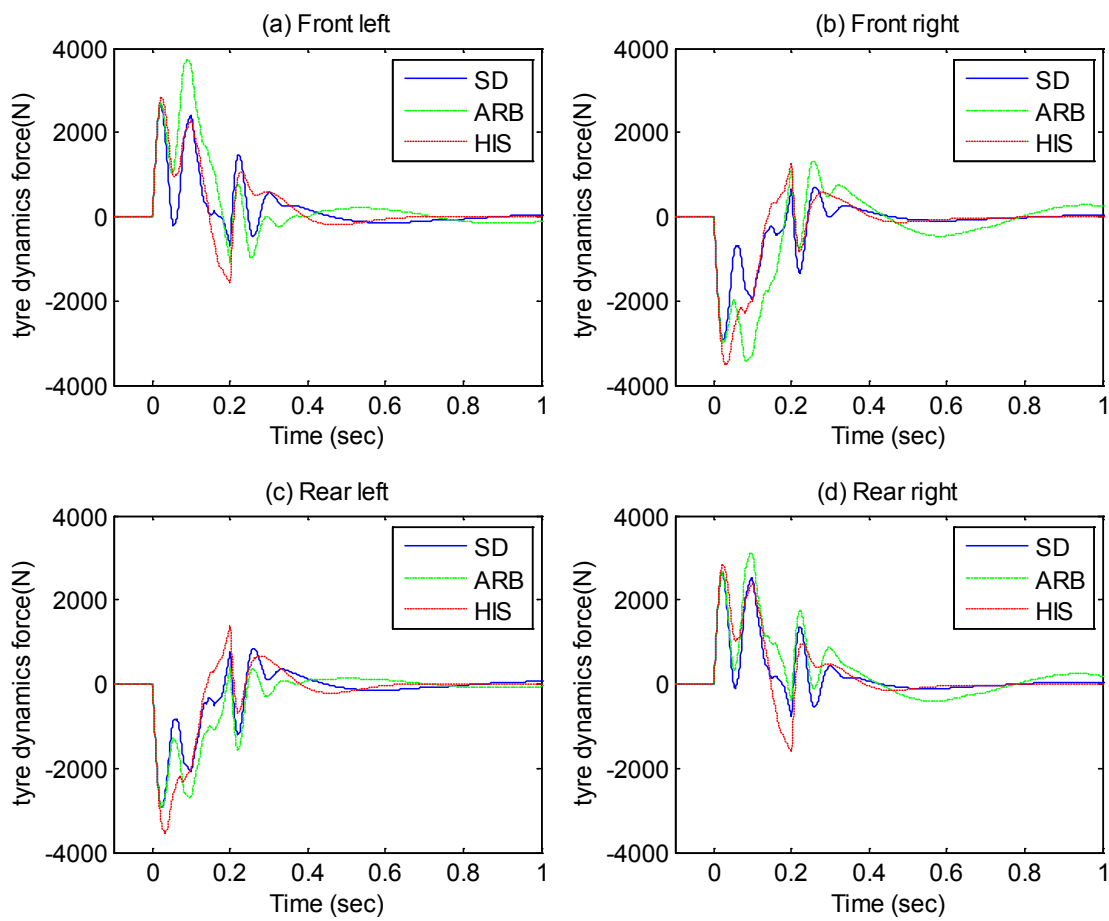


Figure 7.24: Tyre dynamic forces (a) Front left (b) Front right (c) Rear left (d) Rear right

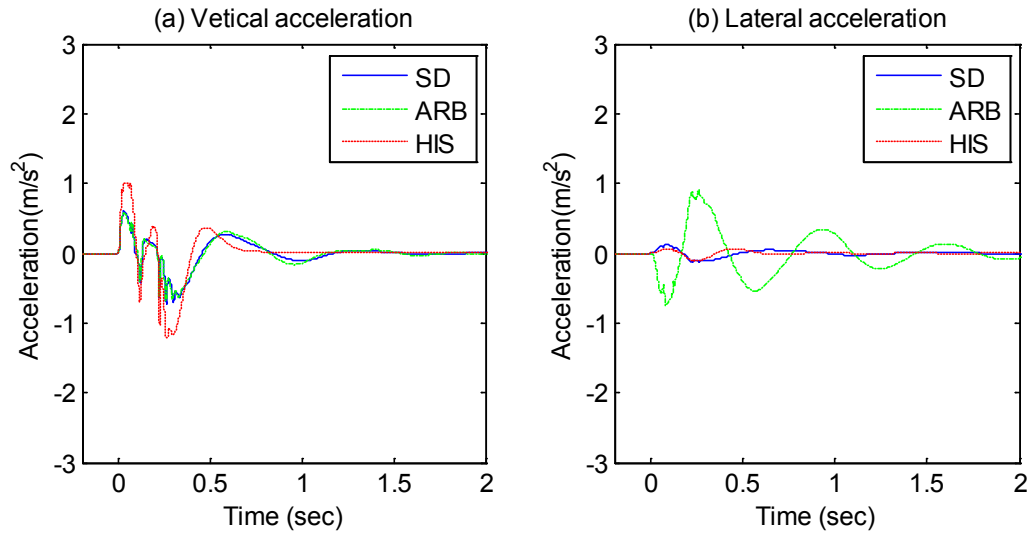


Figure 7.25: Vehicle accelerations at C.G

7.5 Discussion

7.5.1 Experimental limitations

Lab limitations

The lab test conducted in our suspension test lab may have some limitations for the experiments. First is the range limitation of road input. The maximum input range of your hydraulic test rig is $\pm 80\text{mm}$, and the maximum amplitude of our test is set at 50mm . By contrast, the vehicle field test of axle articulation normally has a range of more than 300mm . The vehicle response under extremely large axle articulation cannot be tested in our lab. Second, is the calibration of sensors, especially the load cell calibration. The maximum range of load cell at each corner is up to 4 tons, but due to the limited weights, our calibration is conducted under 300 kg in the static condition. It also lacks dynamic load calibration which may affect the accuracy of the tyre dynamic load measurement. The third limitation is the signal noise of measurement. We have been careful during the sensor installation to shield each wire properly for minimising

the effects of electro-magnetic interference. However certain noise still exists during the test and affects the accuracy of measurement.

Unmodelled effects

The mathematic vehicle model used in the preceding sections overlooked a number of factors that may have contributed to the discrepancy of results in the axle articulation test. The most significant of these is the flexibility of the vehicle body/frame. The vehicle body/frame stiffness has a significant influence on the vehicle's response under axle articulation excitation [105]. The assumption of an infinitely rigid vehicle body may be valid in the vertical bounce vibration mode and roll and pitch vehicle body modes. But the vehicle body/frame is more flexible and easier to deform under the axle articulation inputs. The flexible multi-body dynamics analysis is more appropriate to investigate the vehicle warp mode properties [106].

Some other unmodelled effects could also affect the accuracy of the results. The suspension kinematics and compliance is not considered in the numerical model, but the effects could be large in the real application [107]. The changes of camber and caster angle, and the jack force developed by the control arms play an important role in the suspension characteristics as the suspension moves. The compliance of the bushings, the body, and other parts also modifies the behaviour of the suspension. Particularly, the nonlinearity of the anti-roll bar bushings which connects the bars with the vehicle body/chassis has a major influence on the axle articulation tests. The elasticity and mechanical hysteresis of the roll bar bushings should be accounted for in the dynamic analysis.

For the hydraulic system, the compressibility of the hydraulic fluid is not considered as well as the flexibility of the hose and pipelines. The rigid pipeline and incompressible fluid tend to overestimate the roll stiffness. The pressure loss of pipelines is also ignored in the mathematic model but the effects could become significant under high frequency excitation. The pressure changes produced inside the fluid circuits of interconnected suspensions often lead to vibration of pipelines and associated structures and become a source of structural noise [108].

7.5.2 Suggestions

The rigid body assumption is not valid to be used in practice to evaluate vehicle performance under the axle articulation (warp mode). There is a clear need to consider the vehicle body/frame's deformation (torsional stiffness). A virtual torsional stiffness of vehicle body/frame could be employed in the vehicle modelling to account for the vehicle body/frame deformation under axle articulation (warp) excitation. Another approach is to use flexible multi-body dynamics for the vehicle's axle articulation investigation.

The suspension kinematics and compliance should also be considered in the modelling of the vehicle to more accurately predict vehicle response. There is also a need to obtain accurate empirical hydraulic component models to account for the hydraulic nonlinear effects.

7.6 Summary

The experimental verification of the roll-resistant interconnected suspension was undertaken in the four-post vehicle test rig. The responses of the test vehicle were

compared with the theoretical predictions and the results show that the theoretical model could reasonably predict the vehicle performance under various road excitations, especially the axle articulation. The experiment limitations and unmodelled effects are also discussed and some suggestions are given for future research work. The verified fluidic interconnected suspension model could be confidently applied to the other variant configurations of the interconnected suspension.

Chapter 8: Conclusions and Recommendations

8.1 Summary of the thesis

This research thesis has systematically explored four advanced passive interconnected suspension design concepts, Roll-resistant Hydraulically Interconnected Suspension (RHIS), Pitch-resistant Hydraulically Interconnected Suspension (PHIS), Roll & Pitch Independently Tuned Interconnected Suspension (RPITIS) as well as Zero Warp Hydro-Pneumatic Interconnected Suspension (ZWHPIS) to explore the benefits of suspension mode decoupling and demonstrate the design flexibility of interconnected suspensions.

The static property studies of the proposed interconnected suspensions are performed and the characteristics of suspension stiffness and damping are compared with the conventional suspension. Results illustrate that desirable mode properties can be achieved with the proposed interconnected suspensions. Investigations of the ride and handling dynamic performance of the vehicle with various proposed interconnected suspensions are undertaken with multi-degree rigid body vehicle model coupled with the fluidic model both in the frequency domain and time domain. The trends of the ride and handling performances of the vehicle equipped with the proposed suspensions are examined by the frequency response analysis under road inputs or force moments induced by vehicle accelerations. The time domain studies are also performed using the 14 degree-of-freedom nonlinear vehicle model coupled with the nonlinear fluidic model. The promising improvements both for ride comfort and handling/stability are demonstrated in the simulation results. The theoretical model of the vehicle with the RHIS suspension is verified experimentally by the bench test in our suspension lab, particularly at warp mode inputs. Generally, the testing results agree well with the

simulation results. The un-modelled effects are discussed and further works are suggested.

The detailed summary of the thesis follows.

Chapter 1: the basic problem under investigation was introduced in Chapter 1 and the research objectives were established.

Chapter 2: some essential background information on vehicle system dynamics and suspension system was provided in Chapter 2. It also highlighted a number of key conflicts relating to suspension design that required a compromise such as the ride comfort vs. tyre grip in the vertical dynamics, the attitude control vs. pitch ride in the longitudinal dynamics, the roll stability vs. ride comfort and road holding in the lateral dynamics. Some interconnected suspensions were reviewed and these manifested the unique property to easily decouple the vehicle motion modes. The chapter concluded by stating that more advanced interconnections and the effects of different interconnection configurations to vehicle system dynamics still requires greater exploration.

Chapter 3: the roll-resistant hydraulically interconnected suspension and pitch-resistant hydraulically interconnected suspension were investigated respectively both for static property and dynamic characteristics. The static suspension characteristics illustrated that the roll stiffness is increased by the RHIS with minimal effects on the other modes; similarly, the pitch stiffness is increased by the PHIS with minimal effects on the other modes. It demonstrated the mode decoupling property of the interconnected suspension. The nonlinear roll stiffness/damping of RHIS and nonlinear pitch stiffness/damping of the PHIS were shown to be favourable in terms of improving the compromise between ride comfort and directional stability. The dynamic characteristics of the RHIS and

PHIS suspensions were investigated via the modelling and simulation of the vehicles with fluidic suspension models in the frequency domain. The results showed that the vehicle with RHIS had significantly improved roll natural frequency while bounce and warp natural frequencies still remained at the same levels. The same was the case with the vehicle with PHIS in that the pitch natural frequency was greatly improved while other modes were minimally affected.

Chapter 4: a generalised 14 DOF nonlinear vehicle model was developed to predict the coupling of longitudinal, lateral and vertical dynamics of the on-road two-axle vehicle in this chapter. The magic formula tyre model was used to include the nonlinear behaviour of the pneumatic tyre. The proposed model was validated by the commercial software CARSIM and the results illustrated that the 14 DOF is accurate enough for the vehicle dynamics study. The sensitivity of the vehicle speed and roll stiffness were investigated in the fishhook maneuver test. Severe under-steering was predicted when the vehicle speed was too high. The lateral tyre force saturated at its maximum value so that the vehicle started to slide out when the vehicle speed continued to increase, and the vehicle reached its maximum roll angle and presented a high risk of rollover. The roll stability was critical to vehicle handling and safety. With the same SSF, the stiff roll mode was desirable to inhibit the roll motion and increase the rollover threshold of the vehicle at cornering.

Chapter 5: the vehicle fitted with the Roll and Pitch Independently Tuned Suspension system was presented in this chapter. The static properties of the proposed RPITIS suspension in the four suspension modes were compared with those of conventional suspension. The results showed that the RPITIS system could increase the roll- and pitch-mode stiffness and damping substantially, with minimum influence on the

bounce/warp mode properties. Such enhanced decoupling of the roll/pitch mode from the bounce/warp modes would be beneficial in realising an improved design compromise among various vehicle performance measures under complex driving conditions. The dynamic analysis of the proposed suspension was conducted and compared with conventional suspensions to investigate the potential benefits on the vehicle ride, handling, and the lateral and longitudinal dynamics response under various road excitation and braking/steering maneuvers. The simulation results demonstrated that the proposed RPITIS suspension system could yield considerably enhanced anti-roll and anti-pitch performances. The ride quality of the vehicle was also improved by the reduced vehicle bounce stiffness. The systematic analysis of suspension properties, design sensitivity and vehicle dynamic responses clearly demonstrated the considerable potential of the roll and pitch decoupled interconnected suspension.

Chapter 6: the modelling and tyre load analysis of vehicle with zero warp interconnected suspension system was presented in this chapter based on parameters obtained from a typical sport utility vehicle. Modal analysis results clearly illustrated that proposed ZWHPIS suspension could achieve zero warp suspension stiffness while at the same time maintaining soft bounce and improved roll stability. The results of the tyre load analysis in the frequency domain and time domain under warp excitation both showed that the vehicle fitted with ZWHPIS had a much smaller tyre load variation compared to conventional suspensions at low frequencies. The smaller the tyre dynamic load, the better the road holding ability and the less vehicle body/frame torsional stress which is meaningful for off-road applications such as in military vehicles.

Chapter 7: The experimental verification of the Roll-resistant Hydraulically Interconnected Suspension was undertaken in the four-post vehicle test rig. The test

vehicle responses were compared with the theoretical prediction and the results showed that the theoretical model could reasonably predict the vehicle performance under various road excitations, especially the axle articulation. The verified fluidic interconnected suspension model could be confidently applied to the other variant configurations of interconnected suspension.

8.2 Contributions

The specific objectives and contributions of this thesis, as set out in Section 1.2, were achieved as follows.

1. Theoretical analysis of the interconnected suspension with a focus on the mode decoupling property and warp mode performance.

This was achieved by

- a) presenting a thorough summary of past work relating to vehicle dynamics, suspension modes and interconnected suspensions. (Chapter 2)
- b) the modelling and modal analysis of roll-resistant and pitch-resistant interconnected suspensions. (Chapter 3)
- c) the modelling and dynamic analysis of roll and pitch independently tuned interconnected suspension. (Chapter 5)
- d) the modelling and dynamic analysis of zero warp hydro-pneumatic suspension. (Chapter 6)

2. To develop a generalised full vehicle model with multiple nonlinearities and investigate vehicle responses under different maneuver and road conditions for accurate assessment of vehicle system dynamics.

This was achieved by

- a) the modelling and verification of a generalised 14-dof nonlinear full vehicle system integrated with a nonlinear tyre model. (Chapter 4)
- b) the investigation of vehicle roll yaw coupling during the fishhook maneuver, and a sensitivity study of how vehicle speed or roll stiffness affects vehicle responses. (Chapter 4)

3. To investigate the ride and handling of a vehicle with roll and pitch independently tuned interconnected suspension and demonstrate the capability of mode-based suspension tuning that greatly improves the compromise between ride and handling.

This was achieved by

- a) the modelling of a full vehicle coupled with a roll and pitch independently tuned interconnected suspension system. (Chapter 5)
- b) the static property study of the vehicle equipped with roll and pitch independently tuned suspension. (Chapter 5)
- c) the dynamic analysis of the ride and handling of a vehicle with RPITIS and compared to a vehicle with conventional suspension. (Chapter 5)

4. To present a novel suspension system with zero-warp suspension stiffness and investigate the off-road performance of a vehicle with zero-warp hydro-pneumatic interconnected suspension.

This was achieved by

- a) the modelling of a full vehicle coupled with a zero warp hydro-pneumatic interconnected suspension system. (Chapter 6)
- b) the static property study of the vehicle equipped with a zero warp hydro-pneumatic interconnected suspension system. (Chapter 6)
- c) the dynamic analysis of vehicle tyre load under warp road excitation both in the frequency domain and time domain to demonstrate the zero warp suspension stiffness. (Chapter 6)

5. Experimental verification of the theoretical model of hydraulically interconnected suspension with a focus on the warp model stiffness and tyre dynamic load response.

This was achieved by

- a) the lab testing of a vehicle with roll-resistant hydraulically interconnected suspension under warp mode and single bump excitation. (Chapter 7)
- b) comparison of lab test data with the simulation results of a theoretical model of a full vehicle integrated with roll resistant interconnected suspension. (Chapter 7)

8.3 Suggestions for future work

The hydraulically interconnected vehicle suspension systems offer significant potential as a future suspension owing to its passive principles and enhanced tuning flexibility. Moreover, the hydro-pneumatic interconnected suspension can also provide extensive tuning flexibility for off-road applications. It would be desirable to translate the fundamental and conceptual design studies of these suspension designs into analyses for specific vehicles as well as laboratory prototype developments. It would also be

desirable to explore the semi-active fluidic damping valves integrated within the fluidic systems and alternative compressible fluids to attain variable stiffness suspension. These research efforts would attract interest from the commercial vehicle, military vehicle and motorsport sectors, which have either employed or are planning to employ such design concepts. Particular topics for future work may include the following:

1. There is a clear need to further investigate the effects of vehicle chassis torsional stiffness under axle articulation (warp) mode excitation as the assumption of the rigid vehicle body is not valid anymore at such extreme conditions.
2. The consideration of detailed suspension linkage arm effects in the interconnected suspension design requires further study to facilitate the application of interconnected suspensions in SUVs, commercial vehicles and passenger cars.
3. Experimental study and field test of various interconnected suspension, such as RPITIS, ZWHPIS are recommended for further research.
4. The roll resistant passive interconnected system could be easily upgraded to an active anti-roll controlled suspension by adding a power source to actively control the vehicle roll attitude. The optimized anti-roll control algorithm based on the roll-plane interconnection is worth putting more effort into in terms of future research.
5. The active system is more capable to govern low-frequency large-amplitude vehicle body motions. However for the fully active suspension system, the suspension interconnection can be realised virtually so that physical interconnection is not necessary. Semi-active damping is considered to be most efficient and effective in absorbing high-frequency low-amplitude vehicle dynamic energy. The combination of the semi-active damping system and interconnected suspension could yield more

improved ride comfort and handling performance. The height adjustment and levelling slow-active suspension can also be easily integrated into the interconnected suspension system, either hydraulically or pneumatically. Hence, the integrated semi-active height adjustable interconnected suspension system is recommended as a future research topic.

Appendix: Publications and Patents

The publications resulting directly from the work presented in this thesis are:

Journals:

1. **Guangzhong Xu** and N. Zhang, “Characteristic Analysis of Roll and Pitch Independently Controlled Hydraulically Interconnected Suspension”. *SAE International Journal of Commercial Vehicles*, vol. 7, pp. 170-176, 2014.
2. **Guangzhong Xu**, N. Zhang & H. Roser, “Roll & Pitch Independently Tuned Interconnected Suspension: Modelling and Dynamic Analysis”, *Vehicle System Dynamics*, Accepted for publication.

Conference papers:

1. L. Wang, **Guangzhong Xu**, N. Zhang, and H. Roser, “Experimental Comparison of Anti-Roll Bar with Hydraulically Interconnected Suspension in Articulation Mode”, *SAE Technical Paper Series*, SAE 2013-01-0710, 2013.
2. **Guangzhong Xu**, N. Zhang, H. Roser, “Theoretical Analysis of Roll-plane Hydraulically Interconnected Suspension Compared with Anti-roll Bars”, 23rd *International Symposium on Dynamics of Vehicles on Roads and Tracks*, 2013.
3. **Guangzhong Xu**, H. M. Roser, and N. Zhang, "Experimental Study of a Roll-Plane Hydraulically Interconnected Suspension System under Vehicle Articulation Mode", *ASME 2013 International Mechanical Engineering Congress and Exposition*, 2013, pp. V013T14A011-V013T14A011.

4. W. Sun, Y. Li, **Guangzhong Xu**, and N. Zhang, "Vibration Control of In-Wheel SRM for Electric Vehicle Applications", *INTER-NOISE and NOISE-CON congress*, 2014.
5. **Guangzhong Xu**, N. Zhang, H. Roser, & J. Ruan, "Tyre Load Analysis of Hydro-Pneumatic Interconnected Suspension with Zero Warp Suspension Stiffness", *SAE Technical Paper Series*, SAE 2015-01-0630, 2015.

Patents under examination:

1. **Guangzhong Xu**, Mingyi Zheng, Nong Zhang, "Hydraulic interconnection suspension system and exhausting and sealing method for same," China patent CN103273820.
2. **Guangzhong Xu**, Mingyi Zheng, Nong Zhang, "Hydraulic cylinder" China patent CN103267042.
3. **Guangzhong Xu**, Nong Zhang, "Oil and gas suspension with energy recyclable and motor vehicle," China patent CN204037271.
4. **Guangzhong Xu**, Nong Zhang, "Vehicle suspension units and mutually connected suspension system," China patent WO2015078190.

References

-
- [1] N. Zhang, W. A. Smith, and J. Jeyakumaran, "Hydraulically interconnected vehicle suspension: background and modelling," *Vehicle System Dynamics*, vol. 48, pp. 17-40, 2010.
 - [2] M. C. Smith and W. Walker, "Interconnected vehicle suspension," *Proceedings of the Institution of Mechanical Engineers Part D-Journal of Automobile Engineering*, vol. 219, pp. 295-307, Mar 2005.
 - [3] D. P. Cao, X. B. Song, and M. Ahmadian, "Editors' perspectives: road vehicle suspension design, dynamics, and control," *Vehicle System Dynamics*, vol. 49, pp. 3-28, 2011.
 - [4] T. D. Gillespie, "Heavy truck ride," SAE Technical Paper 850001, 1985.
 - [5] R. S. Sharp and D. A. Crolla, "Road vehicle suspension system design - a review," *Vehicle System Dynamics*, vol. 16, pp. 167-192, 1987.
 - [6] L. Segel, "An overview of developments in road-vehicle dynamics: past, present and future," *Vehicle Ride and Handling*, pp. 1-12, 1993.
 - [7] Z. Y. Jiang, D. A. Streit, and M. El-Gindy, "Heavy vehicle ride comfort: Literature survey," *International Journal of Heavy Vehicle Systems*, vol. 8, pp. 258-284, 2001.
 - [8] E. M. Elbeheiry, D. C. Karnopp, M. E. Elaraby, and A. M. Abdelraaouf, "Advanced ground vehicle suspension systems - a classified bibliography," *Vehicle System Dynamics*, vol. 24, pp. 231-258, Apr 1995.
 - [9] D. A. Crolla, "Vehicle dynamics - Theory into practice," *Proceedings of the Institution of Mechanical Engineers Part D-Journal of Automobile Engineering*, vol. 210, pp. 83-94, 1996.
 - [10] D. J. Cole, "Fundamental issues in suspension design for heavy road vehicles," *Vehicle System Dynamics*, vol. 35, pp. 319-360, 2001.
 - [11] R. M. Chalasani, "Ride performance potential of active suspension systems-Part I: Simplified analysis based on a quarter-car model," in *Proceedings of the 1986 ASME Winter Annual Meeting*, 1986.
 - [12] R. Krtolica and D. Hrovat, "Optimal active suspension control based on a half-car model," in *Decision and Control, 1990., Proceedings of the 29th IEEE Conference on*, 1990, pp. 2238-2243.
 - [13] T. Yoshimura, A. Kume, M. Kurimoto, and J. Hino, "Construction of an active suspension system of a quarter car model using the concept of sliding mode control," *Journal of Sound and Vibration*, vol. 239, pp. 187-199, 2001.
 - [14] H. Rowell, "Principles of vehicle suspension," *Proceedings of the Institution of Automobile Engineers*, vol. 17, pp. 455-541, 1922.
 - [15] ISO, *Mechanical Vibration and Shock: Evaluation of Human Exposure to Whole-body Vibration. Part 1, General Requirements: International Standard ISO 2631-1: 1997 (E)*: ISO, 1997.
 - [16] G. Paddan and M. Griffin, "Evaluation of whole-body vibration in vehicles," *Journal of Sound and Vibration*, vol. 253, pp. 195-213, 2002.

-
- [17] T. D. Gillespie, *Fundamentals of vehicle dynamics* vol. 400: Society of Automotive Engineers Warrendale, PA, 1992.
- [18] M. Gobbi, F. Levi, and G. Mastinu, "Multi-objective stochastic optimisation of the suspension system of road vehicles," *Journal of Sound and Vibration*, vol. 298, pp. 1055-1072, Dec 2006.
- [19] A. Shirahatt, P. S. S. Prasad, P. Panzade, and M. M. Kulkarni, "Optimal design of passenger car suspension for ride and road holding," *Journal of the Brazilian Society of Mechanical Sciences and Engineering*, vol. 30, pp. 66-76, Jan-Mar 2008.
- [20] A. Hać, "Suspension optimization of a 2-DOF vehicle model using a stochastic optimal control technique," *Journal of Sound and Vibration*, vol. 100, pp. 343-357, 1985.
- [21] I. Esat, "Genetic algorithm-based optimization of a vehicle suspension system," *International Journal of Vehicle Design*, vol. 21, pp. 148-160, 1999.
- [22] A. F. Naude and J. A. Snyman, "Optimisation of road vehicle passive suspension systems. Part 2. Qualification and case study," *Applied Mathematical Modelling*, vol. 27, pp. 263-274, Apr 2003.
- [23] J. P. C. Goncalves and J. A. C. Ambrosio, "Optimization of vehicle suspension systems for improved comfort of road vehicles using flexible multibody dynamics," *Nonlinear Dynamics*, vol. 34, pp. 113-131, Oct 2003.
- [24] Y. P. He and J. McPhee, "Application of optimisation algorithms and multibody dynamics to ground vehicle suspension design," *International Journal of Heavy Vehicle Systems*, vol. 14, pp. 158-192, 2007.
- [25] J. H. Crews, M. G. Mattson, and G. D. Buckner, "Multi-objective control optimization for semi-active vehicle suspensions," *Journal of Sound and Vibration*, vol. 330, pp. 5502-5516, Nov 2011.
- [26] D. Karnopp, M. J. Crosby, and R. Harwood, "Vibration control using semi-active force generators," *Journal of Manufacturing Science and Engineering*, vol. 96, pp. 619-626, 1974.
- [27] P. J. T. Venhovens, A. C. M. Vanderknaap, and H. B. Pacejka, "Semiactive attitude and vibration control," *Vehicle System Dynamics*, vol. 22, pp. 359-381, Sep-Nov 1993.
- [28] G. Yao, F. Yap, G. Chen, W. Li, and S. Yeo, "MR damper and its application for semi-active control of vehicle suspension system," *Mechatronics*, vol. 12, pp. 963-973, 2002.
- [29] S. Choi, Y. Choi, E. Chang, S. Han, and C. Kim, "Control characteristics of a continuously variable ER damper," *Mechatronics*, vol. 8, pp. 143-161, 1998.
- [30] G. Georgiou, G. Verros, and S. Natsiavas, "Multi-objective optimization of quarter-car models with a passive or semi-active suspension system," *Vehicle System Dynamics*, vol. 45, pp. 77-92, Jan 2007.
- [31] R. G. Langlois and R. J. Anderson, "Preview control algorithms for the active suspension of an off-road vehicle," *Vehicle System Dynamics*, vol. 24, pp. 65-97, Jan 1995.
- [32] H. D. Taghirad and E. Esmailzadeh, "Automobile passenger comfort assured through LQG/LQR active suspension," *Journal of Vibration and Control*, vol. 4, pp. 603-618, Sep 1998.
- [33] M. Yamashita, K. Fujimori, K. Hayakawa, and H. Kimura, "Application of H^∞ control to active suspension systems," *Automatica*, vol. 30, pp. 1717-1729, 1994.

-
- [34] A. Thompson, B. R. Davis, and C. Pearce, "An optimal linear active suspension with finite road preview," SAE Technical Paper 800520, 1980.
 - [35] W. F. Milliken, D. L. Milliken, and M. Olley, *Chassis design: principles and analysis* vol. 400: Society of Automotive Engineers Warrendale, PA, 2002.
 - [36] R. Sharp, "Wheelbase filtering and automobile suspension tuning for minimizing motions in pitch," *Proceedings of the Institution of Mechanical Engineers, Part D: Journal of Automobile Engineering*, vol. 216, pp. 933-946, 2002.
 - [37] D. A. Crolla and R. P. King, "Olley's "flat ride" revisited," *Vehicle System Dynamics*, vol. 33, pp. 762-774, 1999.
 - [38] D. Cao, A. Khajepour, and X. Song, "Wheelbase filtering and characterization of road profiles for vehicle dynamics," in *ASME 2010 International Design Engineering Technical Conferences and Computers and Information in Engineering Conference*, 2010, pp. 275-285.
 - [39] R. Sharp, "Influences of suspension kinematics on pitching dynamics of cars in longitudinal manoeuvring.," in *The dynamics of vehicles on roads and on tracks*, Pretoria, South Africa, 1999.
 - [40] A. M. C. Odhams and D. Cebon, "An analysis of ride coupling in automobile suspensions," *Proceedings of the Institution of Mechanical Engineers Part D-Journal of Automobile Engineering*, vol. 220, pp. 1041-1061, Aug 2006.
 - [41] D. Cao, S. Rakheja, and C. Y. Su, "Pitch plane analysis of a twin-gas-chamber strut suspension," *Proceedings of the Institution of Mechanical Engineers Part D-Journal of Automobile Engineering*, vol. 222, pp. 1313-1335, Aug 2008.
 - [42] D. P. Cao, S. Rakheja, and C. Y. Su, "Heavy vehicle pitch dynamics and suspension tuning. Part I: unconnected suspension," *Vehicle System Dynamics*, vol. 46, pp. 931-953, 2008.
 - [43] D. Cao, S. Rakheja, and C. Y. Su, "Dynamic analyses of heavy vehicle with pitch-interconnected suspensions," *International Journal of Heavy Vehicle Systems*, vol. 15, pp. 272-308, 2008.
 - [44] F. Ding, X. Han, Z. Luo, and N. Zhang, "Modelling and characteristic analysis of tri-axle trucks with hydraulically interconnected suspensions," *Vehicle System Dynamics*, vol. 50, pp. 1877-1904, 2012.
 - [45] F. C. Wang and M. C. Smith, *Active and passive suspension control for vehicle dive and squat*. Godalming: Springer-Verlag London Ltd, 2003.
 - [46] N. H. T. S. Administration, "Initiative to address the mitigation of vehicle rollover, Docket No," NHTSA-2003-14622-12003.
 - [47] G. J. Forkenbrock, W. R. Garrott, M. Heitz, and B. C. O'Harra, "A comprehensive experimental examination of test maneuvers that may induce on-road, untripped light vehicle rollover—Phase IV of NHTSA's light vehicle rollover research program," *Report No. DOT HS*, vol. 809, p. 513, 2002.
 - [48] R. D. Ervin, "The dependance of truck roll stability on size and weight variables," *International Journal of Vehicle Design*, vol. 7, pp. 192-208, Sep 1986.
 - [49] A. Hac, "Rollover stability index including effects of suspension design," SAE Technical Paper 2002-01-0965, 2002.

-
- [50] N. Zhang, G. M. Dong, and H. P. Du, "Investigation into untripped rollover of light vehicles in the modified fishhook and the sine maneuvers. Part I: Vehicle modelling, roll and yaw instability," *Vehicle System Dynamics*, vol. 46, pp. 271-293, 2008.
- [51] Y. Li, W. Sun, J. Huang, L. Zheng, and Y. Wang, "Effect of vertical and lateral coupling between tyre and road on vehicle rollover," *Vehicle System Dynamics*, vol. 51, pp. 1216-1241, 2013.
- [52] D. Renfroe, A. Roberts, and M. Gilbert, "Vehicle rollover maximum limits," *International Journal of Vehicle Design*, vol. 40, pp. 144-158, 2006.
- [53] M. El-Gindy, "An overview of performance measures for heavy commercial vehicles in North America," *International Journal of Vehicle Design*, vol. 16, pp. 441-463, 1995.
- [54] D. Cebon, *Handbook of vehicle-road interaction*, 1999.
- [55] D. Cao, S. Rakheja, and C.-Y. Su, "Dynamic analyses of roll plane interconnected hydro-pneumatic suspension systems," *International Journal of Vehicle Design*, vol. 47, pp. 51-80, 2008.
- [56] L. Wang, G. Xu, N. Zhang, and H. Roser, "Experimental Comparison of Anti-Roll Bar with Hydraulically Interconnected Suspension in Articulation Mode," SAE Technical Paper 2013-01-0710, 2013.
- [57] A. B. Lovins and D. R. Cramer, "Hypercars, hydrogen, and the automotive transition," *International Journal of Vehicle Design*, vol. 35, pp. 50-85, 2004.
- [58] J. Darling and L. R. Hickson, "An experimental study of a prototype active anti-roll suspension system," *Vehicle System Dynamics*, vol. 29, pp. 309-329, May 1998.
- [59] P. H. Cronje and P. S. Els, "Improving off-road vehicle handling using an active anti-roll bar," *Journal of Terramechanics*, vol. 47, pp. 179-189, 2010.
- [60] D. J. M. Sampson and D. Cebon, "Achievable roll stability of heavy road vehicles," *Proceedings of the Institution of Mechanical Engineers Part D-Journal of Automobile Engineering*, vol. 217, pp. 269-287, 2003.
- [61] F. Yu, D.-F. Li, and D. Crolla, "Integrated Vehicle Dynamics Control—state-of-the art review," in *Vehicle Power and Propulsion Conference, 2008. VPPC'08. IEEE*, 2008, pp. 1-6.
- [62] S. Lu, S. Choi, Y. Li, M. Seong, and J. Han, "Global integrated control of vehicle suspension and chassis key subsystems," *Proceedings of the Institution of Mechanical Engineers, Part D: Journal of Automobile Engineering*, vol. 224, pp. 423-441, 2010.
- [63] D. A. Crolla and D. P. Cao, "The impact of hybrid and electric powertrains on vehicle dynamics, control systems and energy regeneration," *Vehicle System Dynamics*, vol. 50, pp. 95-109, 2012.
- [64] W. A. Smith, *An investigation into the dynamics of vehicles with hydraulically interconnected suspensions*. Ph.D thesis University of Technology Sydney, 2009.
- [65] E. Zapletal, "Balanced suspension," SAE Technical Paper 2000-01-3572, 2000.
- [66] S. Bhawe, "Effect of connecting the front and rear air suspensions of a vehicle on the transmissibility of road undulation inputs," *Vehicle System Dynamics*, vol. 21, pp. 225-245, 1992.
- [67] C.-J. Kat and P. Schalk Els, "Interconnected air spring model," *Mathematical and Computer Modelling of Dynamical Systems*, vol. 15, pp. 353-370, 2009.

-
- [68] D.-I. F. Wolf-Monheim, D.-I. T. Schrüllkamp, and D.-I. S. Loos, "Interlinked Air Suspension Systems," *ATZautotechnology*, vol. 9, pp. 58-61, 2009.
- [69] G. Rideout and R. J. Anderson, "Experimental testing and mathematical modeling of the interconnected hydragas suspension system," SAE Technical Paper 2003-01-0312, 2003.
- [70] N. Rosam and J. Darling, "Development and simulation of a novel roll control system for the Interconnected Hydragas(R) suspension," *Vehicle System Dynamics*, vol. 27, pp. 1-18, Jan 1997.
- [71] P. J. Liu, S. Rakheja, and A. K. W. Ahmed, "Properties of an interconnected hydro-pneumatic suspension system," *Transactions of the Canadian Society for Mechanical Engineering*, vol. 19, pp. 383-396, 1995.
- [72] D. P. Cao, S. Rakheja, and C. Y. Su, "Roll- and pitch-plane coupled hydro-pneumatic suspension," *Vehicle System Dynamics*, vol. 48, pp. 361-386, 2010.
- [73] W. A. Smith, N. Zhang, and J. Jeyakumaran, "Hydraulically interconnected vehicle suspension: theoretical and experimental ride analysis," *Vehicle System Dynamics*, vol. 48, pp. 41-64, 2010.
- [74] W. A. Smith, N. Zhang, and W. Hu, "Hydraulically interconnected vehicle suspension: handling performance," *Vehicle System Dynamics*, vol. 49, pp. 87-106, 2011.
- [75] D. Cao, S. Rakheja, and C.-Y. Su, "Roll-and pitch-plane-coupled hydro-pneumatic suspension. Part 2: dynamic response analyses," *Vehicle System Dynamics*, vol. 48, pp. 507-528, 2010.
- [76] C. B. Heyring, "Vehicle suspension system," ed: Google Patents, 1996.
- [77] J. R. Wilde, G. J. Heydinger, D. A. Guenther, T. Mallin, and A. M. Devenish, "Experimental evaluation of fishhook maneuver performance of a kinetic suspension system," SAE Technical Paper 2005-01-0392, 2005.
- [78] J. R. Wilde, G. J. Heydinger, and D. A. Guenther, "ADAMS Simulation of Ride and Handling Performance of the Kinetic™ Suspension System," SAE Technical Paper 2006-01-1972, 2006.
- [79] W. A. Smith, "An investigation into the dynamics of vehicles with hydraulically interconnected suspensions," PhD thesis, University of Technology Sydney, Australia, 2009.
- [80] M. Ahmadian and Y. K. Ahn, "On-vehicle evaluation of heavy truck suspension kinematics," SAE Technical Paper 2003-01-3394, 2003.
- [81] D. Cao, S. Rakheja, and C.-Y. Su, "Dynamic analyses of roll plane interconnected hydro-pneumatic suspension systems," *International Journal of Vehicle Design*, vol. 47, pp. 51-80, 2008.
- [82] D. Cao, S. Rakheja, and C. Su, "Roll plane analysis of a hydro-pneumatic suspension with twin-gas-chamber struts," *International Journal of Heavy Vehicle Systems*, vol. 14, pp. 355-375, 2007.
- [83] L. Wang, N. Zhang, and H. Du, "Experimental investigation of a hydraulically interconnected suspension in vehicle dynamics and stability control," SAE Technical Paper 2012-01-0240, 2012.

-
- [84] D. J. Cole and D. Cebon, "Truck suspension design to minimize road damage," *Proceedings of the Institution of Mechanical Engineers Part D-Journal of Automobile Engineering*, vol. 210, pp. 95-107, 1996.
- [85] D. Cao, S. Rakheja, and C. Su, "Pitch plane analysis of a twin-gas-chamber strut suspension," *Proceedings of the Institution of Mechanical Engineers, Part D: Journal of Automobile Engineering*, vol. 222, pp. 1313-1335, 2008.
- [86] M. Azman, H. Rahnejat, P. D. King, and T. J. Gordon, "Influence of anti-dive and anti-squat geometry in combined vehicle bounce and pitch dynamics," *Proceedings of the Institution of Mechanical Engineers Part K-Journal of Multi-Body Dynamics*, vol. 218, pp. 231-242, Dec 2004.
- [87] H. Laalej, Z. Lang, B. Sapinski, and P. Martynowicz, "MR damper based implementation of nonlinear damping for a pitch plane suspension system," *Smart Materials and Structures*, vol. 21, p. 045006, 2012.
- [88] T. Shim and C. Ghike, "Understanding the limitations of different vehicle models for roll dynamics studies," *Vehicle System Dynamics*, vol. 45, pp. 191-216, 2007.
- [89] F. Cheli, E. Leo, S. Melzi, and F. Mancosu, "A 14dof model for the evaluation of vehicle's dynamics: numerical-experimental comparison," *International Journal of Mechanics and Control*, vol. 6, pp. 19-30, 2006.
- [90] R. N. Jazar, *Vehicle dynamics: theory and application*: Springer Science & Business Media, 2013.
- [91] H. B. Pacejka and E. Bakker, "The magic formula tyre model," *Vehicle System Dynamics*, vol. 21, pp. 1-18, 1992.
- [92] H. Pacejka, *Tire and vehicle dynamics*: Elsevier, 2005.
- [93] G. J. Forkenbrock, W. R. Garrott, M. Heitz, and B. C. O'Harra, "An experimental examination of J-turn and fishhook maneuvers that may induce on-road, untripped, light vehicle rollover," SAE Technical Paper 2003-01-1008, 2003.
- [94] J. Y. Wong, *Theory of ground vehicles*: John Wiley & Sons, 2001.
- [95] H. Du, N. Zhang, and L. Wang, "Switched control of vehicle suspension based on motion-mode detection," *Vehicle System Dynamics*, vol. 52, pp. 142-165, 2014.
- [96] B. L. Gysen, J. J. Paulides, J. L. Janssen, and E. Lomonova, "Active electromagnetic suspension system for improved vehicle dynamics," *Vehicular Technology, IEEE Transactions on*, vol. 59, pp. 1156-1163, 2010.
- [97] J. Lin and R.-J. Lian, "Intelligent control of active suspension systems," *Industrial Electronics, IEEE Transactions on*, vol. 58, pp. 618-628, 2011.
- [98] http://www.tenneco.com/assets/1/7/Kinetic_Brochure.pdf.
- [99] G. Xu and N. Zhang, "Characteristic Analysis of Roll and Pitch Independently Controlled Hydraulically Interconnected Suspension," *SAE International Journal of Commercial Vehicles*, vol. 7, pp. 170-176, 2014.
- [100] J. Dixon, *The shock absorber handbook*: John Wiley & Sons, 2008.
- [101] P. Andren, "Power spectral density approximations of longitudinal road profiles," *International Journal of Vehicle Design*, vol. 40, pp. 2-14, 2005.

-
- [102] X. Shao, "Modeling and Model Analysis of a Full-Car Fitted with an Anti-Pitch Anti-Roll Hydraulically Interconnected Suspension," SAE Technical Paper 2014-01-0849, 0148-7191, 2014.
 - [103] E. B. Wylie, V. L. Streeter, and L. Suo, *Fluid transients in systems* vol. 1: Prentice Hall Englewood Cliffs, NJ, 1993.
 - [104] M. Rozyn and N. Zhang, "A method for estimation of vehicle inertial parameters," *Vehicle System Dynamics*, vol. 48, pp. 547-565, 2010.
 - [105] M. Arant, "Development and Implementation of a Warp Chassis Model," SAE Technical Paper 2011-01-2172, 2011.
 - [106] A. Deakin, D. Crolla, J. P. Ramirez, and R. Hanley, "The effect of chassis stiffness on race car handling balance," SAE Technical Paper 2000-01-3554, 2000.
 - [107] R. S. Sharp, *Influences of suspension kinematics on pitching dynamics of cars in longitudinal manoeuvring*. Lisse: Swets and Zeitlinger B V, 2000.
 - [108] J. Zhao and N. Zhang, "Vibration of hydraulically interconnected suspensions due to fluid-structure interaction," 2009.